# FOREWORD

This report summarizes work performed in the Liquid Metals Laboratory of the Department of Chemical Engineering at The University of Michigan on Air Force Contract AF33(616)-8277. The work was administered under the direction of the A F Aero Propulsion Laboratory, Research and Technology Division, Wright-Patterson Air Force Base, Ohio. Mr. Charles Delaney, Mr. Kenneth Hopkins, and Mr. Lloyd Hedgepeth have served as Project Engineers for RTD. The project was initiated in June 1961 and the first phase involved the preparation of a literature survey on Liquid Metal Boiling. The final report on this phase, ASD Technical Report 61-594, was released in December, 1961. The experimental efforts discussed in this report originated in January of 1962 and are continuing at the present time under Contract AF33-(657)-11548. The purpose of these studies has been to attain a better understanding of liquid metal boiling heat transfer from both an analytical and experimental point of view.

The program at The University of Michigan has been conducted under the direction of Professor Richard E. Balzhiser of the Department of Chemical and Metallurgical Engineering. Professors Edward E. Hucke, Donald L. Katz, M. Rasin Tek of the Department of Chemical and Metallurgical Engineering, and Professors Herman Merte, Jr., and John A. Clark of the Department of Mechanical Engineering have participated in the studies described herein. Dr. C. Phillip Colver, Messrs. Robert E. Barry, Andrew Padilla, Jr., Lowell R. Smith and Sam Walker have been responsible for individual segments of the project. Other graduate and undergraduate students in the College of Engineering have participated in project activities. The joint efforts of these individuals are responsible for the results conveyed in this final report.

The cooperation of Mine Safety Appliance Research Corporation in the design and fabrication of the liquid metal forced circulation apparatus was very much appreciated. Mr. Earl King and Mr. Guy Kennedy of MSA have provided valuable assistance throughout all phases of these studies. Mr. Robert Brooks of the General Electric Company, Evendale, Ohio has provided valuable technical assistance and services which have greatly facilitated the conduct of portions of this research.

Experimental results for the Forced Convection Heat Transfer Studies and the Agravic Studies with Mercury were not available for inclusion in this report. These studies, along with extensions of the other phases of project activity are continuing, and additional data should be forthcoming in the future. These results will continue to be reported in the quarterly progress reports released under Contract AF33(657)-11548. Those agencies or individuals seeking to be added to the distribution list for these reports should contact Professor Balzhiser at The University of Michigan.

JMR 0280

## ABSTRACT

Personnel in the College of Engineering at The University of Michigan have been conducting both analytical and experimental investigations involving liquid metal boiling heat transfer under contract with the Research and Technology Division, Wright-Patterson Air Force Base, Ohio. A study of saturated pool boiling of potassium in the nucleate regime has supported the nucleate boiling data of Bonilla and coworkers at Columbia University. Values for the critical heat flux were determined experimentally over a pressure range of 0.1 psia to 22 psia. The data fall substantially above the theoretical predictions of Zuber and Tribus, Rohsenow and Kutateladze. The results are of the same magnitude as predicted by Noyes of Atomics International based on his experimental work with sodium at the lower end of this pressure range. The slope of the burnout flux versus pressure curve is much flatter than was predicted by Noyes on the basis of his data and a modified version of the hydrodynamic "correlations." At atmospheric pressure the burnout flux was found to be approximately 600,000 Btu/(hr)(sq ft). Significant temperature fluctuations were observed in the potassium pool during the course of these investigations. Superheating was attributed to the difficulty in establishing nucleating sites at the heat transfer surface in view of the strong wetting tendencies of the potassium and its high thermal diffusivity. The latter served to dissipate rapidly the energy required for nucleation in the boundary layer.

Preliminary data in the stable film boiling regime have not yielded conclusive results. The studies to date have confirmed the superheating tendencies of alkali metal systems. Operation which was believed to have been in a stable film boiling regime produced fluxes much larger than predicted by analytical studies. Further data should be forthcoming from this apparatus shortly.

The forced circulation studies have been plagued by a number of difficulties which have required substantial effort and time to resolve. Loop operation commenced in the spring of 1963, but was terminated shortly thereafter when persistent plugging difficulties in the primary potassium circuit prevented further operation. These difficulties were finally overcome during the summer months following the installation of a zirconium chip hot trap and potassium circulation has proceeded without difficulty since that time. An apparent break in the test section region has prevented the attainment of heat transfer results and has resulted in the contamination of the potassium circuit with sodium. The contamination was slight and it was possible to obtain two-phase pressure drop data and void fraction measurements with this apparatus. These results suggest that the Martinelli-Nelson correlation predicts pressure drops substantially lower than those observed experimentally at qualities up to 40 per cent.

Agravic studies with mercury have not produced data. The fabrication of the apparatus is nearing completion and initial check out procedures should begin shortly. The program calls for the pool boiling of mercury at pressures up to 300 psia and accelerations up to 20 times that of normal gravity. The apparatus is capable of producing fluxes up to 500,000 Btu/(hr)(sq ft).

TABLE OF CONTENTS


| | PAGE |
|---|---|
| SATURATED POOL BOILING OF POTASSIUM UP TO BURNOUT HEAT FLUXES | 1 |
| Introduction | 1 |
| Description of Equipment | 10 |
| Operational Methods and Procedures | 31 |
| Results | 34 |
| Discussion of Results | 56 |
| Conclusions | 64 |
| FILM BOILING OF POTASSIUM | 65 |
| Introduction | 65 |
| Description of Equipment | 66 |
| Operating Procedure | 75 |
| Results | 77 |
| Discussion | 82 |
| FORCED CIRCULATION STUDIES | 83 |
| Introduction | 83 |
| Design of Equipment | 84 |
| Operating Procedure | 95 |
| Results of Operation | 96 |
| Analysis of Loop Performance | 98 |
| TWO-PHASE FLOW INVESTIGATIONS | 100 |
| Literature Review | 100 |
| TWO-PHASE PRESSURE DROP STUDY | 106 |
| Introduction | 106 |
| Description of Equipment | 106 |
| Experimental Procedures | 108 |
| Results | 109 |
| Discussion of Results | 109 |
| VOID FRACTION STUDY | 119 |
| Introduction | 119 |
| Theory | 120 |
| Description of Equipment | 130 |
| Experimental Procedures | 143 |
| Results | 145 |
| Discussion of Results | 145 |
| Conclusions | 147 |
| LIQUID METAL BOILING IN AGRAVIC FIELDS | 148 |
| Introduction | 148 |
| Experimental Program | 151 |
| Experimental Apparatus | 154 |
| BIBLIOGRAPHY | 167 |

## LIST OF APPENDICES


| | | PAGE |
|---|---|---|
| A | Experimental Data | 177 |
| B | Treatment of Data | 195 |
| C | Estimation of Heat Flux and Temperature Profile in Boiling Tube | 197 |
| D | Determination of Power Losses in Boiling Tube Circuitry | 203 |
| E | Estimation of Errors | 205 |
| F | Plots of Nucleate Boiling Potassium Data | 207 |
| G | Procedure for Furnace Calibration of Micro-Thermocouples | 217 |
| H | Furnace Calibration of Micro-Thermocouples | 219 |
| I | Sample Calculation | 221 |
| J | Safety, Sampling, and Cleaning Equipment | 223 |
| K | Uncertainty in Quality Determination | 225 |
| L | Two-Phase Flow Investigations--Experimental Data | 231 |

LIST OF FIGURES


| FIGURE | | PAGE |
|---|---|---|
| 1. | Data of Bonilla and Coworkers (15) for Pool Boiling Potassium | 6 |
| 2. | General View of Experimental Apparatus | 12 |
| 3. | Schematic Diagram of Experimental System | 13 |
| 4. | Sectional Drawing of Experimental Apparatus | 14 |
| 5. | View Showing Uninsulated Test Vessel | 15 |
| 6. | View Showing Bus Bar Assembly | 15 |
| 7. | Cross Sectional Drawing of Boiling Tube Assembly | 17 |
| 8. | View of Boiling Tube Assembly | 18 |
| 9. | Overall View of Boiling Tube with Thermocouple Assemblies | 19 |
| 10. | Views of Boiling Tube Cross Sectionals | 20 |
| 11. | Layout of Entry Holes in Outer Protection Vessel | 23 |
| 12. | Boiling Tube Power Supply | 26 |
| 13. | Guard Heaters Circuitries | 26 |
| 14. | Drawing of Electrode Glands | 27 |
| 15. | View of Boiling Tube Bus Bar Assembly | 28 |
| 16. | Thermocouple Circuitries | 29 |
| 17. | Comparison of Pool Boiling Water Data with Two Previous Investigations | 35 |
| 18. | Boiling Data for Potassium Obtained at 12.2 psia Using Tube 2 (Run K-1) | 37 |
| 19. | Boiling Data for Potassium Obtained in the Range 13-14 psia Using Tube 3 (Run K-8) | 38 |
| 20. | Boiling Data for Potassium Obtained in the Range 3.8-5.0 psia Using Tube 4 (Run K-10) | 39 |
| 21. | Vertical Temperature Profile Based on Free Surface Temperature (Run K-8) | 40 |

LIST OF FIGURES (Cont'd)


| FIGURE | | PAGE |
|---|---|---|
| 22. | Photographs Showing Three Views of Tube 2 After Removal from Apparatus | 42 |
| 23. | Comparison of Data from Tube 2 with Data of Bonilla (15) | 44 |
| 24. | Comparison of Data from Tube 3 with Data of Bonilla (15) | 45 |
| 25. | Burnout Heat Flux Versus Saturation Pressure for Saturated Pool Boiling Potassium | 46 |
| 26. | Photograph of Tube 1 After Removal from Apparatus | 47 |
| 27. | Photograph of Tube 4 After Removal from Apparatus | 49 |
| 28. | Boiling Tube Thermocouple (Side) Trace for Pool Boiling Potassium at 5 psia | 50 |
| 29. | Boiling Tube Thermocouple (Bottom) Trace for Pool Boiling Potassium (Run K-4) | 51 |
| 30. | Boiling Tube Thermocouple (Bottom) Trace for Pool Boiling Potassium (Run K-8) | 53 |
| 31. | Boiling Tube Thermocouple (Bottom) Trace for a Burnout Determination at Constant Pressure | 54 |
| 32. | Boiling Tube Thermocouple (Bottom) Trace for a Burnout Determination at Constant Heat Flux | 55 |
| 33. | Comparison of Saturated Pool Boiling Potassium Results Near Atmospheric Pressure with Correlations | 59 |
| 34. | Comparison of Saturated Pool Boiling Potassium Burnout Data with Burnout Correlations | 60 |
| 35. | Temperature Profile of Graphite Heater in Boiling Tube | 201 |
| 36. | Boiling Data for Potassium Obtained at 9.8 psia Using Tube 2 (Run K-2) | 209 |
| 37. | Boiling Data for Potassium Obtained at 0.7 psia Using Tube 2 (Run K-3) | 210 |
| 38. | Boiling Data for Potassium Obtained in the Range 12.5-14.0 psia Using Tube 2 (Run K-4) | 211 |
| 39. | Boiling Data for Potassium Obtained at 13.7 psia Using Tube 3 (Run K-5) | 212 |
| 40. | Boiling Data for Potassium Obtained at 6 psia Using Tube 3 (Run K-6) | 213 |

LIST OF FIGURES (Cont'd)


| FIGURE | | PAGE |
|---|---|---|
| 41. | Boiling Data for Potassium Obtained at 0.9 psia Using Tube 3 (Run K-7) | 214 |
| 42. | Boiling Data for Potassium Obtained in the Range 37-45 psia Using Tube 3 (Run K-9) | 215 |
| 43. | Schematic Diagram of Film Boiling Experimental System | 67 |
| 44. | Tube Assembly | 68 |
| 45. | Boiling Plate | 69 |
| 46. | Tube Assembly Mounted in Support Flange | 70 |
| 47. | Boiling Plate Top Surface Typical Area (100X) | 72 |
| 48. | Boiling Plate Bottom Surface Typical Area (100X) | 73 |
| 49. | Boiling Curve: Vacuum | 78 |
| 50. | Boiling Curve: 0.7 psia | 79 |
| 51. | Temperature Fluctuations during Nucleate and Film Boiling | 81 |
| 52. | Flow Schematic | 86 |
| 53. | Loop, North Elevation | 88 |
| 54. | Loop, East Elevation | 89 |
| 55. | Test Section | 90 |
| 56. | Loop, North Elevation | 92 |
| 57. | Control Panel | 94 |
| 58. | Typical Section of Taylor Transcope Recorder Chart, Showing Pressure Drop and Flowmeter Traces | 110 |
| 59. | Pressure Drop as a Function of Average Quality at Mass Flow Rate of 376 lb/hr | 111 |
| 60. | Pressure Drop as a Function of Average Quality at Mass Flow Rate of 256 lb/hr | 112 |
| 61. | Pressure Drop as a Function of Average Quality at Mass Flow Rate of 125 lb/hr | 113 |
| 62. | Pressure Drop as a Function of Mass Flow Rate, with Average Quality as Parameter | 114 |

LIST OF FIGURES (Cont'd)


| FIGURE | | PAGE |
|---|---|---|
| 63. | Comparison of Pressure Drop Data with Values Predicted for Steam-Water Flows (82) | 118 |
| 64. | Nonuniform Radiation Beam Passing Through a Nonhomogeneous Absorber | 122 |
| 65. | Two Extreme Cases of Separated Phase Distribution | 126 |
| 66. | Schematic Diagram of Void Fraction Measuring System | 131 |
| 67. | Layout of Void Fraction Measuring Apparatus | 132 |
| 68. | Decay Scheme of Tm-170 | 133 |
| 69. | Typical Energy Spectrum of Tm-170 | 134 |
| 70. | Tm-170 Gamma Ray Source | 136 |
| 71. | Count Rate as a Function of Voltage Impressed on Photomultiplier Tube | 139 |
| 72. | Source and Detector Shields | 141 |
| 73. | Gamma Ray Beam Collimator | 142 |
| 74. | Void Fraction Results | 146 |
| 75. | Variation of Hydrostatic Pressure with Acceleration | 153 |
| 76. | Test Vessel for Boiling Mercury Study under High Gravity | 155 |
| 77. | Copper Heater with Attached Stainless Steel Foil | 156 |
| 78. | Copper Heater, Radiation Shields, and Guard Heaters | 158 |
| 79. | Mercury Container and Heater Support | 158 |
| 80. | Liquid Level Indicator for Mercury | 160 |
| 81. | Pressure Vessel--Disassembled | 162 |
| 82. | Assembled Pressure Vessel and Inner Test Vessel | 163 |
| 83. | Equivalent Thermocouple Circuit for Temperature Measurement | 164 |
| 84. | Mercury Boiling Test Vessel in Centrifuge | 165 |

LIST OF TABLES


| TABLE | | PAGE |
|---|---|---|
| I | Experimental Data for Water | 179 |
| II | Potassium Boiling Data for Run K-1 | 181 |
| III | Potassium Boiling Data for Run K-2 | 182 |
| IV | Potassium Boiling Data for Run K-3 | 183 |
| V | Potassium Boiling Data for Run K-4 | 184 |
| VI | Potassium Boiling Data for Run K-5 | 185 |
| VII | Potassium Boiling Data for Run K-6 | 186 |
| VIII | Potassium Boiling Data for Run K-7 | 187 |
| IX | Potassium Boiling Data for Run K-8 | 188 |
| X | Potassium Boiling Data for Run K-9 | 191 |
| XI | Potassium Boiling Data for Run K-10 | 192 |
| XII | Summary of Potassium Burnout Data | 193 |
| XIII | Film Boiling Results | 80 |
| XIV | Furnace Calibration of Micro-Thermocouples | 219 |
| XV | Potassium Film-Boiling Data | 220 |
| XVI | Average Per Cent Deviation in Properties Between Pure Potassium and Mixture Containing 8 Per Cent by Weight Sodium over the Temperature Range 900-1400°F | 116 |
| XVII | Important Features of the Tracerlab SC-18 Superscaler | 138 |
| XVIII | Pressure Drop Data Obtained at 2 Millivolt Average Flowmeter Output | 233 |
| XIX | Pressure Drop Data Obtained at 3 Millivolt Average Flowmeter Output | 235 |
| XX | Pressure Drop Data Obtained at 4, 5, 6 and 1 Millivolt Average Flowmeter Outputs | 236 |
| XXI | Selected Data Used in Preparing Figure 62 | 237 |
| XXII | Void Fraction Data | 239 |
| XXIII | Froude Numbers for Nucleate Boiling of Saturated Liquids | 150 |

## SYMBOLS

| | |
|---|---|
| $a$ | Thermal diffusivity ($k/C_p\rho$) or acceleration |
| $A$ | Area or term in Equation C-4 |
| $B$ | Term in Equation C-4 |
| $B_L$ | Empirical coefficient in reference (72) |
| $c$ | Conversion factor from watts to Btu/hr, 3.415 |
| $C$ | Constant defined in Equation 35 |
| $C_p$ | Heat capacity |
| $D$ | Diameter |
| $f$ | Friction factor |
| $Fr$ | Froude number, defined in Equations 1 and 41 |
| $g$ | Acceleration due to standard gravity |
| $g_c$ | Gravitational conversion constant, 32.17 $lb_m ft/lb_f\ sec^2$ |
| $h$ | Heat transfer coefficient |
| $h_\ell$ | Enthalpy of saturated liquid |
| $I$ | Current or emergent intensity of radiation beam |
| $I_g$ | Emergent intensity of radiation beam for all-vapor flow |
| $I_\ell$ | Emergent intensity of radiation beam for all-liquid flow |
| $I_o$ | Incident intensity of radiation beam |
| $k$ | Thermal conductivity |
| $K$ | Constant in Equation 10 |
| $\ell$ | Length |
| $L$ | Length along flow channel |
| $\dot{m}$ | Total mass flow rate |
| $n$ | Number of lamina in an absorbing slab |
| $N$ | True count rate |

| | |
|---|---|
| $Nu$ | Nusselt number, $hD/k$ |
| $p$ | Pressure |
| $\Delta p$ | Pressure difference corresponding to superheat |
| $\Delta p_f$ | Friction component of pressure drop |
| $Pr$ | Prandtl number, $C_p\mu/k$ |
| $Q$ | Rate of heat transfer |
| $q/A$ | Heat flux |
| $r$ | Observed count rate |
| $R$ | Bubble radius or electrical resistance |
| $Re$ | Reynolds number |
| $S$ | Slip velocity ratio defined by Equation 14 |
| $t$ | Thickness of boiling tube end or absorber thickness |
| $T$ | Temperature or (temperature in graphite) - (temperature of boiling potassium) |
| $T_o$ | Reference temperature for gamma-ray calibration measurements |
| $\Delta T$ | Temperature difference (Tw-Ts) |
| $U$ | Overall heat transfer coefficient |
| $U_g$ | Superficial vapor velocity |
| $V$ | Voltage, volume, or local superficial mixture velocity |
| $V_g$ | Mean vapor velocity |
| $V_\ell$ | Mean liquid velocity |
| $V_o$ | All-liquid superficial velocity based on total mass flow rate |
| $X$ | Ratio of single phase pressure gradients in Equation 12 |
| $x$ | Length dimension or quality (mass fraction vapor) |
| $\bar{x}$ | Average quality |
| $\Delta x$ | Thermocouple depth from tube surface |
| $y$ | Coordinate direction |

| | |
|---|---|
| $z$ | Coordinate direction |
| $\alpha$ | Void fraction (vapor volume fraction) or thermal diffusivity |
| $\Delta$ | Finite difference operator |
| $\theta$ | Angle of inclination of flow channel from horizontal |
| $\lambda$ | Latent heat of vaporization |
| $\mu$ | Viscosity or linear gamma-ray absorption coefficient |
| $(\mu/\rho)$ | Mass gamma-ray absorption coefficient |
| $\pi$ | 3.14 |
| $\rho$ | Density or electrical resistivity |
| $\bar{\rho}$ | Local mean mixture density |
| $\rho_g$ | Vapor density |
| $\rho_\ell$ | Liquid density |
| $\sigma$ | Surface tension |
| $\tau$ | Dead time |
| | Lockhart-Martinelli two-phase flow correlation parameter (78) |

## SUBSCRIPTS

| | |
|---|---|
| ave | Average |
| b | Bubble or bulk |
| bo | Burnout |
| c | Wall thermocouple |
| g | Graphite or vapor (gas) phase |
| H-25 | Haynes-25 |
| $\ell$ | Liquid phase |
| s | Saturation or solid phase |
| meas | Measured variable |
| prop | Fluid properties |

| | |
|---|---|
| TPF | Two-phase frictional |
| v | Vapor |
| w | Wall |

# SATURATED POOL BOILING OF POTASSIUM UP TO BURNOUT HEAT FLUXES

C. Phillip Colver

## INTRODUCTION

Heat transfer systems utilizing boiling liquid metals provide one method for efficiently exchanging large quantities of heat at relatively high temperature levels. The fact that the first three alkali metals, lithium, potassium, and sodium have densities less than water and possess high latent heats (approximately equal to water for potassium while up to ten times that of water for lithium) makes them extremely attractive as heat carrier fluids in power cycles for space applications.

In order to determine useful design information for such systems it becomes necessary to simulate actual conditions with relatively simple and yet similar experiments. Ultimately, it would be hoped to derive analytical or semi-empirical expressions, or use previously derived relationships substantiated by liquid metal boiling experiments, to provide reliable engineering design information.

Some liquid metal boiling heat transfer data has been reported, but in only one investigation were burnout data obtained. Comparison of both the experimental heat transfer and burnout results with theoretical and semi-empirical predictions has shown at best only fair agreement and indicated that more boiling data with different liquid metals is needed.

### Object of Investigation

Any experiment yielding high flux boiling data would be extremely valuable, especially if burnout data could be obtained. Furthermore, if the investigation covered a range of pressures it would be possible to show the influence of pressure on heat transfer as well as burnout.

This investigation is concerned with the methods and results of pool boiling potassium at heat fluxes up to and including the burnout point. The information gathered is used to test existing correlations for nucleate boiling and for the burnout heat flux. The scope of the investigation included operating at different pressures in the range of a few inches of mercury to over atmospheric pressure.

### Summary of Liquid Metal Boiling Studies

The interest in boiling technology, and specifically boiling liquid metals, has developed at an increasing rate during recent years. Space does not permit discussion of the many scores of investigations covering all phases of the boiling field. The reader is referred to any of the several good overall summaries

Manuscript released by the authors October 1963 for publication as an RTD Technical Documentary Report.

available in the literature for more detailed discussions of the important variables, e.g., liquids properties, types or orientations of heater surfaces, flow conditions, quality, etc. (6, 65, 69, 86, 127). A good concise survey of boiling burnout is also available (40).

Several summaries exist which are devoted exclusively to liquid metal boiling. A literature survey on liquid metal boiling was conducted at The University of Michigan and includes summaries and analyses of all liquid metal investigations through 1961 (6). Nearly 1200 references were included and pertained to all phases of the boiling field. A Russian publication (69) devoted entirely to problems associated with utilizing liquid metals as heat transfer media contains all important liquid metal heat transfer data collected in Russia, up through 1958. A recent paper by Gambill and Hoffman (41) summarizes the boiling metal heat transfer field up to mid-1961.

The first comprehensive boiling study with liquid metals was done by Lyon (79) who investigated boiling mercury, mercury with additives, sodium, NaK, and cadmium. The experimental apparatus consisted of a horizontally oriented stainless steel tube, 3/8-in OD by 5-in long, extending through a stainless steel vessel. Electrical heating gave fluxes up to 130,000 Btu/(hr)(sq ft). All tests were performed at atmospheric pressure under conditions of saturated, natural convection boiling with nitrogen used as a blanket gas. With pure mercury and cadmium high temperature differences were obtained, and indicated that heat transfer was either by simple convection or film boiling. Temperature differences with mercury were as high as 1000°F whereas cadmium gave temperature differences up to 200°F for heat fluxes no greater than 13,000 Btu/(hr)(sq ft). Sodium, NaK, and mercury containing additives gave extremely good heat transfer characteristics with no evidence of the burnout heat fluxes being reached with any liquid at fluxes up to 130,000 Btu/(hr)(sq ft) at atmospheric pressure. Temperature differences of less than 10°F were measured for sodium and NaK at these heat fluxes. Data for mercury containing 0.10 per cent sodium gave a temperature difference of 35°F at 60,000 Btu/(hr)(sq ft), while mercury containing a trace of titanium gave a temperature difference of 12°F at 100,000 Btu/(hr)(sq ft). The effects of additives in mercury gave rise to the speculation that these additives promoted wetting and improved heat transfer.

Lyon noted rather large temperature fluctuations for boiling sodium, NaK, and mercury containing magnesium. For sodium at low heat fluxes, boiling occurred intermittently as indicated by system noise and occasional minor pressure fluctuations. At higher fluxes the amplitude and period of the observed temperature fluctuations were smaller. The qualitative behavior of the fluctuations was given by a sudden drop in wall temperature followed by recovery. He concluded that temperature fluctuations were due to local temperature differences found in the liquid near the surface. As the heat flux increased the surface temperature more nearly approached steady-state conditions with fluctuations diminishing in intensity.

Bonilla (14) and others (4, 66, 67, 76, 69, 79, 110, 117) have conducted boiling mercury investigations. For the most part, the data have not correlated particularly well, and the highest heat flux reached in each study gave no indication of having reached the burnout point.

The pool boiling mercury study of Bonilla (14) was accomplished both with and without wetting agents in the heat flux range 4,000 to 200,000 Btu/(hr)(sq ft) at pressures of 4mm Hg to 45 psia. The boiling $\Delta T$ values covered the range of about 10°F at near atmospheric pressure to over 100°F at lower pressures, with increases in pressure tending to reduce the temperature-driving forces at the same heat flux. The apparatus consisted of a horizontal heating surface of low-carbon steel in a 3-in OD stainless steel vessel. Electrically heated Nichrome strips wrapped around copper fins extending from the bottom of the heating surface served as the heat source. Nitrogen was used as a blanket gas. It was concluded that prolonged boiling, at least on stainless steel, promoted wetting and increased the heat flux for the same temperature-driving force.

A rather interesting study by Avery (4) was conducted to investigate the effect of surface geometry on boiling mercury and mercury with 0.1 per cent sodium. His apparatus was essentially identical to the one used by Bonilla (14) and described above. Upon completion of each set of runs the vessel was disassembled and the boiling surface grooved further. The surface was grooved with parallel, 0.003-in wide by 0.004-in deep grooves, first 3/8-in then 1/8-in apart. Two boiling plates were used. The results demonstrated the significant effect surface geometry has on boiling heat transfer to mercury both with and without additives. For example, with pure mercury at 60,000 Btu/(hr)(sq ft) using the second boiling plate, temperature differences without grooves were in the order of 600°F whereas for grooves 3/8-in apart the temperature difference was about 50°F. Despite efforts to reproduce surface conditions on each plate it was found that each gave considerably different heat transfer curves. The author suggests that differences in microscopic geometry may account for this disagreement.

Romie and co-workers (110) boiled mercury containing traces of additives in a thermal-syphon-type heat transfer loop. Electrical power was supplied through the heating section giving heat fluxes as high as 600,000 Btu/(hr)(sq ft) with 5 per cent vapor qualities. The loop was fabricated from 7/16-in OD stainless steel and contained a 4-in long test section. Deposition of a thin copper layer on the inside wall after it had been thoroughly cleaned was found to promote wetting. It is pointed out that electrical current was passed directly through the surface from which boiling occurred. Since liquid mercury is a reasonably good electrical conductor, the mercury coming in contact with the surface created a parallel circuit. This made it difficult to differentiate between heat generation occurring within the test section wall and that occurring directly in the liquid. The accuracy of results was estimated to be within $\pm$ 20 per cent. There was no indication of burnout even at 600,000 Btu/(hr)(sq ft) and it was emphasized by the authors that the thermal and hydrodynamic performance of the loop gave every indication that even higher heat fluxes could be achieved before reaching burnout.

Madsen and Bonilla (80) pool boiled NaK from a horizontally oriented 3-in diameter low-carbon nickel plate up to over 100,000 Btu/(hr)(sq ft) in the pressure range of 2mm to 790mm Hg. Heat was furnished by molybdenum resistance wire covered with alumina sleeves and wrapped around molybdenum fins brazed to the bottom of the heater plate. The entire system, including heater enclosure, was blanketed with helium gas. Correlation of the data by the method of least-squares showed variations of + 30 per cent or - 28 per cent. It was found that

the boiling temperature difference was an order of magnitude larger than that reported by Lyon (79). The reason postulated for their larger $\Delta T$ values was large temperature gradients that existed in the bulk liquid throughout all runs. It was also suggested that the larger vessel used by Lyon may have promoted strong natural convection currents, thus reducing temperature gradients in the pool. Madsen and Bonilla also reported that during the investigation, the temperature of the boiling plate near the surface fluctuated randomly, the amplitude of fluctuation changing slightly at different heat fluxes. The fluctuating behavior was frequently represented by sudden dips in the boiling surface temperature followed by recovery along a ragged "saw tooth" line. Their data showed that sometimes a rapid temperature rise preceded the temperature drop, the rise and fall both taking place in less than 0.5 seconds. On the average, the fluctuations were in the order of 10°F at 135,000 Btu/(hr)(sq ft) although extreme variations of 25°F were noted. At low heat fluxes the sudden temperature drops were frequently accompanied by audible "bumps."

Noyes (98) has studied pool boiling sodium up to the burnout point in a thermal-syphon pool boiler. A saturated pool was boiled from the surface of a horizontally oriented 3/8-in diameter by 3-in long electrically heated cylindrical test section inserted in a 6-in by 6-in cylindrical boiler. Measurements were made between 1200-1500°F and at heat fluxes up to 800,000 Btu/(hr)(sq ft). Burnout points were determined in the pressure interval 0.5 to 1.5 psia. His burnout data did not correlate well with existing burnout correlations and indicated that for liquid metals, the actual burnout point is considerably higher than that predicted by most burnout correlations. A non-dimensional burnout correlation was developed by alterations in previous predictions in order to bring sodium measurements into agreement with burnout values for other liquids. This correlation is discussed in a later section of this chapter. The nucleate boiling data of Noyes was obtained from five test sections at pressures between 1 and 8 psia. Variations in $\Delta T$ due to pressure variations were not observed. The predictions of Levy (72) and Forster and Zuber (38) were calculated for saturated sodium at 14.7 psia and 3.0 psia and compared to the nucleate boiling data. Although the correlations gave slopes which agree with the data, the $\Delta T$ values predicted by both correlations were higher than those observed. Comparing the data with the sodium results of Lyon (79) shows good agreement below 40,000 Btu/(hr)(sq ft). Both sets of data gave $\Delta T$ values of 8°F. At 100,000 Btu/(hr)(sq ft) Lyons' data gave $\Delta T$ values less than 10°F whereas Noyes found $\Delta T$ values just under 20°F, a disagreement of approximately 10°F. Noyes suggested that the higher $\Delta T$ values in his experiment were probably due to generally lower pressures employed in his investigation.

To obtain burnout data, Noyes operated at constant heat flux and gradually decreased the system pressure. He found that the beginning of the transition to film boiling was characterized by a marked increase in the amplitude of the test section wall temperature fluctuations. His explanation for these pronounced fluctuations was the formation and collapse of vapor patches in the region of the thermocouple. Actual burnout was avoided by cutting off cooling to the condenser, thus raising the system pressure. On two occasions, however, burnout occurred shortly after the pronounced fluctuations occurred. Seven burnout points were determined by this technique at pool pressures between 0.5 and 1.5 psia.

Concurrent with the present study are a number of liquid metal experimental programs in various stages of completion. A list of these is shown elsewhere (6). Liquid metals receiving the most attention in recent studies have been potassium, sodium, NaK, and rubidium. The effects of pressure, velocity, subcooling, surface characteristics, quality, and fluid properties are all being considered.

A current pool boiling investigation with potassium is being conducted by Bonilla and co-workers (15). The pool boiler is very similar to that employed by Madsen and Bonilla (80) and consists of a 3-in diameter high purity (low carbon) nickel boiling plate. The data obtained to date were taken in the pressure ranges 2 to 20mm of mercury and 700 to 1500mm mercury with heat fluxes up to 100,000 Btu/(hr)(sq ft). Figure 1 is a plot of their data. It was found that the data from 700 to 1500mm mercury agreed satisfactorily with correlations (applied at 1400°F) of Forster and Zuber (38), Forster and Greif (37), Chang and Snyder (21), and Levy (72) in location of the curve. However, the data exhibits a somewhat steeper slope than the correlations. The low pressure data had unexpectedly high $\Delta T$ values (80-100°F). It was not believed that film boiling was taking place though no explanation of these high $\Delta T$ values was advanced.

## Nucleate Boiling Correlations

Many theoretical and semi-empirical expressions have been suggested for predicting heat flux in the nucleate boiling regime. For the most part, analyses have been based on postulated models which account for increased heat transfer coefficients over natural convection without surface boiling. A common practice has been to group the influencing physical properties into pertinent dimensionless parameters. The various empirical constants in the expressions are evaluated with actual data to produce a relationship for all boiling liquids.

Several correlations, such as the one derived by Rohsenow (107), necessitate knowing a constant for a particular heating surface and/or fluid combination. Since correlations of this type have limited value in the absence of previously obtained data, they are of little use for engineering purposes. For this reason, only those correlations capable of predicting the nucleate boiling curve under more general conditions will be discussed here.

Forster and Zuber (38) derived analytical expressions for bubble radii and growth rates and then applied them to surface boiling. A Reynolds number was formulated for the liquid flow in the superheated boundary layer adjacent to the boiling surface. The analysis when applied to pool boiling gave the maximum heat transfer rates and yielded the following relationship:

$$Nu = 0.0015\, Re_b^{0.62}\, Pr_\ell^{0.33} \tag{1}$$

where the Reynolds number, $Re_b$, is given by:

$$Re_b = \frac{\rho_\ell}{\mu}\left(\frac{\Delta T\, Cp_\ell\, \rho_\ell \sqrt{\pi a}}{\lambda\, \rho_v}\right)^2 \tag{2}$$

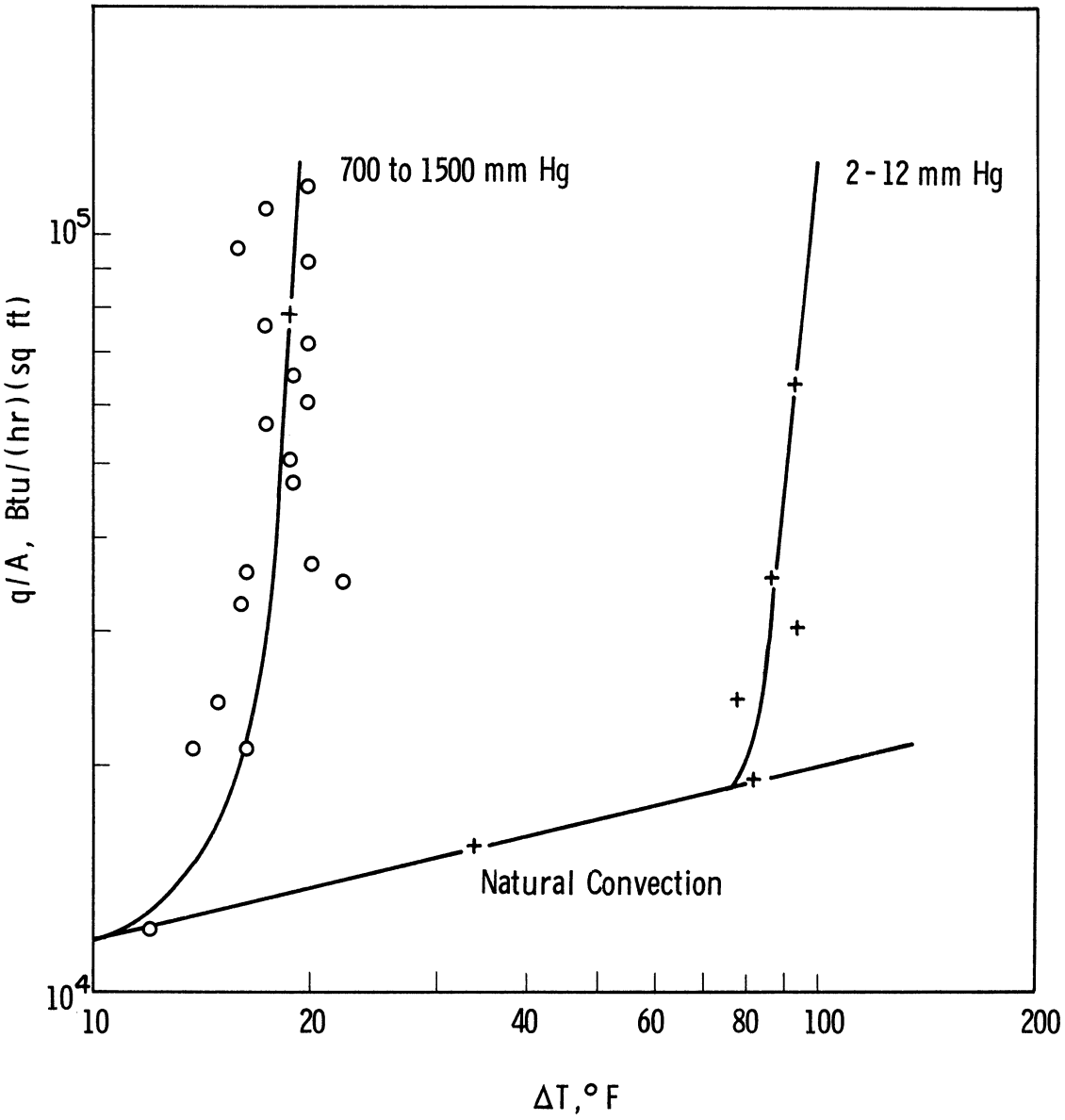


Figure 1. Data of Bonilla and Coworkers (15) for Pool Boiling Potassium.

The Nusselt number, $Nu_\ell$, for the system is:

$$Nu_\ell = \frac{q/A\ R}{(Tw - T_b)}\ 1/k_\ell \tag{3}$$

and where R is given by:

$$R = \frac{\Delta T\ Cp\ \rho_\ell \sqrt{\pi a}}{\lambda\ \rho_v}\left(\sqrt{\frac{2\sigma}{\Delta p}}\ \sqrt[4]{\frac{\rho_\ell}{\Delta p}}\right) \tag{4}$$

The relationship (Equation 1) has favorably predicted data of several liquids including recent studies with sodium (98) and potassium (15).

Forster and Greif (37) in their analysis deduced a correlation for nucleate boiling which gives the dependence of heat flux on the superheat and system pressure. By judicious selection of the important parameters and dimensionless groups in the nucleate boiling process, these authors were able to develop an expression employing the same empirical constants for all liquid-surface conbinations. It is:

$$q/A = 4.3 \times 10^{-5} \frac{a\ Cp_\ell \rho_\ell Ts}{\sqrt{\sigma}(\lambda\rho_v)^{3/2}} \left(Cp_\ell Ts\sqrt{a}\right)^{1/4} \left(\frac{\rho_\ell}{\mu_\ell}\right)^{5/8} Pr_\ell^{1/3}\ p^2 \tag{5}$$

The correlation has satisfactorily predicted the nucleate boiling curves for different liquids varying from water (25) to mercury (14), without necessitating any alteration in empirical constants. Recently the correlation was compared with pool boiling potassium data (15) with acceptable agreement.

Chang and Snyder (21) in their analysis considered the concept of thermal eddy diffusivity as it might relate to nucleate boiling phenomena. Applying dimensional analysis to the fundamental equations of motion and energy and selected boundary conditions they derived a set of parameters characterizing boiling heat transfer. The following expression, good for vigorous boiling, results from their analysis:

$$q/A = 4 \times 10^{-4} \frac{k_\ell \Delta p^{1.4}}{(\rho_v \lambda)^{0.8} \sigma} \left(Cp_\ell Ts\ (\rho_\ell - \rho_v)\right)^{0.4} \Delta T \tag{6}$$

Comparison with mercury data (14) and potassium data (15) has shown satisfactory agreement for engineering design purposes.

An interesting correlation by Levy (72) was derived under the premise that as the generated bubbles attain their maximum diameter, they carry all heat transferred from the boiling surface. The final expression is good for any liquid boiling under saturated conditions. The expression is:

$$q/A = \frac{1}{B_L} \frac{k_\ell \, Cp_\ell \, \rho_\ell^2 \Delta T^3}{\sigma \, Ts \, (\rho_\ell - \rho_v)} \qquad (7)$$

and is independent of pressure and heat transfer surface-liquid combinations. The constant $B_L$ is empirically determined and found to be well represented by plotting it against $\lambda\rho_v$ (see original article in reference 72). Comparison with sodium (98) and potassium (15) data shows fair agreement.

It is not known which of the above correlations is superior for predicting all nucleate boiling heat transfer data. Mercury data has been equally well predicted by all correlations. For sodium and potassium all correlations give good agreement in view of the fact that data to date has exhibited a great deal of scatter. The correlation of Levy, however, appears to predict slightly high $\Delta T$ values, particularly when compared to sodium data of Noyes.

Burnout Correlations

According to a recent survey (40) of boiling burnout, some fifty equations have been proposed for predicting the critical or burnout heat flux under various conditions, i.e., free or forced convection, with subcooling or quality, etc. Many of these are based on experimental data obtained from specific systems and may not be recognized as generalized correlations. Several theoretical or semi-empirical correlations. Although these correlations correctly predict burnout for several liquids, only one expression (developed using sodium burnout data) has shown even fair agreement when applied to liquid metals.

No burnout data is available for liquid metals boiling under subcooled conditions. All burnout data for other liquids indicates that the burnout point is raised with increased subcooling at all pressures. At lower pressures subcooling has been shown to have the greatest effect (6, 70, 130). Several correlations are available for predicting burnout for different levels of subcooling (6, 63, 130). These correlations will not be considered here as the present investigation is concerned with only saturated pool boiling burnout measurements.

Rohsenow and Griffith (108) developed an expression for the burnout point on the premise that at burnout, the active sites on the boiling surface become so numerous that growing bubbles on the surface coalesce to form a vapor blanketing layer. The final equation in their derivation contained empirical constants which when correlated with experimental data (1, 16, 25) gave:

$$(q/A)_{bo} = 143 \, \rho_v \lambda g^{1/4} \left( \frac{\rho_\ell - \rho_v}{\rho_v} \right)^{0.6} \qquad (8)$$

Comparison of the above expression with burnout data for water and organic liquids gave a deviation range of $\pm$ 11 per cent. Poor agreement is given with sodium burnout data (98).

Zuber and Tribus (130) derived an analytical expression which permits the prediction of pool boiling burnout. Their analysis considered the hydrodynamic instabilities and geometrical configurations of boiling systems. It was found that the maximum heat flux was limited by combined effects of Taylor and Helmholtz instabilities on the flow of the two-phase mixture. Their expression is:

$$(q/A)_{bo} = \frac{\pi}{24} \lambda \rho_v \left( \frac{\sigma g (\rho_\ell - \rho_v) g_c}{\rho_v^2} \right)^{1/4} \left( \frac{\rho_\ell}{\rho_\ell + \rho_v} \right)^{1/2} \quad (9)$$

Although comparison with some data, including that of Westwater and Santangelo (128) with methanol, has shown agreement the prediction does not agree with sodium (98) burnout data.

Kutateladze (68) has derived an expression very similar to that of Zuber and Tribus, the principle difference being the value for the constant. In his analysis, Kutateladze considered the basic equations of motion and mechanical interaction which apply to the hydrodynamics of a two-phase boundary layer adjacent to a boiling surface. Employing dimensional analysis the following equation was derived:

$$(q/A)_{bo} = K \lambda \rho_v \left( g^2 \sigma \left( \frac{\rho_\ell - \rho_v}{\rho_v^2} \right) \right)^{1/4} \quad (10)$$

When compared with data for water and some organic liquids for saturated pool boiling, the best value for K was found to be 0.16.

Noyes (98) in a recent publication presented a modified dimensionless burnout correlation supported not only by published data for water and various organic liquids, but also his data for sodium. In essence the correlation was developed by modifying previous expressions to produce agreement with his burnout data.

$$(q/A)_{bo} = 0.144 \lambda \rho_v \left( \frac{\rho_\ell - \rho_v}{\rho_v} \right)^{1/4} \left( \frac{g\, g_c\, \sigma}{\rho_\ell} \right)^{1/4} Pr^{-0.245} \quad (11)$$

The major difference between this correlation and those developed from hydrodynamic theory, i.e., Zuber-Tribus and Kutateladze, is the inclusion of a Prandtl number effect.

## DESCRIPTION OF EQUIPMENT

### Introduction

The scope of this study necessitated design considerations which would permit the pool boiling of potassium up to heat fluxes slightly over 1 x $10^6$ Btu/(hr)(sq ft). The pressure range necessary extended from a few millimeters of mercury up to about 200 psia; the temperature range up to over 1800°F. Further, since the investigation included burnout measurements, it was imperative that a heat transfer assembly be designed which could be easily removed for inspection or completely replaced after it failed.

To satisfy these requirements, high strength, high temperature materials were selected when available and financially feasible. In addition, those materials in contact with potassium were selected because of their excellent corrosion resistant properties.

The experimental apparatus consisted primarily of a vertical boiling vessel containing an electrically heated bayonet-type boiling tube inserted horizontally. Other major components included a water jacketed condenser, an outer pressure vessel, guard heaters, an inert gas supply, a vacuum system, a potassium charge and dump system, and instrumentation.

All process lines and equipment coming in contact with potassium or potassium vapor were made from either Haynes-25* or stainless steel 304 or 316. Welds involving Haynes-25 were made using Haynes-25 welding rods exclusively, with no less than two passes per weld.

As an added precaution against leaks in the test vessel, all thermocouple wells and tubes extending into the boiling vessel were welded on both the outside and inside surface, with two passes per surface. A total of four passes was used when the top and bottom plates were welded to make up the test vessel.

Connections made in the potassium system, where welding was impractical, used Swagelok (type 316) stainless steel compression fittings exclusively. Whenever possible, pressure gland sealants, gasket materials, insulation, brazing filler, etc. were selected to withstand the highest temperatures possible. The thermocouple and tube pressure glands were Conax glands using lava as the sealant. Electrode glands located in outer vessel top flange utilized silicone rubber O-rings in lava seats. The upper temperature limit of these O-rings was 650°F and represented the temperature limiting material in the experimental apparatus.

A controlled atmosphere of helium was maintained around the boiling vessel. This served to reduce oxidation of the boiling vessel, and by balancing the helium pressure with the system pressure, permitted operation at elevated pres-

* Also referred to as L-605 metal (composition: 10Ni - 48.9Co - 20Cr - 15W - 3Fe - 0.1C - 1Si - 2Mn).

sures (temperatures) with minimum pressure stresses in the test vessel. During normal operation and particularly at lower pressures, a slight positive pressure was maintained outside the boiling vessel. In this way, small leaks in the test vessel would not result in potassium contamination of outer vessel.

A photograph showing the experimental apparatus and most of the instrumentation is shown in Figure 2. A schematic diagram of the experimental system is shown in Figure 3.

Boiling Vessel and Filling Line

A drawing of the experimental system is shown in Figure 4. Photographs of the test vessel are shown in Figures 5 and 6.

Boiling took place in a vertical 2 foot section of thick walled Haynes-25 pipe, 2.15-in OD by 1.36-in ID. The vessel ends were formed by welding on 5/16-in thick by 2 1/4-in diameter Haynes-25 plates.

Four holes were drilled in the top plate of the test vessel. A 3/4-in diameter, 16 BWG, type 304 stainless steel tube was welded into a 3/4-in diameter hole in the center of the plate. This tube in turn was welded through the outer pressure vessel and served as the vacuum and inert gas entry into the vessel. Three thermocouple wells equally spaced circumferentially around the center hole in the top plate extended into the test vessel 3, 13, and 16 inches. Each well was made from tubing 0.188-in OD by 0.032-in wall thickness and closed at one end with a Heliarc welder.

The bottom plate to the test vessel contained a 3/8-in diameter hole into which was welded a Haynes-25 tube 3/8-in OD by 0.057-in wall thickness. This tube served as the potassium charge line and was welded flush to the inside bottom plate to insure complete draining of potassium from the test chamber for tube replacement. Two Haynes-25 thermocouple wells, 2 and 4 inches, were welded through the bottom plate. They were made from the same tubing as those extending down from the top plate. A 9/16-in diameter hole was drilled 2 1/2-in from the bottom of the test vessel and threaded for a 3/8-in IPS male fitting. The hole was threaded completely through the 0.395-in vessel wall so that, when the boiling tube assembly was screwed in place, the boiling tube would be completely inside the boiling chamber. The threaded fitting would then be exactly flush with the inside vessel wall.

The liquid metal filling line was a Haynes-25 tube, 3/8-in diameter by 0.057-in wall thickness, welded to the bottom of the test vessel as mentioned above. It extended through the protection vessel as seem in Figure 5 and was connected to the potassium charge system. A Conax (No. PG-4) stainless steel packing gland (using lava as the sealant) sealed the tube as it passed through the top flange. This gland permitted the tube to slide either way upon expansion and contraction of the boiling vessel. A 3/8-in Swagelok union (No. 600-6-316) connected the filling line to the charge system.

Condenser and Cooling Lines

The condenser consisted essentially of three parallel cooling systems welded around a stainless steel pipe press-fitted over the test section. As an

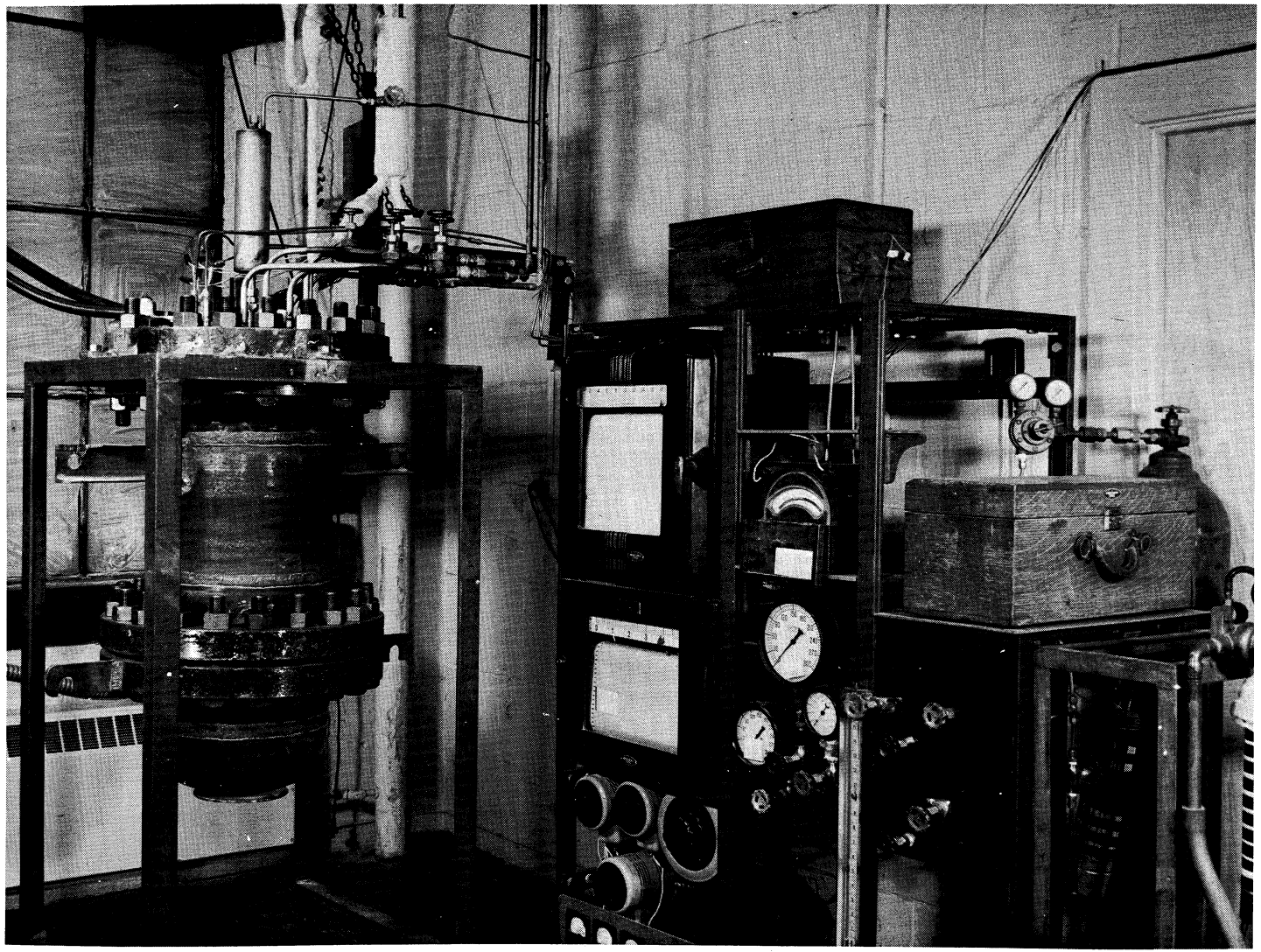

Figure 2. General View of Experimental Apparatus.

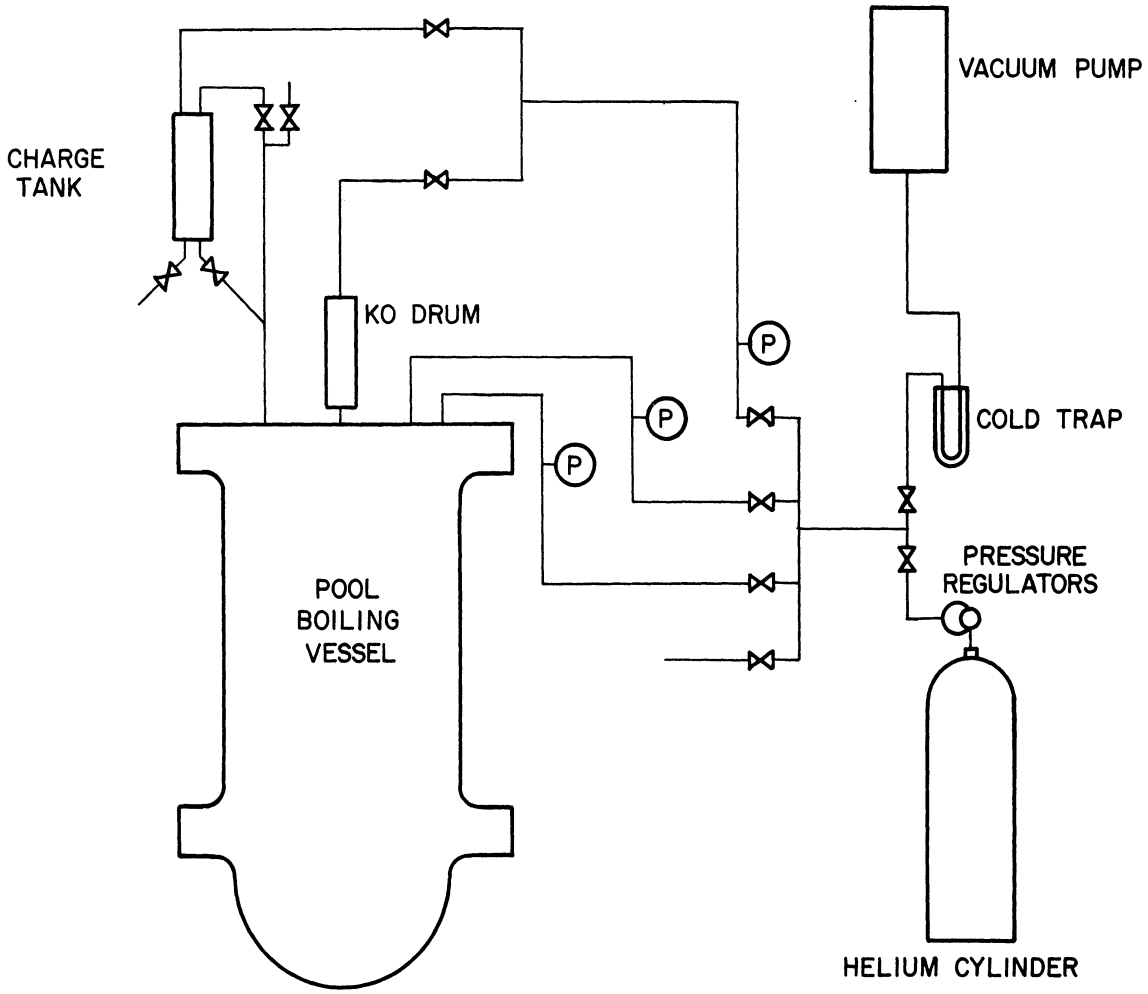


Figure 3. Schematic Diagram of Experimental System.

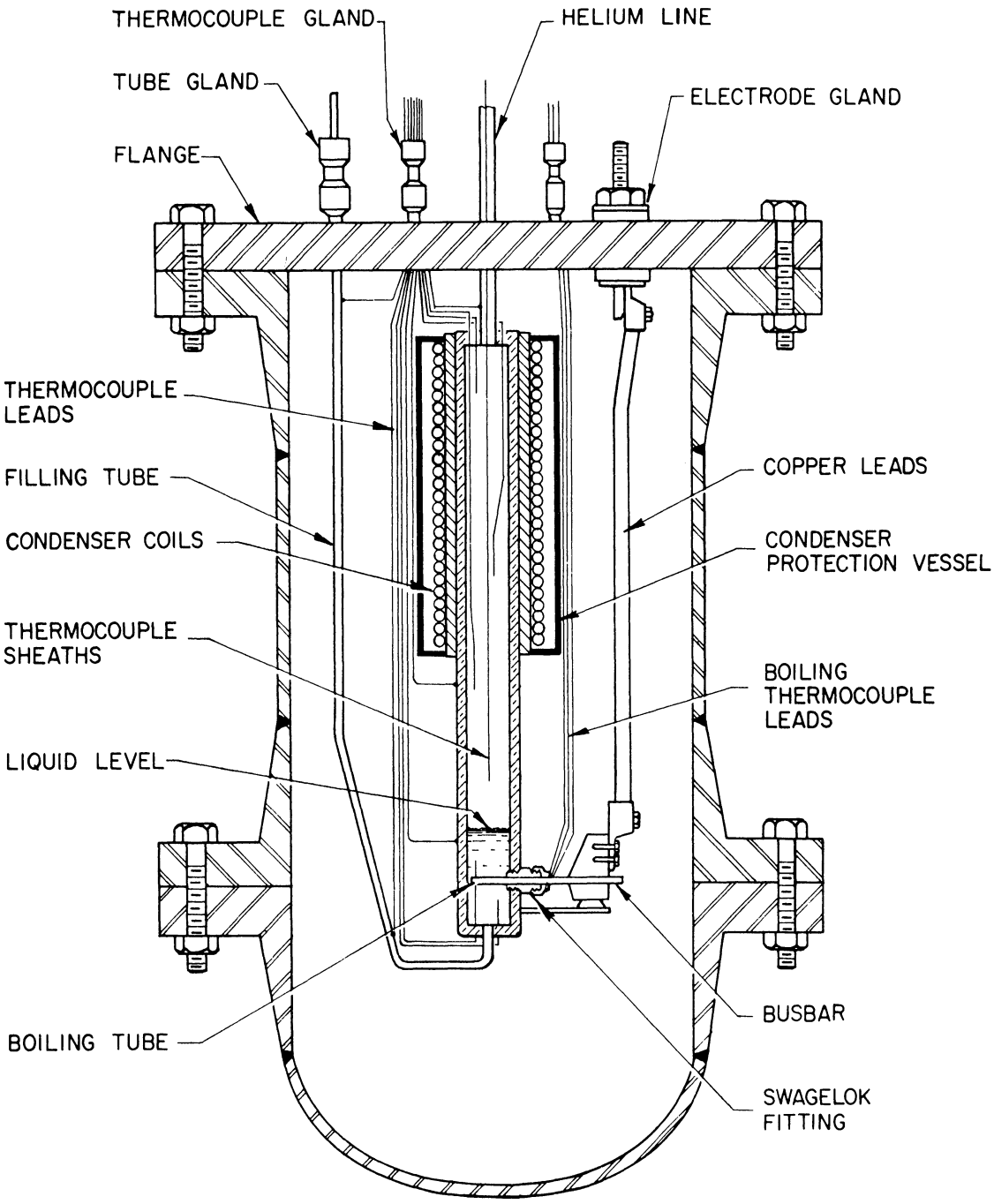


Figure 4. Sectional Drawing of Experimental Apparatus.

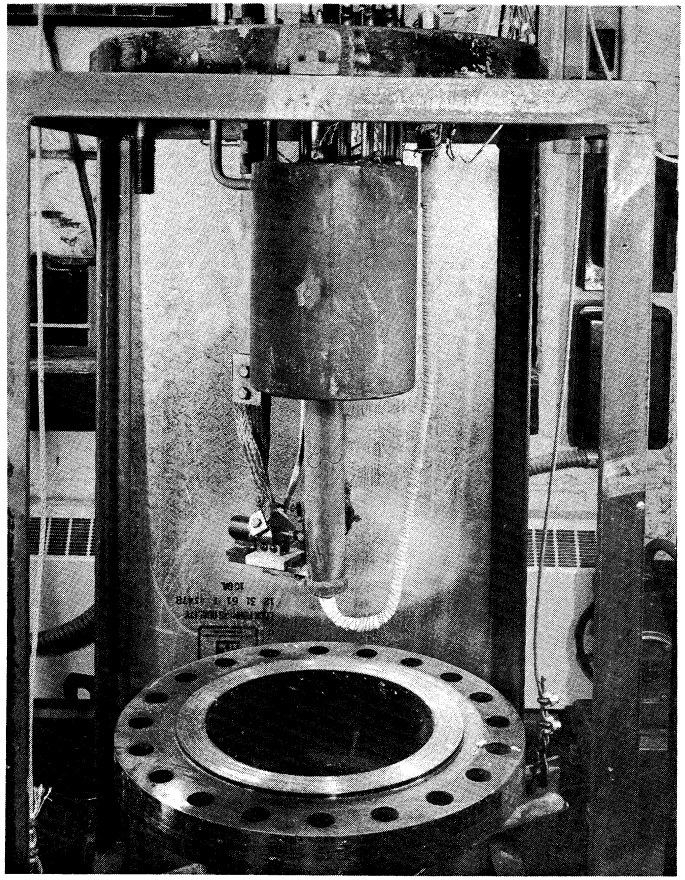

Figure 5. View Showing Uninsulated Test Vessel.

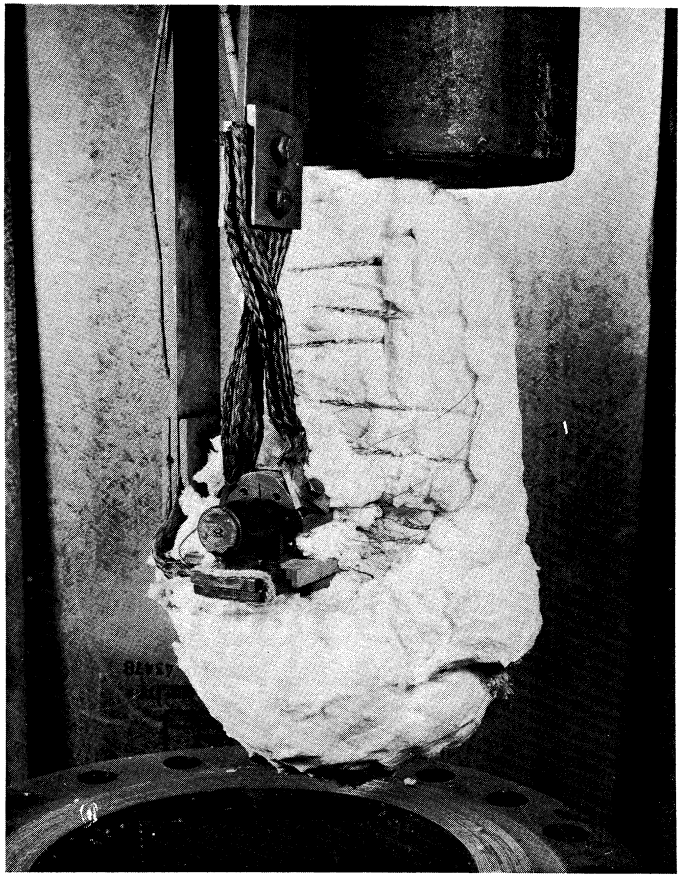

Figure 6. View Showing Bus Bar Assembly.

added precaution against water leaks a welded steel protection vessel enclosed the condenser. The condenser was designed to allow for removal of about $4 \times 10^6$ Btu/(hr)(sq ft) while operating the system at 1000°F.

The section making up the condenser sleeve was a one foot by 2 1/2-in diameter, sch 60, type 304 stainless steel pipe. The inside surface was reamed to obtain a press-fit over the boiling vessel. An Atlas compound mandrel press was used to force the sleeve down over the boiling vessel.

The cooling coils were 5/8-in diameter, type 304, 16 BWG stainless steel tubes bent around and welded to the sleeve to make up three separate and parallel cooling systems. The cooling systems were arranged in three, five and nine coils each, numbering from the bottom of the condenser, and connected in such a way that water entered each set of coils at the bottom. Tubes to and from the condenser were welded through the top flange of the outer pressure vessel and connected to a water manifold system. This arrangement made it possible to operate all or any part of the condenser system and gave more flexibility to the operation of the equipment. Each cooling line contained a nominal 3/8-in pipe Crane gate valve. The valves were connected with 5/8-in diameter copper tubing. City water was used as the condenser coolant.

A one foot section of 6-in diameter black iron pipe was welded around the cooling coils; 1/4-in thick by 6-in in diameter cold rolled steel plates were welded to form each end. A 5/8-in diameter, type 304, stainless steel tube was welded through the top flange of the outer pressure vessel and welded to a 5/8-in diameter hole made near the top along the side of the condenser pressure vessel. This line was connected to the inert gas system.

Boiling Tube

At the outset of this investigation it was hoped that a composite-electrically heated tube extending completely through the boiling vessel, with a stabilizer gas flowing through the center, could be fabricated for use in this study. A tube of similar design was used by Ellion (35) in his study of boiling water under force convection. This design would have permitted determining the critical heat flux directly while minimizing the probability of burnout. Also, boiling could have been accomplished in the transition boiling regime. Unfortunately, this tube assembly design was found to be extremely difficult to fabricate and would in all probability not stand up for more than one heating cycle.

It was finally decided that a tube design similar to that first used by Noyes (98) could satisfactorily yield high flux nucleate boiling data and permit burnout determinations. Although this design was a compromise from the original design, nevertheless it could yield nearly as much information as originally planned and, in addition, would allow for rapid and easy replacement of the heater assembly.

A cross sectional drawing of the bayonet heater assembly is shown in Figure 7. Photographs of the boiling tube and tube cross section are given in Figures 8 through 10. Figure 8 is a view of the boiling tube assembly showing the boron nitride sleeve and graphite heater before installation. Figure 9 is an overall

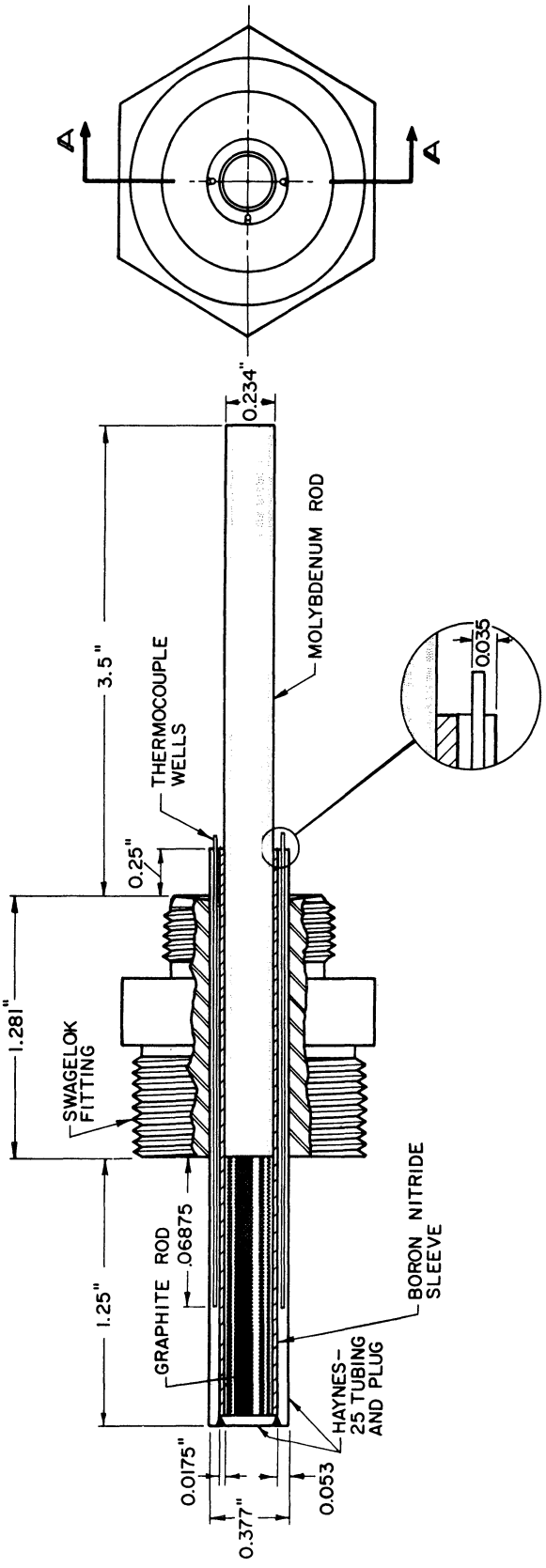


Figure 7. Cross Sectional Drawing of Boiling Tube Assembly.

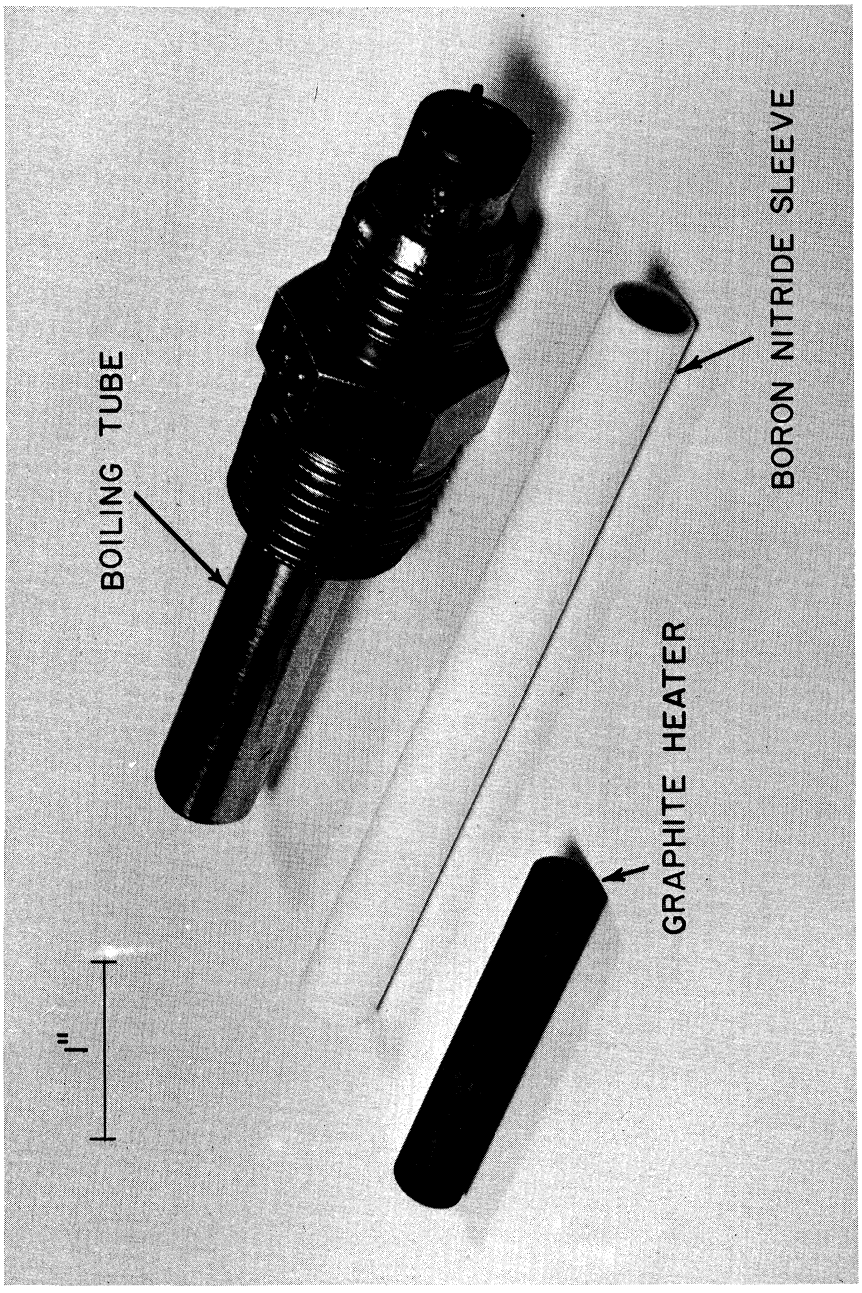


Figure 8. View of Boiling Tube Assembly.

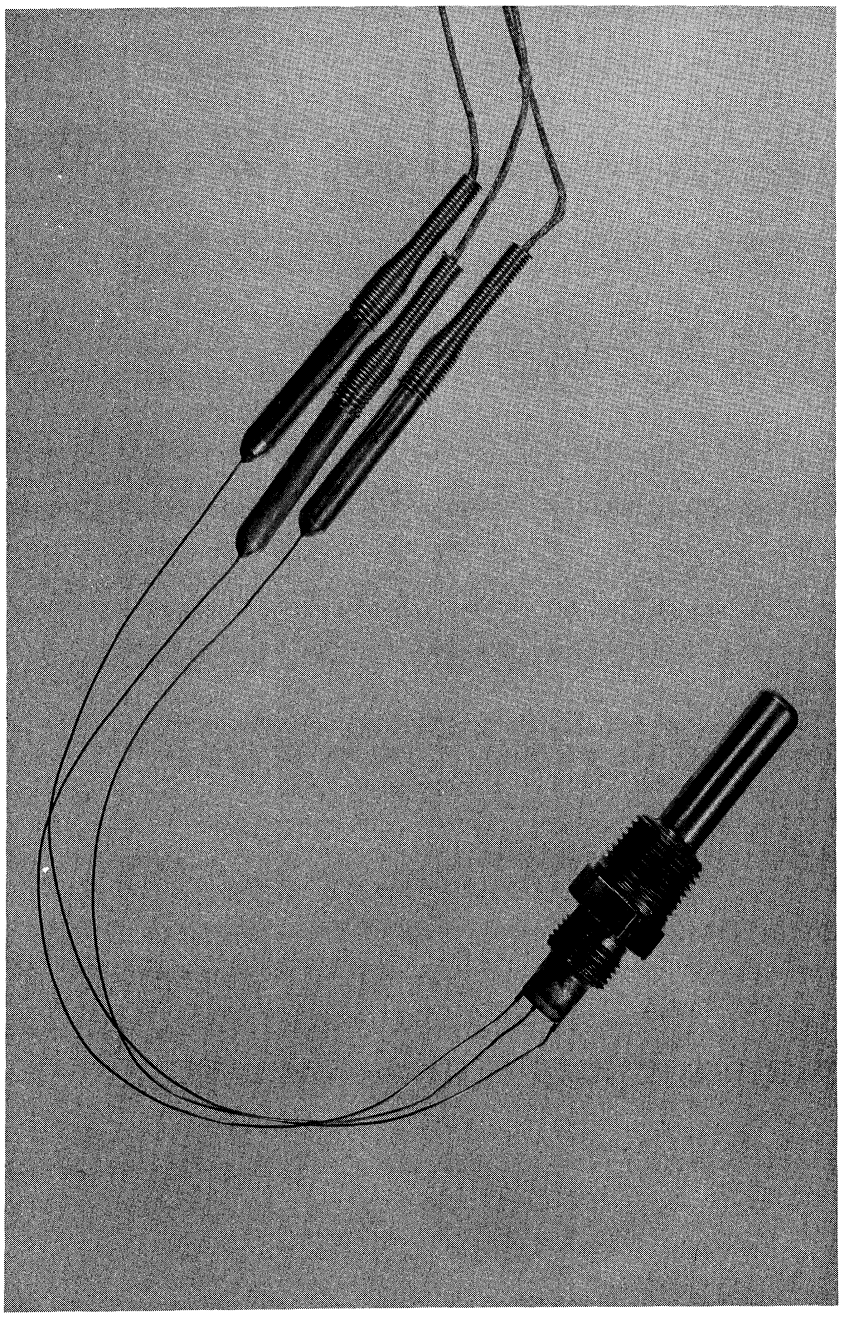

Figure 9. Overall View of Boiling Tube with Thermocouple Assemblies.

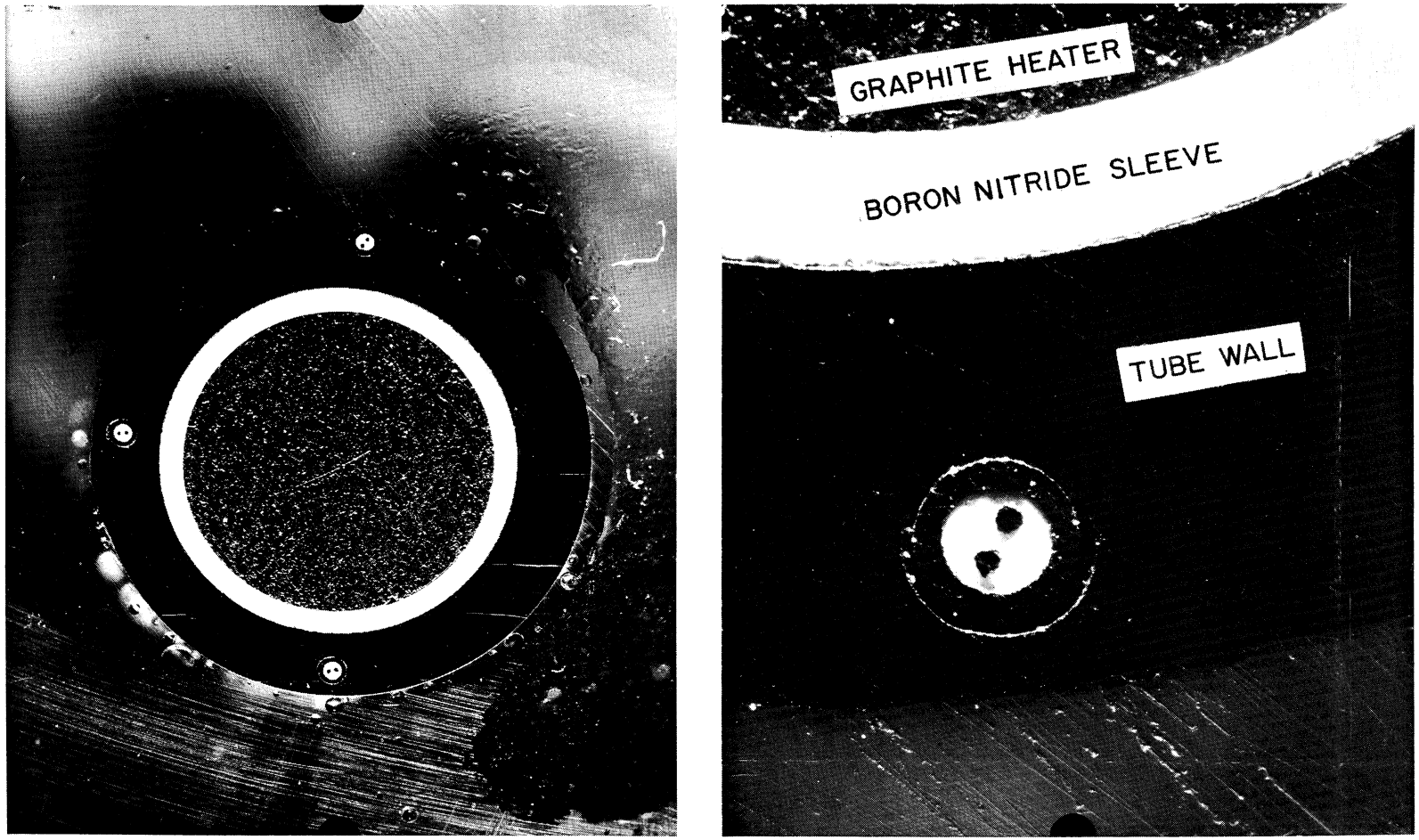


Figure 10. Views of Boiling Tube Cross Sectionals.

view of the tube showing the thermocouple assemblies extending from the thermocouple wells. Figure 10 gives cross sectional photographs of the composite tube.

The bayonet heater arrangement is made up of a cylindrical graphite heating element, a boron nitride insulating sleeve, and the boiling tube. Because of the importance of limiting large thermal gradients radially through the composite layers, it was imperative that each component be machined to the closest tolerances possible. To meet these requirements it was found that the following fabricating procedure gave quite satisfactory results:

The boiling tube was a 0.377-in OD by 0.053-in wall thickness Haynes-25 tube. Three longitudinal grooves 2 3/8-in long by 0.040-in wide by 0.040-in deep were made 90° apart in the tube with a surface grinder using a 0.035-in thick cut-off wheel. In tube 4 the three tube thermocouple grooves were placed at different locations longitudinally along the tube length. The three grooves in this tube instead were made 2 1/8, 2 3/8, and 2 7/8-inches long respectively. Stainless steel (type 304) hypodermic tubes 2 1/4-in long by 0.035-in OD by 0.022-in ID, closed with a Heliarc welder at one end, were then nicrobrazed into each groove. At the same time, the tube was nicrobrazed into a 3/8-in (type 316) stainless steel bore-thru Swagelok male connector (No. 600-1-6-316BT). By brazing the tube into the fitting, it was not necessary to use ferrules with the Swagelok fitting to make the seal. The braze filler used was a nicrobraze paste type B (LM nicrobraze AMS 4777)* purchased from Wall Calmonoy Company, Detroit, Michigan. The excess braze on the tube surface was machined off, the tube polished, and a 1/16-in thick by 0.277-in diameter Haynes-25 plug welded to close the end of the boiling tube. To give the required smoothness to the inside surface of the boiling tube, the tube was then reamed to 0.270-in diameter.

A 1/2-in diameter rod of boron nitride, purchased from the Carborundum Company, Latrobe, Pennsylvania, was drilled and reamed to 0.230-in ID. The sleeve was then put on a mandrel and finished to 0.2695-in OD.

The graphite used for the heating element was ultra-purity graphite purchased from Ultra Carbon Corporation, Bay City, Michigan. It was machined to a 1.25-in length by 0.230-in diameter. Extreme care was taken to assure that each end of the graphite element was cut off at a right angle in order that good electrical contact might be obtained at both ends of the tube.

The small end of a stepped molybdenum rod, 2-in long by 0.25-in diameter and 1 3/4-in long by 0.23-in diameter, slipped in the boron nitride sleeve and was forced up against the graphite element. Along the 0.25-in diameter length of the rod the bus bar was clamped. The end of the molybdenum rod was then fitted into the spring mechanism support (discussed later in this chapter). This mechanism forced the molybdenum rod against the graphite and also the graphite against the inside end of the boiling tube.

Litharge (PbO) mixed with glycerine (to a consistency of thick paste) was used on the tube assembly threads. This mixture prevented the seepage of liquid potassium through the threaded joint. With the tube assembly tightened in the

* Composition: 6.5Cr - 3.5B - 4.5Si - 2.5Fe - 0.15C - BalNi.

test vessel, the vessel was pressurized with helium and the threaded joint checked with a helium leak detector. The detector was a type 24-210 manufactured by Consolidated Electrodynamics Corporation, Pasadena, California. In no instance initially after tube installation, did the threaded connection leak, even at the most sensitive setting on the detector.

Outer Pressure Vessel

A photograph of the outer vessel is shown in Figure 2. A drawing of the vessel is given in Figure 4.

This vessel was fabricated from a one foot length of sch 40, 14-in diameter, black iron pipe; three 400-lb, 14-in diameter, forged steel weld neck flanges; one 400-lb, 14-in diameter, forged steel blind flange, and a 14-in diameter tube turn (Part No. 81XS) welding cap. Flange gaskets were standard, 14-in diameter, XH asbestos ring gaskets. Each flange contained 20 bolt holes and used 1 1/4 by 8-in carbon steel machine bolts and hex head nuts.

A block and tackle was used to lift the outer vessel in place for bolting. Two 1/4-in diameter steel cables with hooks, extended from a bar connected to the block and tackle. Steel arms (see Figure 2) welded to the outer vessel and lower flange extended out from the vessel to facilitate hooking the block and tackle cables.

All necessary entries into the pressure vessel were made through the blind flange. A layout drawing of these entry holes is shown in Figure 11. Thermocouples, voltage taps, guard heater leads, and the charging line entered the vessel through Conax glands while the water lines and gas lines were welded directly to the flange. The electrode glands were specially designed and are discussed in a later section of this chapter.

Potassium Charging System

All lines in the charge system were made from 3/8-in diameter, type 304, 16 BWG stainless steel tubing and were connected as shown in Figure 3. Valves were nominal 3/8-in vee-seat (No. 7VF6-316) Whitey valves with 0.312-in diameter orifices and high temperature (rated at 1100°F) asbestos packing. Stainless steel, type 316, Swagelok male connectors (No. 600-1-6-316) were used with each valve.

The charge vessel was a 2-in diameter by 14-in long section of sch 40 stainless steel pipe. Stainless steel discs, 1/4-in thick by 2-in diameter were welded to form each end. Two 3/8-in diameter drain holes were drilled in the bottom plate and welded to the system loading and test vessel charging lines. The two 3/8-in diameter holes in the top plate were welded to the inert gas line and an alternate potassium dump line. A 3/16-in diameter stainless steel thermocouple well extended six inches into the charge vessel. This well was made from 16 BWG (type 304) stainless steel and was closed at one end with a Heliarc welder.

The inert gas line leading from the charge vessel used a 1/4-in (No. Y353H), type 316, stainless steel Hoke valve with asbestos packing. This valve

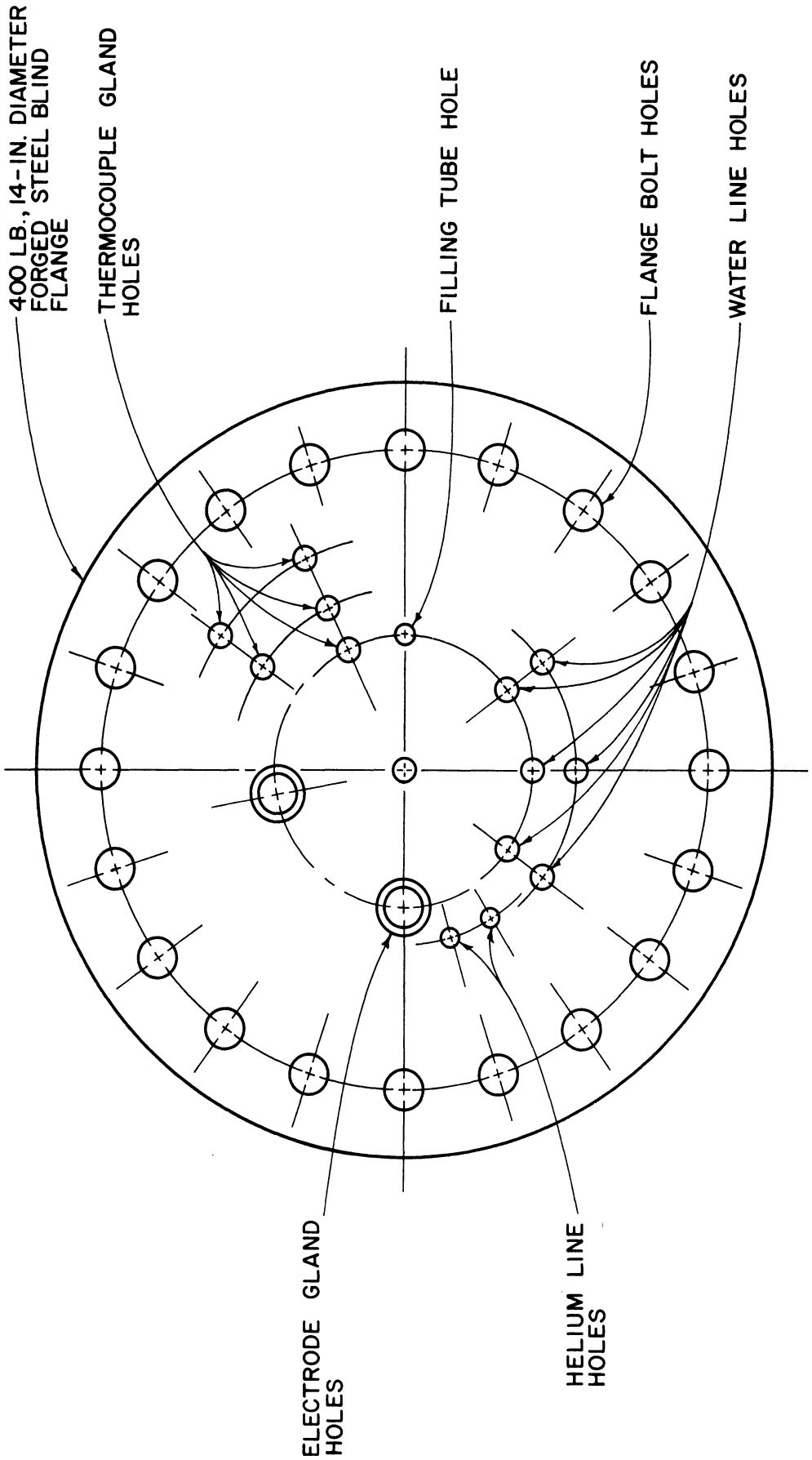


Figure 11. Layout of Entry Holes in Outer Protection Vessel.

was connected to the inert gas supply through a 1/4-in diameter copper line.

When initially charging potassium to the charge system, a 6-in length of 3/8-in diameter stainless steel tubing connected the system loading valve to the potassium shipping container. A 3/8-in Cajon (No. 6SW-7-4-316) socket weld female connector was welded to the end of this line and could be screwed to a 1/4-in male pipe fitting on the shipping drum.

An auxiliary access line to the charging loop was installed to be used as the feed line during the cleaning operation. A vessel containing methanol (or other cleaning fluid) could be attached to this line and methanol circulated in the charge system and boiling vessel.

Inert Gas Lines, Vacuum System and Knockout Drum

The inert gas lines are schematically shown in Figure 4. Helium from a gas cylinder was supplied to a maniford system by a two-stage 0-3000 psig and 0-200 psig Meco pressure regulator. Hoke 1/4-in (No. Y353H) type 316 stainless steel valves, with asbestos packing, regulated the gas supply to each of the three systems, i.e., test vessel and potassium charge system, condenser protection vessel, and outer pressure vessel. A fourth valve was used for exhausting to the atmosphere.

All gas lines not coming in contact with potassium were of 1/4-in copper tubing. Standard Imperial compression fittings were used for all connections.

The vacuum system was connected to the manifold system as schematically shown in Figure 3. The valve in the vacuum line was a 1/4-in (No. Y353H) type 316 stainless steel Hoke valve. The vacuum pump was a (Cat. No. 91305) Cenco Hyvac 2 pump. A nitrogen cold trap of standard design was used to remove condensibles and avoid contamination of the vacuum pump oil.

Calibrated bourdon pressure gauges (0-300 psig) measured pressures in each system. In addition, an open end mercury manometer was used in the test vessel system. Valves could cut out each pressure gauge and/or the manometer when operating outside the range of the gauge (manometer).

The line above the test vessel contained a knockout drum to trap and condense any potassium vapor which migrated beyond the condenser. This drum was made from a 2 1/2-in diameter by one foot long section of sch 60 (type 304) stainless steel pipe, packed with stainless steel lathe shavings. Discs 1/4-in thick were welded to form each end. A 3-in length of 3/4-in diameter, 16 BWG, (type 304) stainless steel tubing was welded through the bottom of the knockout drum and connected to a similar piece of stainless tubing extending down to the test vessel. A (no. 1210-6-316) Swagelok union made the junction. A 3/8-in diameter stainless steel tube extending from the top of the knockout drum was connected to the inert gas line. A Hoke valve of the type used in the inert gas manifold was installed in the line leading from the knockout drum. In the top of the knockout drum a 3/16-in diameter (No. PG-2) Conax stainless steel tube gland was welded and fitted with a thermocouple well. This well extended through the knockout drum into the test vessel and could be adjusted to read temperatures vertically throughout the boiling vessel. It was approximately

five feet long and made from 0.188-in diameter by 0.032-in wall thickness Haynes-25 tubing.

Power Supply, Power Leads, and Guard Heaters

Power to the boiling tube was furnished from a 12KW, 3-phase, full wave Udylite rectifier with a rated output of 250 - 2000 amps at 18 - 6 volts DC respectively. It was made by the Udylite Corporation, Detroit, Michigan. The boiling tube electrical circuit is shown in Figure 12.

Heavy power leads (300 AWG copper welding cables) carried current from the rectifier to the electrode glands passing through the top flange of the outer pressure vessel. The glands, shown in Figure 14, were made from 1 1/4-in diameter copper rods and used rubber silicone O-rings in lava seats. The O-rings were (No. GRC30-7 S1185) supplied by Goshen Rubber Company, Goshen, Indiana. Lava spacers (seats) were machined to size, cured at 1800°F, then slowly cooled to room temperature.

Two 1/4-in thick by 2-in wide copper bus bars directed the current inside the outer pressure vessel to the boiling tube circuit. One bus bar was connected with heavy flexible copper straps to the nickel-A bus bar. The second was connected with silimar heavy flexible copper straps to the bus bar support (see Figure 6). The flexible straps allowed for any differential in expansion between the copper bus bars and the boiling vessel.

Figure 15 is a photograph of the nickel bus bar and spring loaded mechanism for the molybdenum shunt.

Guard heaters were used around the test vessel, charge vessel, and all potassium lines. Their circuitries are shown in Figure 13. All heaters were 20 ga Chromel-A wire, electrically insulated from the containers and lines by 1/16-in thick asbestos sheeting. Copper (14 ga) leads from the guard heaters inside the protection vessel went through a (No. TG-14-A6) Conax bare-wire gland using a lava sealant. Power to the test vessel guard heaters utilized 1 KW 110v AC Powerstats. A 0-25 amp model 331-S AC Triplett ammeter was used with the test vessel guard heater. Simpson (model 157) 0-10 amp AC ammeters were used with all other guard heater circuits.

Instrumentation

A majority of the boiling vessel thermocouple locations are shown in Figure 4. Figure 16 gives the circuitry for all thermocouples.

All temperatures, except those in the boiling tube, were measured using 20 and 28 ga Chromel-Alumel thermocouple wires (Hoskins 3G-178 grade). Fabrication of each thermocouple junction was accomplished by using the standard gas welding technique as recommended by the thermocouple supplier. Conax bare wire thermocouple glands (No. TG series) were used to seal each thermocouple lead as it passed through the outer pressure vessel.

The three Chromel-Alumel boiling tube thermocouples (see Figure 9) were

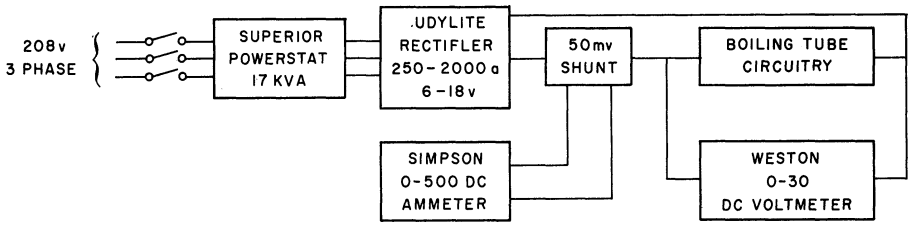


Figure 12. Boiling Tube Power Supply

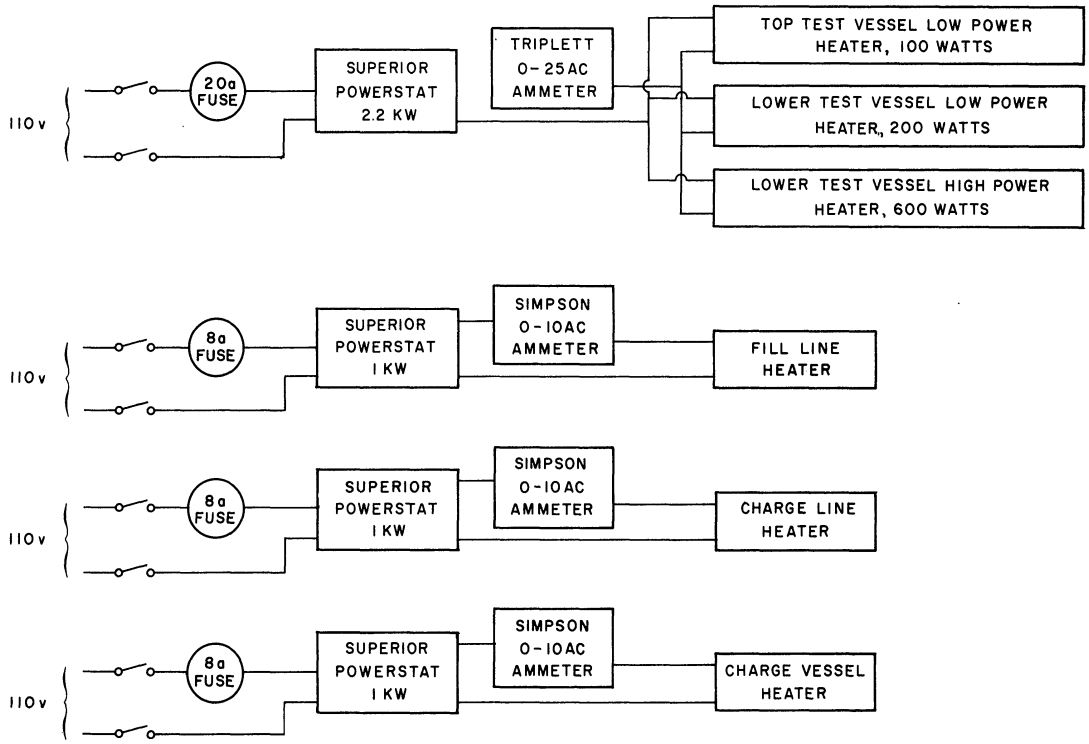


Figure 13. Guard Heaters Circuitries

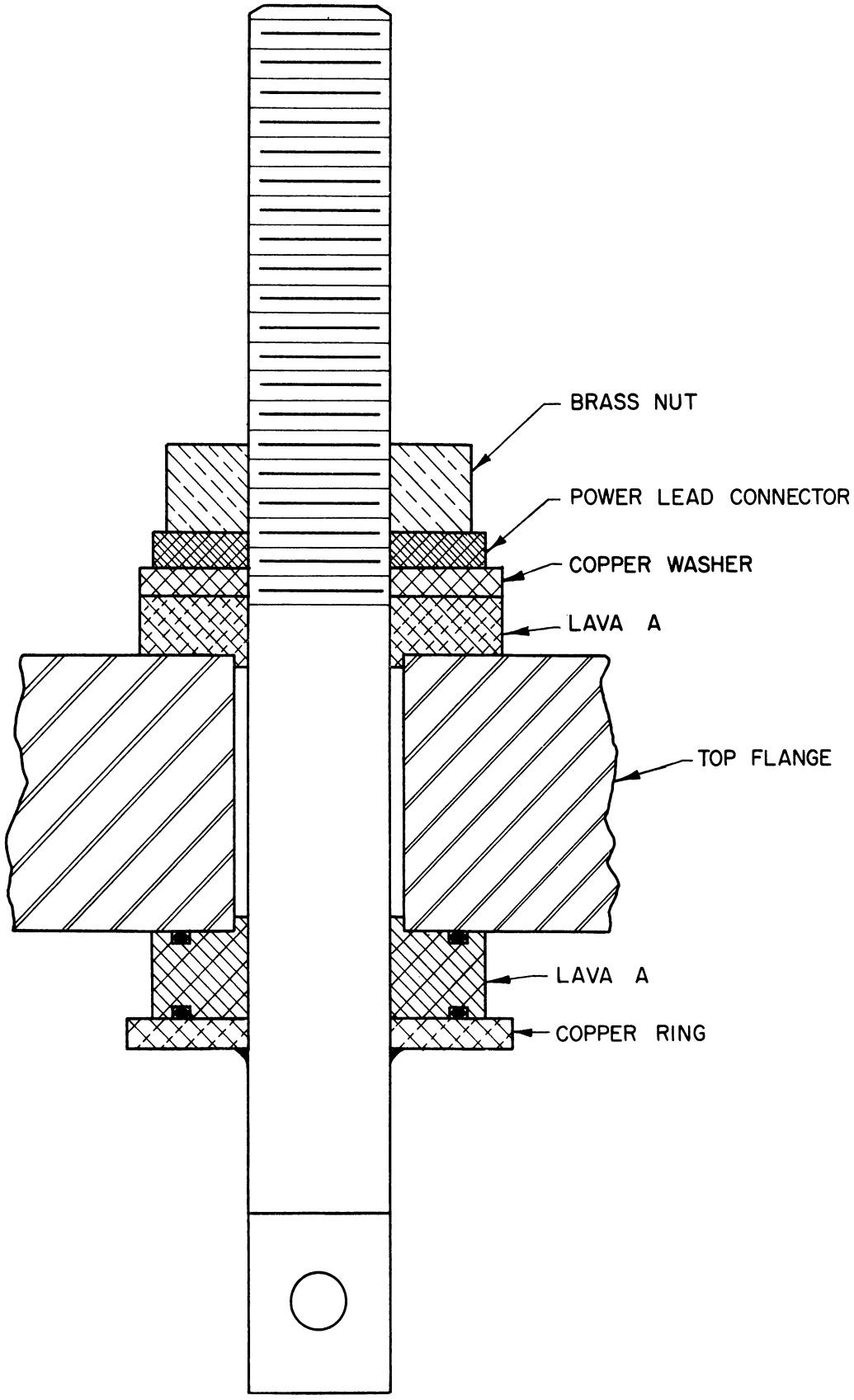


Figure 14. Drawing of Electrode Glands.

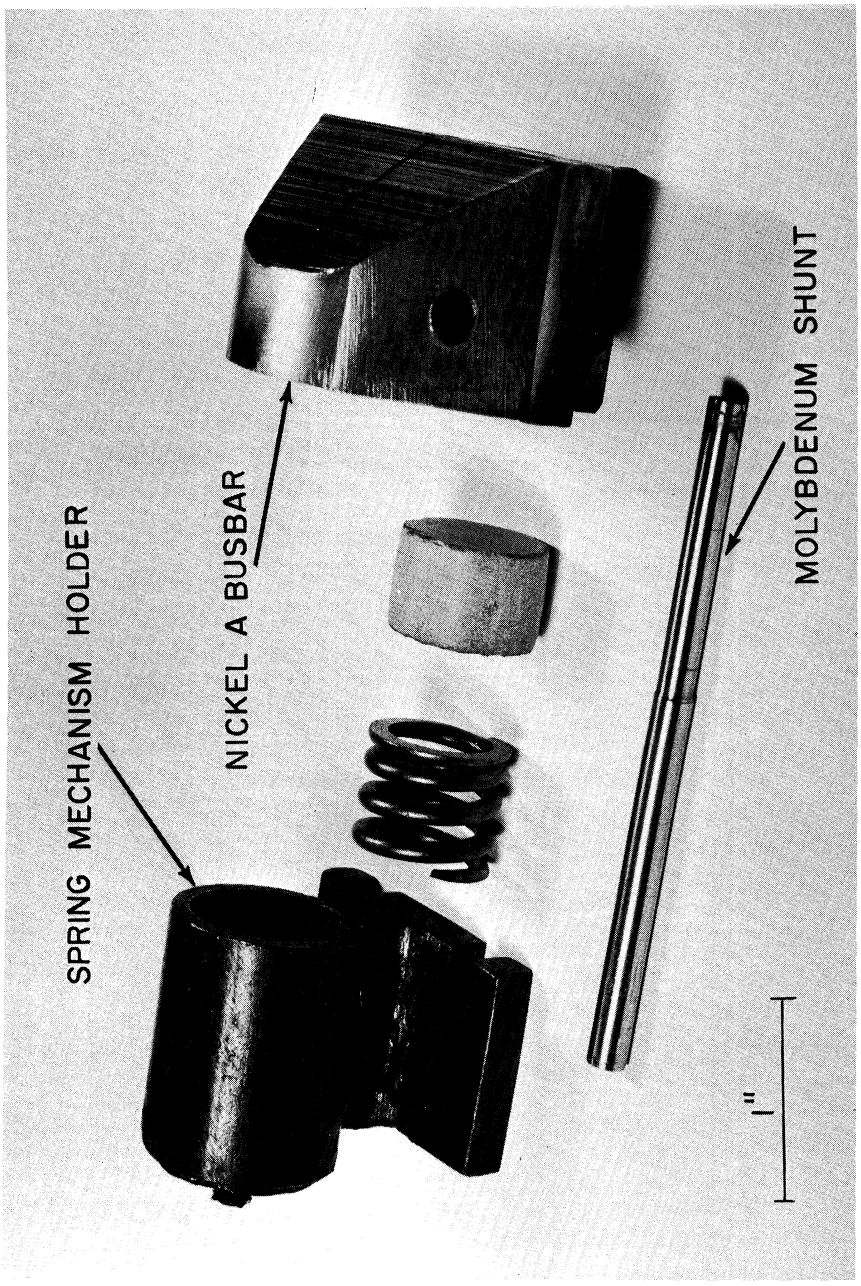


Figure 15. View of Boiling Tube Bus Bar Assembly.

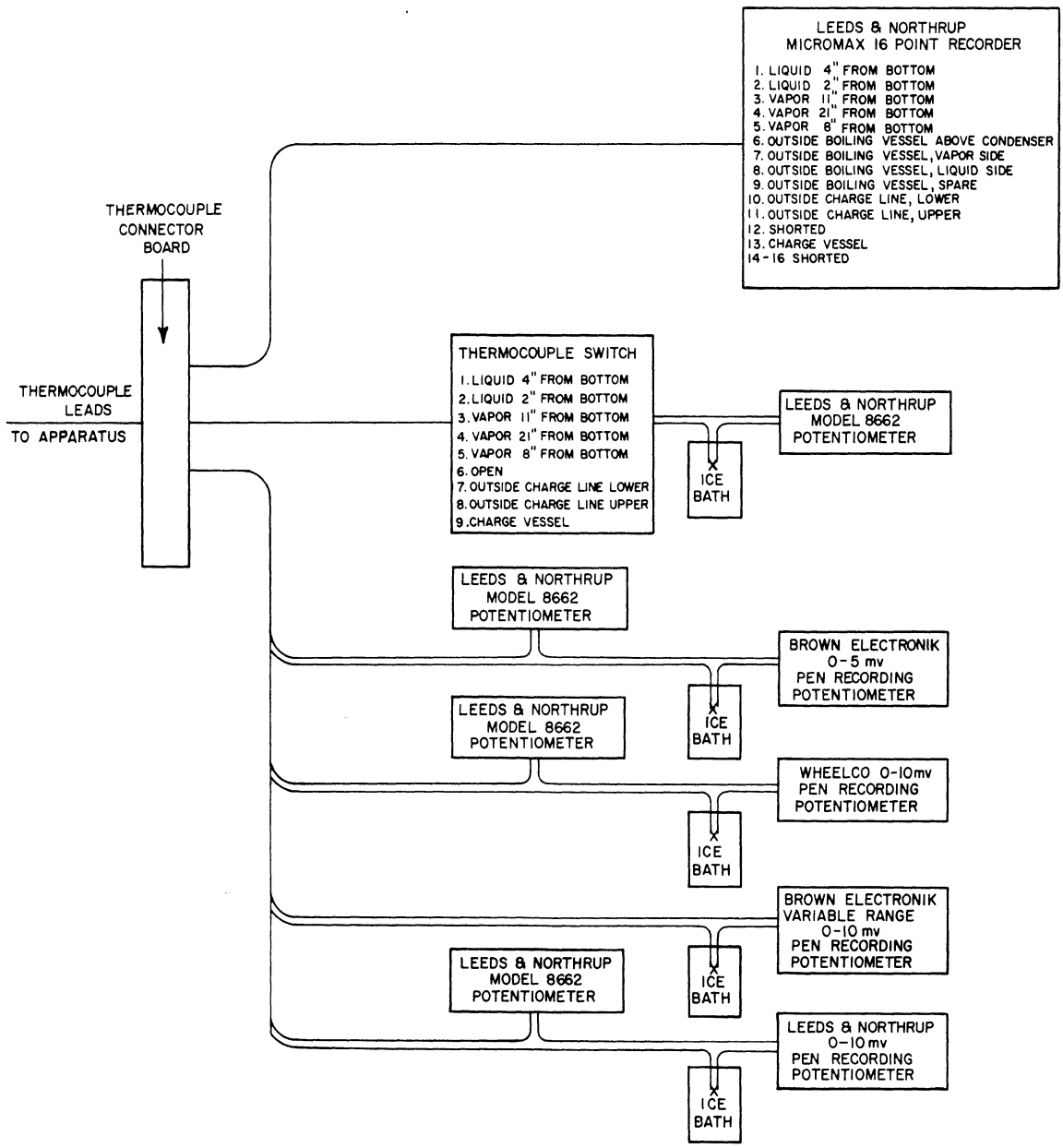


Figure 16. Thermocouple Circuitries.

swaged assemblies with a 0.020 ± 0.0005-in diameter Inconel sheaths. The matched thermocouple wires were 38 ga Chromel-Alumel (Hoskins 3G-178 grade) and were electrically insulated with magnesium oxide. Each thermocouple used a grounded junction. The thermocouples were calibrated and gave average deviations from standard tables of 0.32 per cent at 1100°F. They were purchased from Pyro Electric Company, Walkerton, Indiana.

The vertically adjusting thermocouple measured temperatures at any desired location throughout the test vessel and was used as a liquid level finder when charging potassium.

Three pen recorders were used to record the three boiling tube temperatures. Two of the recorders were 0 - 10mv full scale and used hand balancing Leeds and Northrup (model 8662) potentiometers in series to obtain the temperature ranges desired. One recorder was a Leeds and Northrup Speedomax while the other was a Brown Electronik. The third recorder was a Brown Electronik with an adjustable scale of 0 - 10mv span.

A 0 - 5mv fast responding Brown Electronik pen recorder was used with the adjustable thermocouple. This recorder also used a standard Leeds and Northrup (model 8662) laboratory potentiometer in series with it to give the desired temperature ranges. Other temperatures were recorded on a Leeds and Northrup Micromax, 16 point, recorder with a range of 200 - 2000°F. It was also possible to read a number of temperatures with another standard laboratory Leeds and Northrup (model 8662) potentiometer connected to an 8 point thermocouple switch.

A pre-calibrated ammeter (0 - 500 amps) and voltmeter (0 - 30 volts) were used to measure power to the boiling tube. Voltage tap connections were made across the boiling tube circuit which included the molybdenum shunt, graphite heater, Haynes-25 tube end, potassium, and vessel wall.

## OPERATIONAL METHODS AND PROCEDURES

### Preliminary Procedures

Upon completion of equipment installations the apparatus was thoroughly cleaned and tested. The boiling system and auxiliary lines were made helium tight up to 200 psig. All thermocouples and instrumentation were checked out.

The system was then flushed several times and heated to boil distilled water. The test vessel charging procedure, method for determining liquid level, operation of condenser system, etc. were checked out and/or refined using water as the test fluid.

As a means of determining what might be the best operational procedure with potassium, seven nucleate boiling runs were made with water. These runs covered a pressure range of one atmosphere to 150 psig with fluxes up to 0.5 million Btu/(hr)(sq ft). Operation of equipment and the method of taking data were essentially identical to that subsequently used with potassium (discussed later in this chapter).

Upon completion of the water test, the water was withdrawn from the system, the test vessel and charging lines were heated to over 200°F and the experimental system outgassed for several days. This completely removed the last traces of water from the system. The apparatus was then heated up to 1000°F and held for several hours.

Commercial grade potassium was charged through the load valve from a standard 3-lb capacity MSA Research Corporation shipping container. The shipping container was connected for filling as per instructions (92) furnished by MSA Research Corporation, Callery, Pennsylvania. A hot plate placed under the shipping container melted the potassium for charging while a propane torch (small portable fuel cylinder torch) heated the connecting lines. All lines and vessel heaters were set at over 250°F. The liquid potassium was drawn up into the charge vessel by applying a slight pressure to the shipping container. The thermocouple in the charge well indicated when the potassium had reached the correct level by a sharp change in the thermocouple reading. At this point the loading valve was closed, the apparatus and shipping container allowed to cool to room temperature, and the container disconnected. The loading tube was then cleaned of residual potassium, using methanol. A cap was screwed on the loading valve connection.

During the filling step a potassium leak developed at the threaded fitting between the shipping container and the filling line. In the course of filling, potassium completely solidified in the loading line and necessitated remelting with the propane torch. The first potassium to reliquify was blocked off on both sides in the line by solid potassium. This resulted in liquid potassium being forced through one fitting and causing a minor fire. Extreme care was exercised to prevent this from happening again.

With the potassium in the apparatus all instrumentation, connections, etc. were checked out. Finally, the test vessel charging procedure was reviewed and carried out. Necessary refinements were made.

## Start-Up Procedure

Before the initial run for each tube, the test vessel was charged to the desired depth. This was accomplished simply by equalizing the pressures in the test vessel and charge vessel, then draining the liquid potassium into the test vessel to the desired depth as indicated by the thermocouple liquid level finder. The charge line test vessel guard heaters were set to give system temperatures over 250°F. Lowering the test vessel level could be accomplished by applying slight positive pressure over the liquid in the test vessel.

With the potassium at the correct depth in the test vessel, power to the test vessel and fill line guard heaters was increased to give the desired heat up rate. The normal rate for heating was usually about 300°F/hr. When the bulk temperature reached bulk saturation, the potassium was allowed to pool boil using only the guard heaters, for a sufficient time to reach thermal equilibrium throughout the test system. Sometimes power to the boiling tube was turned on and the pool boiled for 30 to 60 minutes at fluxes approximating 200,000 Btu/(hr)(sq ft).

The adjustable thermocouple served to measure bulk temperature and was normally positioned to read the temperature at a pool depth of approximately 4 to 6 inches. When system temperatures, at zero power to the boiling tube, remained constant over a period of time, the system was considered to be at steady state and ready for a boiling run.

## Operating Procedure for Nucleate Boiling Runs

Following the start-up procedure, as described above, the system was ready to commence a boiling run. With the tube power source cut off, all boiling vessel liquid thermocouples, i.e., adjustable bulk thermocouple, and three boiling tube thermocouples, were read and recorded.

The power to the boiling tube was then turned on and increased in steps up to the desired maximum heat flux. For each step the system was allowed to reach steady state, after which the following readings were recorded: (1) boiling tube amperage, (2) boiling tube voltage, (3) bulk thermocouple reading, and (4) the three boiling tube thermocouple readings. Since temperatures in the bulk liquid and boiling tube generally fluctuated, it was necessary to average the readings. It should be mentioned that throughout each run, pen recording potentiometers continuously recorded the bulk and the three boiling tube thermocouple readings. The system pressure was read and recorded about every third power setting.

The three condenser temperatures were checked periodically, as these temperatures were used as an indication of when more condenser cooling was needed. It was found that for the most part cooling water had to be turned on only periodically and then only long enough to refill the condenser coils with water. The condenser was operated by filling the top nine coils with water and then letting it boil out. This technique worked quite satisfactorily on all runs except the lowest pressure runs when it was necessary to let a very slight continuous flow of water go through the condenser. At all times only the top nine coils of the condenser were used.

In all runs there was a slight increase in system pressure as the heat flux was increased. This increase was generally due to the generation of increased amounts of potassium vapor and subsequent compression of helium cover gas.

When a run was completed the power was returned to zero and all liquid bulk thermocouples read and recorded; the pressure was also recorded. To start a run at a different pressure, the helium cover gas was regulated to the desired pressure and the system allowed to reach equilibrium saturation conditions. The procedure was then repeated.

Operating Procedure for Burnout Determinations

The experimental procedure for obtaining a majority of the burnout points was very similar to that used by Noyes (98) in his burnout measurements with sodium. In short, the method consisted of holding the heat flux constant at the desired value and slowly decreasing the pressure until incipient burnout was reached. It was felt that measurements made in this manner were very reliable and permitted time for cutting off the tube power before actual tube failure occurred. In one nucleate boiling run, burnout was inadvertently reached by increasing the heat flux at a constant pressure. When burnout was reached, it was not possible to shut off the power supply before complete tube failure occurred. For this reason most subsequent burnout measurements were made by holding the flux constant while decreasing the system pressure.

Usually the system pressure was set 30-in Hg above the anticipated burnout pressure. With the pressure regulated, the power was slowly increased to the desired heat flux. When the system reached steady state, the vacuum line (with vacuum pump operating) and boiling system valves were regulated to give a gradually (maintaining steady state conditions) decreasing system pressure. The rate of pressure decrease was usually controlled to less than 20-in Hg per hour. Because of the unsteadiness of the pressure decrease in some instances it was necessary at times to readjust the vacuum line valve.

Incipient burnout was indicated by an instantaneous rise (at least 300°F) of the boiling tube thermocouple. The rectifier was cut off immediately and the final thermocouple and pressure readings made. The procedure was repeated to obtain new burnout points.

## RESULTS

All results were obtained through direct measurements or observations and are categorized under the general headings: Nucleate Boiling Water Data, Nucleate Boiling Potassium Data, Potassium Burnout Results, and Temperature Fluctuations.

The nucleate boiling data consisted of measurements of heat flux, system pressure, and the temperature difference between the boiling surface and liquid saturation temperature. The liquid saturation temperature here denotes the bulk temperature at the liquid-vapor interface, frequently referred to as the free surface temperature. In the burnout determinations, only measurements of heat flux and system pressure were necessary.

Power input to the boiling tube assembly was used to calculate the heat flux while thermocouples in the liquid and tube wall furnished temperatures. Determination of power losses in the boiling tube circuitry are discussed in Appendix D while the errors associated with each experimental measurement are estimated in Appendix E. Tabulations of all experimental data are given in Appendix A. A section covering the treatment of data is given in Appendix B.

### Nucleate Boiling Water Data

This phase of the investigation was undertaken to check the operability of the apparatus and to provide a standard for comparison of results obtained in this equipment with those from similar systems using the same test liquids. Water was boiled at fluxes up to 500,000 Btu/(hr)(sq ft) in the pressure range from one atmosphere to approximately 150 psig.

Boiling tube temperatures during the water runs were measured using only one thermocouple. It was located in the tube surface approximately 45° from the vertical. The other two thermocouples in the surface had previously shorted out, thus a comparison between $\Delta T$ values measured around the tube was not possible.

All data were taken by starting at zero heat flux and increasing the flux in steps to the desired levels. At each flux setting the system was allowed to reach a steady boiling condition before taking data. A summary of the data is shown in Figure 17 while a tabulation of all measurements is in Table I of Appendix A.

The atmospheric data compares well with atmospheric water data obtained by Lyon (79) who also obtained data from the outside of an electrically heated 3/8-in diameter tube. Atmospheric water data of Addoms (1), from a 0.024-in diameter platinum wire, gave lower $\Delta T$ values than the present investigation. It is seen in the present data, that with an increase of operating pressure from one atmosphere to 150 psig, the pressure effect on the $\Delta T$ is significant.

At no time were pronounced temperature fluctuations observed. Since other investigators (57, 89, 91, and others) have reported fluctuating temperatures in a boiling surface while boiling water, it is felt that perhaps the response time of the temperature recorders used in this study was too slow to pick up such variations.

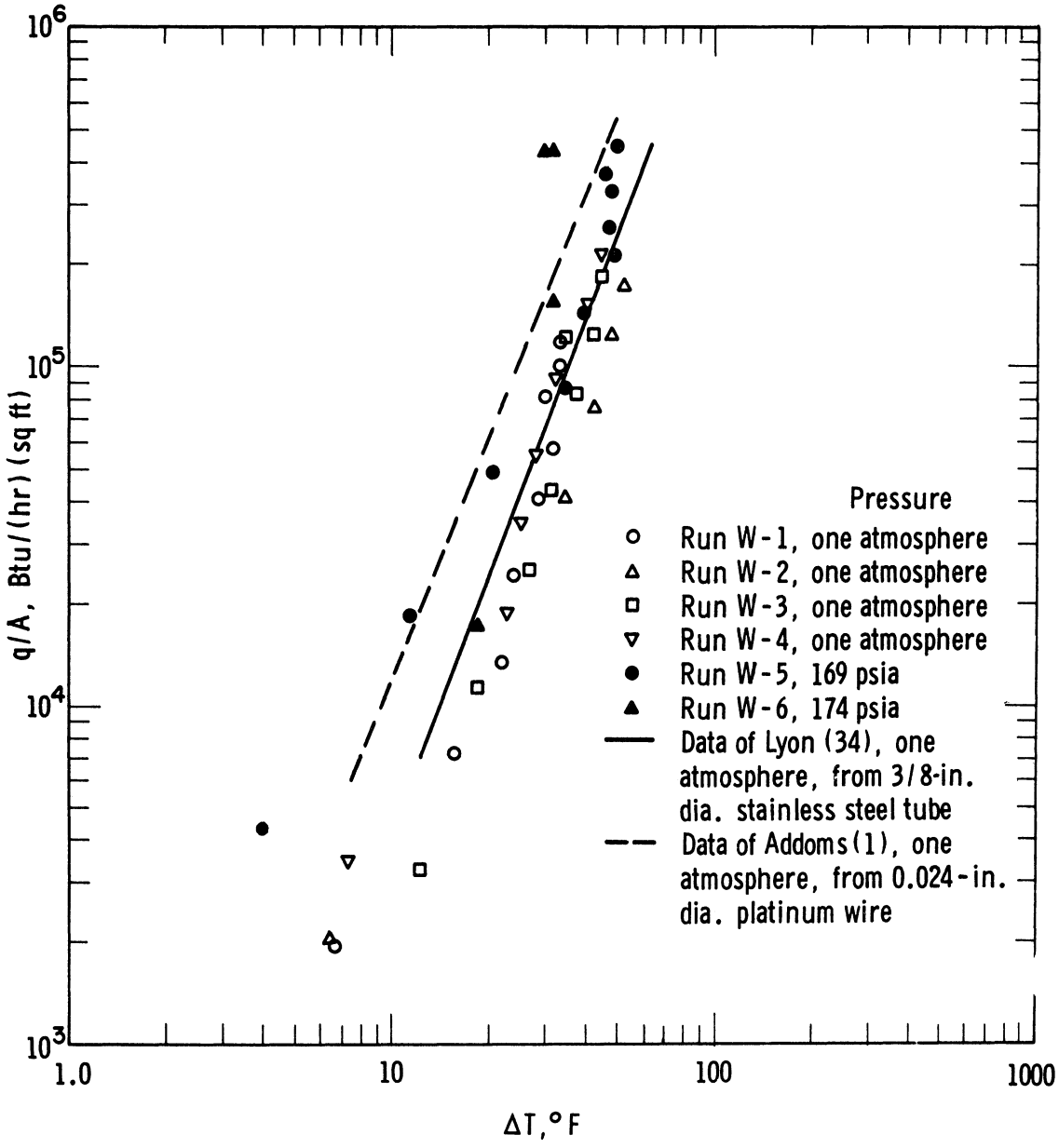


Figure 17. Comparison of Pool Boiling Water Data with Two Previous Investigations.

The boiling runs with water were made using a boiling tube assembly with a slightly different thermocouple installation than those used for the potassium runs. Nevertheless, the thermocouple sensitivity should have been comparable in the two designs.

In the development of a satisfactory boiling tube assembly several alternate designs were tested before arriving at the final design. One design which, at the time, was thought feasible called for brazing a 0.032-in diameter swaged thermocouple directly into longitudinal grooves made in the outer tube surface. The first tube fabricated in this manner proved satisfactory and was installed in the apparatus. All water runs were made using this tube. Later, upon charging the apparatus with potassium, the last thermocouple in the boiling tube assembly was shorted out on the first run attempted. Subsequent tubes fabricated in this manner had on the average 2 out of 3 thermocouples in each tube with open circuits. This fact necessitated a slight modification of the tube design for the potassium runs.

Nucleate Boiling Potassium Data

Figures 18 through 20 present typical plots of nucleate boiling data for potassium taken on three, 0.377-in OD by 1.25-in long, Haynes-25 tubes. Ten runs were performed from zero to burnout fluxes in the pressure range 1 to 45 psia. A complete tabulation of the original data is given in Tables II to XI in Appendix A. Plots of data for all individual runs not presented in this section are given in Appendix F.

Each figure presents data determined from the three boiling tube thermocouples, i.e., top, side, and sottom, aor a single run. Scatter of the data prevented plotting data in the same figure for more than one run. No attempt was made to evaluate numerically the reproducibility of the data. An attempt was made to correlate the data using the least-square method to determine the best straight line log-log relationship. Curvature of the boiling curves at low fluxes prevented a good correlation, thus the method was discarded. A smooth curve was more representative of the data. The burnout level for each run is shown as a horizontal line in each figure.

During run K-8 (Figure 19) the bulk temperature for each heat flux setting was measured at different depths in the liquid pool. Figure 21 is a graphical presentation of these measurements and shows that mixing in the potassium pool, at least in this run, was insufficient to maintain a constant pool temperature. In the plot, the temperature difference is the temperature above the liquid-vapor interface (free surface) temperature. Similar behavior was reported by Madsen and Bonilla (80) in their study of pool boiling NaK.

As a result of these bulk temperature gradients, the temperature to be used as the bulk saturation was not so clearly defined. Madsen and Bonilla found that free surface temperatures equalled the equilibrium temperatures corresponding to saturation pressures. It also correlated better when used to determine the boiling $\Delta T$. This fact was found to be true in the present investigation, thus the free surface (or liquid-vapor interface) temperature was used in $\Delta T$ determinations.

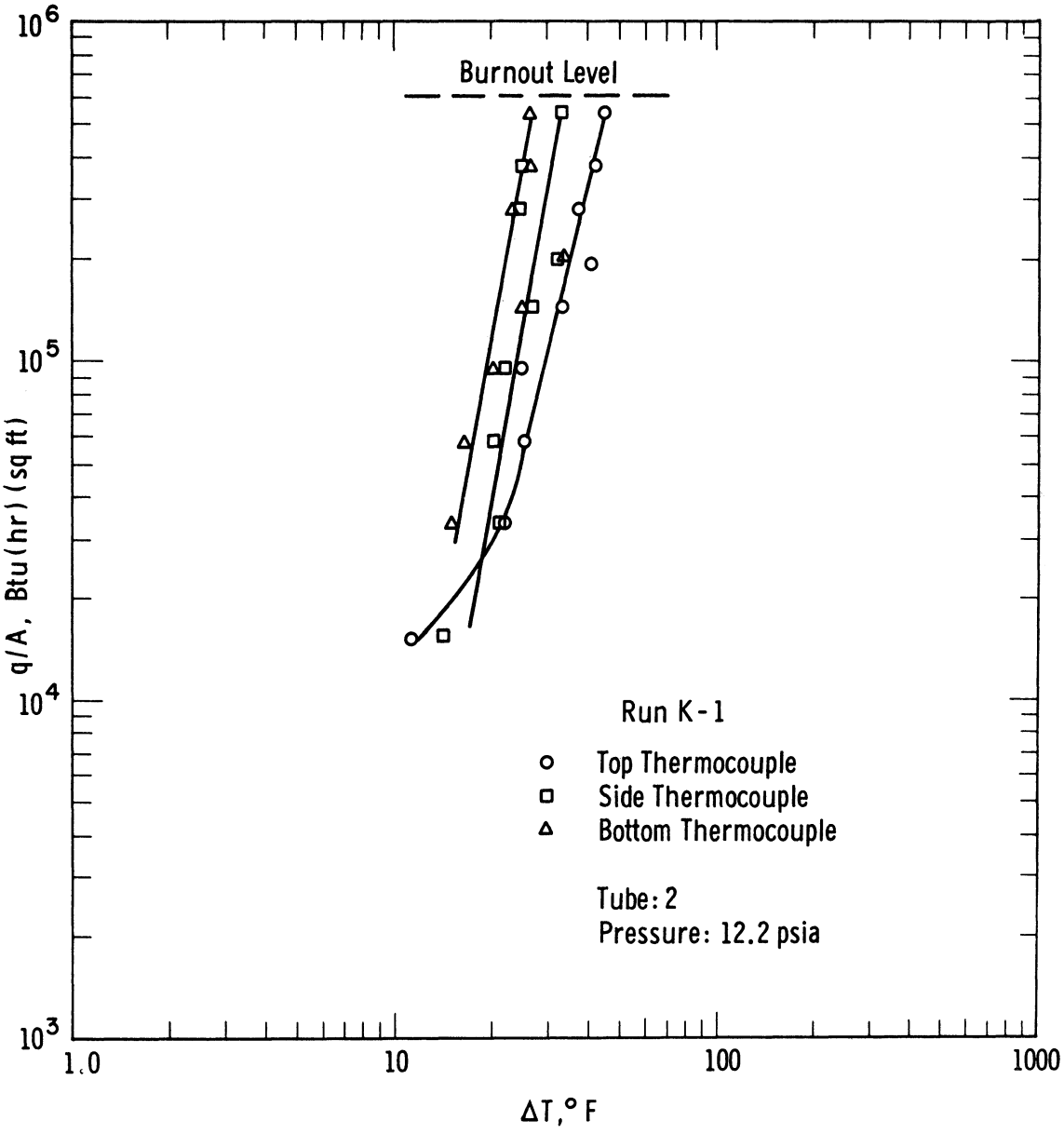


Figure 18. Boiling Data for Potassium Obtained at 12.2 psia using Tube 2 (Run K-1).

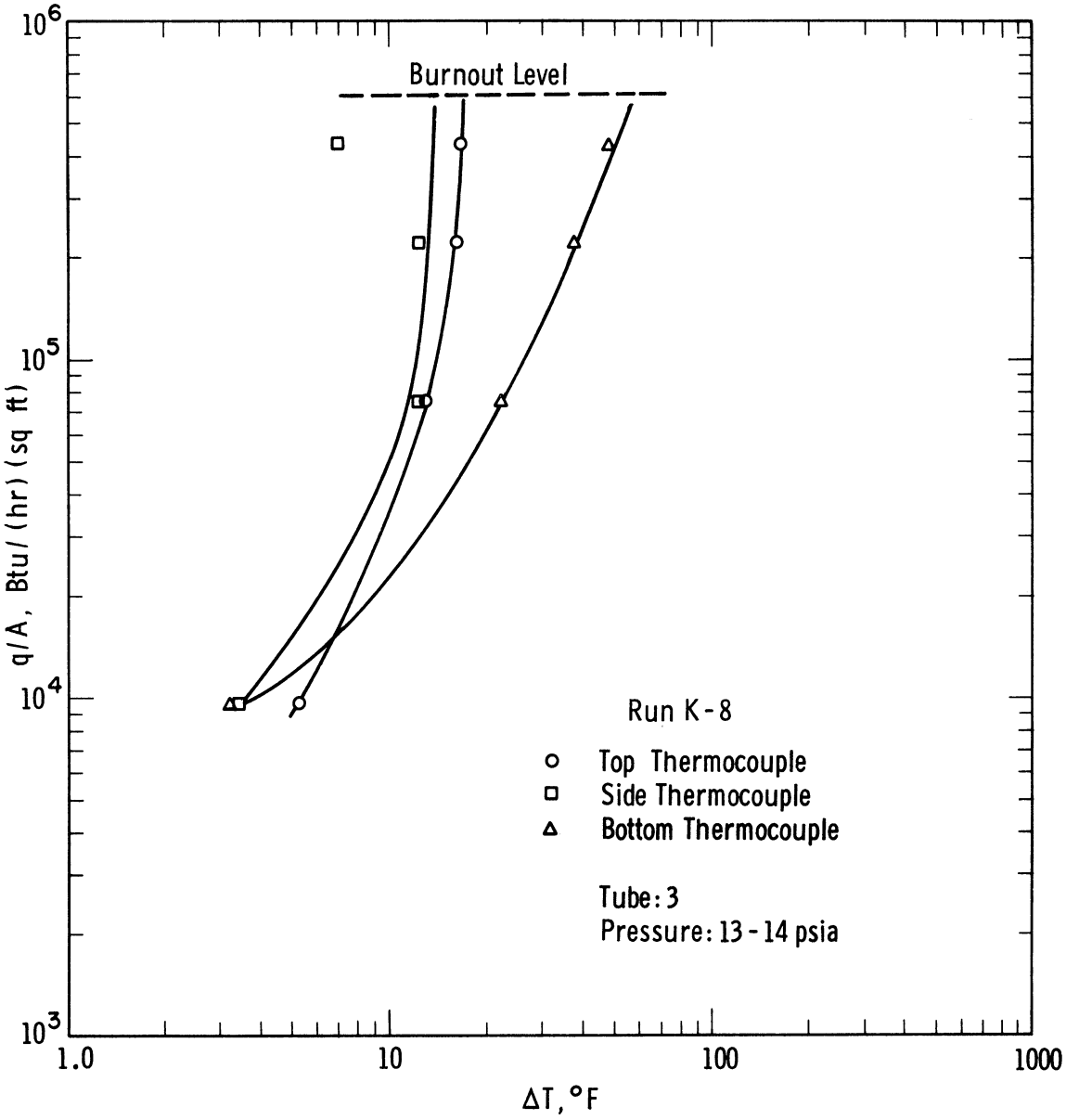


Figure 19. Boiling Data for Potassium Obtained in the Range 13 - 14 psia using Tube 3 (Run K-8).

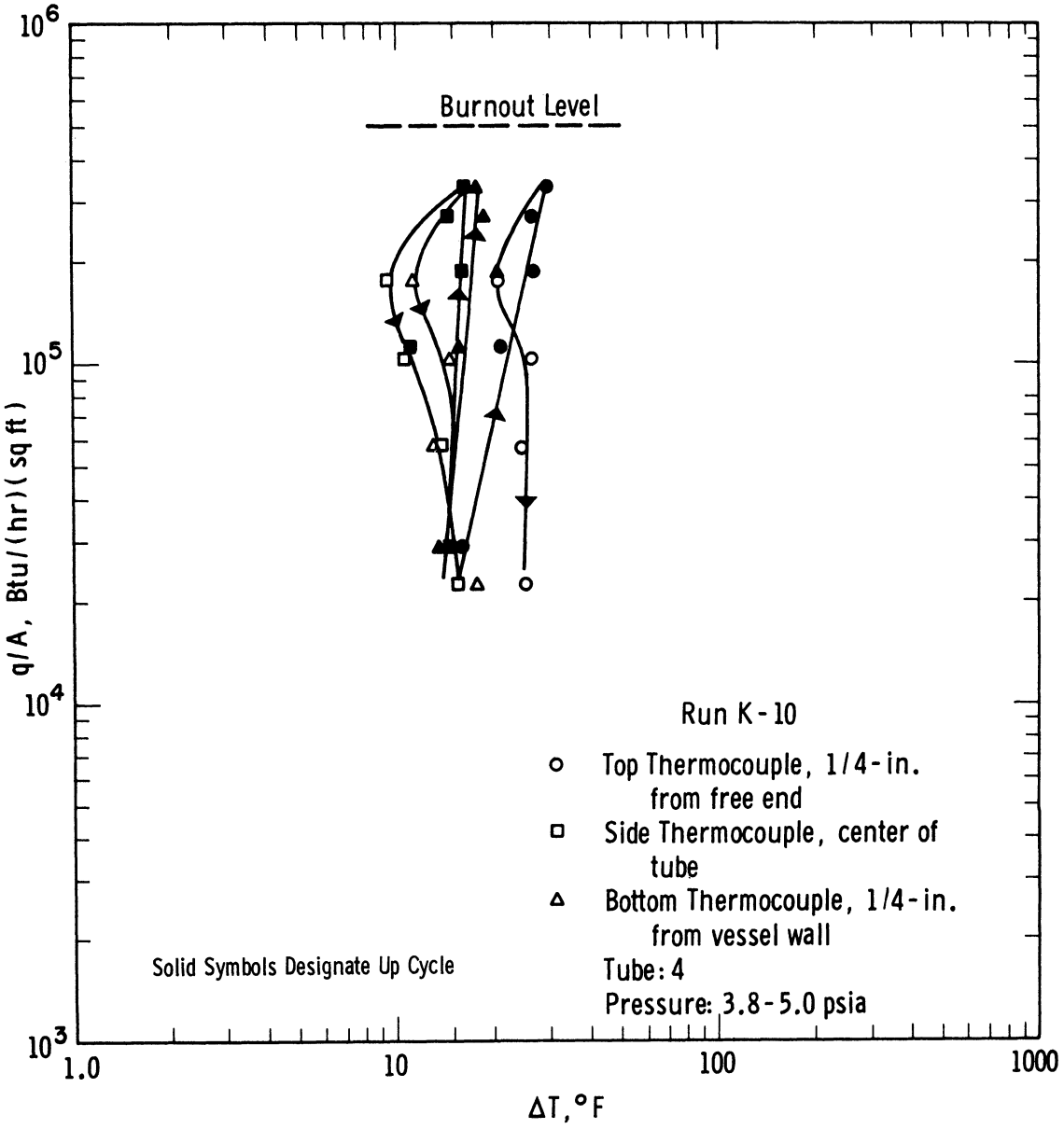


Figure 20. Boiling Data for Potassium Obtained in the Range 3.8 - 5.0 psia using Tube 4 (Run K-10).

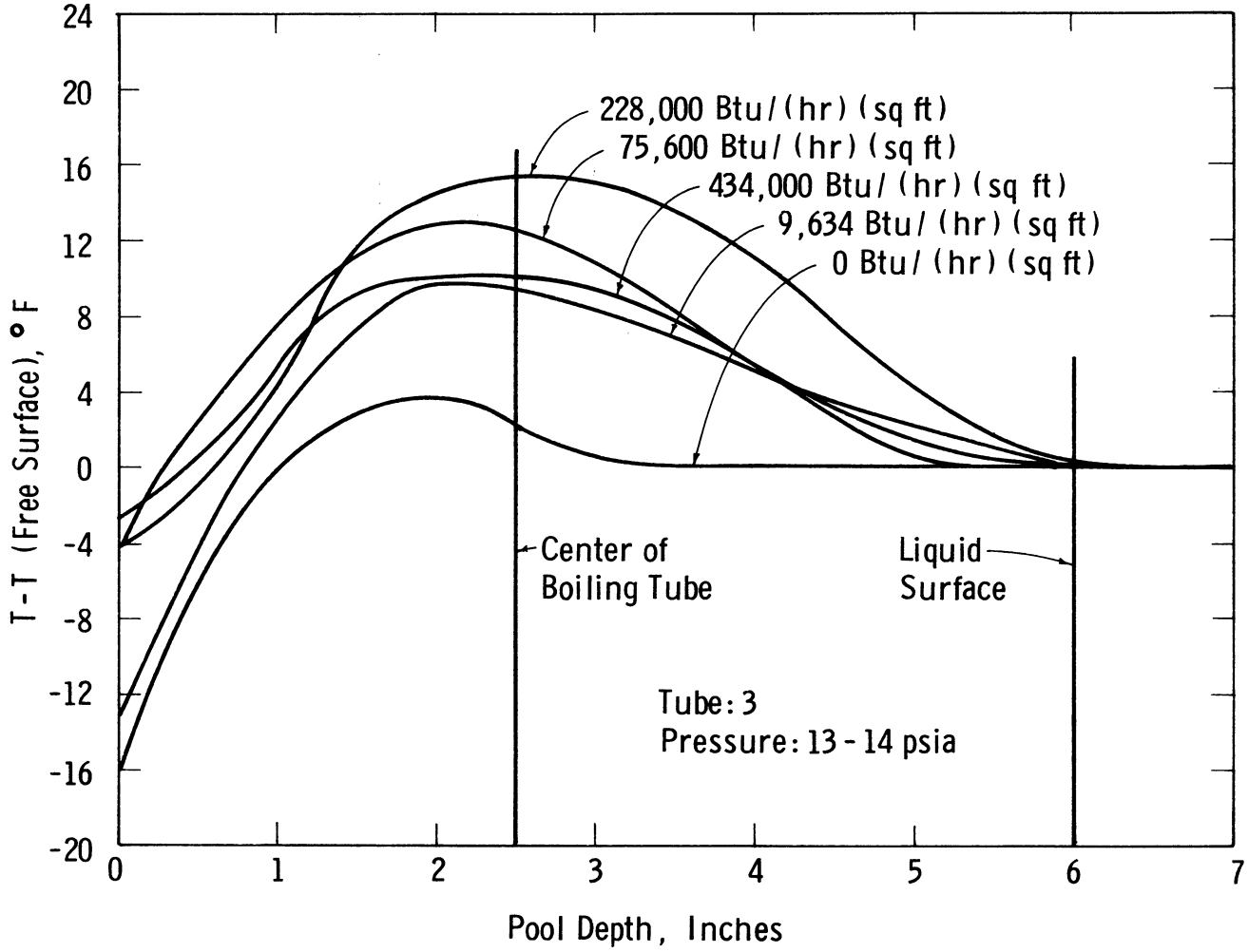


Figure 21. Vertical Temperature Profile Based on Free Surface Temperature (Run K-8).

In all runs except K-10 (tube 4), data were taken by increasing the flux in steps from zero to the highest value. No readings were taken for decreasing flux conditions. In each case an attempt was made to obtain data as near the burnout point as possible without actually reaching it. In run K-10 data were taken for stepped increases in flux from zero to over 300,000 Btu/(hr)(sq ft) and for stepped decreases back to zero. The data are shown in Figure 20. The apparent break (displacement) to the right on the down cycle is easily distinguishable.

Also, recall that tube 4 was fabricated with the three thermocouples placed at different locations along the tube length to detect any longitudinal temperature gradients during boiling. One thermocouple was located directly in the middle of the tube length while the other two were placed 1/4-in from each end. It can be seen from Figure 20 that the scatter of data is similar to other runs and does not show the existence of any distinguishable longitudinal temperature gradients.

Pronounced temperature fluctuations were observed in the three boiling tube thermocouples during all runs. In several runs and particularly at fluxes below 100,000 Btu/(hr)(sq ft), temperature fluctuations were also significant in the bulk liquid and were usually accompanied with significant pressure fluctuations. The last section of this chapter is devoted to these temperature fluctuations, therefore, only their existence is noted here.

Inconsistencies and scatter of the data prevented drawing any conclusions concerning the existence of characteristic variations in $\Delta T$ values for the top, side, or bottom tube surface. Also, the data showed no distinguishable pressure effect on $\Delta T$ over the intervals 0.7 - 14 psia and 0.9 - 45 psia.

Upon completion of each set of runs the boiling tube assembly was removed from the apparatus and inspected to see what effect prolonged high flux boiling and incipient burnout had on the heat transfer surface. The tube (tube 2) used in runs K-1 through K-4 appeared as it did initially with no noticeable surface changes except at the end of two of the brazed thermocouple grooves beyond the thermocouple junction. At this point a slight amount of braze in the last 3/16-in of each groove was eaten away giving the appearance that there may have been melting, erosion, or dissolution of the braze at these locations. Fortunately, the thermocouple junctions in each of the two cases were far enough removed (about 1/4-in) from these indentations that it was felt the thermocouple readings were not affected significantly.

Photographs showing three views of the tube assembly after removal from the apparatus are shown in Figure 22. The dull finish and residue seen on portions of the tube surface resulted from the cleaning operation. Lead deposits coming from the litharge (PbO) -glycerin pipe dope mixture can be seen on the threads of the fitting.

The tube (tube 3) used in runs K-5 through K-9 showed no effects of boiling and upon slight polishing of the surface it looked exactly as it did before installation. The tube (tube 4) used in run K-10 underwent destructive burnout on the last of six burnout determinations. A photograph of the tube is shown in Figure 27. A description of the burnout effects on the tube is given in the next section.

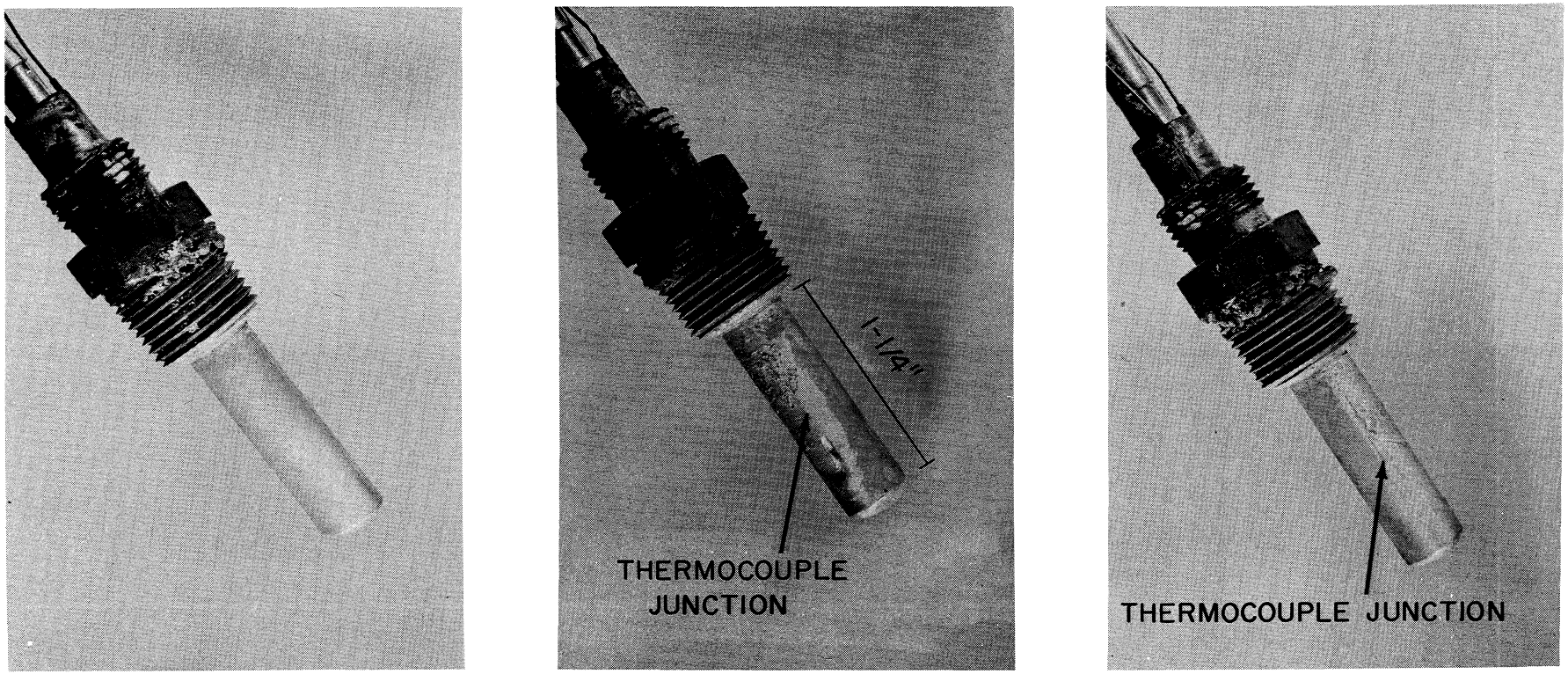


Figure 22. Photographs Showing Three Views of Tube 2 After Removal from Apparatus.

The data from tubes 2 and 3 are compared with the data of Bonilla (15) in Figures 23 and 24. The present data shows more scatter at the same pressure than data of Bonilla (see Figure 1), however, it must be pointed out that Bonilla obtained data up to only 115,000 Btu/(hr)(sq ft) with only three runs in the range 700 - 1500mm Hg and one run at 2 - 12mm Hg.

Potassium Burnout Results

Figure 25 is a plot of the burnout data taken with four boiling tube assemblies in the pressure range 0.15 to 22 psia. A summary of the burnout measurements is given in Table XII, Appendix A. All tubes were 0.377-in diameter by 1.25-in bayonet heaters made from Haynes-25 tubing. Heat fluxes were determined from a measurement of the power to the tube assembly. See Appendix B for method of calculation. The system pressure determined the liquid free surface temperature as discussed in the previous section.

The most satisfactory method for making burnout determinations consisted of holding the heat flux constant and decreasing the system pressure until burnout was reached. This method is discussed in the preceding chapter. The other method consisted of holding the pressure constant and slowly increasing the power to the tube stepwise until a temperature excursion was observed in the tube thermocouples. Although the latter technique was more straightforward the probability of destroying the tube was much greater. Of the nine burnout points determined by this method, two ended in complete tube failure, while the other method gave nine values with no failures. Typical traces of the boiling tube thermocouples during burnout runs by both methods are presented in the next section (Figures 31 and 32).

Three burnout points were determined using tube 1, two at subatmospheric pressures (0.15 and 0.16 psia) and one at atmospheric pressure. The latter point was inadvertently obtained at the last power increase during a nucleate boiling run. When burnout was reached it was not possible to shut off the power supply before complete tube failure occurred. Since the power at burnout was not accurately read, the data point for this determination in Figure 25 represents the last stable heat flux measurement. This value should not be significantly different from the actual burnout flux since the flux increase creating burnout was very small.

Removal of tube 1 showed that it had completely melted at its midpoint. A photograph of the tube is shown in Figure 26. Only the half attached to the wall could be recovered for examination, thus the condition of the other half subsequent to burnout was unknown.

Burnout determinations on tube 2 were all made at constant flux. Four burnout points were obtained from 1 to 14 psia. Photographs of the tube assembly after operation are shown in Figure 22. The only noticeable changes (discussed in previous section) in the tube surface after removal were the development of small indentations in the surface at the end of two thermocouple grooves.

Five burnout determinations were made on tube 3 in the pressure range 0.7 to 22 psia. Two of these measurements were inadvertently made during nucleate boiling runs at constant pressure while the rest were determined by decreasing

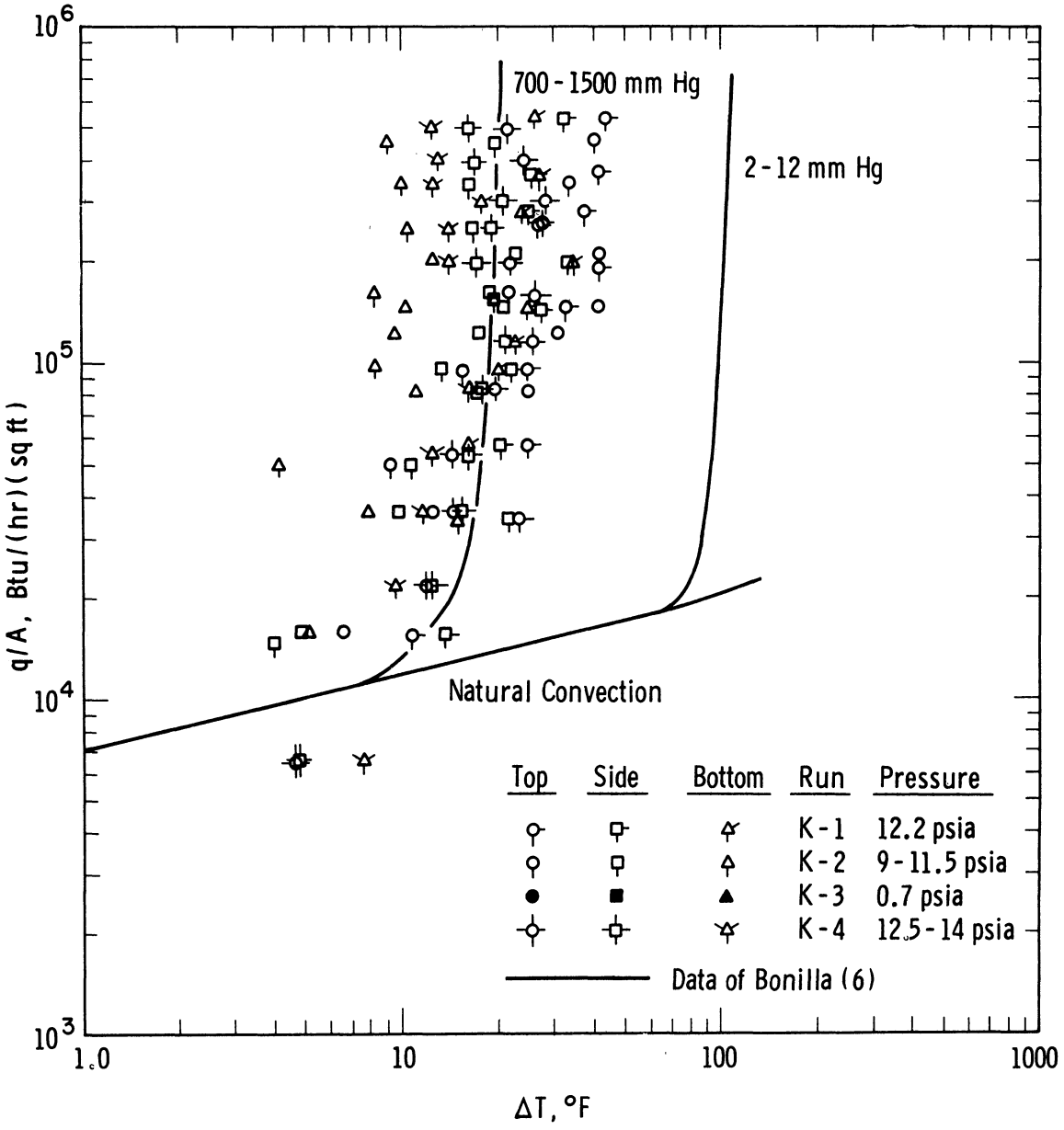


Figure 23. Comparison of Data from Tube 2 with Data of Bonilla (15).

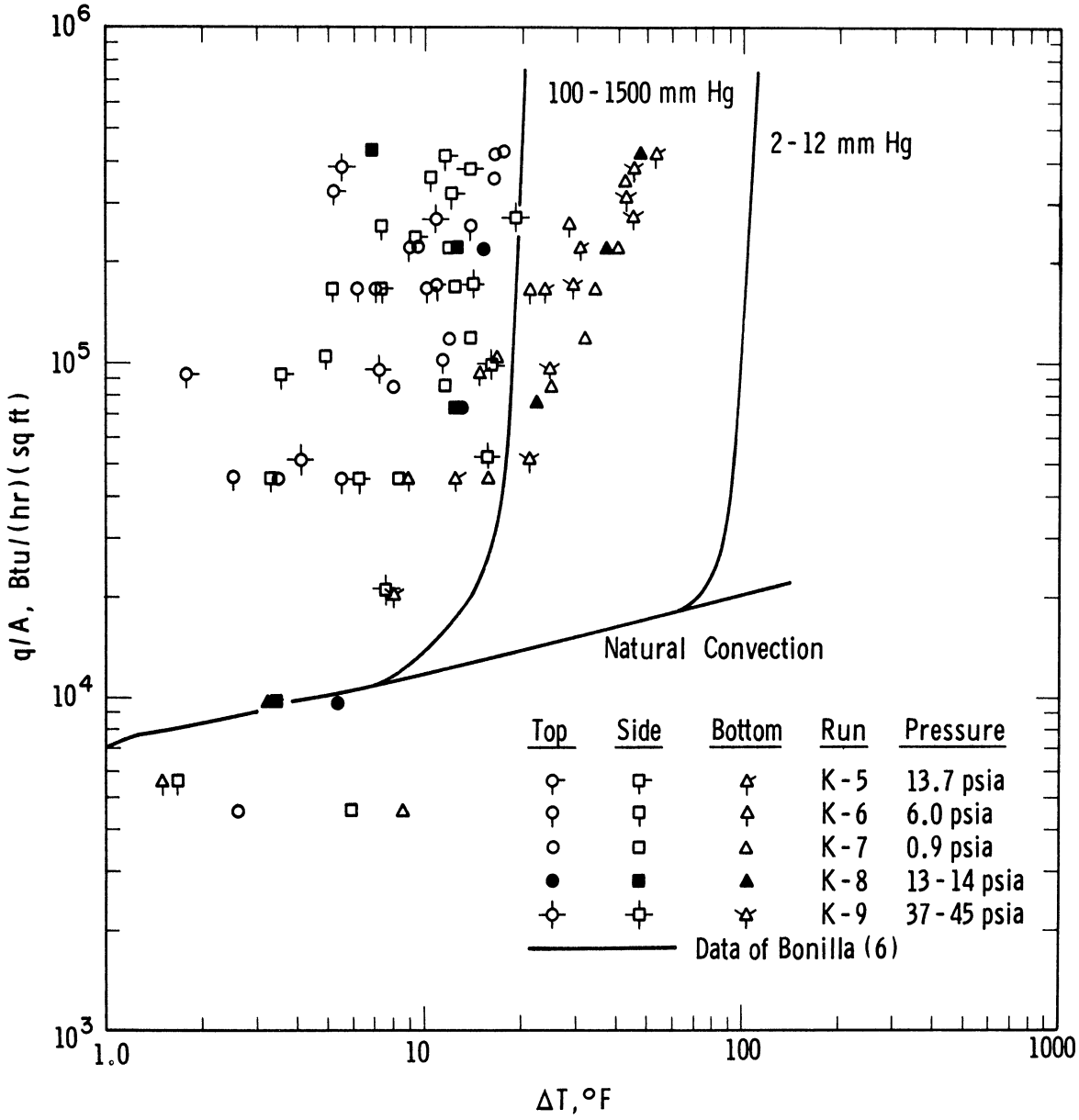


Figure 24. Comparison of Data from Tube 3 with Data of Bonilla (15).

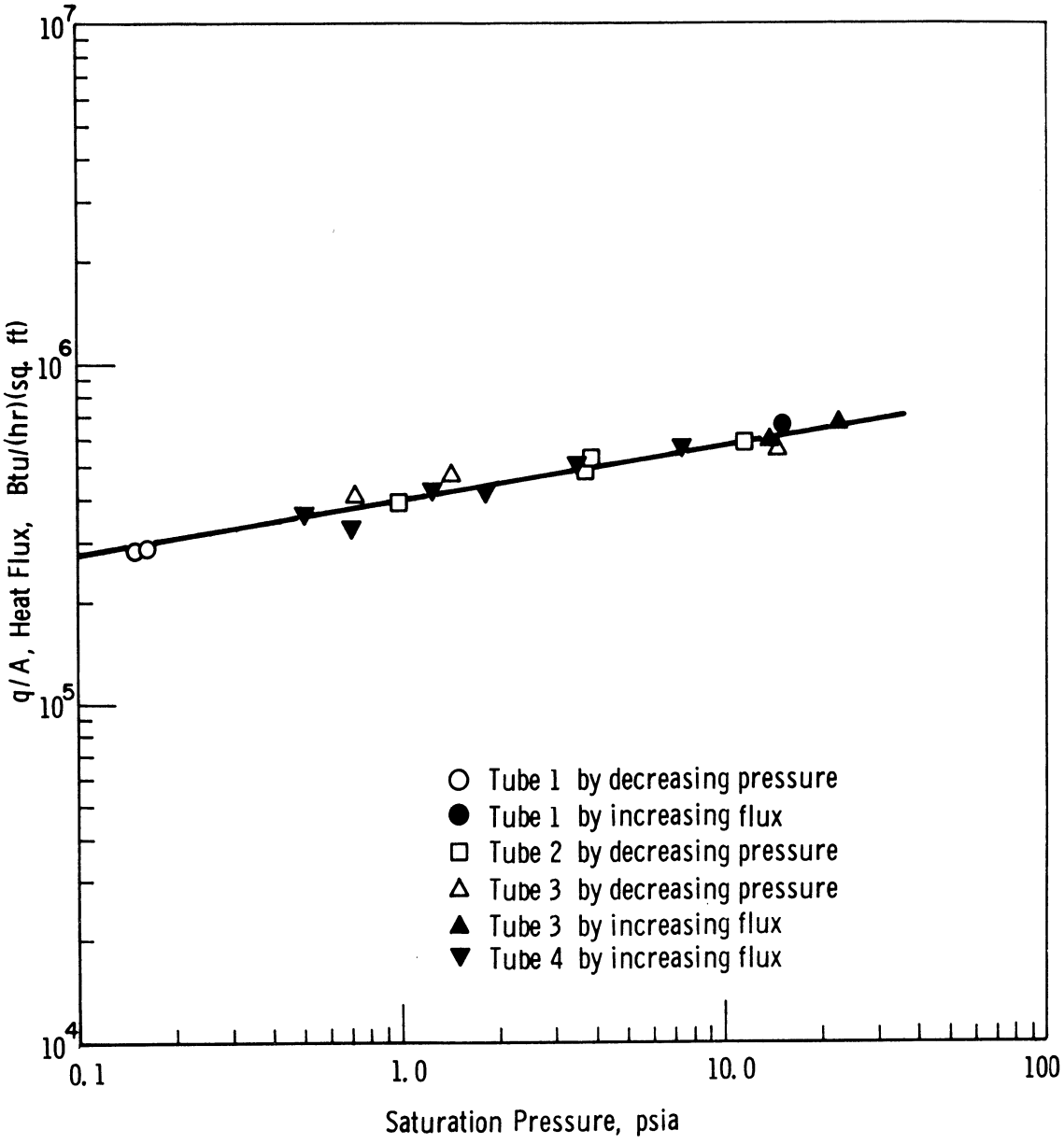


Figure 25. Burnout Heat Flux Versus Saturation Pressure for Saturated Pool Boiling Potassium.

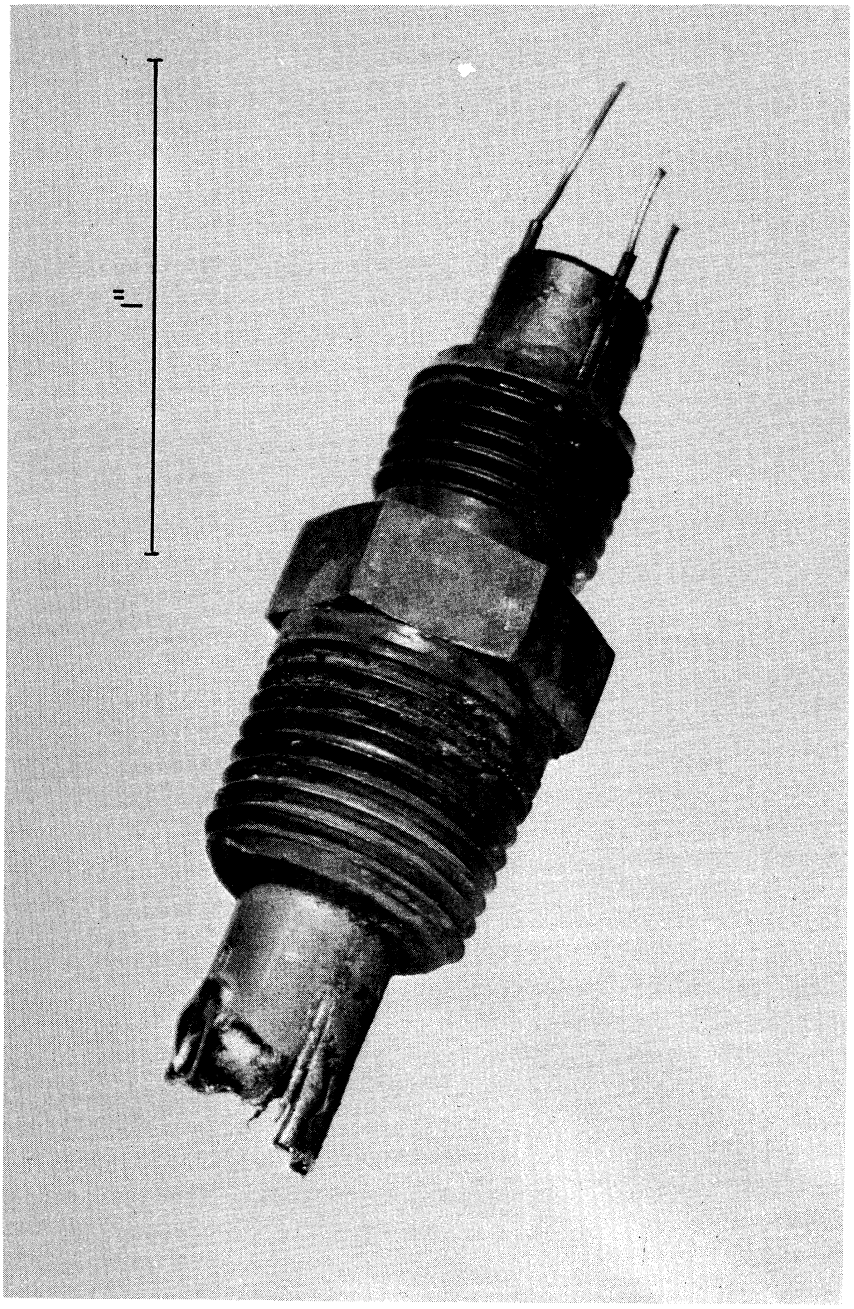

Figure 26. Photograph of Tube 1 After Removal from Apparatus.

the pressure at constant flux. Fortunately, the last increase in flux each time burnout was reached in the former determinations was small enough that the power source could be cut off before complete tube failure. The tube, after removal from the equipment, appeared as it did initially with no noticeable surface changes.

Burnout measurements using tube 4 were made by increases of heat flux at constant pressure. Six determinations were made in the pressure range 0.7 to 7.4 psia. The tube failed on the last burnout determination (7.4 psia), making it necessary to shut down the equipment.

A photograph of tube 4 is shown in Figure 27. It can be seen that a longitudinal crack, nearly 3/4-in long, had developed along the top thermocouple groove, thus exposing the graphite heating element to the potassium pool. In addition, the end of the tube extending into the pool had a hole of approximately 1/16-in diameter melted through it. Either of these failures would have caused the current to short around the graphite heating element and caused tube failure.

Temperature Fluctuations

Temperature fluctuations were observed in the boiling tube thermocouples during all runs. During several runs, pronounced bulk temperature fluctuations as well as pressure fluctuations were observed at low flux levels. Similar fluctuations have been reported in the literature (28, 57, 79, 80, 89, 91).

Figure 28 is a trace of the side tube thermocouple during a 5 psia nucleate boiling run using tube 1. Temperature fluctuations up to 150°F can be noted at flux levels below 250,000 Btu/(hr)(sq ft). In some cases the temperature increased rapidly to a point, then slowly (approximately 1°F/sec) to a maximum value. At this point it instantaneously dropped to the original value. Many times this drop exceeded the initial temperature rise and fell as much as 50°F below the original level. Similar behavior was observed on the other tube thermocouples and to a lesser degree in the liquid bulk. Each instantaneous drop in temperature was accompanied by a drop in the system pressure and an audible bump. The largest bulk variation, measured 1/2-in below the liquid surface (total depth 6-in), was 70°F. This coincided with a tube temperature fluctuation of 150°F shown in Figure 28 at 184,000 Btu/(hr)(sq ft). Above 250,000 Btu/(hr)(sq ft) the amplitude of fluctuations in the boiling tube decreased significantly. Although upward spikes as great as 50°F were frequently observed no significant downward drops in temperature were observed. Above 250,000 Btu/(hr)(sq ft), the bulk temperature and system pressure remained essentially constant. The only significant changes in pressure were gradual increases that followed an increase in flux. This resulted from an increased generation of potassium vapor and subsequent compression of the helium cover gas.

Figure 29 shows a trace of the bottom tube thermocouple for run K-4. A plot of the complete data for this run is shown in Figure 38. Fourteen flux settings are shown on the plot with no level maintained for more than one minute duration. It can be observed that at no time at low flux levels were pronounced fluctuations observed as in the previous figure. Similar fluctuations were recorded during this run for the other boiling tube thermocouples while the bulk temperature remained constant throughout the run. No fluctuations in the system pressure were observed.

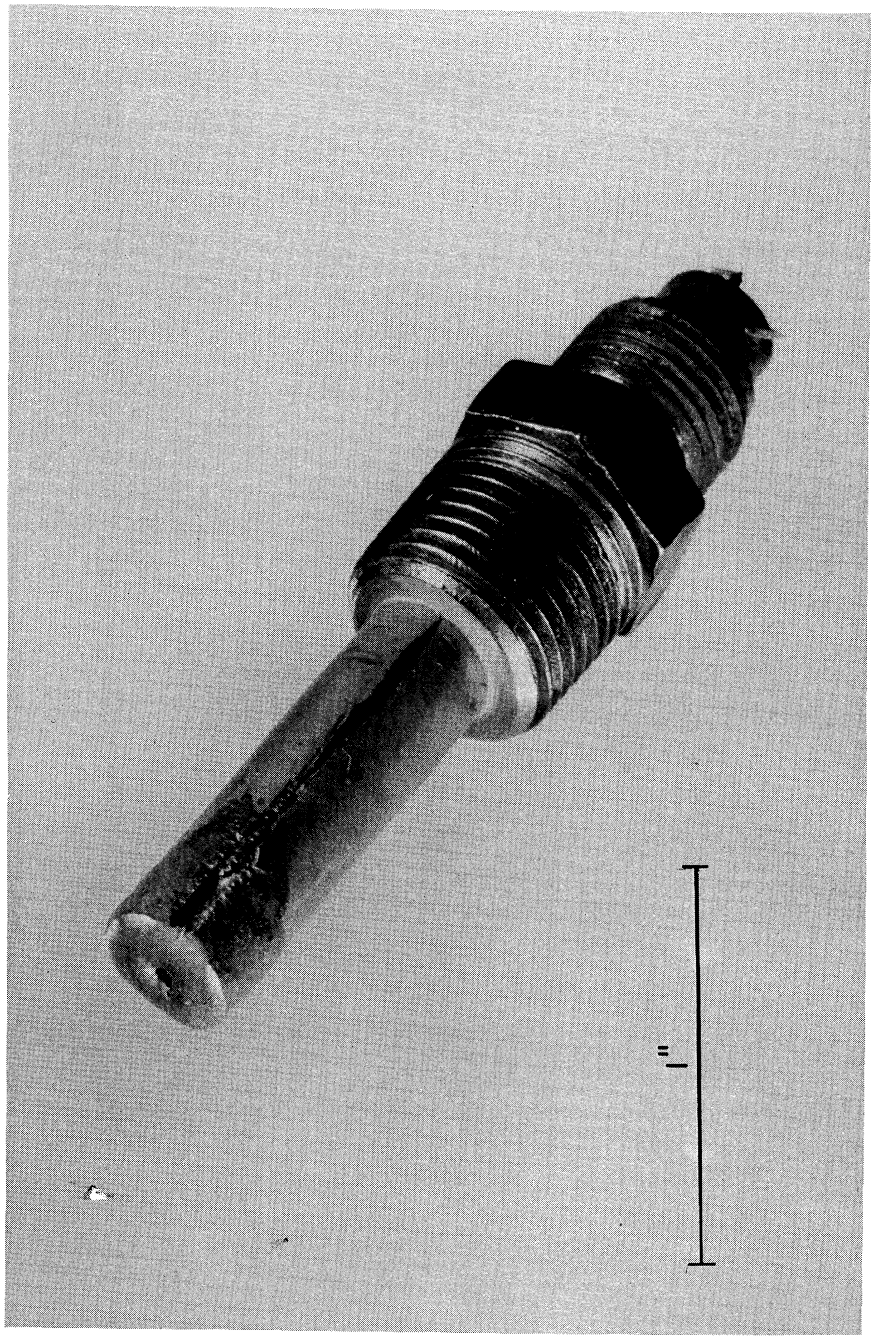

Figure 27. Photograph of Tube 4 After Removal from Apparatus.

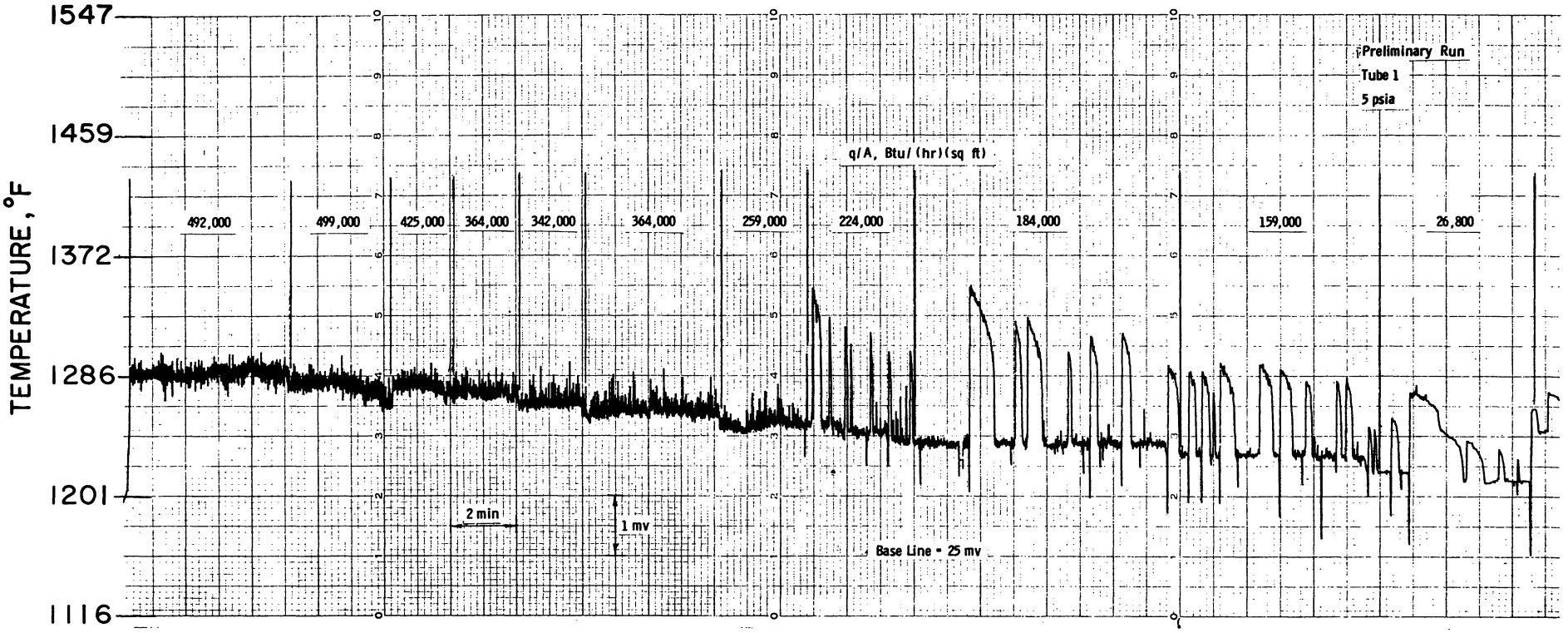


Figure 28. Boiling Tube Thermocouple (side) Trace for Pool Boiling Potassium at 5 psia.

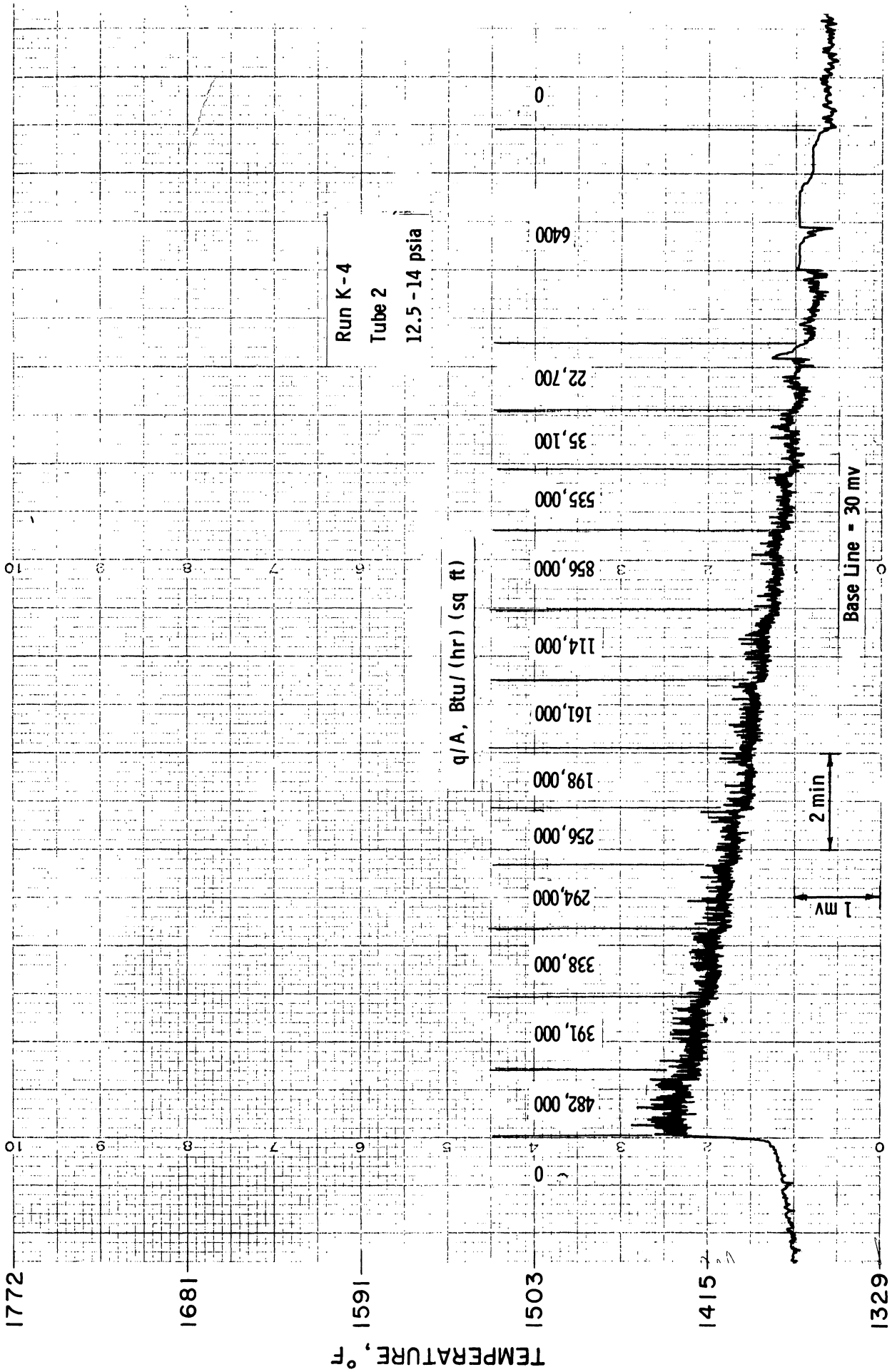


Figure 29. Boiling Tube Thermocouple (bottom) Trace for Pool Boiling Potassium (Run K-4).

The trace for the bottom tube thermocouple in run K-8 is given in Figure 30. Each flux setting in this run was held for at least 7 minutes. The fast response of the system after each flux increase is apparent. Fluctuations at low flux levels seem more pronounced but with a lower frequency than at higher levels. An occasional downward spike can be observed at the lowest flux whereas the only significant spikes at the higher fluxes occur upward. The other tube thermocouples showed similar behavior whereas the bulk temperature or pressure did not fluctuate at any flux level.

Figure 31 is the bottom tube thermocouple trace showing a burnout determination at a constant pressure of 14.6 psia using tube 3. The burnout flux was 359,000 Btu/(hr)(sq ft). Traces for the other tube thermocouples were essentially identical. The emf rise at burnout represents a temperature increase of over 300°F. The sharp drop to bulk temperature following burnout occurred when the boiling tube power supply was turned off. Subsequent temperature rise resulted when the power supply was turned back on and raised to a flux of 434,000 Btu/(hr)(sq ft). This was done to check for possible tube or thermocouple failures. At no time during this run were bulk fluctuations observed.

A trace of the bottom tube thermocouple showing a burnout determination at a constant heat flux of 399,000 Btu/(hr)(sq ft) is shown in Figure 32. At burnout the system pressure was 1.0 psia and was decreasing at the rate of about .02 psia/min. The temperature rise after burnout was over 400°F before the power supply could be shut off. The temperature then dropped to the bulk saturation temperature. Similar behavior at burnout was observed on the other tube thermocouples.

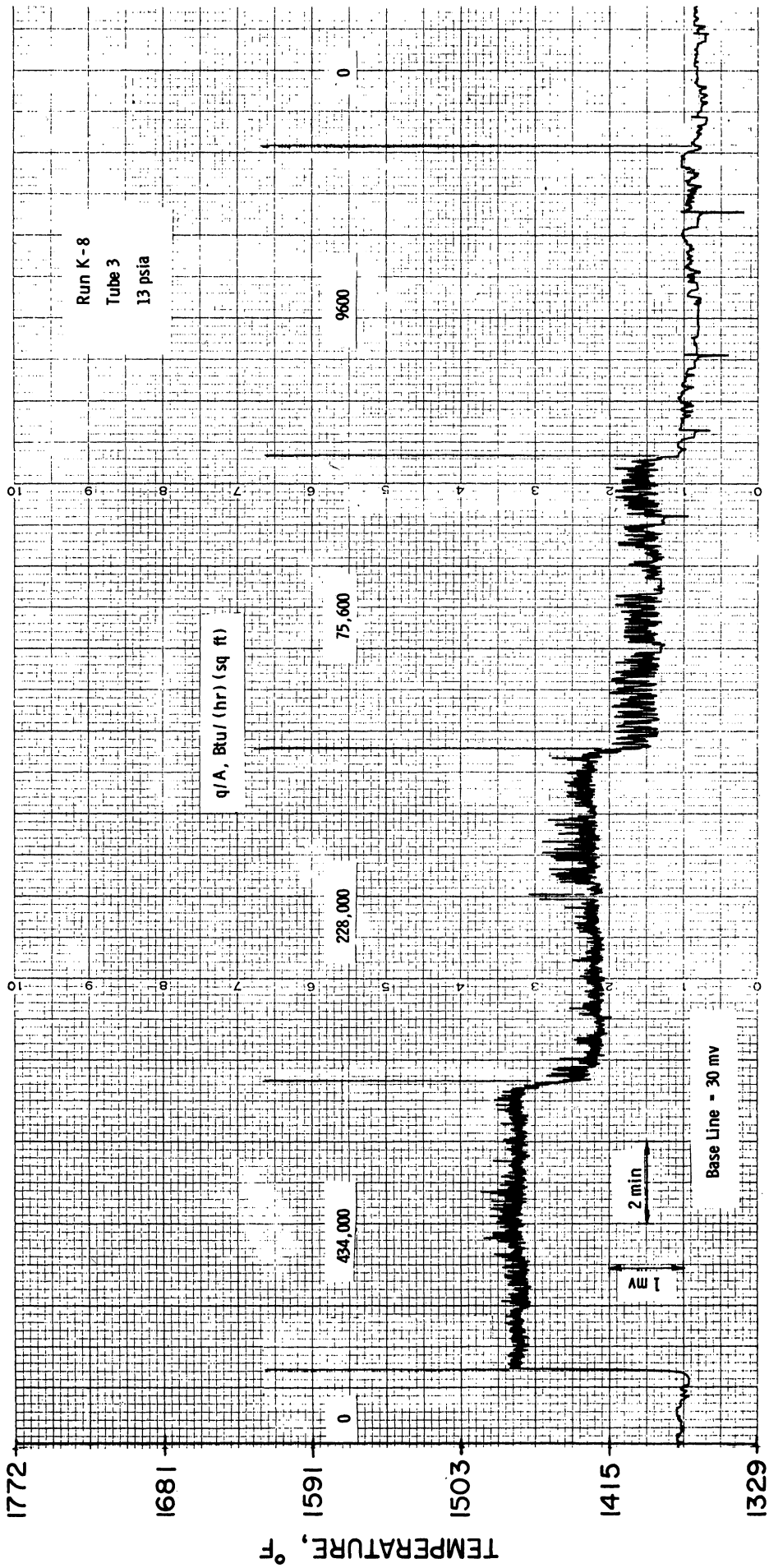


Figure 30. Boiling Tube Thermocouple (bottom) Trace for Pool Boiling Potassium (Run K-8).

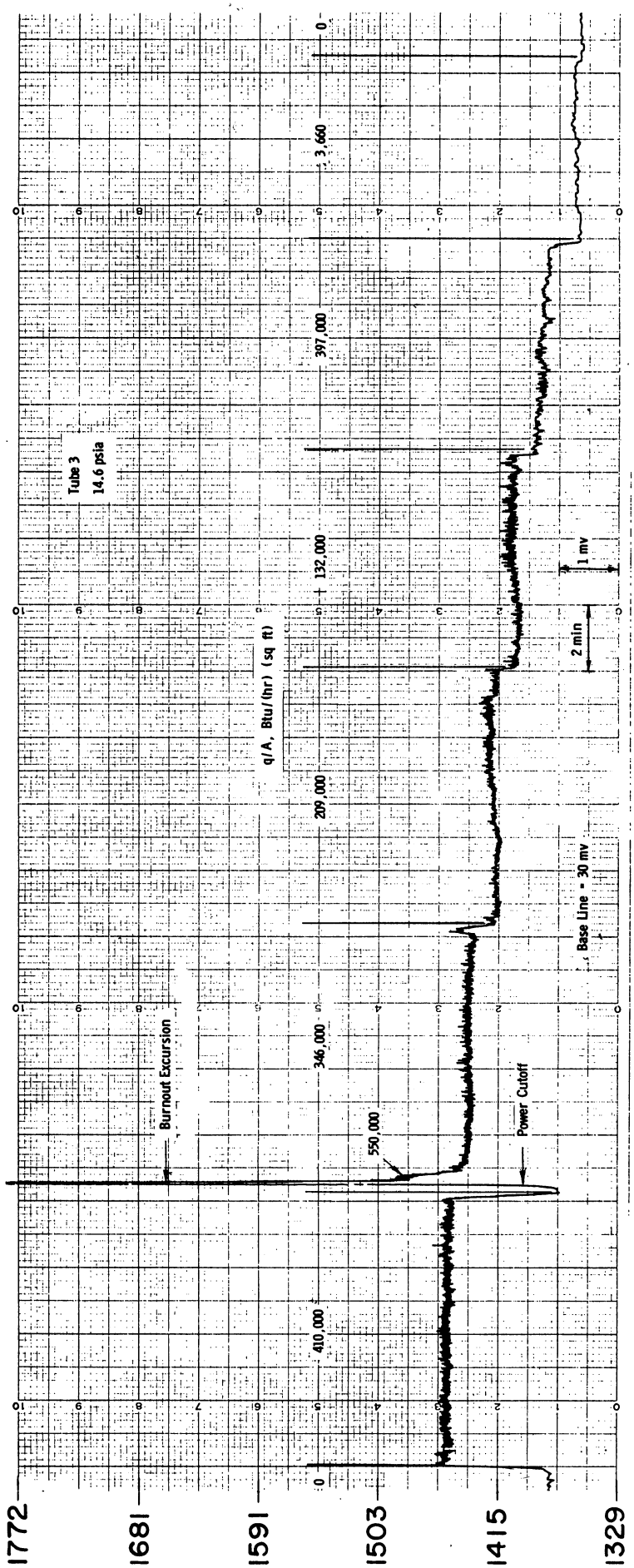


Figure 31. Boiling Tube Thermocouple (bottom) Trace for a Burnout Determination at Constant Pressure.

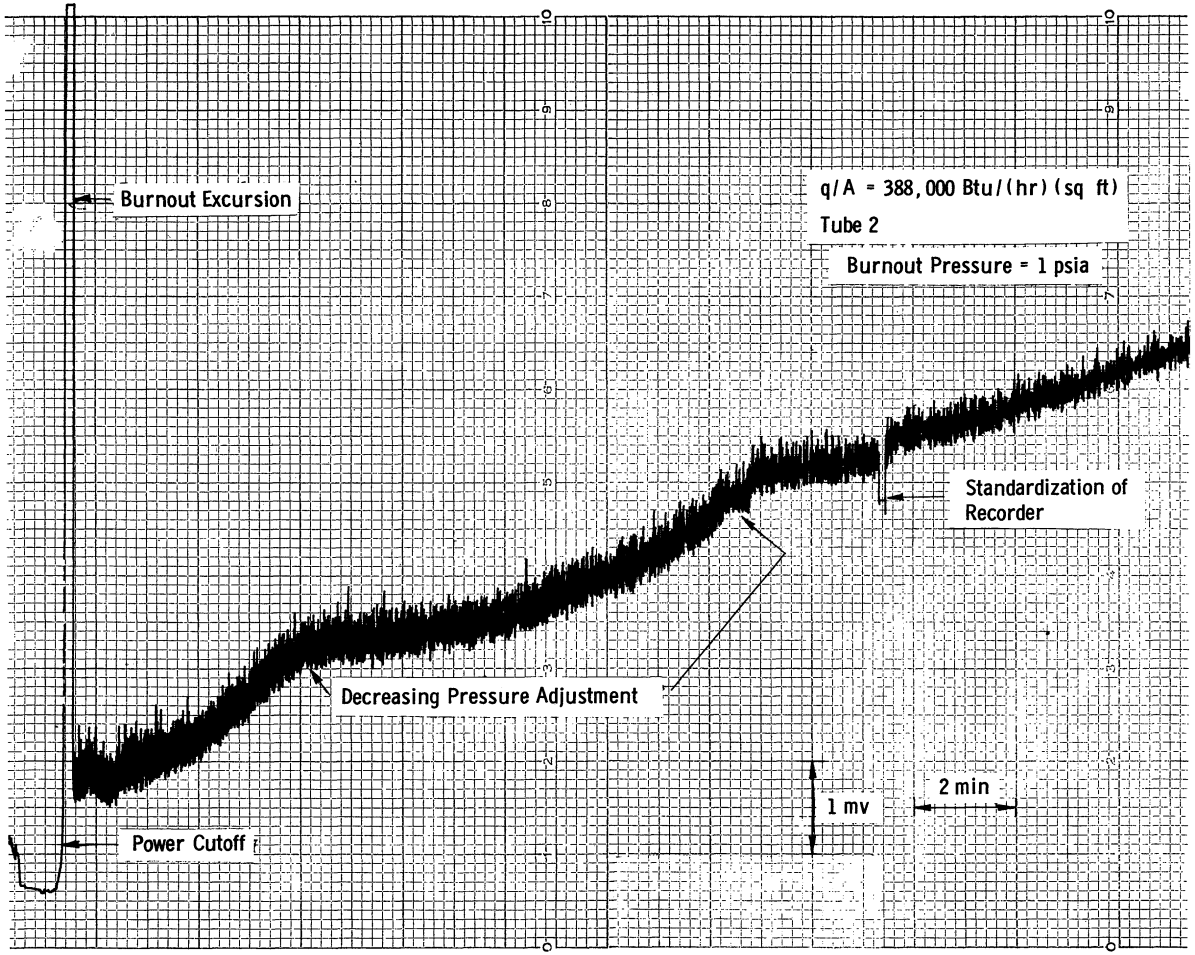


Figure 32. Boiling Tube Thermocouple (bottom) Trace for a Burnout Determination at Constant Heat Flux.

## DISCUSSION OF RESULTS

The potassium results presented in the previous section have provided data which should be very valuable to the understanding and prediction of alkali metal boiling heat transfer. This section will discuss these results and attempt to explain some of the phenomena encountered. Also, comparisons will be made for both the nucleate boiling data and burnout data with existing correlations.

### Nucleate Boiling Potassium Data

The existence of temperature gradients in the potassium bulk liquid was not unexpected. Madsen and Bonilla (80) in their study of NaK pool boiling on a horizontal surface found a similar behavior when they measured temperatures as a function of pool depth up to heat fluxes of 100,000 Btu/(hr)(sq ft). They found that with heat fluxes ranging from 40,000 to 100,000 Btu/(hr)(sq ft) the temperature of the liquid metal in the pool increased with depth to between 80-120°F, based on the free surface temperature. The profile changes with each new heat flux setting. No correlatable behavior could be detected from their data.

The same behavior was observed in the present data for run K-8 shown in Figure 21, however, temperature differences were never greater than 22°F. At zero power input to the tube the liquid pool was not at a constant temperature, but increased 4°F when going 3 to 2 inches from the pool bottom, then fell nearly 22°F from a depth of 2 inches to the bottom of the liquid pool. This superheat, around 2 inches depth, was attributed to heat input from the guard heaters, whereas the filling inlet extending from the bottom of the test vessel was enough to subcool the potassium at the bottom of the vessel. As the flux was increased it was noticed that the gradients similarly increased to a pool superheat of 15°F at 228,000 Btu/(hr)(sq ft). Subcooling on the pool bottom continually decreased for each increase in flux. Above 75,600 Btu/(hr)(sq ft) the level of subcooling at the bottom was 4°F or less with the pool becoming superheated above one half an inch from the bottom. The decrease in superheat at the highest flux was probably due to increased circulation of the liquid promoted by vapor generation.

The nucleate boiling potassium data in this study displayed considerable scatter. By examination of the complete data of tubes 2 and 3 (Figures 23 and 24) it is seen that the $\Delta T$ values, when operating at heat fluxes less than 10,000 Btu/(hr)(sq ft), varied as much as 8°F and were in the range of 1.5°F to nearly 9°F. At fluxes in the order of 500,000 Btu/(hr)(sq ft) the $\Delta T$ values varied as much as 40°F and were in the range from less than 10°F to, in one case, over 50°F. Nevertheless, the general location of the data agrees with data of Bonilla (15) in the range 700 - 1500mm Hg.

The uncertainty in calculating the boiling $\Delta T$ values probably accounted for much of the scatter in the processed data. Appendix B treats this subject in detail, therefore it will be only briefly discussed here. The boiling surface temperatures were determined by averaging thermocouple variations in the tube wall and then extrapolating to the surface. The calculation to extrapolate temperatures to the surface required accurate knowledge of three items: the boiling tube heat flux, depth of thermocouple junction from the tube surface,

and the thermal conductivity for the boiling tube material in the vicinity of the thermocouple junction. Since the boiling $\Delta T$ values in most cases were never larger than 30°F--even at the highest fluxes--it is seen that even the slightest error in any of the above values would significantly distort the boiling $\Delta T$ values. For example, at 500,000 Btu/(hr)(sq ft) a 10 per cent error in any of the above values, singularly, would account for an error of over 5°F in the $\Delta T$.

Although there were undoubtedly errors associated with both the heat flux determinations and the method for measuring the depth of thermocouple junctions, it was felt that the uncertainty in the value for the thermal conductivity, k, of the tube wall was the major source of error. The considerable mass of Nicrobraze, of different thermal conductivity than Haynes-25, surrounding each thermocouple made it very difficult to estimate a good value of thermal conductivity. Using the value of Haynes-25 alone gave $\Delta T$ values (in nearly all runs at high fluxes) that decreased markedly with each increase in flux. This suggests that the mass of the braze was indeed significant and the effective thermal conductivity should be an intermediate value between the braze and Haynes-25. Calculations using the individual thermal conductivities gave $\Delta T$ values at 500,000 Btu/(hr)(sq ft) which differed by 25°F. Using the two-dimensional relaxation method for heat conduction, and using a heat flux of 500,000 Btu/(hr)(sq ft), the boiling $\Delta T$ values were calculated and found to be on the order of 10°F higher than those using the thermal conductivity of Haynes-25 alone. Even these were frequently still as much as 5°F less than those required to give non-decreasing boiling $\Delta T$ values. For this reason it was felt that the best value to use for the effective thermal conductivity should be that value which gave a curve for all runs of the same tube and thermocouple with no reversal in slope.

The lack of any characteristic relation between the heat flux and the temperature profiles which existed in the liquid pool may have contributed to the scatter of the boiling data. Inconsistencies in the temperature profiles for run K-8 (Figure 21) gave reasons to believe that during other boiling runs slightly different gradients could possibly have existed. These, of course, would have been directly related to the boiling $\Delta T$.

Another factor which could have affected boiling $\Delta T$ values was the fact that burnout measurements were made between many of the boiling runs. High flux and high $\Delta T$ values inherent with these determinations may have significantly changed surface properties which in turn could have affected the $\Delta T$. For example, it is known that such factors as surface aging and surface roughness alter the average surface temperature and hence the boiling $\Delta T$ (86).

The one boiling run (run K-10) in which measurements were made on both the increasing and decreasing flux cycle indicated the possibility of significant hysteresis effects with boiling potassium. Although one run is hardly sufficient to substantiate this effect, the apparent break of the boiling curve on the downward cycle is easily distinguished in Figure 20. Behavior of the type suggested by this run is certainly not uncommon. Several investigators haae reported displacements or breaks in the boiling curve on both the increasing and decreasing cycle. The general phenomena has been labeled as hysteresis effects of boiling. Several investigators (8, 29, 122) have found a temperature overshoot on the increasing cycle just before the boiling process transforms from

totally convective to nucleate boiling. This is shown by an extension of the convection boiling curve beyond the point where it normally bends upward due to contribution of nucleate boiling. More will be said about this behavior in the last section of this chapter. Some investigators (63, 71) have found for water that on the decreasing cycle the curve is displaced to the left with a slope similar to the up cycle. Still other investigators (1, 8, 122) have found for water and seven different organic liquids that on the down cycle the curve shifted to the right and possessed a greater slope, by a factor of over two, than that of the increasing cycle.

The present data on the down cycle for all thermocouples first appears to be displaced to the left and then changes in slope and gradually tends back to the right. It seems probable that the low $\Delta T$ of the first heat flux setting on the decreasing cycle resulted from the retention of most of the nucleating sites of the previous setting. It is possible that with further stepped decreases in flux, a disproportional amount of sites became inactive, thus the $\Delta T$ continually increased.

The boiling data for tubes 2 and 3 near atmospheric pressure were averaged and compared to the nucleate boiling correlations presented earlier. This comparison is summarized in Figure 33. The correlations were evaluated using the properties for saturated potassium at 1400°F. The prediction of Levy appears to give somewhat high values for $\Delta T$ even in light of the above discussion on the errors associated with the $\Delta T$. The other predictions give good agreement not only in the location of the curve, but also in the prediction of the slope of the curve within the uncertainty limits of the experiment. The fact that the correlations were developed from the boiling behavior with non-metals indicates the significance of the agreement.

Potassium Burnout Results

The burnout data obtained from either decreases of pressure at constant heat flux or increases in heat flux at constant pressure proved exceptionally reproducible. In no instances did individual data points vary more than 15 per cent from the average curve of Figure 25. Comparison of the determinations made by the two methods gave very favorable agreement and indicated the reliability of measurements by either method. An empirical fit of the pool boiling burnout results is represented by the following equation:

$$q/A = 4 \times 10^5 \, p^{0.167}$$

where q/A is expressed in Btu/(hr)(sq ft) and the saturation pressure, p, in psia.

Figure 34 compares burnout data obtained in this study to several burnout predictions. The predictions are based on theoretical considerations and have in most cases been substantiated with burnout data. Discussions of all predictions except Addoms' are given in the first section of this report. The prediction of Addoms was obtained from reference (86) from a correlation of

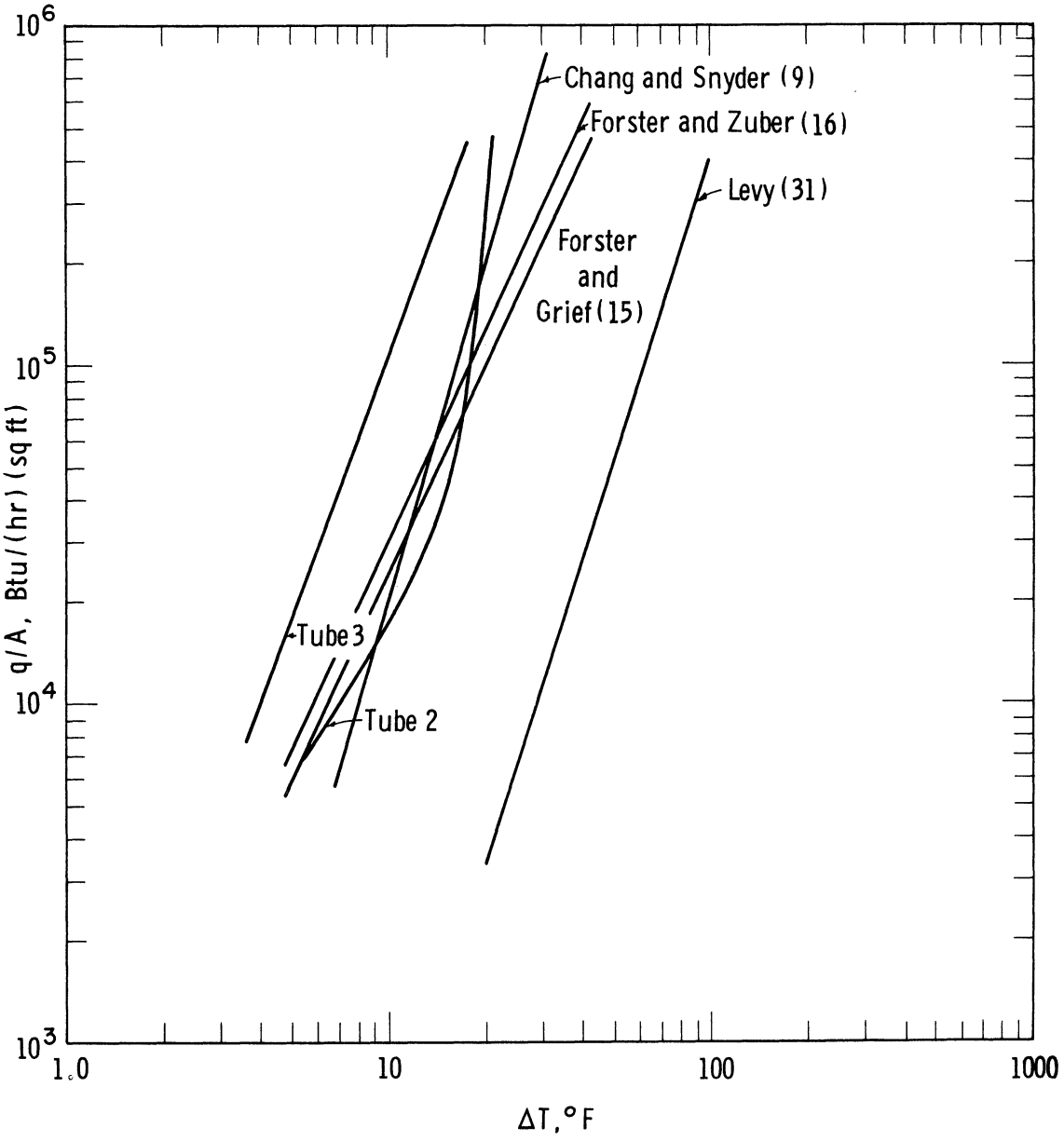


Figure 33. Comparison of Saturated Pool Boiling Potassium Results Near Atmospheric Pressure with Correlations.

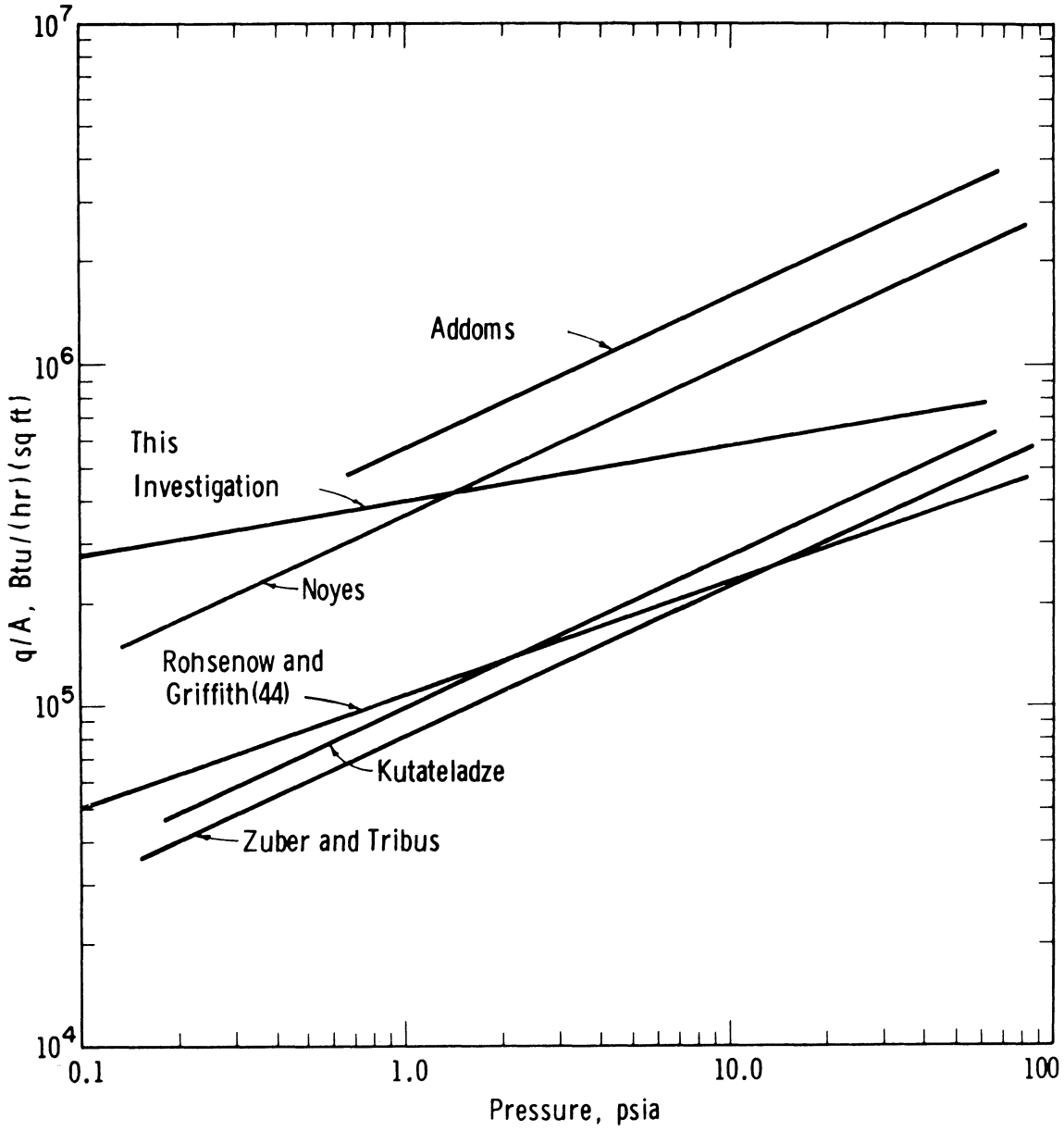


Figure 34. Comparison of Saturated Pool Boiling Potassium Burnout Data with Burnout Correlations.

$(q/A)_{bo}/\lambda\rho_v(gk/\rho Cp)_L^{1/3}$ versus $(\rho_\ell-\rho_v)/\rho_v$ for water and organic liquids. None of the relationships successfully predict the experimental data although Noyes' successfully estimates the magnitude of the burnout level. Recall the fact that Noyes developed his equation by alterations in previous predictions in order to make them compare with his sodium burnout data. It would therefore be expected that his equation would best predict the correct magnitude of the potassium burnout curve.

The theory of Zuber and Tribus (130) for subcooled boiling predicts burnout values (with only a few degrees subcooling) of the same magnitude and slope of the present data. Since this suggests that significant subcooling may have existed, the burnout results and experimental procedures were thoroughly reviewed. Examination of pool temperatures recorded in run K-8 (Figure 21) for fluxes well below burnout indicated that the pool was actually superheated except on the pool bottom where subcooling existed. Since this region of subcooling extended less than one-half an inch into the pool (or two inches below the tube), and superheating existed beyond that point, it was concluded that this would not have had a significant effect on burnout measurements. Also, recall that a majority of burnout determinations were made by gradually lowering the pool saturation temperature (pressure). Obviously, this procedure would have completely eliminated any tendency for subcooling that might have temporarily existed.

The question may also be raised whether the boiling tube end losses had a significant effect on burnout determinations, particularly since tube 1 underwent destructive failure by completely melting at its midpoint. Although an analytical estimate (Appendix C) indicated that these end effects were minor and did not contribute significantly to the boiling results, it was felt that a definitive check should be made. In order to do this, the last boiling tube assembly was fabricated with the three thermocouples located at different locations along the tube length, and, in addition, had a thermocouple fitted into a hole drilled into the Swagelok fitting. This latter thermocouple was intended to indicate the significance of heat losses out the end of the graphite heater contacting the molybdenum. Actually, before any runs could be performed using this tube, the main guard heater surrounding the test vessel shorted out. Thus the temperatures indicated by this thermocouple were lower than would normally be expected and indicated that even under this adverse condition the heat losses out the end of the tube ranged from a high of 7.4 per cent at heat flux of 22,600 Btu/(hr)(sq ft) to a low of 0.13 per cent at a heat flux of 333,000 Btu/(hr)(sq ft).

As previously mentioned, it was found that at any flux level, axial temperature gradients could not be detected with the wall thermocouples. Considering these findings, the conclusion therefore was that end effects were not significant to the burnout behavior in this study.

Temperature Fluctuations

Temperature fluctuations seem to be typical of all boiling systems although with liquid metals the magnitude of fluctuation appears to be greater and more easily identified. Boiling studies of non-liquid metals, which have used conventional temperature recording equipment, have found that temperature fluctuations were usually no greater than about 5°F and were difficult to characterize.

The general temperature behavior observed in the present study was in qualitative agreement with previous liquid metal boiling studies. The rather large temperature fluctuations encountered in the tube wall were also observed by Lyon (79) in boiling sodium, NaK and to lesser degree with mercury containing magnesium and by Madsen and Bonilla (80) in boiling NaK. For sodium boiling at 23,600 Btu/(hr)(sq ft) Lyon frequently observed sudden drops (2 sec. duration) in the wall temperatures followed by recovery. The total cycle covered 15 seconds. Similarly Madsen and Bonilla observed a fluctuating behavior which was also represented by sudden dips in the boiling surface followed by slow recovery. Their data sometimes showed a rapid temperature rise preceding the temperature drop, the rise and fall both taking place in less than 0.5 seconds. Note similar temperature behaviors of the present data at low flux levels in Figures 28, 29, and 30.

The pronounced variations of Figure 28 at low flux levels occurred in nearly all runs early in the study, although throughout the experiment fluctuations of this type were generally experienced at the onset of operation with each new tube. It is interesting to note that fluctuations very similar to these were measured by Moore and Mesler (91) in a study of pool boiling water. By measuring thermocouple voltage signals with an oscilloscope, they were also able to observe characteristic behaviors in regular time intervals. However, instead of cycle periods measured by seconds they found the total time required for a cycle to be in the order of 20 milleseconds. They further found that at higher fluxes the behavior was identical but the temperature dips occurred more frequently.

Careful scrutiny of the fluctuating behavior at low heat flux levels in Figure 28 certainly gives an interesting contrast to the fluctuations at higher fluxes. Recalling the behavior recorded by Moore and Mesler at high fluxes, it is seen by inspection of the present data that although it was not possible to discern any characteristic behavior at the higher flux levels, other than the existence of an occasional upward spike, their significance may become more apparent by examination of the variation encountered at the lower heat fluxes in Figure 28.

Consider a system boiling in the convective region such that the bulk liquid is superheated and actual vaporization occurs only at the liquid surface. As the heat flux is increased, it is obvious that a point will be reached when the temperature difference between the heating surface and the liquid bulk is great enough so that the heat transfer surface instantaneously breaks into nucleate boiling. Corty and Foust (29) found that it was possible to retain convection boiling heat transfer to a much higher T than would be normally required for vigorous nucleate boiling. This is a type of boiling hysteresis discussed earlier in this chapter. Using water Corty and Foust found that superheats as great as 40-50°F above the saturation temperature were possible even though stable nucleate boiling normally began when the $\Delta T$ reached only 25°F. When the flux was further increased to the point that it spontaneously broke into nucleate boiling, the $\Delta T$ then decreased to the normal expected value. Similar behavior was observed by Bankoff, et al (8) in his study of boiling methanol.

Examination of the temperature behavior shown in Figure 28, at heat fluxes below 250,000 Btu/(hr)(sq ft), indicates that the same behavior may have exist-

ed. However, for a given heat flux instead of the nucleate boiling process remaining stable, it was periodically lost with the system reverting back to convection boiling. The upward spikes then may represent a superheating of the system necessitated by a dying out of active nucleation sites. When the superheat again became great enough, the system broke into vigorous boiling with a resultant drop in temperature. Many times this drop exceeded the initial temperature rise and approached the liquid saturation temperature. The behavior agrees with previous investigations of both liquid metals and non-liquid metals discussed earlier in this section. Immediately after this temperature drop the temperature fluctuations indicated stable boiling. After a time--dependent on heat flux level--stable boiling was lost and the process repeated.

As the flux level was increased, these upward temperature spikes occurred more frequent and with shorter duration. Finally, the upward spikes were of such short duration that the subsequent drop in temperature was almost instantaneous. At the higher fluxes if the temperature of the surface dropped below the normal nucleate boiling value, the rapid recovery was nearly always faster than the response time of the recorder thus dips were generally not detected. This would explain why downward spikes were markedly less frequent than those occurring upward.

## CONCLUSIONS

The following conclusions may be drawn as a result of this investigation:

1. The agreement of the water data with a previous investigation (79) demonstrated the reliability of the results obtained with the experimental apparatus.

2. The nucleate boiling curve for potassium in a saturated pool may be predicted within the uncertainties of this study by the equations of Chang-Snyder (21), Forster-Grief (37), and Forster-Zuber (38). In addition, the data compared favorably with the potassium results of Binilla (15). Mean wall superheats were in the order of 20°F for heat fluxes over 100,000 Btu/(hr)(sq ft).

3. Measurements made on both increasing and decreasing heat flux cycles indicated the possibility of significant hysteresis effects with boiling potassium.

4. Mixing of the potassium pool in this study was insufficient to maintain a constant pool temperature. The temperature gradients which existed throughout the liquid potassium pool were associated with liquid superheat. In general, increases in heat flux gave similar increases in pool superheat.

5. Saturated pool boiling potassium burnout data can be represented by a straight line when plotting the burnout heat flux versus the saturation pressure. An empirical equation representing the data is:

$$(q/A)_{bo} = 4 \times 10^5 \, p^{0.167}$$

Furthermore, burnout measurements obtained at constant flux by decreasing the pressure or at constant pressure by increasing the heat flux give consistent and reliable results.

6. Existing burnout correlations based on liquid thermal transport properties as well as hydrodynamic properties of a two-phase system do not successfully predict the experimental potassium burnout data obtained in this study.

7. Pronounced temperature fluctuations between 10 and 150°F exist in the heat transfer surface during the boiling of potassium. Below 250,000 Btu/(hr)(sq ft) temperature fluctuations in the bulk liquid are common and are usually accompanied with noticeable pressure fluctuations.

# FILM BOILING OF POTASSIUM

Andrew Padilla, Jr.

## INTRODUCTION

Unlike the forced-convection and nucleate-boiling regimes, the film-boiling region has been the subject of relatively few analytical studies and very few experimental investigations. The process is physically characterized by a layer of vapor which separates the boiling liquid from the heating surface. Energy transfer through the vapor layer occurs by conduction, convection, and radiation and the fluxes expected at reasonable temperature levels are substantially lower than those in the nucleate-boiling regime.

Since the apparatus for the present investigation utilizes a horizontal disc as the boiling surface, it is important to note the film-boiling correlations in the literature for a horizontal surface. These analytical studies have been undertaken only within the last five years. In 1959, Chang (22) introduced his wave theory based on hydrodynamic considerations. He assumed that the phenomenon might exhibit waves whose wavelengths would be equal to the critical value for the existence of a standing wave over a horizontal surface. He then proceeded to derive an expression for the heat transfer coefficient. Later, Zuber (131) assumed that a more significant wavelength might be the most dangerous wavelength; that is, the one for which the amplitude grows most rapidly. By assuming that the process is governed by a two-phase Taylor instability, he derived equations for predicting the minimum heat flux. Berensen (12) modified and extended the hydrodynamic approach used by Zuber and obtained relationships for both the heat transfer coefficient and the temperature difference at the minimum.

The correlations of Zuber and Berensen have been used to predict the temperature differences and the fluxes corresponding to the minimum point for various liquid metals boiling at 1 atm.

| | Zuber | Berensen | |
|---|---|---|---|
| | $(q/A)_{min}$ Btu/hr-ft$^2$ | $(\Delta T)_{min}$ °F | $(q/A)_{min}$ Btu/hr-ft$^2$ |
| Rb | 4,760 - 6,230 | 301 | 3600 |
| K | 11,100 - 14,500 | 323 | 4700 |
| Na | 12,000 - 15,700 | 201 | 5100 |
| Li | 12,600 - 16,500 | 220 | 9500 |

Data on film boiling from a 2-inch diameter horizontal surface was obtained by Berensen (12) for n-pentane and carbon tetrachloride. The experimental values of temperature differences and fluxes at the minimum agreed within ± 10 per cent with his correlation. Hosler and Westwater(55) investigated water and Freon-11 on an 8-in square horizontal surface and found that their heat fluxes at the minimum were approximately twice that predicted by Berensen's correlation. However, Berensen's prediction of the film boiling curve at higher

temperature differences agreed well with their data. They concluded that Chang's correlation was not reliable. Ishigai, et al. (61) studied the film boiling of water on a flat surface facing downward.

The purpose of the present study was to investigate heat transfer in the stable film boiling regime for potassium boiling at 1400°F to 1800°F.

## DESCRIPTION OF EQUIPMENT

When ebullition is governed by the heat flux (electrical heating), as opposed to control by the temperature-driving force (condensing media), any increase in heat flux above the critical heat flux causes the surface temperature to rise rapidly in an effort to compensate for the decreasing coefficient. If this temperature rise causes the surface to exceed its melting point, the phenomenon of "burnout" occurs. A system governed by the heat flux is basically unstable near the critical heat flux since, for a given value of the heat flux, three values of temperature difference corresponding to operation in the nucleate- transition- and film-boiling regimes are possible. However, operation in only one regime is observed for a given temperature difference. Consequently, the present apparatus has been designed to control the temperature difference, using a condensing medium as the heat source.

A schematic diagram of the experimental system with details of the tube assembly and the boiling plate are shown in Figures 43, 44, and 45 respectively. Figure 46 shows the tube assembly mounted in its support frame. Sodium is boiled in the bottom chamber of the tube assembly by means of a radiation heater and condenses on the bottom surface of a horizontal boiling plate. The potassium boils on the top surface of the plate and condenses in the upper part of the tube assembly which radiates to the walls of the containing vessel.

### Tube Assembly

The tube assembly is a composite Cb-1 Zr/Haynes-25 assembly 4-ft 2 1/2-in long fabricated by the Space Power and Propulsion section of the General Electric Company. Welded to the 2-inch boiling plate section are 10 inches and 6 inches of Cb-1 Zr tube at the top and bottom respectively. The wall of Cb-1 Zr tube is machined from 150 mils to 60 mils 3 inches above and 2 inches below the boiling plate to reduce axial conduction around the boiling plate. The bottom sodium chamber is reduced from 1.10 inches to 0.45 inch diameter with 4 inches of Cb-1 Zr and 2 inches of Haynes-25 added to reduce the temperature before transition to a stainless steel fitting. The relatively long section of Haynes-25 tube at the top radiates to the walls of the outer vessel before passing through the supporting flange. Water coils tacked onto the 6-in section of Haynes which extends above the flange can be used if radiation proves inadequate in maintaining reasonable temperature levels in the vicinity of the flange.

### Boiling Plate

The boiling plate was machined from a solid rod 1.10 inches in diameter and 2 inches long. The plate is 196.5 mils thick and contains eight 21-mil thermocouple holes at three different depths below the boiling surface and at

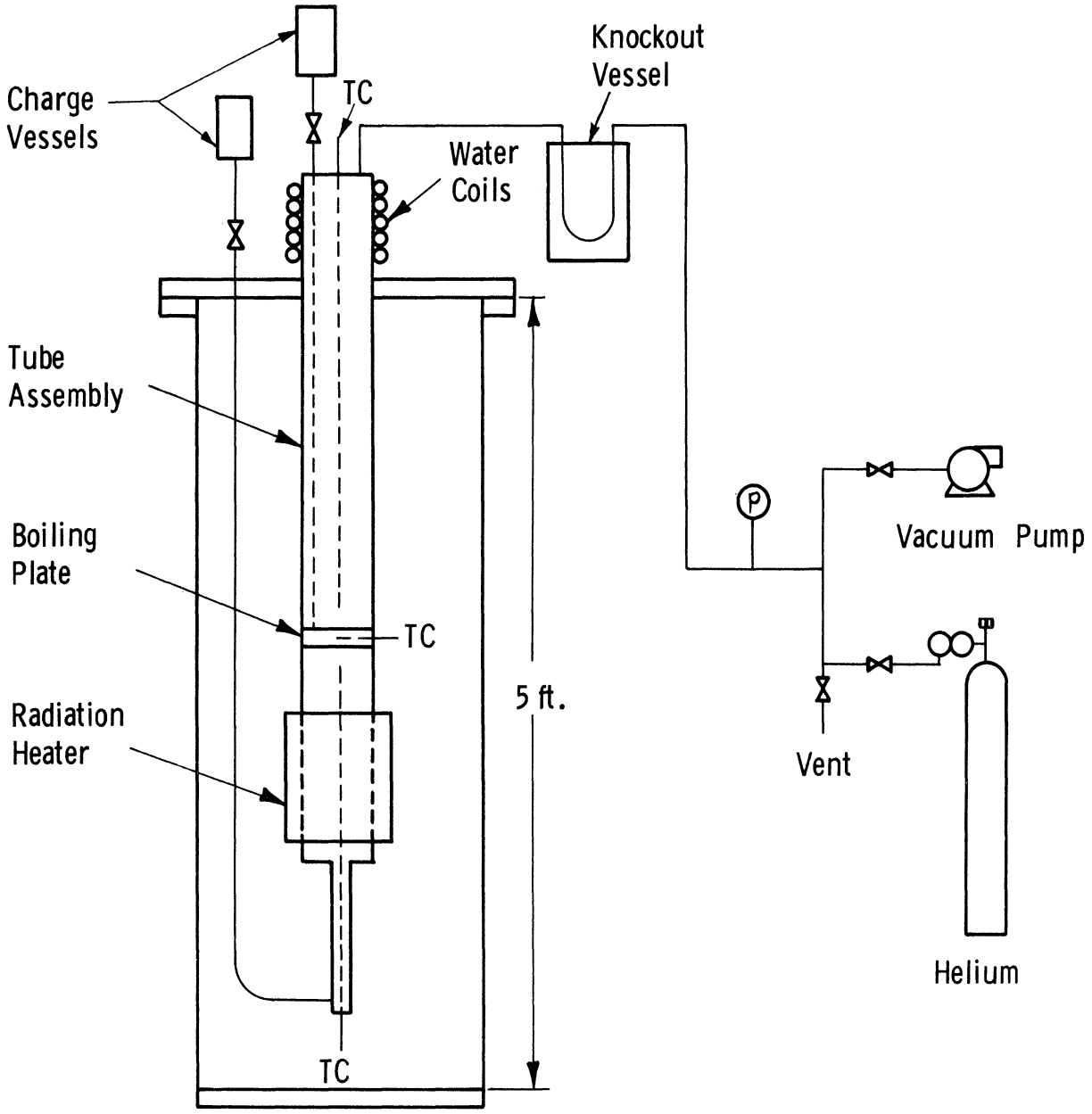


Figure 43. Schematic Diagram of Film Boiling Experimental System.

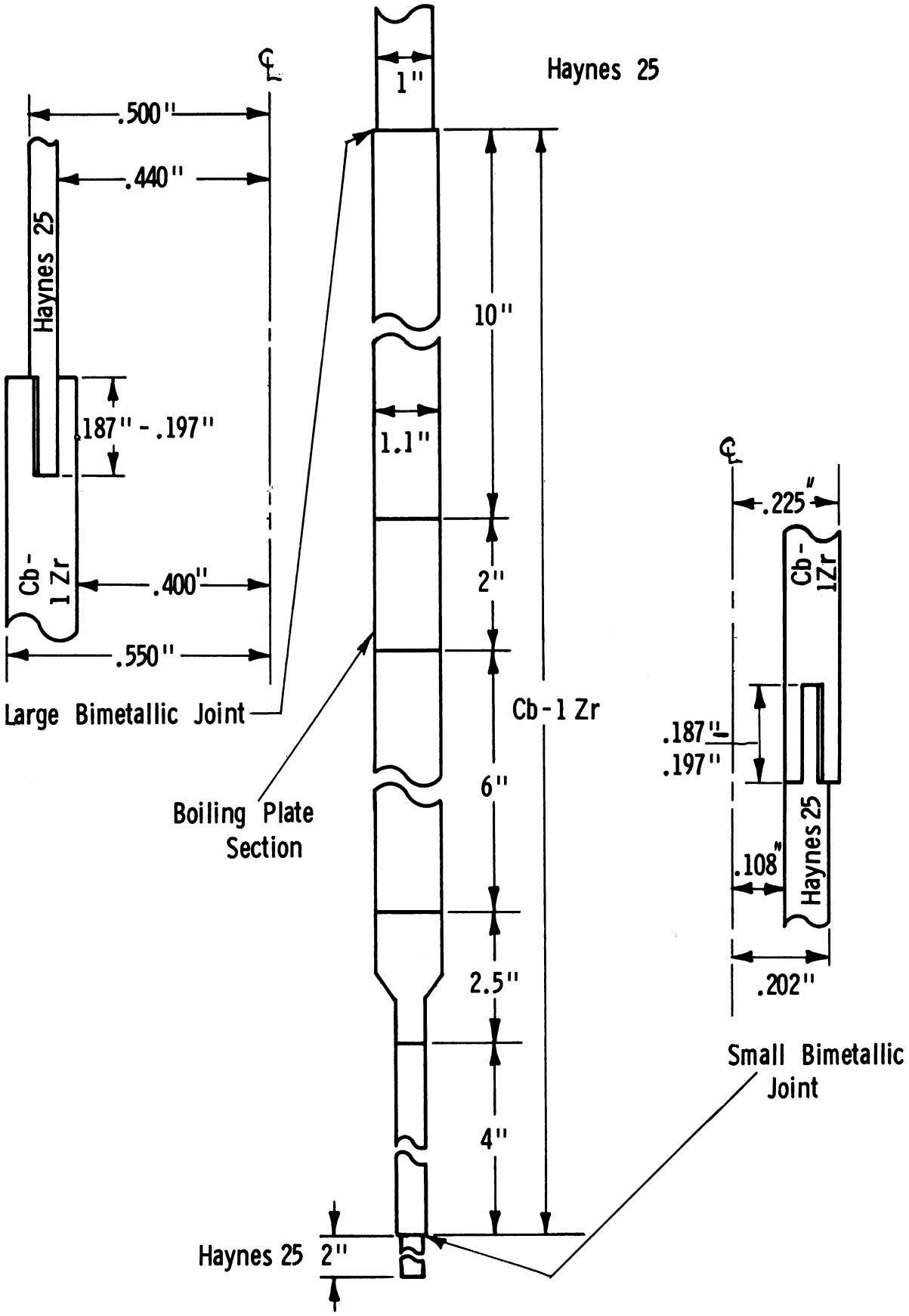


Figure 44. Tube Assembly.

Thermocouple Hole Diameter 0.021"
Radial Depth of Thermocouple Holes

| | |
|---|---|
| 1 | .250" |
| 2 | .450" |
| 2A | .450" |
| 3 | .250" |
| 4 | .450" |
| 5 | .280" |
| 5A | .250" |
| 6 | .450" |

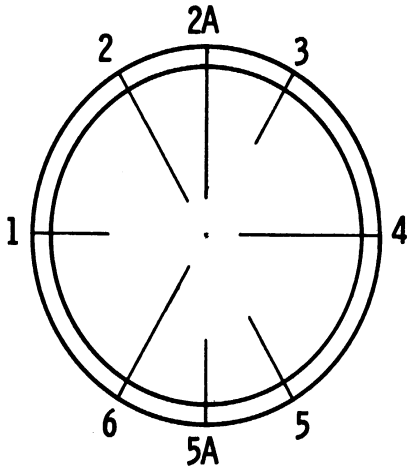


Inner Thermocouple Holes - 120° Apart
Outer Thermocouple Holes - 120° Apart
#2A Hole - 30° from #2
#5A Hole - 30° from #5

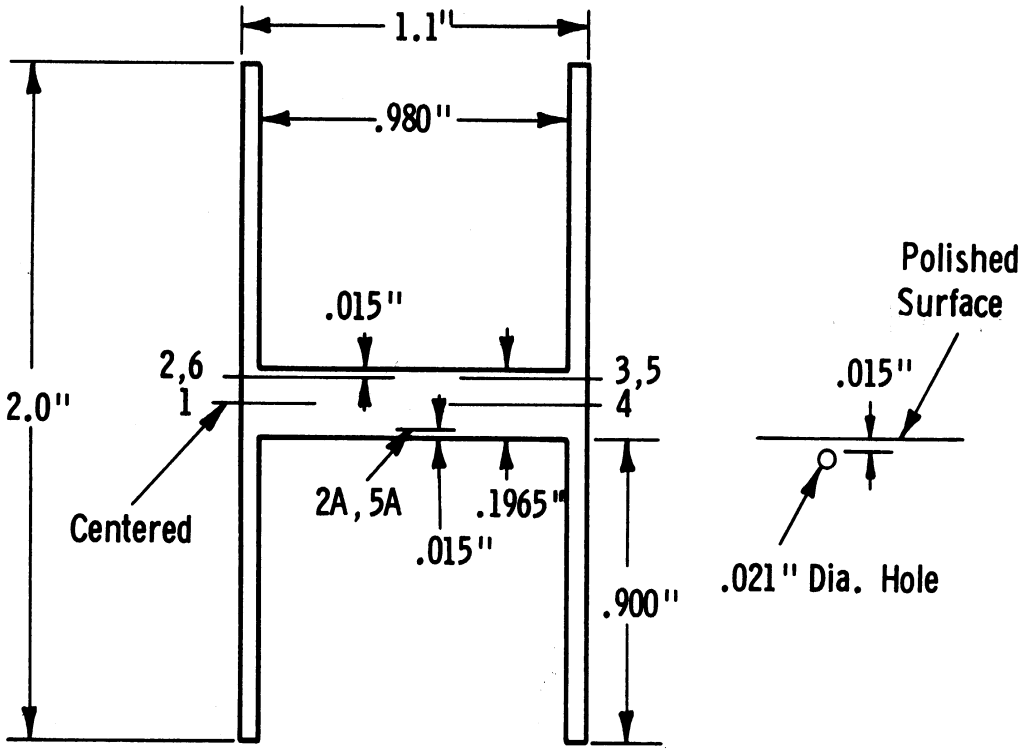


Figure 45. Boiling Plate Section.

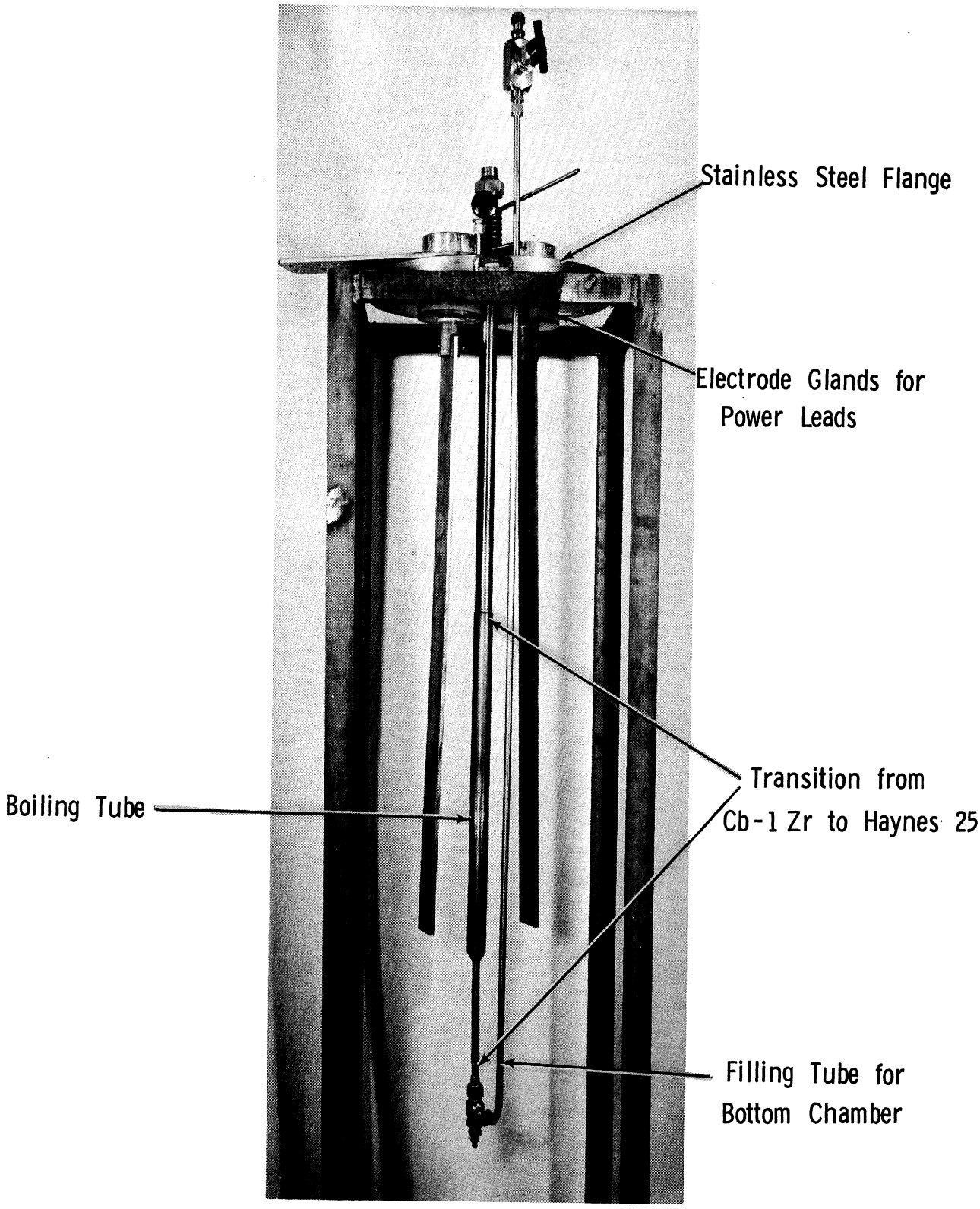


Figure 46. Tube Assembly Mounted in Support Flange.

two different radii. The tube wall above and below the boiling plate is 60 mils thick, giving a 0.98-in diameter boiling and condensing surface. Both surfaces were mechanically polished and photographed prior to assembly of the composite tube. (See Figures 47 and 48.)

Outer Vessel

The tube assembly is supported by a 150-lb stainless steel blind flange and surrounded by a 5-ft long, schedule 5, 8-in stainless steel pipe. The pipe is capped off at the bottom with a stainless steel plate with a 125-lb stainless steel slip-on flange at the top. A Viton O-ring is used to obtain a vacuum seal. A 5/8-in hole in the side of the pipe allows for evacuation of this environmental chamber. Four Conax thermocouple glands through the top flange provide flexibility in making electrical and thermocouple connections. A bus bar system extends through the top flange and serves to introduce DC current from the rectifier. Copper rods 1 1/4 inches in diameter connecting copper tongues on the outside to bus bars inside the vessel are electrically insulated from the flange by lava glands using O-ring seals.

Auxiliary Lines

Access to the bottom sodium chamber of the tube assembly is made through a 3/8-in stainless steel filling line through the top flange. A vacuum seal is obtained using a Veeco O-ring coupling which permits longitudinal movement of the filling line to avoid stresses due to thermal expansion of the tube assembly. The filling line for the potassium chamber is a 3/16-in Haynes-25 tube which extends down from the top of the tube assembly to approximately 1/4-in above the top surface of the boiling plate. The line to vacuum and inert gas pressure at the top of the tube assembly runs through a knockout vessel filled with stainless steel shavings.

Heaters

Several radiation heaters for the bottom sodium chamber have been tried. These include the use of tantalum foil, graphite cloth, and Hevi-Duty electrical heaters. The first heater was made from two 2 1/2-in by 4-in sections of 3-mil tantalum foil formed into two half cylinders. Tantalum strips 1/2-in wide by 30-mils thick were used to hold the foil in place at the top and bottom, the result being a split cylinder approximately 2 inches in diameter and 4 inches long around the 1.1-in tube assembly. Power to the tantalum heater was supplied through the bus bar system from the 12 KVA Udylite rectifier.

The tantalum heater was used during the initial runs with water. However, inadequate environmental control of the outer vessel resulted in catastrophic oxidation of the tantalum. Although another tantalum heater was fabricated, it was decided to use a different type of heater because of the acute oxidation problem which would have been encountered at higher temperatures.

A graphite cloth heater with the same split-cylinder shape using stainless steel clamps was constructed. Flexible copper strap connected the clamps to the bus bar system. This heater was successful in obtaining film boiling of potassium under vacuum. However, electrical arcing occurred between the stain-

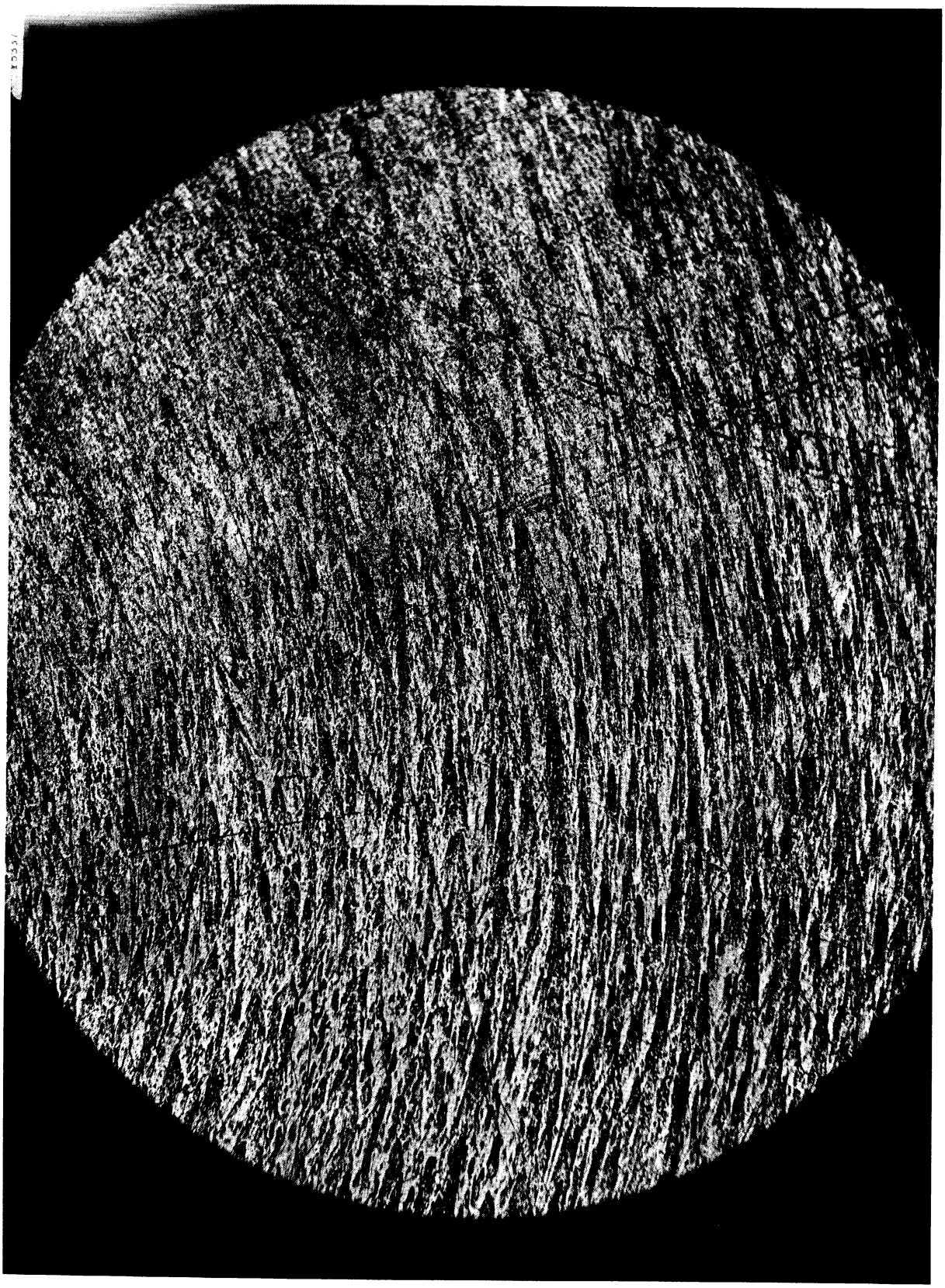

Figure 47. Boiling Plate Top Surface Typical Area (85X)

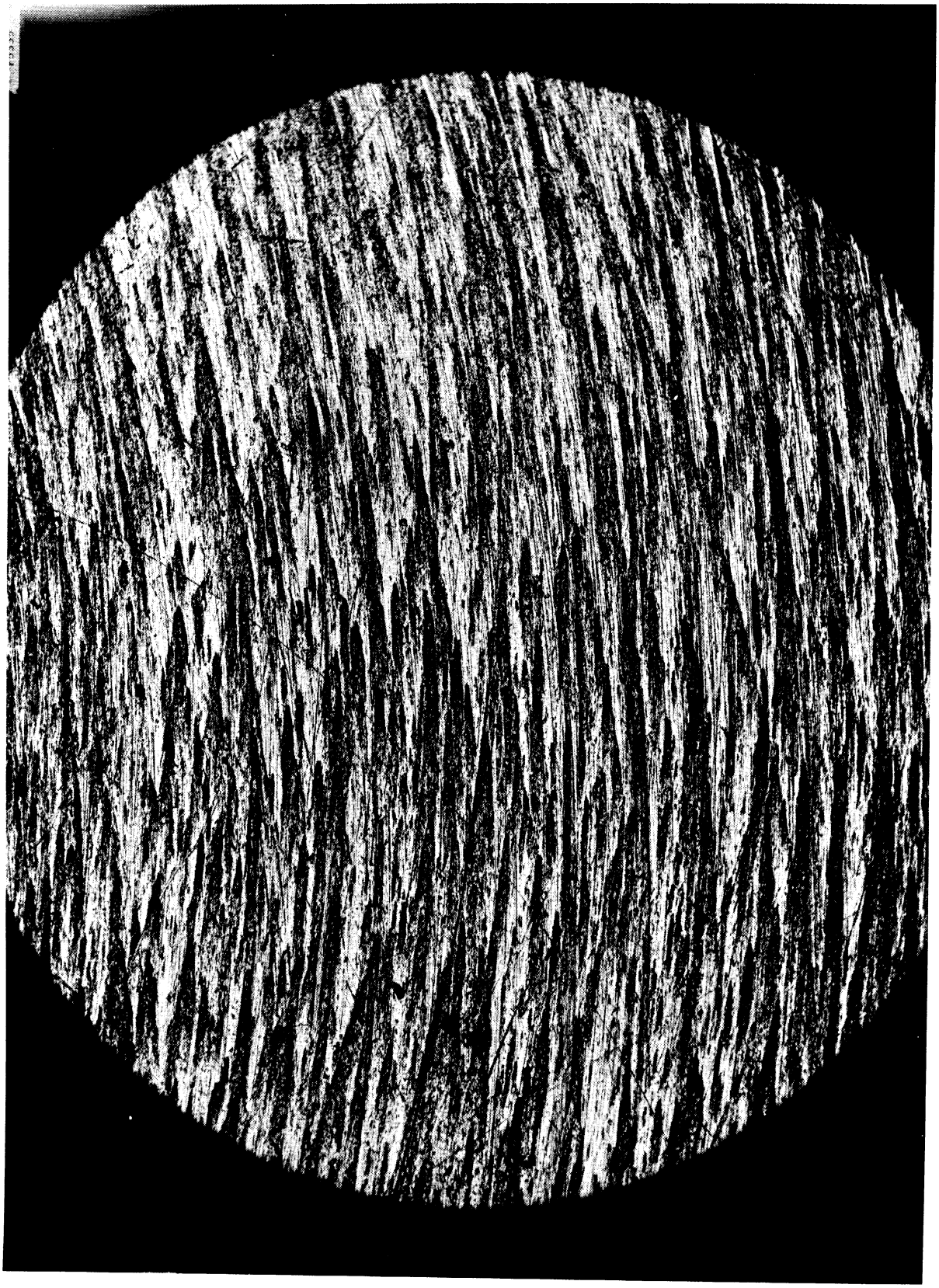

Figure 48. Boiling Plate Bottom Surface Typical Area (85X)

less steel clamps and the graphite cloth at higher currents causing failure of the heater. To avoid excessive contact resistance at high currents, graphite leads would have had to be used.

The heaters currently being used are Hevi-Duty furnace elements. A 2 1/8-in OD by 1 1/4-in ID by 8-in long element is placed around the sodium boiler with a larger 3 1/4-in OD by 2 3/8-in ID by 8-in long element placed around it to insure adequate power. These two heaters are surrounded by four concentric stainless steel shields to minimize radial heat loss outward. Another Hevi-Duty element with two radiation shields is used above the boiling plate to prevent subcooling of the boiling potassium. Power to the inner sodium boiler heater is supplied through a 220-volt variac while the other two are connected to 110-volt variacs. The electrical connections are made through the Conax glands. Using the sodium boiler inner heater alone, film boiling of potassium under vacuum has been obtained with boiling plate temperatures up to 1500°F.

Instrumentation

The temperature of the boiling potassium is measured with an adjustable Haynes-25 thermowell extending down from the top of the tube assembly through a Conax gland. The temperature of the condensing sodium is measured by means of a tantalum thermowell extending up from the bottom of the tube assembly through a stainless steel Swagelok fitting. Both of these thermowells contain thermocouples made from 24 gauge Chromel/Alumel wire.

The eight micro-thermocouples in the boiling plate are 20-mil OD, inconel-sheathed, Chromel/Alumel thermocouples with MgO insulation. Control temperatures inside the vessel include the outer surface of the guard heater, the outer radiation shield around the sodium boiler, and the stainless steel fitting at the bottom of the tube assembly.

Temperatures are monitored on a 12-point temperature recorder. When steady-state conditions are obtained, a double-switch circuit allows either temperatures or temperature differentials to be measured. Stable outputs are measured with a Leeds and Northrup No. 8662 portable potentiometer while fluctuating temperatures are recorded on a continuous temperature recorder.

The pressure in the potassium chamber is measured with a mercury manometer. A 0-60 psig Bourdon gauge is also in the line for leak-testing purposes.

## OPERATING PROCEDURE

### Water Runs

The apparatus was operated with water as the fluid in both compartments to predetermine the importance of edge effects arising from the use of a relatively small boiling surface. The film-boiling data would have been compared with the results of Hosler and Westwater. However, operation was severely limited because of the undesirability of heating Cb-1 Zr over 400°F while in contact with water.

Nucleate boiling data at 1 atm was obtained but these runs did not yield film-boiling data as anticipated. Boiling at reduced pressures was also carried out in an attempt to lower the temperature at which film boiling could be attained, but overloading of the condenser occurred in the nucleate boiling regime. Another technique tried was to heat the boiling plate with the upper chamber empty and them slowly introduce fluid onto the boiling plate. Due to inadequate $\Delta T$, film boiling was initially obtained but quickly reverted to nucleate boiling with the addition of more water.

### Liquid Metal Runs

Cylinders of solid sodium approximately 1/2-in in diameter by 2-in long were cut by means of a corkborer. Oxide was removed by immersion in a 20 per cent solution of isopropanol in kerosene until a shiny metallic surface was obtained. The cylinders were transferred to a tared beaker containing n-heptane, adjustments being made in the number of cylinders to obtain the desired weight.

The sodium cylinders were then transferred to the charge vessel also containing n-heptane. The hydrocarbon overflowed the top of the vessel as more sodium was put in, keeping the sodium always immersed. The top flange of the charge vessel was then tightened down on a gasket. The vessel was evacuated from the top to remove air and then from the bottom to drain out the liquid n-heptane.

The charge vessel was then attached to the filling line assembly and further evacuated to remove all n-heptane adhering to the sodium. The sodium chamber and filling lines, which had been flushed three times with helium, were heated up to approximately 300°F with heating tapes. The charge vessel was heated with a propane torch until the temperature of the sodium was 450°F. The electrical contact between the thermowell and the outside wall of the charge vessel was monitored and as the valve was cracked liquid sodium was allowed to drop into the bottom of the tube assembly. The valve was closed when the electrical contact was broken, indicating that the level of sodium had fallen below the thermowell.

The same procedure was used for charging the potassium. In this case, however, the oxide on the solid potassium pellets was removed with a 20 per cent solution of iso-amyl alcohol in kerosene. With the outer vessel on and evacuated, the guard heater was used to heat the potassium chamber to approximately 700°F prior to charging.

Operation

Two techniques were considered for achieving film boiling. The first consisted of traversing the entire boiling curve under reduced pressures while the second involved heating the boiling plate to a high enough temperature so that the slow introduction of potassium would immediately yield film boiling. Traversal of the boiling curve at normal pressures was not feasible because of the thermal stresses induced in the boiling plate due to the large value of the critical heat flux. The first technique was successful in obtaining film boiling.

Hence, the initial liquid-metal runs were made at reduced pressure. The outer vessel was evacuated for one day prior to operation. This vessel was always filled with helium prior to removal for repairs or adjustments, thereby decreasing the pumping-down time. Since outgassing is highly temperature dependent, the vessel was initially pumped down to 1 micron. The vacuum system remained in operation to remove gases released as the system temperature increased.

The potassium chamber was evacuated and the power to the radiation heater around the sodium boiler slowly increased. The power to the guard heater around the potassium chamber was adjusted so that its temperature corresponded approximately to that of the boiling plate. Transition from natural convection to nucleate boiling was easily noted by the sound of bubbles forming and collapsing and by temperature fluctuations in the liquid potassium. A point was eventually reached at which a slight increase in power to the sodium heater caused the temperatures in the boiling plate to rise several hundred degrees. This was accompanied by a marked decrease in the sound of boiling and a stabilization of the liquid potassium temperature, suggesting that film boiling had been attained. Operation in the transition regime could be obtained by slowly decreasing the power to the sodium heater. Film boiling at higher pressures could be obtained by slowly introducing helium into the potassium chamber.

A second technique for obtaining film boiling at reduced pressure was attempted. The potassium was heated to approximately 1200°F under helium pressure to prevent boiling. Maintaining constant power to the sodium boiler, the pressure in the potassium chamber was slowly decreased by means of a vacuum pump. Full vacuum was eventually reached with the potassium still at 1200°F but not boiling. It was concluded that the potassium had achieved 400°F superheat without boiling. No attempt was made to induce boiling by disturbing the system (for example, with the light tap of a hammer).

After investigating film boiling under vacuum, helium was slowly bled into the potassium chamber while simultaneously increasing the power to the sodium boiler to insure continuous film boiling. When the temperature of the potassium was approximately 1000°F, surges in the sodium chamber occurred causing the boiling plate to fluctuate between 1500°F and 1000°F. It now seems that excessive superheating of the sodium may have occurred causing surges in the boiling sodium. A failure of the thermocouple in the sodium chamber prevented close monitoring of behavior in that system.

Measurements

At each incremental power setting for the sodium heater, sufficient time was allowed for conditions to reach steady-state (approximately 30 minutes). The temperatures and temperature differentials in the boiling plate as well as the potassium temperature were recorded on a continuous recording chart. The pressure in the potassium chamber was obtained from the mercury manometer.

RESULTS

The results are summarized in Figures 49 and 50 and Table XIII. The data for the vacuum runs were obtained by traversing the boiling curve in both directions. The 0.7 psia data was obtained by moving down the nucleate boiling curve towards natural convection region. Two sets of curves, corresponding to thermocouples at two different radii in the boiling plate, are shown. The inner flux is considerably larger than the outer flux due to axial losses up the sides of the boiling tube. This radial transfer in the plate will be minimized in future runs by adjustment of guard heaters.

Considerable fluctuations in temperature occurred in the plate during boiling. Individual temperatures in the plate varied 30°F to 100°F in nucleate boiling up to 200°F in the transition regime. Temperature fluctuations during film boiling were about 100°F. The present data are based on average values as read from the recording chart. In the calculation of the heat flux the temperature difference between the bottom and top thermocouples at the same radial position was used. The temperature of the boiling surface was obtained by extrapolation using the calculated flux and the temperature of one of the thermocouples. Figure 51 shows the fluctuations encountered during operation.

The data from the furnace calibration of the micro-thermocouples is presented in Table XIV in Appendix G. A least-square analysis was applied to the data to obtain the best estimate of the true temperature as a function of the indicated temperature as obtained from the actual emf generated by the thermocouple. The resulting equations were:

| Boiling Plate Location | | Equation |
|---|---|---|
| Inner radius: | bottom | $T = 1.0043\ T' - 13.9$ |
| | top | $T = 1.0238\ T' + 18.0$ |
| Outer radius: | bottom | $T = 1.0050\ T' - 14.1$ |
| | top | $T = 1.0040\ T' + 2.7$ |

$T$ = best estimate of true temperature, °F
$T'$ = indicated temperature obtained from emf, °F

These equations were used to calculate the expected temperatures for the furnace calibration data. As shown in Table XIV, the equations give a good fit to the data.

The thermocouple calibration was carried out after the boiling runs and was found to differ significantly from that obtained from the first calibration several months earlier. A check run, also included in Table XIV, shows that the micro-thermocouples are at least not drifting at a defectable rate.

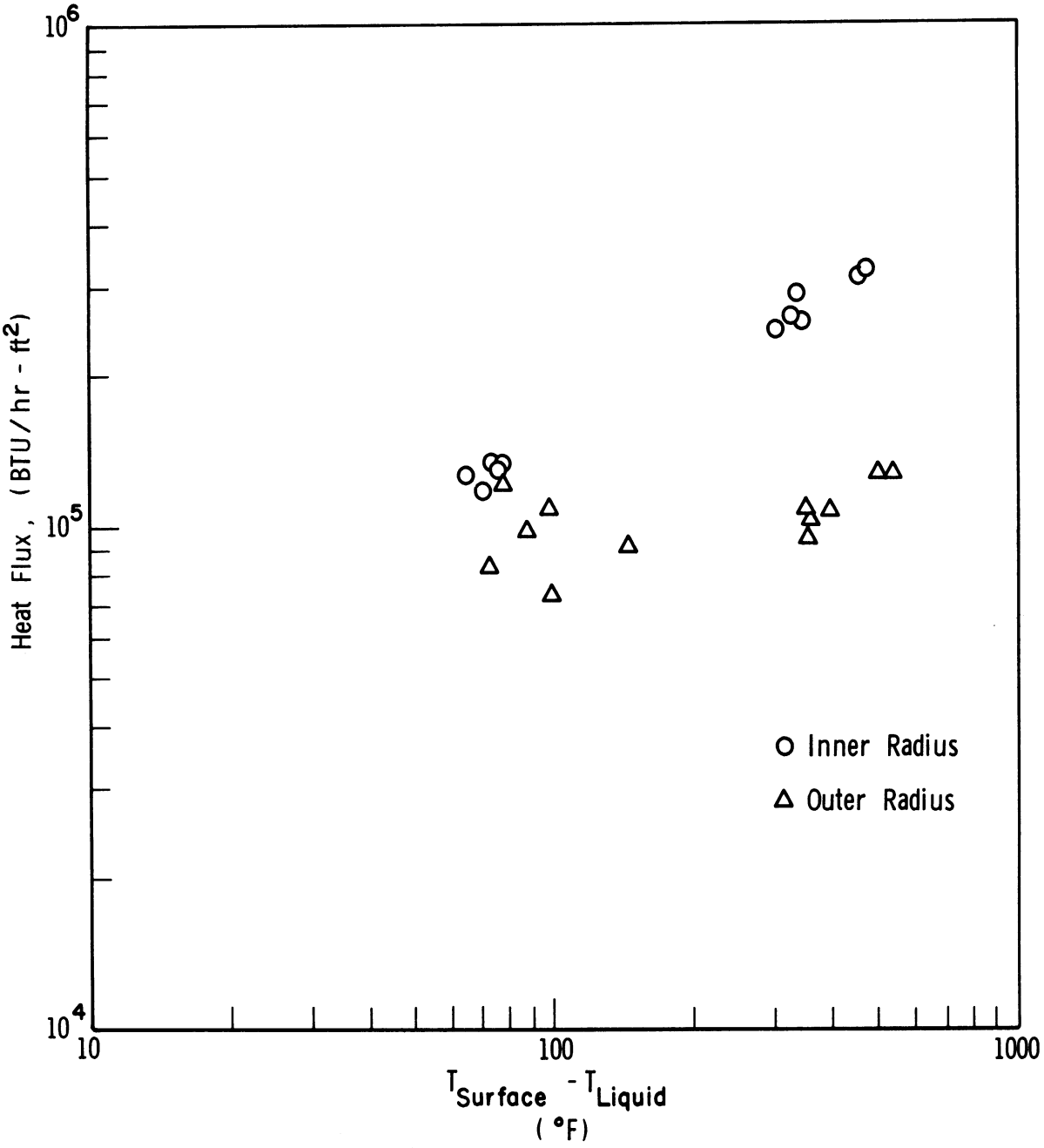


Figure 49. Boiling Curve: Vacuum.

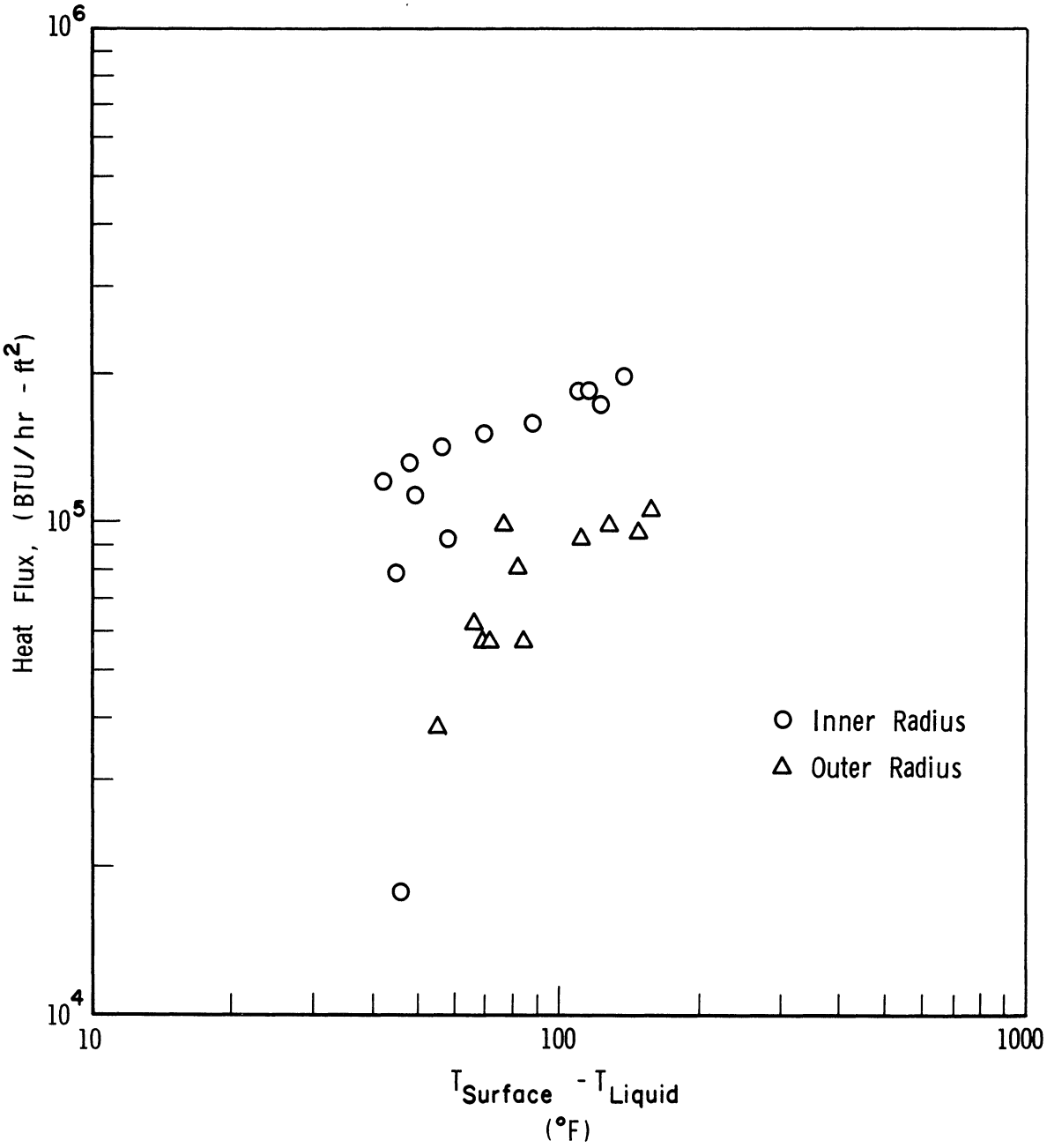


Figure 50. Boiling Curve: 0.7 PSIA

TABLE XIII

FILM BOILING RESULTS

| Potassium Temperature °F | INNER RADIUS ΔT °F | INNER RADIUS Heat Flux Btu/(hr)(sq ft) | OUTER RADIUS ΔT °F | OUTER RADIUS Heat Flux Btu/(hr)(sq ft) |
|---|---|---|---|---|
| Vacuum Run | | | | |
| 751 | 70 | 118,000 | 99 | 73,000 |
| 751 | 65 | 128,000 | 77 | 121,000 |
| 752 | 76 | 133,000 | 72 | 83,000 |
| 751 | 77 | 136,000 | 143 | 91,000 |
| 760 | 74 | 136,000 | 87 | 98,000 |
| 805 | 300 | 249,000 | 348 | 95,000 |
| 810 | 324 | 263,000 | 346 | 109,000 |
| 825 | 332 | 291,000 | 391 | 107,000 |
| 836 | 340 | 257,000 | 353 | 104,000 |
| 757 | 75 | 131,000 | 97 | 108,000 |
| 769 | 449 | 315,000 | 496 | 127,000 |
| 803 | 468 | 327,000 | 533 | 128,000 |
| 0.7 psia | | | | |
| 846 | 46 | 18,000 | 55 | 38,000 |
| 889 | 45 | 79,000 | 84 | 56,000 |
| 909 | 58 | 92,000 | 66 | 62,000 |
| 930 | 49 | 113,000 | 69 | 57,000 |
| 940 | 42 | 121,000 | 71 | 57,000 |
| 946 | 48 | 132,000 | 81 | 80,000 |
| 954 | 56 | 143,000 | 76 | 99,000 |
| 959 | 69 | 151,000 | 100 | 102,000 |
| 962 | 88 | 159,000 | 111 | 92,000 |
| 964 | 122 | 174,000 | 158 | 106,000 |
| 960 | 109 | 184,000 | 128 | 97,000 |
| 958 | 115 | 184,000 | 148 | 95,000 |
| 948 | 137 | 197,000 | 150 | 95,000 |

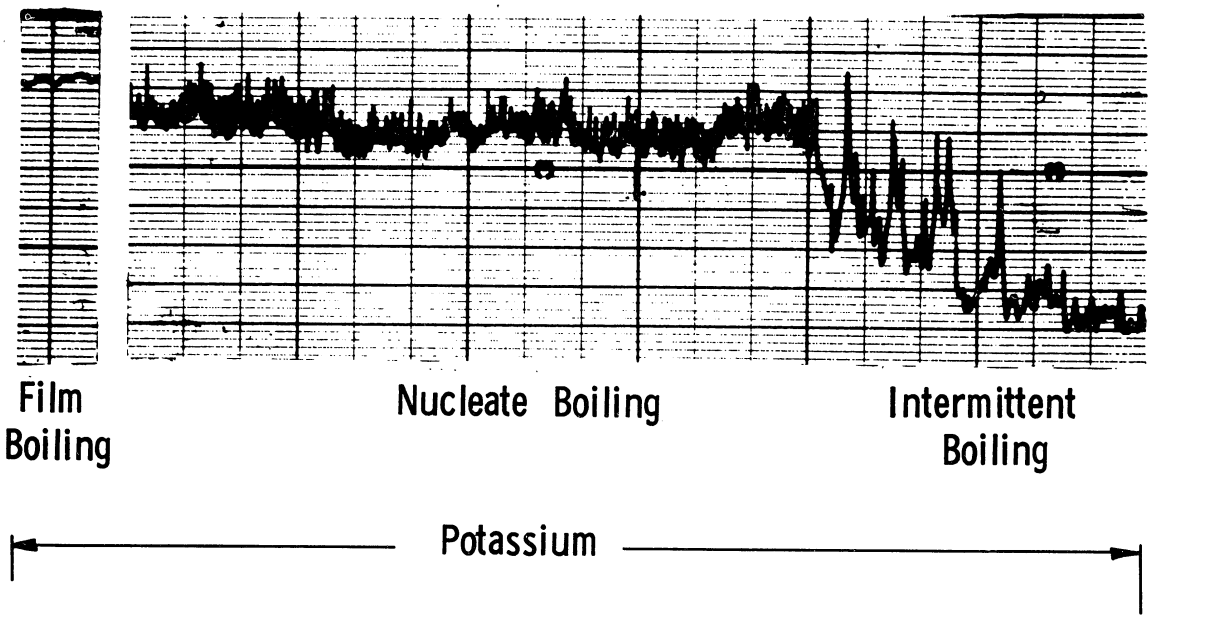


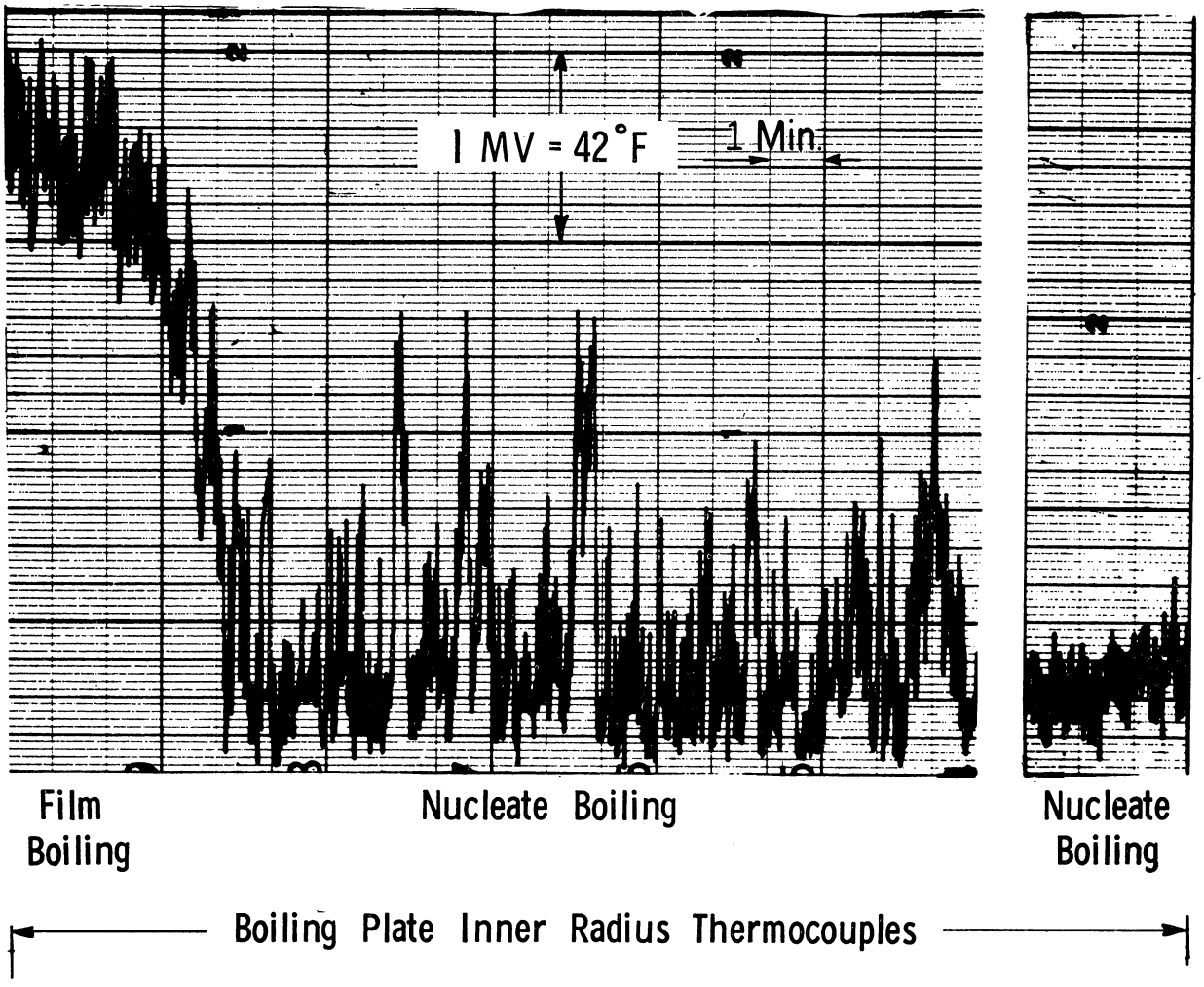


Figure 51. Temperature Fluctuations during Nucleate and Film Boiling.

## DISCUSSION

From the boiling curves, it is seen that the fluxes obtained in what is apparently the film-boiling regime are higher than those in nucleate boiling. One obvious question is whether film boiling had been attained at all. The considerable reduction in noise and the marked stabilization of the boiling potassium temperature indicated that the mechanism of the boiling process had changed.

One would expect that the fluxes in film boiling would be substantially lower than nucleate boiling at reasonable temperature differences. In this case, however, the temperatures involved are high. For a temperature difference of 600°F with the heating surface at 1500°F, the heat flux due to radiation alone would be 24,000 Btu/hr-ft$^2$ assuming black body radiation. However, this cannot account for the high values of the flux in film boiling.

The expected temperature difference at the minimum point was predicted to be 323°F at 1 atm. At reduced pressures, one would expect this temperature difference to decrease and this is borne out by the data. Two uncertainties existed in the processing of the temperature data. The first concerned large fluctuations in the temperature of the boiling plate, since each average value had to be determined by inspection from one minute of recorded data. The other depended on the accuracy of the furnace calibration of the micro-thermocouples.

The large fluctuations encountered were not expected and the only method of allowing for the lack of precision which they caused was to obtain as many experimental points as possible. In several cases, two sets of readings were taken for each power setting, thus allowing one hour for the system to reach steady state. The fact that the micro-thermocouples did not drift significantly following the boiling runs does not insure that they were not drifting rapidly during the runs. However, considerable cycling of the thermocouples in the heater development stage gives some basis for hoping that they were stable when the data was obtained.

The temperature of the boiling potassium varied during runs. This was attributed to the slight pressure changes due to the inability to control the condensation rate. The saturation temperature-pressure relationship changes rapidly at such reduced pressures. The guard heater was not in operation during most of the runs and there is the possibility that subcooled nucleate boiling occurred. In film boiling, this probability was reduced since the walls of the potassium chamber were at a higher temperature. Future runs using the guard heater should determine the existence of a difference.

Steps are being taken to stabilize the boiling process in both the sodium and the potassium. Consideration is being given to creating a "hot finger" at the bottom of the sodium chamber to act as a nucleation source. Operation of the guard heater to obtain nucleate boiling along the walls of the potassium chamber may suffice to obtain more stable potassium boiling.

The micro-thermocouples will be recalibrated before being replaced by new ones. New heaters will also be installed. Present plans call for operation in the film-boiling regime at higher pressures, at least up to 1 atm and hopefully up to a boiling temperature of 1800°F. Operation will be limited by the temperature differences encountered in the film-boiling regime.

# FORCED CIRCULATION STUDIES

Robert E. Barry

## INTRODUCTION

Energy conversion cycles employing liquid metals as intermediate heat transfer fluids in the process of generating electricity have been the subject of intense study in recent years. Such an application requires a much improved understanding of the heat transfer process occurring across a solid-liquid interface at high flux levels. High flux operation permits minimization of heat transfer surface for a given power and hence a reduction in size. For applications employing a turbine-like converter driven by metallic vapor it is important that liquid droplets be eliminated to reduce wear on the rotor surfaces. Pumping requirements are also reduced by achieving high qualities in a single pass. Therefore, the study of heat transfer at high fluxes with varying qualities is of major importance in forced circulation studies. The determination of pressure drop in two-phase metallic systems is also of importance because of its effect on pumping requirements.

Academically, a better understanding of the phenomena that lead to variations of flow patterns and heat transfer characteristics are sought. Studies with aqueous and other simple systems have produced some insight regarding the two-phase heat transfer and burnout problem. Data with metallic fluids should permit a substantial extension of the ranges of certain important physical parameters such as density ratio, interfacial energies and the more common transport properties. These studies should subject existing theories and correlations to more severe tests.

The objective of the forced circulation studies was to determine the parameters characterizing heat transfer and pressure drop in the two-phase flow of liquid metals. In particular, the effect of flow rate and temperature on the value of quality at which significant changes in heat transfer coefficients occurred was desired. These changes might be expected to correspond to transitions between nucleate boiling and film boiling or between annular flow and a "dry-wall" condition both of which could effect significant change in the heat transfer coefficient.

In September 1961, design studies were initiated for a proposed forced circulation liquid-metal loop resulting in the specification of the following operating conditions:

| | |
|---|---|
| Working fluid | Potassium or Sodium |
| Fluid operating temperatures | 1400-1800°F |
| Design pressure | 200 psi |
| Flow rate | 0.2 to 2 GPM |
| Total power input | 40 KW |
| Heat flux at the test section | 1,000,000 Btu/(hr)(sq ft) |
| Test section diameter | 0.5 inch |

Potassium and sodium were chosen as the working fluids because of their ready avilability and relatively low cost. The 1800°F maximum operating temperature was specified to permit the use of Haynes-25 (L-605) in the critical sections, rather than a refractory metal which would have necessitated enclosing the loop in an evacuated chamber and added substantially to the cost. Originally, a maximum flow rate of 3 GPM and a power input of 65KW were specified, but both requirements were reduced in proportion to conform with the performance of an existing electromagnetic pump. The operating conditions would allow the attainment of 100 per cent quality at .2 GPM entering the test section, assuming no losses.

Formal specifications were prepared and requests for proposals for the design and construction of the loop were issued in November 1961. Mine Safety Appliance Research Corporation, Callery, Pennsylvania was awarded a contract in May 1962 and delivered the loop in February 1963.

DESIGN OF EQUIPMENT

The most critical component of the loop was the test section where extremely high heat fluxes were desired. Several possibilities were considered.

1. Resistance Heating.

   a. Flame-spray Technique. In this method, the base tube would be sprayed with 5-mils of berylium oxide and 3-mils of tantalum. About 1000 amps would pass through the outer layer and the heat generated would be transferred through the layers to the fluid. The success of this method would depend on maintaining a thin layer of insulating oxide which would keep the temperature drop small but prevent any leakage of current through the insulation to the fluid. Two such tubes were made, one with 5-mils of aluminum oxide and the second with 10-mils. Both tubes had a direct short through the insulation and metallographic examination revealed threads of tantalum extending through the alumina. This method was abandoned since it apparently required further development.

   b. Wire-wound Technique. In this method, sheathed insulated resistance wire would be brazed to the tube surface. In 1961, Brookhaven National Laboratory was conducting a series of experiments to determine a suitable brazing alloy for this purpose. At that time, this method had not yet proved reliable.

2. Radiant Heating. An element temperature of about 5000°F would be required to transfer one million Btu/(hr)(sq ft) to the tube wall by radiation. A refractory metal element would have to be enclosed in an evacuated chamber to prevent oxidation and the difficulties of maintaining the electrical lead seals over a temperature range of 2000°F appeared formidable.

3. Induction Heating. High fluxes can be obtained with high-frequency induction heating. This would involve placement of thermocouples in the cross section of the tube to determine the local heat flux. Since the heat is generated within a small thickness at the outside diameter of the tube, there is conduction along the tube which must be taken into account. There is also the risk of failure of the tube wall if the critical flux is exceeded.

4. Liquid-Liquid Heat Exchange. This method would consist of a double-pipe exchanger with 1900°F liquid metal in the annulus and the working fluid in the tube. While high coefficients can be achieved, this method requires another electromagnetic pump, a cooling system to reduce pump inlet temperatures to 1300°F and more power to heat the fluid to 1900°F again. This method was discarded because of the increased costs.

5. Condensing Vapor. Work at Columbia University (90) had indicated heat transfer coefficients of about 11,000 Btu/(hr)(sq ft)(°F) for condensing sodium at low fluxes. While extrapolation of the data was uncertain, it did not seem unreasonable to expect coefficients of about 7000 at a flux of $10^6$ Btu/hr $ft^2$. This would result in a temperature drop of about 150°F on the condensing side. Since the maximum temperature on the condensing side was limited by the strength of the metal and since potassium temperatures of up to 1800°F were desired, it was necessary to use as thin a wall between the fluids as was consistent with structural considerations. This method had the advantages of low cost and the elimination of the burnout problem since the flux was controlled by the temperature differential. It had the disadvantage of not allowing a temperature reading in the thin wall, but at the time it was felt that this limitation would not seriously affect the objectives of the program. Accordingly, this was the method chosen.

A schematic diagram of the final loop design is shown in Figure 52. The system utilizes two separate fluid circuits. The primary circuit contains potassium as the working fluid and the secondary circuit utilizes condensing sodium as the heating fluid. The liquid metal in the primary circuit is pumped by an electromagnetic pump through a throttle valve and an electromagnetic flowmeter. The flow is then equally distributed into the three parallel heating sections of the preheater and exits into a common header at the test section inlet. The liquid metal flows through the tube side of the test section and passes through a horizontal straight section of pipe for pressure drop measurement. The flow then continues into a condenser section, through a hot well and into a subcooler from whence the flow is returned to the pump. In the secondary circuit, the sodium is vaporized in the boiler section, condensed in the shell side of the test section, and returned by gravity to the boiler.

Each circuit is equipped with a diffusional cold trap for maintenance of a low oxide concentration, and a supply tank. Valves and auxiliary lines are located in each circuit for bleeding, pressurizing, venting, leveling and drainage. A more detailed description of the system components follows.

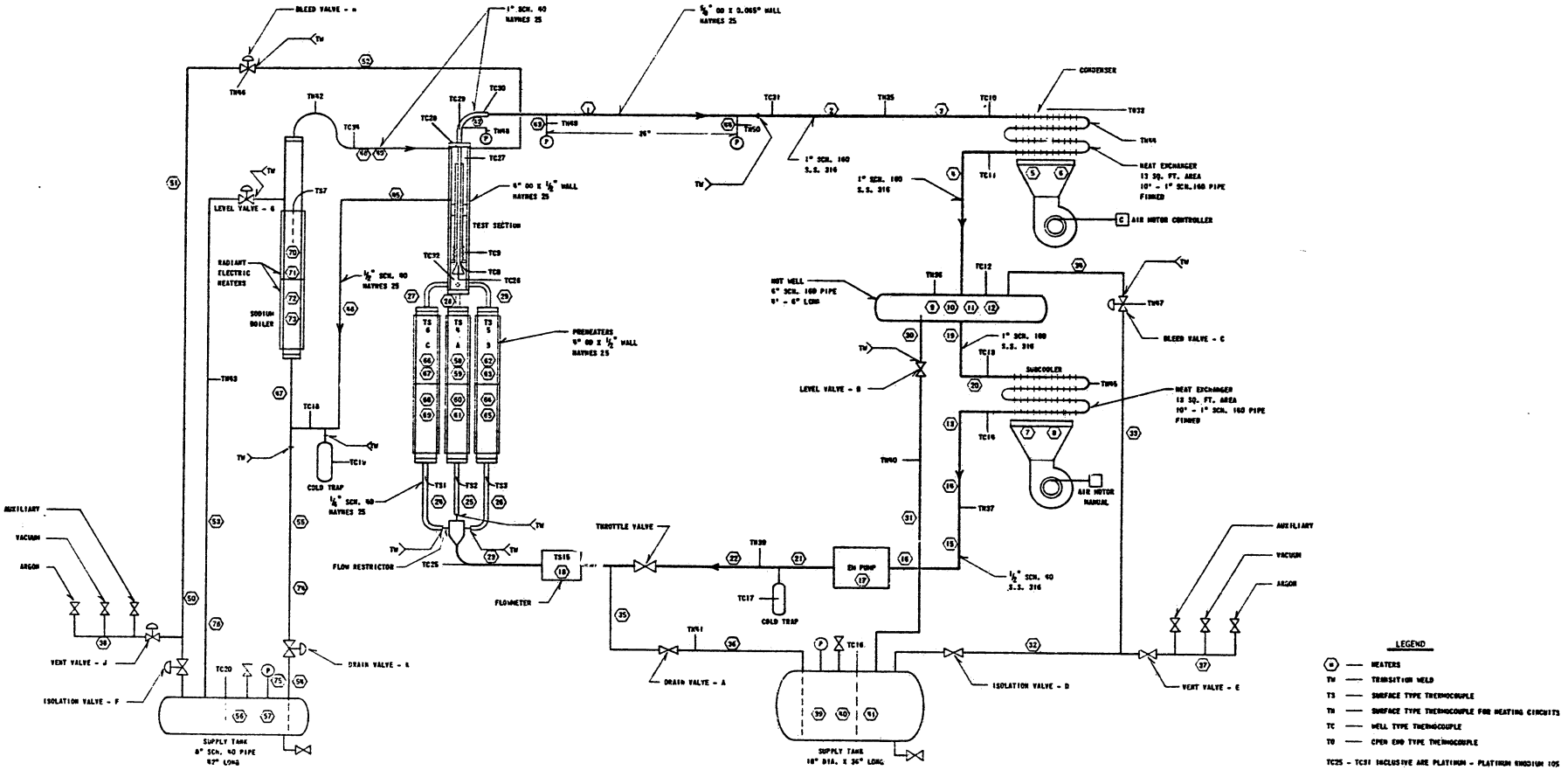


Figure 52. Flow Schematic.

AK2246-28

Pump: This is a MSAR Style II electromagnetic conduction pump. (Shown in Figure 53.) The pumping section consists of a 1-ft length of 3/8-in stainless tube flattened so as to provide an inside width of 1/16-in. The developed pressure is rated at 100 psi at no flow and 80 psi at 2 GPM. The flow rate is controlled by varying the applied voltage from 0 to 270 V with a variable transformer or by regulating the throttle valve. A 10 KVA capacitor is connected across the pump to correct the power factor and reduce the line current. The pump is equipped with two blowers for cooling the coils.

Throttle Valve: This valve is a General Kinetics Corporation 1/4-in Hi-100 stainless steel valve with a bellows seal. A ball whose position is controlled by an air operated cylinder floats in the fluid between the inlet and outlet seats. The valve provides a linear response to the air signal.

Flowmeter: The flowrate in the primary circuit is measured by a MSAR Style FM-2 magnetic flowmeter. (Shown in Figure 54.) This consists of two voltage taps diametrically mounted on 3/8-in stainless tube and perpendicular to the field of a permanent magnet.

Preheater: The preheater consists of three sections of 4-in OD by 3-in ID by 45-in long Haynes-25 pipe mounted in parallel. Approximately 3-ft of each section is heated by four radiant clam shell heaters. These heaters are Hevi-Duty 5718 KSP rated at 2.5 KW at 230 V, and with an allowable element temperature of 2200°F. The twelve heaters provide for a total of 30 KW rated power. An orifice is located in the entrance line of each of the preheaters to help maintain uniform flow in the three sections.

The preheaters were mounted in parallel to maintain a reasonable height. A fairly extensive experimental program was conducted on a full scale model of this arrangement using air and water (7). It was demonstrated that such an arrangement would provide reasonably stable flow in the test section if a funnel was placed above the point where the three streams re-united prior to entering the test section.

We also considered the use of direct resistance heating for the preheater section. In this method, three electrical leads would be placed directly on the pipe and the resistance of the potassium would internally generate the required heat. This method was abandoned because it was felt that the relatively long lengths of pipe required would lead to a substantial pressure drop before the test section entrance and further, that there was a distinct possibility of overheating the pipe in the region of two-phase flow when the pipe would be required to carry substantially all the current.

Test Section: The test section was designed to deliver a flux density of one million Btu/(hr)(sq ft) to a 2-in long section of 1/2-in tube. It is shown in Figure 55. The flow from the preheaters enters tangentially at the bottom of a 4-in OD by 3-in ID by 36 1/2-in long Haynes-25 pipe. The flow then enters a funnel leading to 23 inches of 1/2-in tube having a wall thickness of .010-in. All but 2 inches of this tube is enclosed in a length of 1-in pipe which is welded to the 1/2-in tube at the top and connected to the 4-in pipe by means of a bellows. The 2 inches of exposed tube serves as the heat transfer test section.

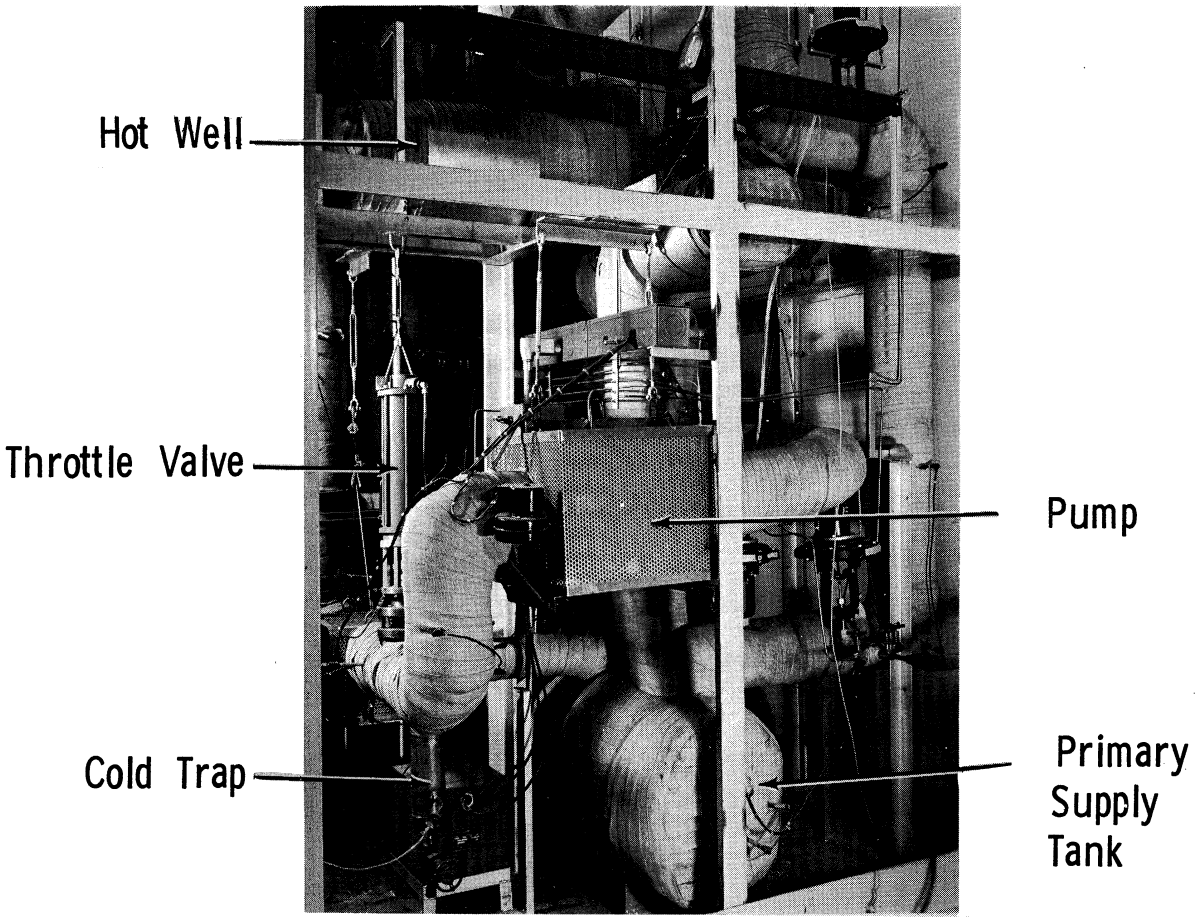


Figure 53. Loop, North Elevation.

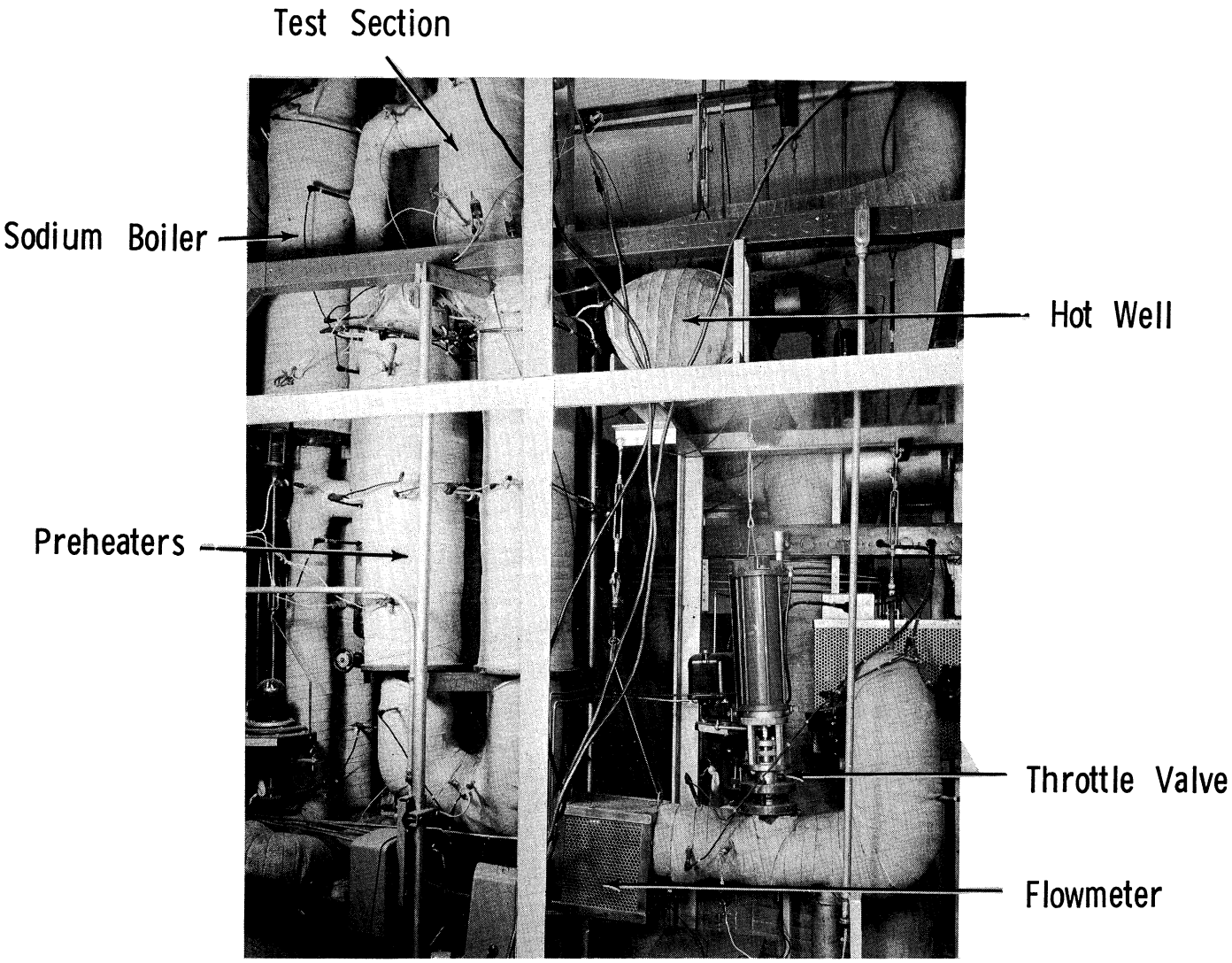


Figure 54. Loop, East Elevation.

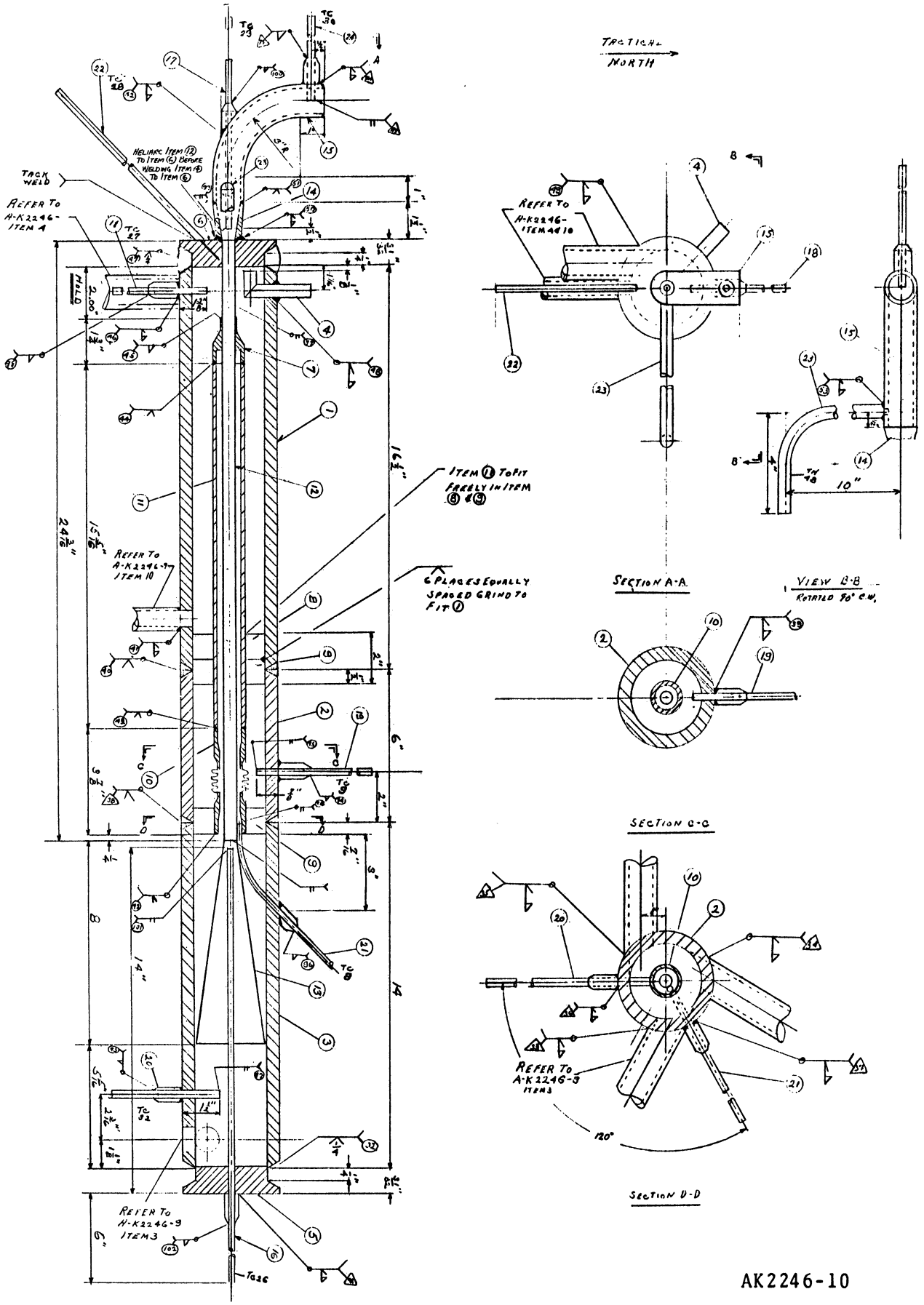


Figure 55. Test Section.

In operation, sodium vapor enters tangentially at the top of the test section as shown in section A-A, and condenses on the exposed 2 inches. The resulting liquid then falls down the outside of the 1-in pipe and runs out through the overflow pipe (half-way up the 4-in pipe) back to the sodium boiler. The annulus below the overflow tube is filled with sodium down to the bellows. A loosely fitting disc just below the sodium overflow serves as a "thermal block" to maintain a lower temperature in the sodium surrounding the bellows. The space between the 1-in pipe and the 1/2-in tube is normally filled with vapor (since the funnel is not attached to the wall of the 4-in pipe) and serves as an insulator. This vapor barrier was designed to reduce the heat loss while the velocity profile of the potassium was developing prior to entering the 2-in heat transfer section. Calibration of the test section entrance would provide the magnitude of this heat loss. Thermocouples are located below the funnel, in the funnel, at the bellows, in the sodium annulus, the sodium vapor space, the test section outlet and in the heavy wall after the test section. Absolute pressure is read at the test section outlet by means of a diaphragm type sensing element back filled with NaK leading to a pressure transmitter.

Pressure-Drop Measurement Section: This section consists of a horizontal 3-ft length of 5/8-in OD by .495-in ID Haynes-25 tube. (Shown in Figure 56.) Differential pressure across this length is read by two diaphragm sensing elements, back filled with NaK, which are connected to each side of a diaphragm in a pressure transmitter. The transmitter has three ranges; 100, 300 and 600 inches of water. Thermocouples are located upstream and downstream of this section.

Condenser: The condenser consists of 10 feet of 1-in, Sch 160, stainless steel finned tube encased in a blower duct. Air is supplied by an 800 cfm blower and the condenser is rated at 105,000 Btu/hr. The air flow is controlled by louvres at the discharge of the blower and the louvre position is controlled by an air signal.

Hotwell: This is a horizontal 54-in section of 6-in pipe which serves to insure a liquid level above the pump even in the event of large instabilities. It also serves as an accumulator of liquid when the preheaters contain a large vapor fraction.

Subcooler: The subcooler is identical in design to the condenser and serves to cool the liquid to 1400°F before it enters the pump.

Sodium Boiler: The sodium boiler consists of a 4-in OD by 3-in ID by 54-in long section of Haynes-25. The bottom 3 feet are heated by four clam shell heaters of the same type as in the preheater. The rated output is 10 KW.

Valves: The auxiliary valves are Hoke, Inc. HY473, 1/2-in bellows-sealed globe valves rated for liquid metal service at 1500°F and 50 psi.

Piping: In the primary circuit, the preheater, test section and pressure drop section are constructed of Haynes-25 alloy. 1-in, Sch. 160, 316 stainless pipe is used from the pressure drop section to the subcooler and 1/2-in, Sch 160, 316 stainless pipe is used from the subcooler to the preheater inlet.

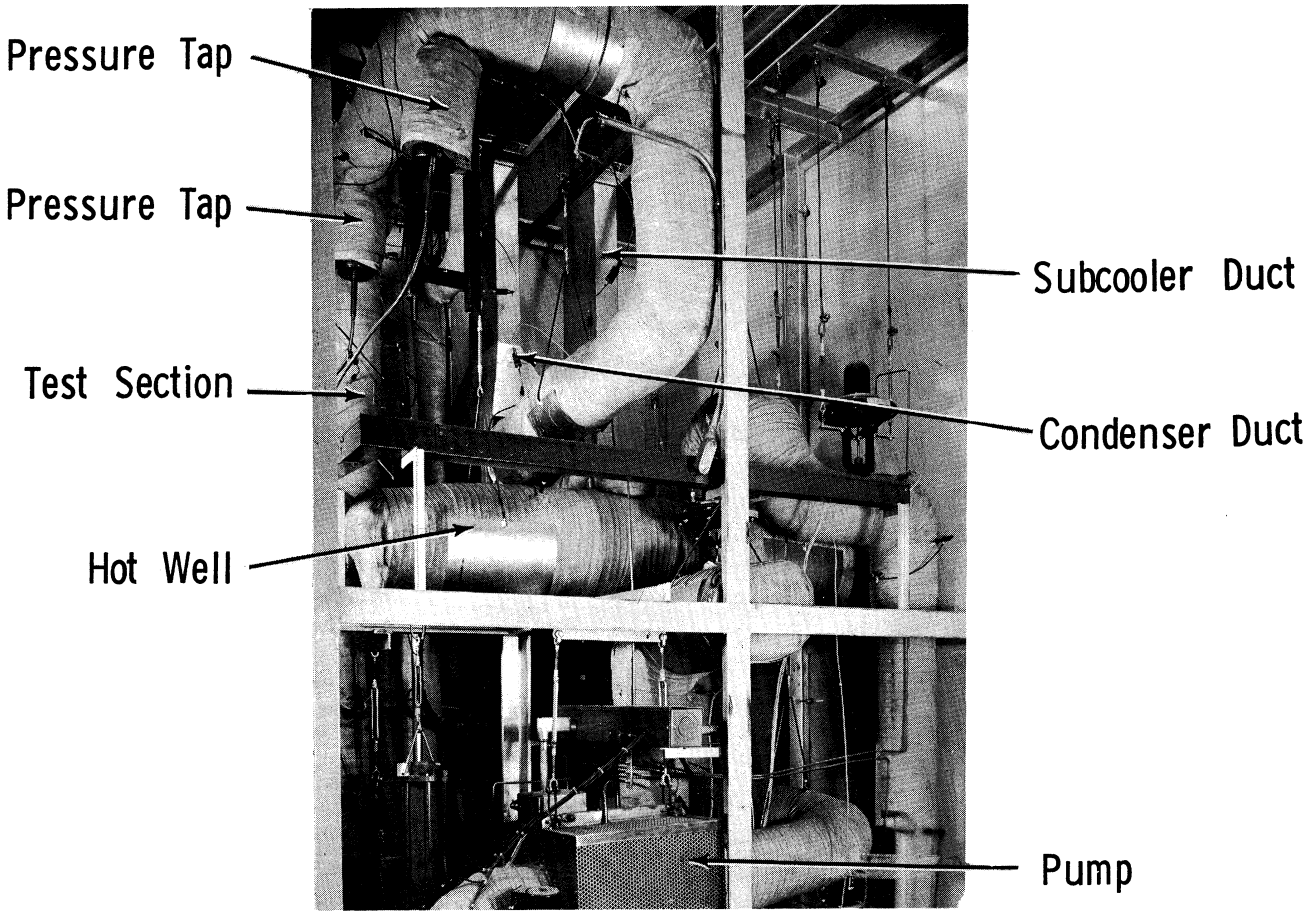


Figure 56. Loop, North Elevation.

In the secondary circuit, the sodium boiler, the 1-in vapor line and the 1/2-in condensate return are made of Haynes-25 alloy. All lines in both systems are traced with warm-up heaters.

Control: The control panel (shown in Figure 57) was assembled by R. T. Brokaw and Company, Ann Arbor, Michigan, using instruments supplied by the University of Michigan. Variable transformers control the voltage to the preheaters, sodium boiler and pump, the power being read on wattmeters accurate to 1 per cent of full scale. Thermocouples used to monitor loop operation are read out on a 12-point recorder used in conjunction with a 48-point stepping switch. Thermocouples on the walls of the preheaters are connected to a temperature indicator equipped with a high temperature alarm which automatically cuts off the preheaters in the event of a temperature excursion. A thermocouple on the sodium boiler wall is similarly connected. An indicating recorder-controller provides continuous read-out of the platinum/platinum-rhodium thermocouples, loop pressure and differential pressure. It may be adjusted to control the condenser louvre either by a temperature signal or by loop pressure. The platinum/platinum-rhodium thermocouples (used in heat transfer calculations) are read out on a K-2 potentiometer. These thermocouples were calibrated against a secondary standard calibrated by the National Bureau of Standards. The positions of the throttle valve, the subcooler louvre and the primary and secondary drain valves are controlled by manually operated air regulators. The millivolt signal from the flowmeter can be read out either on a millivoltmeter or on a Wheelco "Limitrol" equipped with a low-signal alarm to cut off the pump, preheater and boiler power. All auxiliary valves are controlled by solenoid valves actuated by switches on the control panel. In the event of a serious emergency, the contents of both loops may be drained to their respective supply tanks and all power cut off by use of a "scram" button.

Facilities: The University of Michigan provided the facilities to house the forced circulation loop. The 25 by 40-ft building is constructed of cinder blocks on a slab foundation and contains a 14 by 25-ft bay, 17-ft high. A compressor supplies air for the instruments and valves, and a 112 KVA tapped transformer supplies the electrical power. Connections between the control panel and the loop terminal boxes were made by the University.

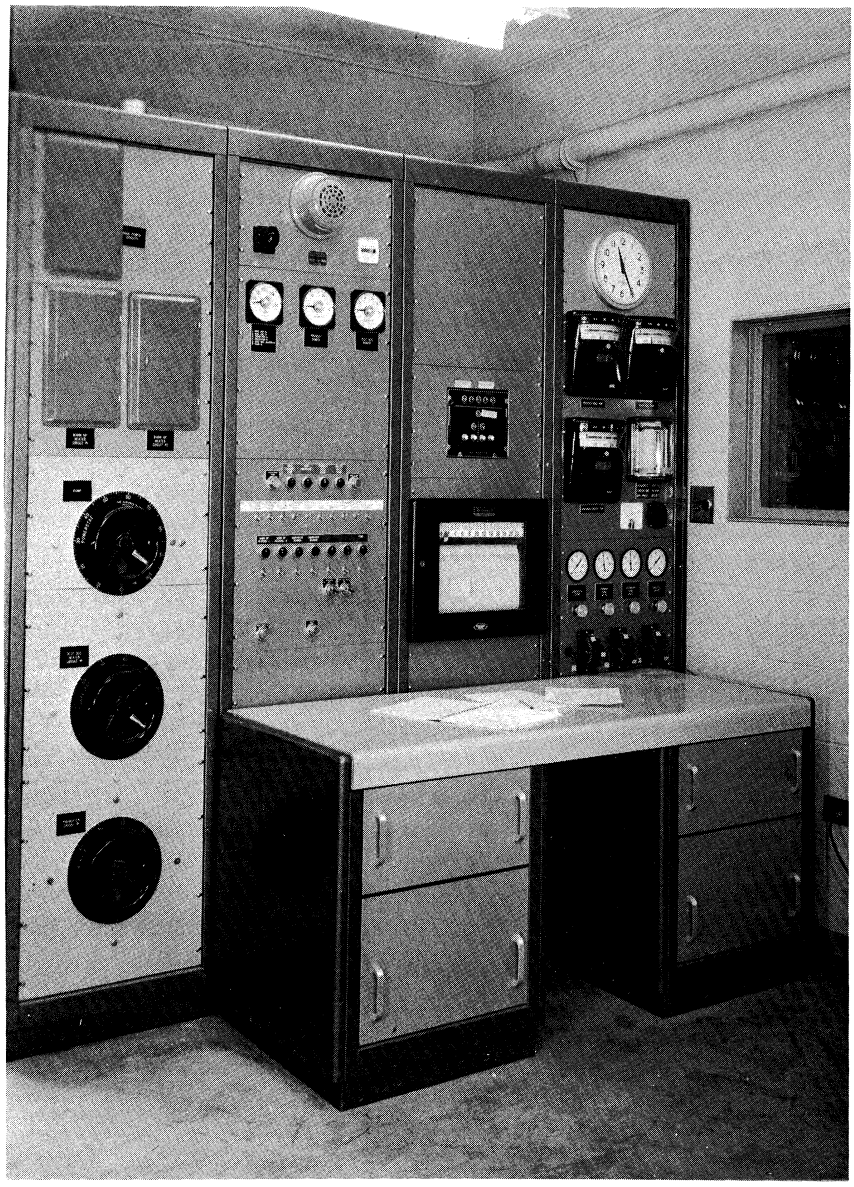

Figure 57. Control Panel.

## OPERATING PROCEDURE

Once the loop was charged with sodium and potassium, circulation would be initiated at low temperatures (500°F) under inert gas pressure. The potassium would then be gradually heated by the preheater while the sodium vapor temperature was maintained within 25°F of the potassium temperature. As the potassium was heated an independent calibration of the flowmeter would be made by running a heat balance over the preheater and test sections. The power delivered to the fluid would be determined by measuring the power input to the preheaters and deducting the losses which would be estimated from correlations for natural convection heat transfer from vertical surfaces. Measurement of the bulk temperature entering and leaving the preheater would then permit determination of the flowrate for a particular millivolt signal from the flowmeter.

The next phase of the planned program was to determine the sodium condensing coefficient. This was necessary in order to determine the heat transfer characteristics of boiling potassium in later phases of the work. To determine the condensing coefficient the loop was pressurized and potassium circulated without phase change. Thermocouples before and after the two inch length of test section would be used to determine the heat input to the potassium and the average potassium temperature. The sodium temperature would be measured directly. From these measurements and overall heat transfer coefficient would be calculated. At the same time power input to the sodium boiler could be measured and the heat losses determined as a function of temperature. This determination would permit heat flux determinations in subsequent two phase potassium flow experiments by simply measuring power input to the sodium system.

A knowledge of the condensing coefficient would be required if an estimate of the forced convection boiling coefficient was to be made. Knowing the conductivity of Haynes-25 it is possible to calculate the thermal resistance of the 10 mil wall. Analytical and experimental studies would be used to estimate the single phase forced convection coefficient on the potassium side.

Once these studies were completed, the loop was to be evacuated and the boiling heat transfer runs begun. At a particular heat input, temperature and pressure, the potassium quality entering the test section would be varied by changing the flow rate. From the previously determined knowledge of the sodium condensing coefficient, it would be possible to determine the heat transfer characteristics of boiling potassium as a function of flow rate, heat flux, quality and physical properties. During these runs, the pressure drop for horizontal two-phase flow would also be measured.

RESULTS OF OPERATION

On March 27, 1963 the loop was charged with potassium from the supply tank and circulation was begun under argon pressure at 800°F. After three hours of circulation at 1.6 GPM, the flow rate began to drop off in a manner suggesting plugging and finally ceased altogether in another two hours. Durint the next two weeks efforts were made to dislodge the plug by the application of heat and pressure. These methods failed and it was necessary to drain the loop and cut the pump out of the line. The restriction in the pumping section was found to be plugged and was cleaned by alternately rodding and flushing with methanol and methanol-water mixtures.

Commercial grade potassium containing about 2 per cent sodium had been provided with the loop. It was believed that the sodium present in the potassium has been selectively oxidized and precipitated. Plots in the Liquid Metals Handbook (64) show that the solubility of sodium oxide in potassium is quite low. There is some question as to the source of the oxygen. The potassium charged to the supply tank had been filtered through stainless steel frit and, although the commercial grade argon used as a cover gas was found to contain 150 ppm oxygen, this was not enough to account for the amount of oxide formed.

To eliminate oxygen contamination in the cover gas a NaK bubbler was installed on the inert gas line. The loop was flushed with high purity potassium (less than 200 ppm Na, less than 800 ppm $O_2$) at 1000°F. The pump was reinstalled and a second charge of high purity potassium was circulated at 1000°F and drained. Finally, a third charge of potassium was introduced. Unfortunately, before the first flushing, more oxygen was inadvertently introduced into the loop through a leak to the atmosphere.

On May 14, circulation was begun at 1.3 GPM with the temperature increasing gradually from 740° to 900°F. After 6 hours of operation, the flow had dropped to 0.6 GPM and circulation was terminated before the loop became completely plugged.

It was concluded that there were still oxides on the internal surfaces of the loop which were being dissolved and then precipitated at the cooler restricted sections. The preheater and hotwell, having the largest surfaces, were considered to be the main cause of the trouble. The loop was cleaned by charging potassium to the preheaters and hotwell, heating them to 1000°F, draining to the supply tank and cooling the supply tank to 200°F in order to precipitate the dissolved oxides. This procedure was followed three times, after which hot potassium was forced in both directions through the pump with the pump alternately connected for forward and reverse flow. Finally, 600°F potassium was left in the pump for two days in an attempt to redissolve any precipitated oxides. This appeared to have a beneficial effect and it was repeated for five days. At the end of this period the pump and the throttle valve were completely plugged and it was necessary to remove them from the system.

In July the pump was reinstalled along with a bypass filter (a 1/8-in thick stainless steel frit in a 4-in pipe) upstream of the pump and in parallel

with the main line. The main line could be frozen using a mixture of dry-ice and antifreeze and all the flow diverted through the filter. Thus, by heating the preheaters to 1000°F, cooling the potassium to 200°F in the subcoolers and operating the filter at 200°F the oxides could be dissolved in the hot parts of the loop and collected in the filter. When the filter plugged it was cut out and replaced and the operation repeated. Four such cycles were run for 24 hours at a flow rate of about 1/4 GPM before the filter plugged. This "cold" filtering served to reduce the oxide load on the hot-trap which was installed to insure trouble free operation with regard to oxide plugging.

The loop was then shut down for installation of a hot-trap system and reinstallation of the throttle valve. The hot trap consists of a 4-ft bed of zirconium chips which was connected in parallel with the main line of the primary circuit across the inlet and outlet of the pump. A portion of the flow can be recycled through the hot trap at 1200°F where the zirconium removes the oxygen from the potassium. This operation was carried out for 8 days with 0.2 GPM flowing through the primary circuit at 1000°F and 1.2 GPM flowing through the hot trap. The potassium in the supply tank was also cleaned up by dumping and recharging the loop.

The hot-trapping operation cleared up the problem of plugging and efforts were initiated to calibrate the flowmeter and measure the sodium condensing coefficient. During this period, it was determined that the calibration of the flowmeter by a heat balance was impossible. The air temperature varied around the circumference of the preheater and the "flat plate" correlations were unuseable. The flowmeter was calibrated by measuring the time to fill a known volume of the loop between two thermocouples. Eight determinations at various flow rates showed that the theoretical calibration curves supplied with the flowmeter were quite satisfactory.

On August 11, the secondary system was evacuated to 2 microns and heat was applied to the sodium boiler with the potassium circulating at 2.6 GPM. However, boiling of the sodium did not occur despite superheat of 150° to 200°F. Nucleation was indiced by striking the boiler and the temperature in the vapor space rose rapidly. The condensing heat transfer coefficients were about 700 Btu/(hr)(sq ft)(°F), much lower than anticipated. The boiler was heated to 1770°F during which time vapor temperatures of around 1200°F with fluctuations of 100°F were observed. Although natural circulation boiling loops are known to be subject to instability, the low heat transfer coefficient and the large temperature difference between the boiler and the vapor space suggested that a significant amount of non-condensible gas remained in the system. An attempt to evacuate the sodium circuit resulted in liquid metal being carried over into the trap and pump. The metal was found to contain 52 per cent potassium indicating a failure in the test section package which had allowed the sodium circuit to fill completely with liquid. This explained the anamolous operating characteristics of the sodium circuit. It is impossible to determine exactly when the test section failed.

It was decided to gather two-phase pressure drop data prior to repairing the test section. The sodium circuit remained full of liquid metal but a pressure differential was maintained to minimize sodium leakage into the potassium. Two phase mixtures were generated in the preheaters and pressure

drop readings taken. These runs are described in a later section of this report. After final shutdown on August 30, an analysis of the potassium showed 8 per cent sodium. Fortunately, the various two-phase flow parameters (such as quality) were affected by less than 1/2 per cent.

ANALYSIS OF LOOP PERFORMANCE

Sodium Boiler: The large instabilities in this circuit are believed to be due primarily to a lack of nucleating sites. Since hitting the boiler with a hammer produced nucleation, a vibrator mounted on the loop might prove beneficial. A better method, however, appears to be to introduce a localized "hot-spot" in the boiler. A small heating element would be inserted in the bottom of the boiler to produce continuous boiling. The bubbles of vapor formed would prevent superheating in the main body of the liquid and permit stable operation.

As noted previously, the boiler is heated by four clam shell heaters. Each heater contains two heating elements embedded in a refractory. These elements are rated at 2200°F but five of the eight elements burned out at sodium temperatures below 1770°F. Conservative calculations indicate that the element temperature should not have exceeded 1960°F. The reason for the failure may appear when the heaters are disassembled.

Test Section: The 8 per cent sodium found in the potassium corresponds to what one would expect if the leak were in the bellows. This section will be disassembled and examined. In view of the recent evidence that fluxes of 1 million Btu/(hr)(sq ft) may not be necessary for studying forced convection heat transfer at high qualities, the various methods of supplying heat to the test section are being re-evaluated.

Preheaters: Boiling instabilities were experienced in the preheaters with temperature fluctuations of 18°F observed. The period of the oscillations was about 3 minutes. This condition necessitated throttling the flow with full power to be applied to the pump in order to produce steady flow. A nucleating device in the preheater would stabilize operation.

Three of the 24 heating elements burned out at fluid temperature below 1450°F. Since the loop never operated near the maximum design conditions in either the primary or secondary circuit the failure of these elements is unexplained.

Although the preheaters were rated at 30 KW at 240 V, they only delivered 22.1 KW at 227 V which corresponds to 24.7 KW at 240V. This situation can be improved, however, by changing the taps on the main power transformer to provide 250 V.

Heat Losses: With full power (19 KW after the 3 elements burned out) on the preheater, it was impossible to operate above 1450°F at the preheater exit. This was due to the substantial losses in the rest of the loop which resulted in a maximum preheater inlet temperature of about 870°F. By operating all the trace heaters and circulating part of the flow through the 1200°F hot-trap, it was possible to raise the preheater inlet temperature to only 1030°F. This was substantially below the 1400°F which was the design condition.

The principal heat loss occurred in the condenser and subcooler. With the line heaters on and no air flow, the condenser lost 6 KW at 1400°F, and the subcooler lost 5 KW at 1300°F making it impossible to independently vary the quality and the pressure. This situation can be corrected most satisfactorily by shortening the length of exposed pipe. The line from the subcooler to the preheater lost 2 KW at 1000°F; the preheaters lost 3 KW at 1400°F; and the test section lost about 1.5 KW at 1400°F. The test section loss would have been less if the space between the 1/2-in tube and the 1-in pipe had not been filled with liquid.

Since the line heaters cannot be operated above 1000°F without danger of burning them out, the line losses will have to be made up either by clamshell heaters between the pump and the preheaters or by adding another heating section to the preheaters. Further insulation of piping and components is also under consideration.

Pump: The pump exhibited some anomalous behavior for which an explanation was not immediately evident. It was possible to distinguish three sounds in the pump: (1) a 60 cycle continuous whine when the pump was operating normally, (2) a growl when the pump operated against a plugged line or was empty, (3) a rasping sound which was attributed to cavitation. Coincident with this rasping sound, there occurred an immediate drop in flow rate. This latter condition has appeared intermittently without an apparent pattern. When it occurred, the voltage was reduced across the pump (and thus the flow rate) until it stopped. The voltage was then increased and the throttle valve adjusted to obtain the desired flow rate. This condition has appeared at low and high values of flow rate, inert gas pressure, and fluid temperature. Further experience has indicated that a vapor pressure of about 5 psia is required in the hotwell to attain flows above 0.4 GPM.

Line Heaters: The line heaters attached to the condenser and subcooler piping both burned out prematurely necessitating replacement. Radiant type heaters were designed, fabricated and installed by project personnel in order to get the facility back in operation immediately. Satisfactory operation has resulted since. Failure of the original elements must be attributed to faulty manufacture, design or installation.

# TWO-PHASE FLOW INVESTIGATIONS

Lowell R. Smith

The importance of studies to provide insight into the nature of two-phase flow cannot be overemphasized. Theoretical developments are necessary to the establishment of general prediction methods, while the gathering of reliable experimental data is essential for verification of theory and development of empirical correlations in the absence of adequate theory. Liquid-vapor flows commonly occur in boilers, evaporators, refrigerators, heat exchangers, and chemical reactors. Of more recent interest are the two-phase flows which occur in nuclear power plants and proposed space power generation systems. The very accurate designs required in these latter applications necessitate being able to predict two-phase flow phenomena to a high degree of accuracy. The possibility of using various liquid metals as heat transfer media in nuclear power and space power systems has led to a large degree of activity in the many aspects of metallic two-phase phenomena.

This report deals with studies of two-phase flows of potassium which are being performed at The University of Michigan. Specifically, pressure drops and vapor volume (or void) fractions are being investigated. To date a significant amount of pressure drop data for horizontal flows have been obtained. Some void fraction data have also been gathered using the gamma-ray attenuation method, but these data exhibit a high degree of scatter and more data will be necessary before a correlation can be made.

The studies are being performed in a liquid metal heat transfer test loop. Flows studied are horizontal and of the essentially adiabatic, evaporating type. In such cases, the pressure drops are accompanied by significant temperature drops, and the mixture qualities increase across the test section due to flashing. The flow regimes for all data are predicted as annular or dispersed. It is hoped that the data will be described by a recently derived mathematical model for annular flow. This theoretical work is still in development.

The experimental data and methods of measurement will be presented, together with pertinent conclusions and recommendations.

## LITERATURE REVIEW

It is not possible here, nor is it the purpose, to make an exhaustive review of the two-phase flow literature. This literature is voluminous, to say the least, representing a large technical endeavor. The treatments of two-phase flow are generally empirical in nature and lend little insight into the prevailing physics of the problem. It is further noteworthy that of all the papers written on this subject, few represent fresh approaches to the problem. These facts arise from the complexity of the phenomena encountered, and do not depreciate the competence of workers in the field.

In examining the literature one finds that the majority of investigations have been concerned with two-component two-phase flows, such as occur in the

air-water system. Considerably less work has been done in single-component systems, although quickening interest has led recently to intensified efforts in this area.

Although a tremendous amount of data on gas-liquid pipe flows has been published, only four basic methods of analysis have been used. The most satisfying but also most difficult approach is the analytical one. Because of the complexities encountered in two-phase flow, only two relatively simple flow regimes have been attacked by this method. Anderson and Mantzouranis (2) and Calvert and Williams (19) performed theoretical analyses of annular upward flow in vertical pipes, applying the classical von Karman-Prandtl-Nikuradse work on turbulent velocity profiles. Dukler (33) performed a similar but more advanced analysis which yielded only numerical solutions for downward annular flows. Hewitt (52) extended Dukler's work to upward annular flows. Street (116) performed an accurate analysis of the vertical slug flow regime.

Bankoff (9) recently analyzed the bubble flow regime for vertical upward flows, proposing a variable density single-fluid model. His model supposes that the mixture flows as a suspension of bubbles in the liquid, where radial gradients exist in the concentration of the bubbles. The bubble concentration is maximum at the center of the pipe, decreasing to zero at the wall. The slippage at any point is considered negligible, and the mixture thus may be considered as a single fluid with density varying radially in the pipe. It was not possible to obtain the radial void distribution, since information on turbulent diffusivities of bubbles was lacking. Nevertheless, the model's predictions of void fractions and frictional pressure drops compared very favorably with data obtained from steam-water flows. Bankoff's approach has received wide attention, since it represents a high degree of creative thinking.

The second basic approach to two-component two-phase flow problems was first developed by Lockhart, Martinelli, et al. (78, 81, 83). The method predicts pressure drops and void fractions occurring in horizontal, isothermal gas-liquid flows. The authors assumed that the frictional pressure loss is the same for each phase and is equivalent to the static pressure drop, i.e., momentum losses are neglected. An empirical correlation of the following form was developed.

$$\frac{(\triangle p/\triangle L)_{TPF}}{(\triangle p/\triangle L)_{g(\text{or } \ell)}} = \phi^2_{g(\text{or } \ell)}(X) \qquad (12)$$

where $(\Delta p/\Delta L)_{TPF}$ = two phase frictional pressure gradient

$(\Delta p/\Delta L)_{g\ (\text{or } \ell)}$ = pressure gradient computed for gas (or liquid) flowing alone in the tube at the same mass rate as in the two-phase stream

$X$ = ratio of single-phase pressure gradients,

$$\frac{(\Delta p/\Delta L)_\ell}{(\Delta p/\Delta L)_g}$$

The Martinelli procedure utilizes a notion of "flow type" based on whether laminar ($Re < 1000$) or turbulent ($Re > 2000$) flow would exist if the phases were flowing alone. The $\phi$ parameters, therefore, are correlated as a function of X in four curves. Although the correlation leaves a great deal of scatter in the data, the method has been perhaps most widely used of all available correlations.

Several attempts have been made to improve the Lockhart-Martinelli approach. Hoogendoorn (53) and Chenoweth and Martin (23) presented improved correlations for high gas densities. Chisolm and Laird (24) made corrections for pipe roughness to the Martinelli correlation, and Hughmark and Pressburg (59) indicated that total mass velocity appears to be an important variable in two-phase flow. Earlier, Levy (73) in an analytical effort established that the $\phi$ parameters do have theoretical significance.

The third type of approach to two-phase flow is through the friction factor concept, which has been used for both horizontal and vertical cases. Govier and coworkers (17, 18, 44, 45, 46) treated the two-phase system as a single phase and presented plots of friction factor as a function of Reynolds number with gas-liquid ratio taken as a parameter. Bertuzzi, Tek, and Poettman (13) used the same general technique to achieve a correlation for horizontal flows which they claimed to be independent of flow pattern. Their correlation curves did show a shift with liquid phase Reynolds number.

The fourth basic approach is illustrated by the work of Ros (111) who performed a general dimensional analysis on vertical two-phase pipe flow. He considered twelve independent variables which account for geometry, liquid and gas physical properties, flow properties, and interactions between phases. Using pressure gradient and liquid holdup as dependent variables, he obtained ten dimensionless groups. Some groups were eliminated because they were physically insignificant in the subsequent experiments. After treating 20,000 experimental points, Ros found only four of the original nine groups had significant effect on pressure drop. His resulting correlation for frictional pressure gradient and liquid holdup involve a rather large number of constants. Although the method is strictly empirical, Ros' correlation does give impressive accuracy.

Most of the literature mentioned so far has been concerned with two-component flows. Linning (77) and Pike (100) performed analyses of horizontal, adiabatic flows of pure evaporating fluids in pipes. The flows were assumed to be in the annular regime, and the authors achieved excellent agreement with their steam-water experiments. Pike's void fraction predictions were within $\pm$ 10 per cent of measured values. His model produced a series of non-linear differential equations which took into account different phase velocities, fluid accelerations, wall shear forces, interface shear forces, and mass and energy transfer between the phases. Pike's analysis is similar to Linning's, but Pike's model did not require information concerning flow variables at some point downstream from the point of initial vaporization, as was the case with Linning's model.

It must be recognized that the pressure drop occurring in the flow of a pure fluid which is boiling or flashing includes, in addition to the frictional loss, a loss resulting from rate of increase of momentum. Such momentum losses are often quite significant, and in order to predict them one needs to know the true gas velocity, demanding in turn knowledge of void fractions. The analyses of Linning (77) and Pike (100) accounted for the momentum effects. A very early attempt to predict boiling pressure drops resulted in the still widely used method of Martinelli and Nelson (82). Their correlation is based on few data and is strictly valid only for steam-water flows. The correlation resulted from an integration of the Lockhart-Martinelli correlation (78), thus accounting for changing quality. However, since the Lockhart-Martinelli method was based primarily upon air-water data, an empirical extrapolation was necessary to make predictions agree with expectations at the critical pressure. Working charts are given which can be used in making rough pressure drop estimates. Goldmann (42) recently extended the Martinelli-Nelson method to sodium flows. His results are purely computational and have yet to be verified by experiment.

Soviet workers have been interested in two-phase flow in boiling systems. Armand (3) correlated the ratio of two-phase pressure gradient as a function of volumetric steam content, taking the ratio of volumetric steam content to void fraction as a parameter. Kutateladze, et al. (69) report the results of Lozhkin, Krol, and Gremilov who studied two-phase mercury flow. They report that wetting has negligible effect on two-phase mercury flow systems, and they propose the following equation for pressure drop.

$$\Delta p = \frac{f V_o^2 \rho_\ell L}{2 g_c D} \left[ 1 + \left( 1 - \frac{\rho_g}{\rho_\ell} \right) \frac{U_g}{V_o} \right] \qquad (13)$$

The discussion thus far has said little about void fractions, although it was recognized that this parameter appears to be fundamental in the correlation and interpretation of two-phase phenomena. Indeed, most of the analytical approaches produce void fraction as a variable. The Martinelli methods (78,82) give empirical correlations for void fractions occurring in horizontal flows, and Ros' work (111) gives values for vertical flows based on his empirical treatment. Linning (77), Pike (100), and Bankoff (9), paid particular attention to prediction of void fraction values in their analytical treatments. Hughmark (58) recently published a method for determination of liquid holdup (one minus the void fraction) in gas-liquid flow.

Levy (74, 75) in some high-level analytical work has tried to predict void fractions (as well as pressure drops). One of his efforts resulted in a momentum model (74) for predicting slip phenomena--the condition, due to unequal density and viscosity between gas and liquid, in which the gas flows at a higher absolute velocity than the liquid. The model gave reasonably good agreement with available experimental results for steam-water horizontal and vertical flows with and without heat transfer, at pressures from 12 to 2000 psia. In a very recent paper (75), Levy treated the two-phase system as a continuous medium and applied to it the single-phase turbulent mixing length methods. Two-phase density and velocity distributions as well as pressure

drops were thus derived analytically. Good agreement was found between theoretical predictions and available data.

A number of papers have presented void fraction data, at the same time emphasizing the experimental techniques used. Radiation (primarily gamma-ray) attenuation has been the most widely utilized technique for obtaining void fractions. Maurer (85), Petrick (99), Hooker and Popper (54), and Richardson (106) all give good developments of the theory of gamma-ray attenuation as applied to measuring void fractions. Petrick (99) and Richardson (106) developed a traversing technique in which a narrow gamma beam is passed across the pipe. This technique was shown to be superior to the "one-shot" method, especially for wide flow channels. These authors present void fraction data for flows in vertical and horizontal rectangular channels. They also determined the effect of a sudden change in flow area on significant parameters and present pressure drop measurements as well. Hooker and Popper (54), in addition to developing the basic theory for void fraction measurements by radiation attenuation, analyze the principal sources of error inherent in the method and evaluate their magnitude for a specific test facility. Maurer (85) presents an excellent review of the method, summarizing the apparatus used by many previous workers. Egen, Dingee, and Chastain (34) obtained void fractions occurring in forced circulation boiling of water in a vertical rectangular test section at 2000 psia. Their paper also furnished an excellent discussion of temperature effects on the gamma-ray attenuation method.

Other methods are available for measuring void fractions, although they are less widely employed. Heineman, Marchaterre and Mehta (51) have used electromagnetic flowmeters to measure void fractions in two-phase metallic flows. The flowmeters must be calibrated before use, and the method is applicable to vertical flow channels in which the quality is less than 0.01. This restricts the void fractions to values below about 0.65. It should be mentioned that the gamma-ray method is good up to qualities of about 0.15. Neal and Bankoff (96) developed an electrical resistivity probe which allows high-order resolution of local void fraction, bubble frequency, and bubble size distribution function in two-phase flows in the bubble regime. The probe was satisfactorily tested in a mercury-nitrogen system. This technique is good only for two-phase flows where the liquid phase is electrically conducting and of course would be applicable for potassium flows. However, the problem of sealing the probe entrance against leakage at the high temperature involved was too formidable to allow anything but preliminary consideration of such a method.

Of the several papers cited so far, few have included work in metallic systems. Indeed, few investigations to date have been involved with metallic fluids. As previously mentioned, Kutateladze, et al. (69) summarize the results of Gremilov and coworkers who studied the vapor-liquid flows of mercury. Kutateladze (69) also presents Siryi's results for the mercury-mercury vapor system as well as those of Korneev who worked with a magnesium amalgam-mercury vapor system. These workers obtained void fraction values and correlated them against the ratio of superficial vapor velocity to total liquid velocity, using an all-liquid Froude number as a parameter. Froude numbers were between 1 and 20. Smith, Tang, and Walker (115) obtained void fractions occurring in two-phase flows of mercury. The Froude numbers reported in this investigation were of the order of $10^{-4}$. A correlation similar to

Gremilov's was given.

Neal (97) describes the same electrical probe as in reference (96) and also discusses development of an impact probe for measuring local liquid velocity. These instruments were used to measure local parameters in co-current mercury-nitrogen flow. A concomitant photographic study showed that the structure of mercury-nitrogen flow is much different from air-water flow, rendering inapplicable the air-water correlations.

Recently Baroczy (10) presented a generalized void fraction correlation and proposed its use for all fluid systems, including liquid metals. The correlation is based on water-air and mercury-nitrogen data. Verification of the correlation with single-component metallic systems was not possible, due to a lack of data. The correlation, which is of the Martinelli type, predicted other steam-water data and data for an organic coolant quite accurately. On the basis of this agreement, calculated values are offered for single-component flows of sodium, potassium, rubidium, and mercury.

This discussion, as mentioned at the outset, does not provide an exhaustive review of the two-phase flow literature. It was intended to cite work which is pertinent to the potassium results soon to be discussed. More and more experimental work in liquid metals is reaching the reporting stage (104, 105). Some work involving several aspects of two-phase flow was presented in a recent symposium (103), but none of the studies was specifically concerned with metallic systems. Several bibliographies are available which may be referred to for a more complete coverage of the two-phase flow literature (6, 11, 48, 60, 84, 124).

## Two-Phase Pressure Drop Study

### INTRODUCTION

Although an extensive literature exists, as illustrated, on the subject of two-phase fluid flow, few investigations have been reported on flows in metallic systems. It was recognized that there was a need to experimentally study metallic two-phase flows. Moreover, it was evident that such a study should, in addition to providing reliable data, indicate whether existing two-phase flow correlations might be applied for making pressure drop estimates in metallic systems. It was expected that the existing correlations would at least require modifications, since the single-component metallic systems of current interest have much higher liquid-to-gas density ratios than the systems used in developing the correlations.

Since a heat transfer test loop for studying forced circulation boiling of potassium was to be procured, this facility offered the opportunity of making pressure drop and void fraction measurements in two-phase flow of potassium.

### DESCRIPTION OF EQUIPMENT

The pressure drop measurement section, an integral part of the test loop, is a horizontal tube of Haynes-25 alloy 5/8-in OD by 0.065-in wall (0.495-in ID) as indicated in Figure 52. The section is oriented horizontally, its level being the highest of all loop components. The differential pressure taps are 1/4-in schedule 40, 4-in long Haynes-25 pipe nipples welded vertically onto the bottom of the tube. They are spaced 36 inches apart.

Two-phase flows are generated in the three parallel 3-in ID preheaters which are vertical. The three streams merge into a 0.476-in ID tube and flow proceeds vertically upward through the heat transfer test section. Just downstream of the heat transfer section, the two phase mixture is turned by an elbow into a 10-in long (20 tube diameters) horizontal calming section from which it enters the pressure drop measurement section. The calming section is merely a portion of the pressure drop tube, extending upstream from the first pressure tap.

Pressure drop is measured with a Taylor Transaire Volumetric D-P Transmitter. Pressure transmitting diaphragm assemblies of 316-stainless steel are transition-welded to the Haynes-25 pressure taps. These 5-ply diaphragms lie in a horizontal plane and are 5 1/8-inches in diameter. At time of installation, the volume above the diaphragm was empty. This volume was filled with potassium upon startup of loop operations. Trace heaters lie alongside the pressure taps and upper portion of the diaphragm housings, the purpose of which is to keep the potassium in contact with the diaphragms liquid at all times. The upper diaphragm housings and pressure taps are insulated with Johns-Manville Cerafelt and Banrock insulation materials. The insulated assembly is shown in Figure 56.

Attached to the lower side of the diaphragm housings are flexible stainless steel capillary hoses. These hoses from the pressure transmitting diaphragms are attached to opposite faces of a single diaphragm which is a component of the transmitter. The capillary hoses and lower portions of transmitting diaphragm housings are filled with sodium-potassium eutectic alloy. This alloy is liquid at room temperatures, and these static legs thus do not require trace heating.

The differential transmitter is horizontally mounted at floor level. Because a pressure drop occurs in the flow test section, the transmitter's single diaphragm receives unequal signals from the two static legs and thus is deflected. Such deflection, being proportional to the pressure drop, causes a deflection on a lever assembly. The differential pressure transmitter, which is a pneumatic force balance system, translates the lever deflection into a proportional air signal at the loop control panel.

Differential pressure is recorded on the strip chart of a Taylor Transcope Recorder. Values are read as per cent of either 100, 300 or 600 inches of water. Taylor Differential Transmitters are usually permanently set at the factory to a single full scale range between 100 and 600 inches of water. However, to add flexibility to the experiments, Taylor Instrument Company in this case provided three calibrated notches on the force beam. One thus has a choice of ranges--100, 300 or 600 inches of water.

The differential pressure measurements made by this system are accurate to within 1 per cent of maximum range--i.e. to within 6 inches of water or about 0.2 psi. Further details on the instruments are given in bulletins issued by the Taylor Instrument Company (118, 119, 120).

Fluid temperatures at the inlet to the calming section and about 6 inches from the downstream pressure tap are measured with platinum--platinum plus 10 per cent rhodium thermocouples. These thermocouples were calibrated against a National Bureau of Standards standard thermocouple. The thermocouples are well type and electrically insulated from the loop. Millivolt signals were read on a Leeds and Northrup type K-2 potentiometer, and the temperatures recorded to within 0.1°F with the aid of the calibration charts. Standardized thermocouple lead wire connects all thermocouples to the read-out switch at the control panel.

In treatment of data to obtain qualities in the flowing two-phase mixtures, the power supplied to the preheaters is an important experimental measurement. Total preheater power was read to within 0.2 KW on a General Electric AC Kilowatt meter which has a 0-30 KW range. The maximum power attainable in the preheaters, in experiments to date, was 19 KW. A Superior Electric Company Powerstat variable transformer is used to vary the power input to the preheaters.

Another important variable in the interpretation of two-phase flow results is the mass flow rate. The liquid metal flow rate is measured by a Mine Safety Appliance Research, Style FM-2 magnetic flowmeter. The flowing liquid metal cuts the lines of force of a permanent magnet and generates a voltage which is proportional to the flow rate. A calibration curve for

reducing millivolt readings to GPM, as a function of metering temperature, was supplied with the meter. This calibration was checked and found accurate. Flow rates were read to within 0.05 millivolt. Accuracy of flow rates is about $\pm$ 7 lbm/hr corresponding to a maximum of about 5.5 per cent uncertainty at the lowest flow rates run to date.

## EXPERIMENTAL PROCEDURES

Pressure drop data were obtained for flow rates ranging from 110 to 740 lb per hour and for preheater power settings ranging from 7.3 to 19 KW. Once the loop was running essentially steady at given pump and preheater settings, the necessary loop data were recorded and the Taylor differential pressure chart marked appropriately. For most operating conditions several sets of data were obtained. These data included readings on all platinum-platinum plus 10 per cent rhodium thermocouples for heat balance determination, flow rate (in millivolts on the K-2 potentiometer), flow meter temperature, and preheater power settings.

The differential pressure transmitter was zeroed frequently. Although the zero of the instrument exhibits a drift, the zero was checked often enough so that there is negligible error in the data due to this zero drift.

For most of the data reported, the pressure drop fluctuated regularly about a mean value which is the result reported. The pressure drop fluctuations were accompanied by oscillations in the flow rate (also recorded on the Taylor chart during most of the experiments). It is evident that the potassium loop exhibited instabilities, a situation commonly found in such two-phase test loops. Data reported at given power and pump settings are for steadiest possible conditions in flow rate--i. e., at conditions of zero or minimum flow rate fluctuations.

The differential pressure fluctuations are greatest at high preheat power values and low pumping rates. The inverse to this situation is also true. Superheating of the liquid in the preheaters is believed to be the explanation for this trend. At low flow rates the liquid moves into the preheater with little disturbance and the higher power level causes it to superheat as it "crawls" upward. Periodically a sudden nucleation occurs, producing a large volume of vapor which pushes a liquid slug up through the heat transfer section and through the pressure drop section. This surge shows up as a fluctuation in the pressure drop trace. At lower power settings the magnitude of the liquid superheat is less, and increased flow rate also provides disturbance for more frequent nucleation. Thus, the surges are less violent.

Prior to running two-phase flow experiments, a series of data were taken to determine heat losses from the preheaters, heat transfer section, and pressure drop section. The losses were determined as enthalpy changes in single phase flow. Preheater losses were correlated against outlet temperature (TC26), test section and pressure drop section losses were correlated against inlet temperature (TC26 and TC30, respectively). The preheater and heat transfer section heat losses were found to be independent of mass flow rate, but pressure drop section losses display a parametric flow rate effect.

The heat loss determinations are necessary for determination of quality in the two-phase flow runs. Quality is defined as weight fraction vapor and is calculated by enthalpy balance. The physical and thermodynamic properties given by Weatherford, et al. (125) are used.

## RESULTS

A typical section of the Taylor chart showing pressure drop and flow rate (millivolts) traces is given in Figure 58. The section shown is for a flowmeter output of about 4 millivolts and 18.5 KW preheater power. The pressure drop here is being recorded in the 0-300 inches of water range. The zero for this pressure drop trace is 30 per cent. Thus the mean pressure drop at 3:00 is 2.38 psi.

The pressure drop data are presented in Tables XVIII, XIX and XX. Tables XVIII and XIX show data at essentially constant mass flow rates. These data were obtained while keeping the flowmeter output as nearly constant as possible at 2 and 3 millivolts. Table XX presents data at a series of nearly-constant mass flows. Inlet and outlet temperature and quality are presented in addition to average pressure drop section quality and preheater power. The fact that the parametric mass flow rates vary over a range is due to a shift in flowmeter temperature with a preheater power change.

The tabulated results are presented graphically in Figures 59, 60, 61 and 62. Figures 59, 60 and 61 show pressure drop as a function of average quality occurring in the test section at nearly-constant values of mass flow rate. Figure 62 shows the variation of pressure drop with mass flow rate, taking average test section quality as a parameter. This plot most effectively presents the data obtained at higher flow rates, which are fewer in number than low flow rate data. The data in Figure 62 do not represent truly constant values of quality, but rather narrow ranges of quality. Table XXI summarizes the data used in Figure 62.

The overall ranges of pertinent variables may be summarized as follows:

| | | |
|---|---|---|
| a) | Pressure Drop, psi | 0.0545 - 3.10 |
| b) | Mass Flow Rate, lb/hr | 110 - 740 |
| c) | Inlet Quality | 0.0091 - 0.402 |
| d) | Average Quality | 0.0159 - 0.400 |
| e) | Inlet Temperature, °F | 926 - 1432 |

## DISCUSSION OF RESULTS

An examination of Tables XVIII, XIX, XX shows that in nearly all cases the pressure drop is accompanied by a temperature drop and a corresponding increase in quality. For the entire set of data, the heat losses from the pressure drop section ranged from 800 to 2000 Btu/hr. Since the heat supplied to the fluid in the preheaters ranged from about 20,000 to 55,000 Btu/hr (accounting for preheater losses), it is evident that the pressure drop section losses represent a small portion of the fluid's total enthalpy. Thus, the two-phase flows in the pressure drop section occur nearly adiabatically over the entire range of data. It follows that the two-phase flows

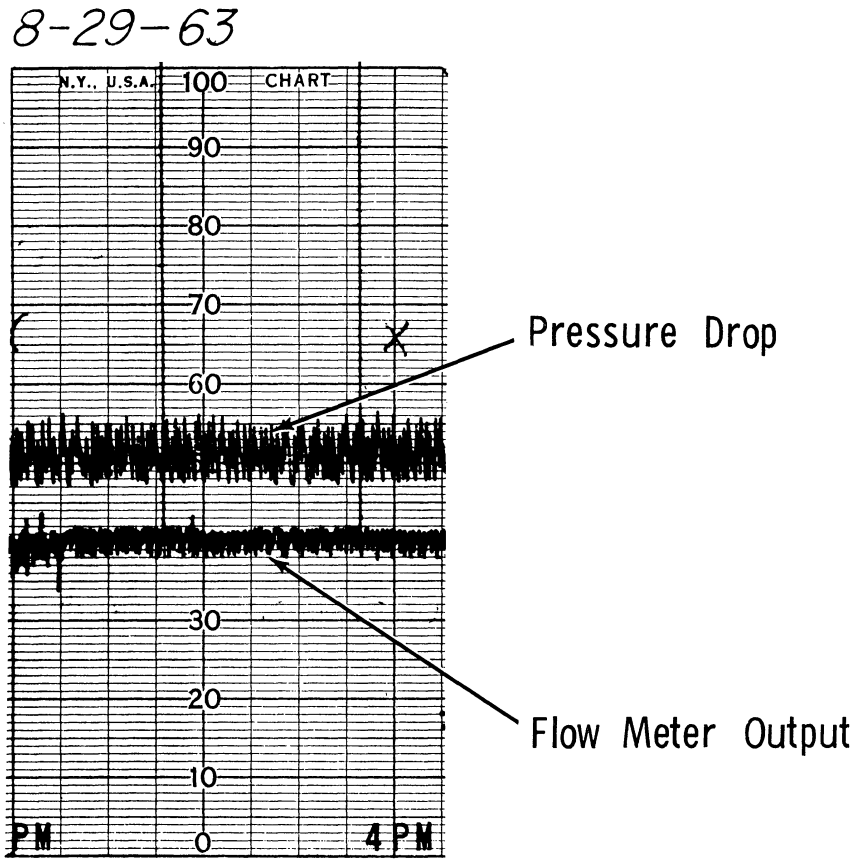


| | |
|---|---|
| Preheat Power | 18.5 KW (Full) |
| Pressure Drop Scale | 0-300 in. of Water |
| | zero = 30% |
| Flow Meter Scale | 0-10 Millivolts |

Figure 58. Typical Section of Taylor Transcope Recorder Chart, Showing Pressure Drop and Flow Meter Traces.

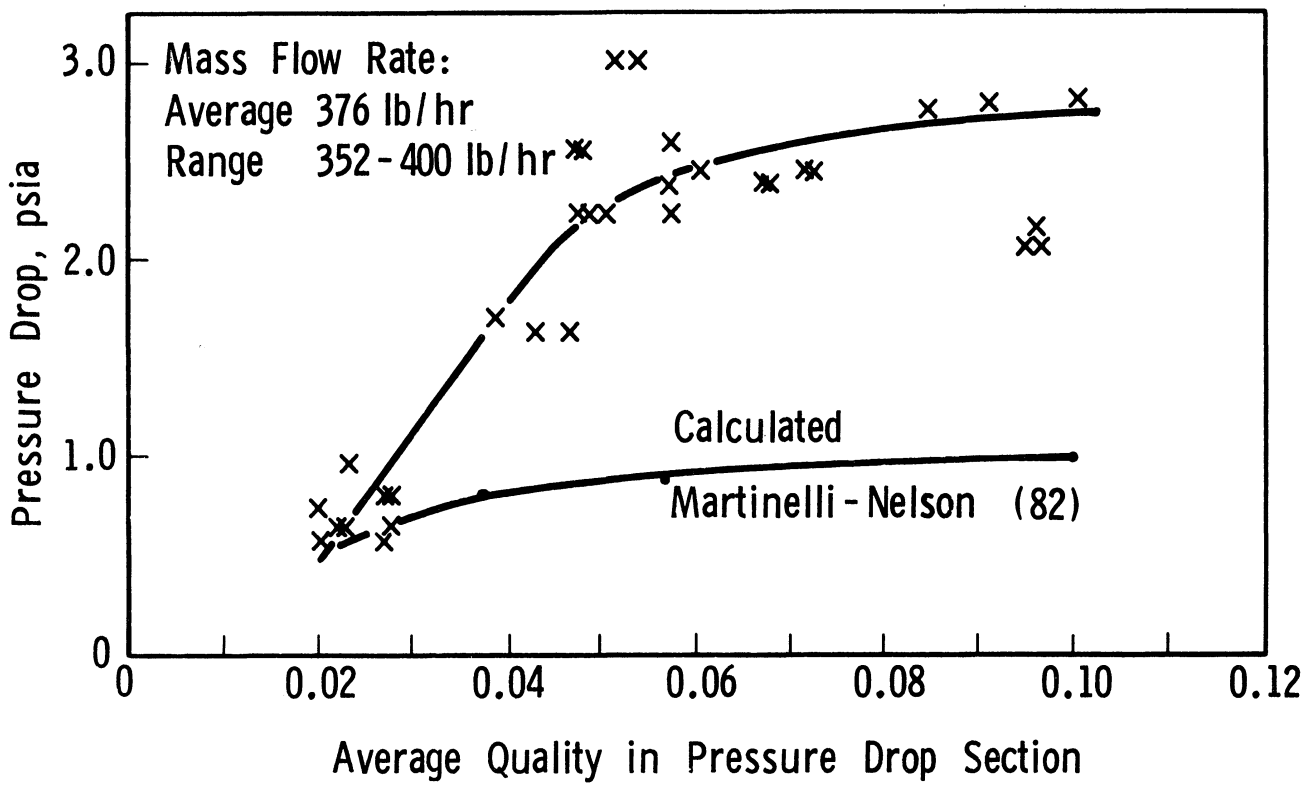


Figure 59. Pressure Drop as a Function of Average Quality at Mass Flow Rate of 376 lb/hr.

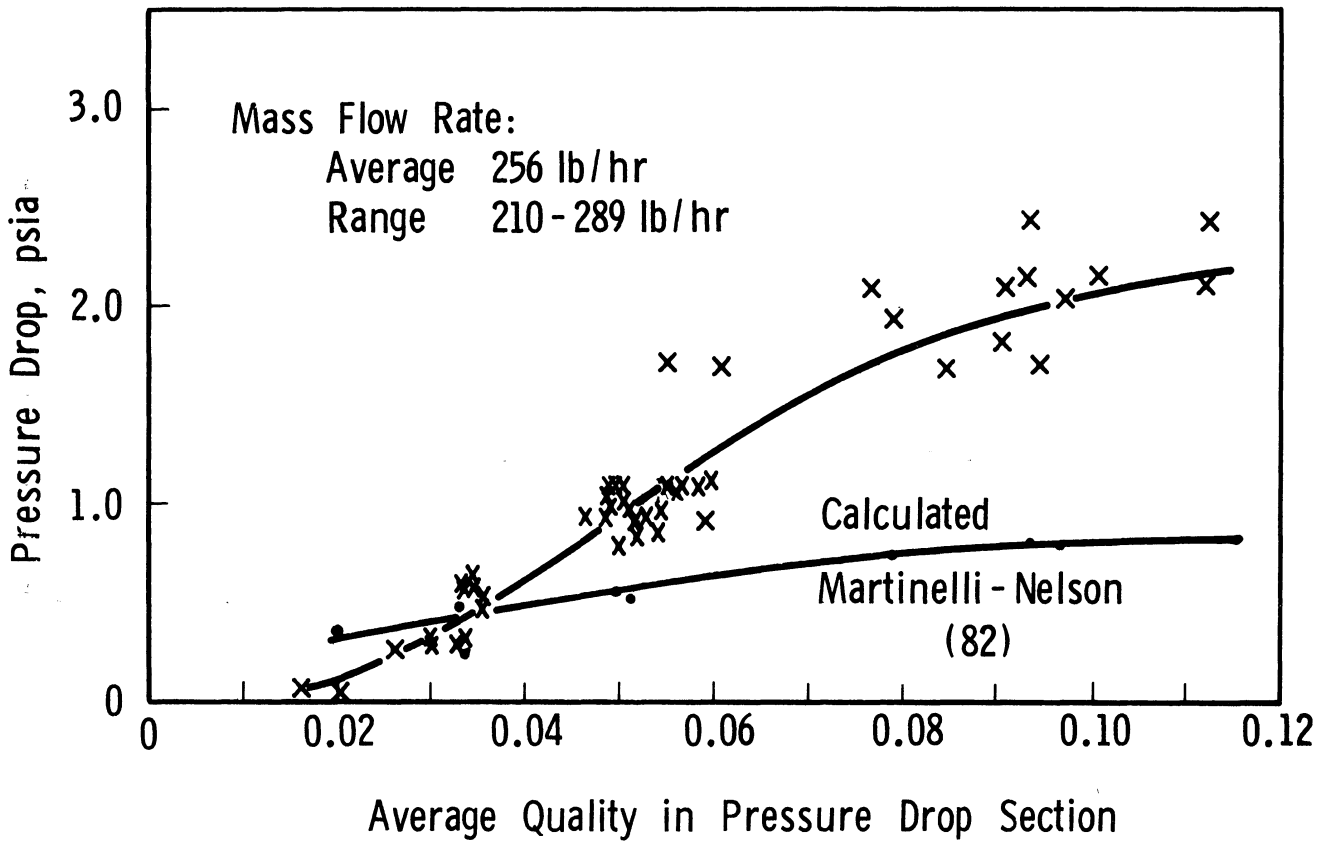


Figure 60. Pressure Drop as a Function of Average Quality at Mass Flow Rate of 256 lb/hr.

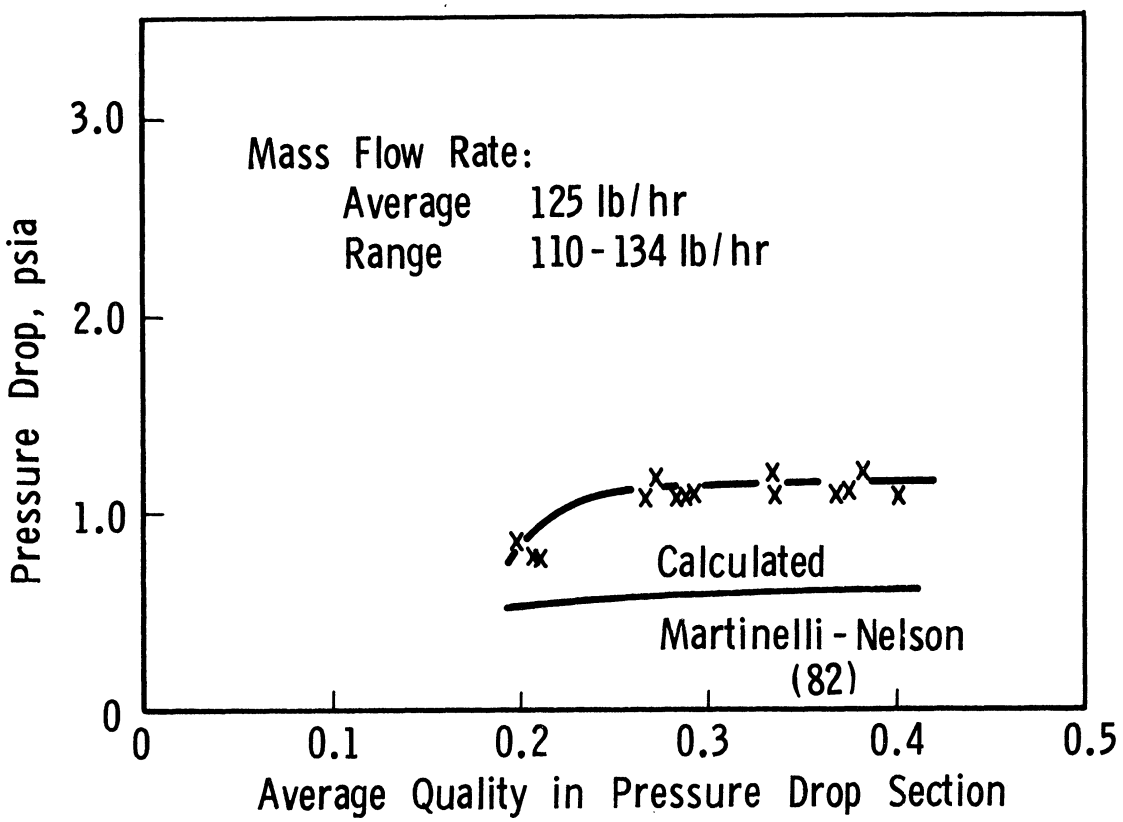


Figure 61. Pressure Drop as a Function of Average Quality at Mass Flow Rate of 125 lb/hr.

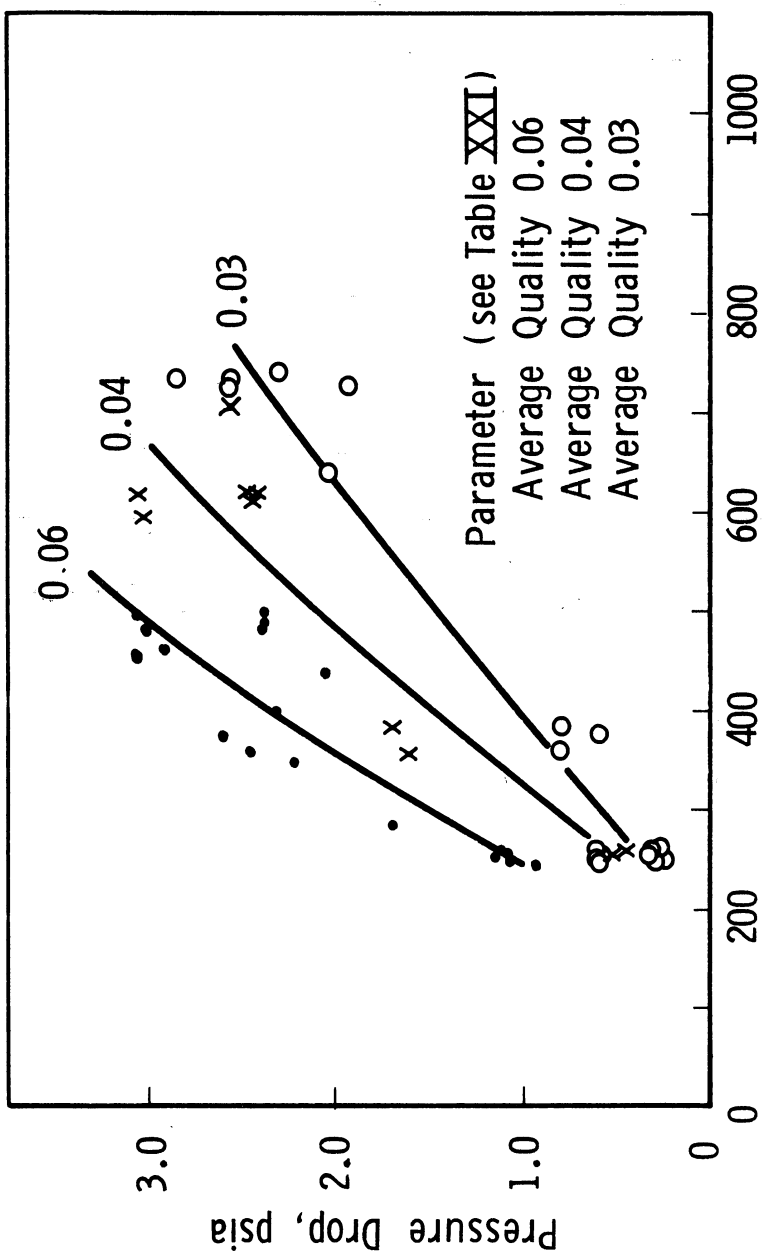


Figure 62. Pressure Drop as a Function of Mass Flow Rate, with Average Quality as Parameter.

under consideration here are the "nearly-adiabatic, evaporating" type. The evaporation or flashing occurs because thermodynamic equilibrium is maintained--i.e., because the rate of heat transfer is small decreasing pressure and temperature leading to increased quality, a consequence of the First Law. Adiabatic, evaporating flows have been examined by Linning (77) and Pike (100). Both authors assumed thermodynamic equilibrium and wrote differential equations based on an annular flow model. The methods of Linning and Pike are being studied, and the equations are being adapted to see if the model agrees with the data presented here.

Prior to making pressure drop runs, it was found that the thin-walled heat transfer section had somewhere failed and potassium had leaked into the secondary sodium system. It was then decided to run two-phase flow experiments, the data from which are under consideration here. After shutdown of operations and after much of the data had been reduced, a chemical analysis showed that leakage had also occurred into the potassium side and the experiments had been run with a mixture containing 8 per cent sodium. Since the data had been processed using pure-potassium properties, the question arose as to what effect the presence of 8 per cent sodium has on quality calculations.

Referring to the Liquid Metals Handbook (64), it is a relatively simple matter to adjust pertinent physical and thermodynamic properties, giving values for potassium-sodium mixtures. Properties were examined in the temperature range 900-1400°F, and the average deviations between the two systems are presented in Table XVI.

Appendix K gives an analysis of uncertainty in quality calculation, based upon known precision in experimental measurements as well as neglecting presence of the sodium in the fluid. The results in Table XVI are used in this analysis. Examination of a "worse case" shows that a 5 per cent error results from neglecting sodium--i.e., the error amounts to 5 per cent of the quality value obtained by using pure-potassium properties. Thus, not a great deal of accuracy is lost in presenting the data on the basis of pure-potassium properties. The important point, however, is that property values can be adjusted.

The error analysis in Appendix K includes an examination of the uncertainty in quality values arising from uncertainty in experimental measurements. The variables considered are preheat power, all pertinent heat losses, and flow rate. A "worse case" examination shows the uncertainty to be about 10 per cent--i.e., the uncertainty amounts to 10 per cent of the calculated quality value.

One interesting aspect of two-phase flow which has not been mentioned so far is flow regime. This is an area of study in itself but cannot be entirely separated from other facets of the problem. Vohr (123) presents a survey of two-phase flow pattern investigations. He points out that Baker's work (5) represents one of the few flow regime studies that includes the effect of different fluid physical properties. Although the results are somewhat preliminary, they are derived from horizontal flow data.

TABLE XVI

AVERAGE PER CENT DEVIATION IN PROPERTIES BETWEEN PURE POTASSIUM AND MIXTURE CONTAINING 8 PER CENT BY WEIGHT SODIUM OVER THE TEMPERATURE RANGE 900-1400°F

| Property | Average deviation of mixture from pure potassium |
|---|---|
| Liquid Density | 1.6 per cent higher |
| Liquid Viscosity | 1.0 per cent higher |
| Liquid Heat Capacity | 5.1 per cent higher |
| Liquid Enthalpy * | 5.1 per cent higher |
| Vapor Pressure ** | 11.3 per cent lower |
| Heat of Vaporization *** | 3.6 per cent higher |

* Saturated Liquid, referred to 0°F

** Raoult's Law assumed

*** Based on equilibrium vapor composition --i.e., for partial vaporization

Baker's plot (5) was used to predict flow regimes in the potassium data. The entire range of mass flow rates, qualities, and temperature levels was included in this examination. All data fell in the annular, dispersed, or annular-dispersed transition areas of Baker's plot. It is believed that slugging effects on the pressure drop trace are due to instabilities in the preheaters and the flows are inherently annular or dispersed. It is rather fortuitous that this is the case, for it increases hope that the annular flow theory (in development) will adequately predict the effects observed. In general, dispersed flows are predicted at higher qualities, annular flows at lower qualities. Total mass flow has an effect as well.

One of the primary goals of this study was to compare potassium pressure drop data with existing correlations. For the type of flow observed the method of Martinelli and Nelson (82) has been widely used for making pressure drop predictions in nonmetallic systems. Recognizing the fact that the Martinelli-Nelson correlation is derived for steam-water flow, it was decided to compare the experimental data with pressure drop values predicted by the correlation. Experimental conditions of total mass flow, exit quality, average test section pressure and temperature were used. The frictional component of pressure drop was predicted using the actual exit quality. However, since the acceleration pressure drop component arises primarily from the quality increase, the acceleration multiplier in the correlation was evaluated at a pseudo exit quality equal to the quality increase. It was necessary to extrapolate the correlation curves to the low pressure range (0.3 to 14.7 psia).

The pressure drops calculated by the Martinelli-Nelson technique are shown in Figures 59, 60 and 61. It is evident that the potassium two-phase pressure drops are much higher than those occurring in steam-water flows over most of the quality range.

Figure 63 summarizes the comparison of the data with the Martinelli-Nelson predictions, including values at the higher flow rates. Predictions were not made for each data point, but the trend of the comparison is clear. A curve is shown through values at the four lowest flow rates. Points at the two highest flow rates scatter away from the curve.

An interesting trend can be seen in Figures 59, 60 and 61. In Figure 59 the slope of the curve decreases in the 0.045 to 0.065 quality region, and from about 0.07 quality upward the curve flattens out. This change in slope is not so pronounced in Figure 60 but is clearly present in Figure 61. Comparing these three figures, it is evident that the quality level where the curve "bends over" is dependent on total mass flow rate. It appears that the bend occurs at lower qualities for higher flow rates.

Two further features are obvious from Figures 59, 60, 61 and 62. First, pressure drop increases with quality for any given mass flow rate. Second, for a given quality the pressure drop varies as the flow rate. These results are quite in keeping with physical expectations. Frictional forces increase with increased mass flow, and also with increased quality.

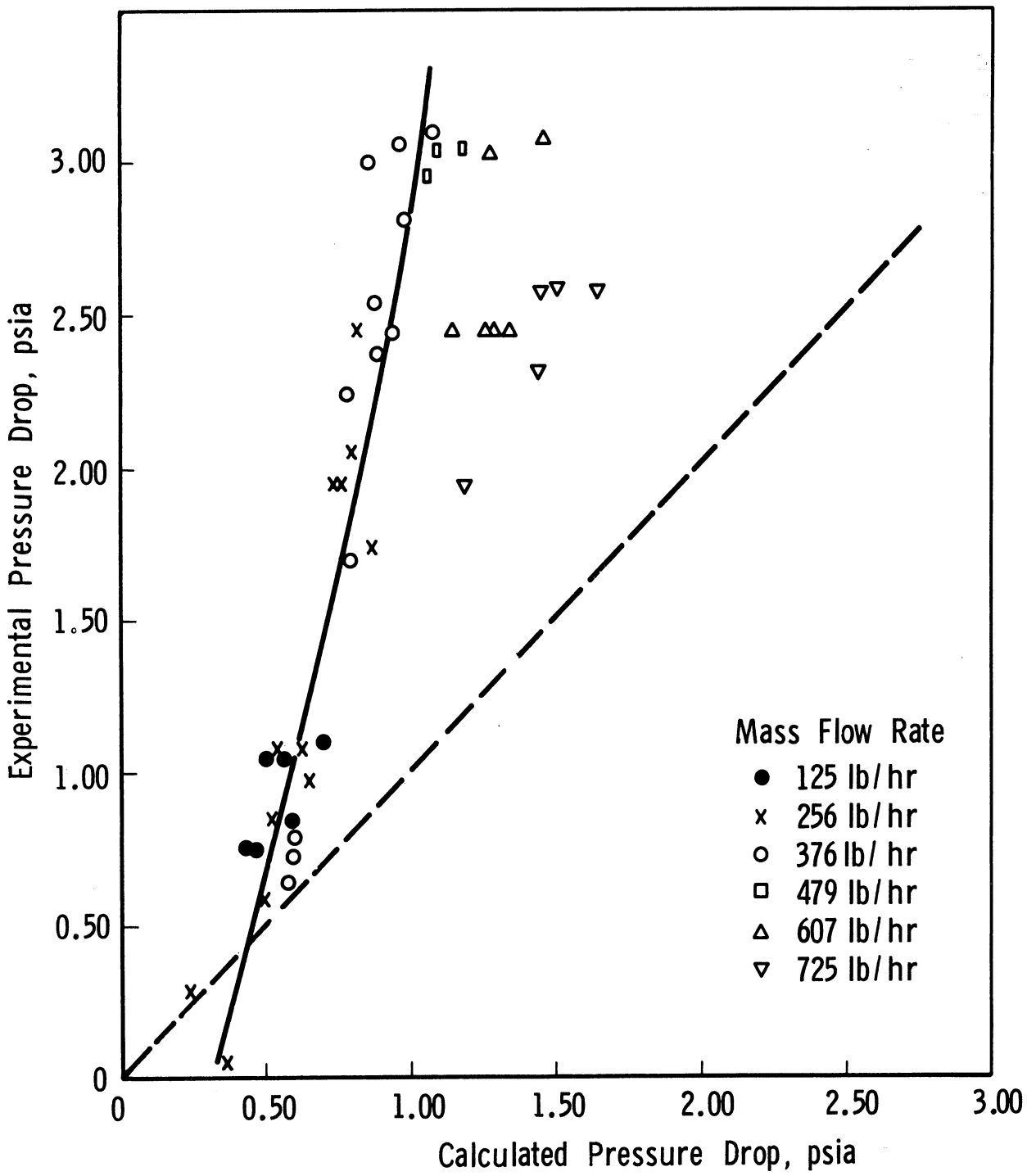


Figure 63. Comparison of Pressure Drop Data With Values Predicted for Steam-Water Flows (82).

## Void Fraction Study

INTRODUCTION

In the experimental study of two-phase flow of any fluid system, it is desirable to obtain void fraction data, the value of which will be outlined here.

In gas-liquid flow, the mean velocities of the two phases may not be equal. The mean velocities referred to here are those based on the cross sectional area occupied by each phase. This inequality of velocities, known as "slip," occurs in both horizontal and vertical flow. The true fraction of the pipe cross section occupied by either phase differs from that calculated, if the calculation is based on the volumes of liquid and gas passed through the flow channel. From considerations of mass balance the slip velocity ratio is given by

$$S = \frac{V_g}{V_\ell} = \left(\frac{x}{1-x}\right)\left(\frac{1-\alpha}{\alpha}\right)\left(\frac{\rho_\ell}{\rho_g}\right) \tag{14}$$

where $V_g$, $V_\ell$ = vapor and liquid average velocities

$\rho_g$, $\rho_\ell$ = vapor and liquid densities

$x$ = quality, mass fraction vapor

$\alpha$ = void fraction (or vapor volume fraction)

The hydraulics of two-phase flow are influenced by the void fraction. In a flow system in which a change of phase is occurring, the differential pressure drop can be written as

$$-dp_{\text{overall static}} = -dp_{\text{friction}} - dp_{\text{acceleration}} - dp_{\text{hydrostatic}} \tag{15}$$

which merely reduces the overall pressure drop into a summation of the pressure drops arising from the major physical processes taking place. The above relationship can be expressed more quantitatively as

$$dp = dp_f + \bar{\rho}\,\frac{V\,dV}{g_c} + \bar{\rho}\,dL\sin\theta\,\frac{g}{g_c} \tag{16}$$

where $\bar{\rho}$ = local mean density of the two-phase mixture

$p_f$ = frictional pressure loss

$V$ = local superficial mixture velocity

$L$ = length along channel

$\theta$ = angle of inclination of channel from horizontal

$g_c$ = force-mass conversion constant

$g$ = acceleration of gravity

For a flowing two-phase mixture with slip, the local mixture density is given in terms of the local void fraction and individual phase densities as

$$\bar{\rho} = \alpha \rho_g + (1-\alpha) \rho_\ell \qquad (17)$$

Examination of Equations 16 and 17 shows that without knowledge of the void fraction, the hydrostatic and accelerative components of pressure drop cannot be separated from the overall static pressure drop to yield friction losses. Thus, the usefulness of void fraction measurements is realized.

Gamma-ray attenuation methods have been used by many workers to obtain void fraction data. This technique, in general, is reliable for qualities up to about 15 per cent. Basically, the method measures the mean mixture density of the two-phase fluid. As has been shown in Equation 17, the void fraction is related to the mean two-phase density. However, because appropriate gamma ray absorption coefficients are usually lacking, the experimental technique is actually indirect, Equation 17 not being used to calculate void fraction. Rather, the usual procedure is to interpolate between detector signals read for all-liquid and all-vapor flows. The type of interpolation valid for certain two-phase flows can be derived theoretically. The resulting expressions depend on the spatial orientation of the fluid phases with respect to the gamma-ray beam, as will be shown subsequently.

Void fractions occurring in the horizontal two-phase potassium flows were obtained, using the radiation attenuation method. A nominal 5-curie Tm-170 gamma-ray source and a scintillation detection system were employed. The low gas-liquid density ratios encountered (of the order of $10^{-4}$) required low energy radiation in order that a large portion of the beam impinging on the channel be attenuated. This consideration led to the choice of Tm-170 as the gamma-ray source.

The void fraction data obtained to date exhibit a high degree of scatter and have not been successfully correlated. These data will be presented, together with discussions of apparatus and theoretical background.

THEORY

Maurer (85), Petrick (99), Hooker and Popper (54), and Richardson (106) all give developments of the theory of gamma-ray attenuation as applied to measuring void fractions.

Following Maurer's discussion, the intensity of a monoenergetic beam of electromagnetic radiation emerging from an absorber is given by

$$I = I_o \, e^{-\left(\frac{\mu}{\rho}\right)\rho t} \qquad (18)$$

where $I_o$ = intensity of beam entering the absorber

$t$ = absorber thickness

$\rho$ = absorber density

$\left(\frac{\mu}{\rho}\right)$ = mass absorption coefficient of absorber

$\mu$ = linear absorption coefficient (dimensions are reciprocal length)

Equation 18 is a statement of the well-known Beer-Lambert law, in which the absorber is presumed to be homogeneous and the radiation beam is presumed to consist of parallel rays.

Referring to Figure 64, if the incident beam has a finite size and passes through several materials, the intensity of emerging radiation will be given as

$$I = \int_o^{y_1} \left\{ \frac{I_o}{y_1} \cdot \exp\left[ -\int_o^{z_1} \left(\frac{\mu}{\rho}\right)_{z,y} \rho_{z,y} \, dz \right] \right\} dy \qquad (19)$$

where the subscript (z, y) denotes that $\left(\frac{\mu}{\rho}\right)$ and $\rho$ are functions of z and y. Implied in this integration is the fact that in the general two-dimensional case, the incident beam intensity $I_o$ varies with the y coordinate. The result I is a pseudo uniformly strong beam due to the normalizing factor $1/y_1$. The case considered here is not completely general in the sense that it could be extended to three-dimensional geometry. Since the radiation is passing through a slab composed of several materials, one must deal with discontinuities in the functions $(\mu/\rho)_{z,y}$ and $\rho_{z,y}$.

Consider the more common and less complicated case where a uniform beam impinges on a laminated slab. If each of the n lamina is taken as having constant density and constant mass absorption coefficient, Equation 19 reduces to

$$I = I_o \cdot \exp\left[ -\sum_{i=1}^{n} \left(\frac{\mu}{\rho}\right)_i \rho_i \, t_i \right] \qquad (20)$$

If density or thickness of material are the only variables, the density or thickness can be measured using the basic Equation 18 if $I_o$ and $(\mu/\rho)$ are known.

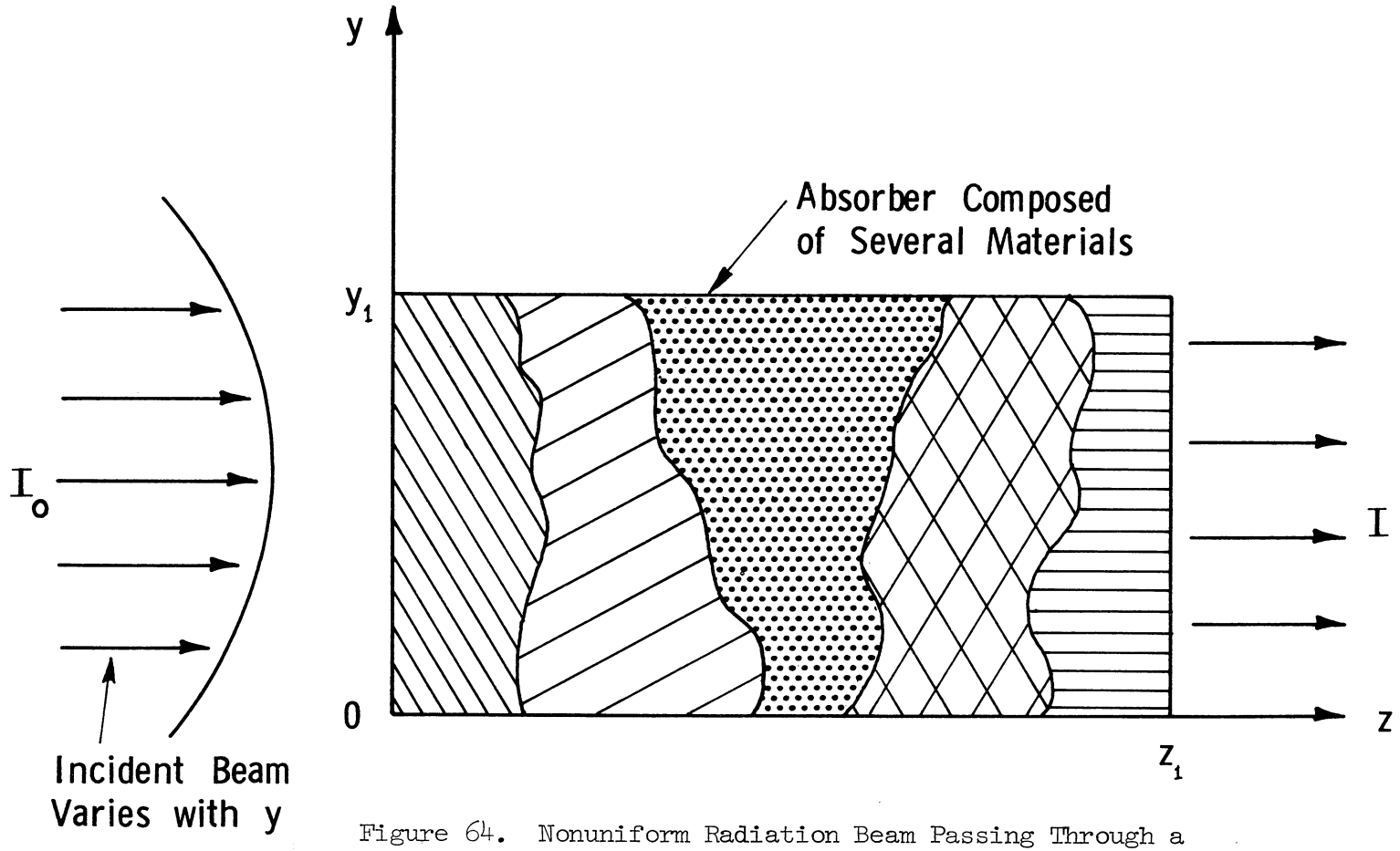


Figure 64. Nonuniform Radiation Beam Passing Through a Nonhomogeneous Absorber.

$$t\rho = \frac{\ell n \left(\frac{I}{I_o}\right)}{-\left(\frac{\mu}{\rho}\right)} \qquad (21)$$

The value of I is measured experimentally. In practice it is often impossible to predict $(\mu/\rho)$ and $I_o$, so it is necessary to resort to calibration techniques which eliminate the difficulty.

Consider now the use of a gamma-ray source to measure the mean density of a two-phase fluid. A suitably collimated beam of radiation is passed through a flow channel, with the emergent beam intensity measured by a suitable detector. One way of circumventing the difficulties caused by not knowing $I_o$ and $(\mu/\rho)$ is to take readings with all-vapor and all-liquid flows. Let

$I_\ell$ = intensity of emergent beam with all-liquid flow

$I_g$ = intensity of emergent beam with all-vapor flow

Then

$$I_\ell = I_o \cdot \exp\left[ - \left(\frac{\mu}{\rho}\right) \rho_\ell \, t_\ell - \left(\frac{\mu}{\rho}\right)_s \rho_s \, t_s \right] \qquad (22)$$

$$I_g = I_o \cdot \exp\left[ - \left(\frac{\mu}{\rho}\right) \rho_g \, t_g - \left(\frac{\mu}{\rho}\right)_s \rho_s \, t_s \right] \qquad (23)$$

The subscript s refers to the solid channel wall through which the beam must pass. By dividing Equations 22 and 23, taking logarithms and rearranging,

$$\left(\frac{\mu}{\rho}\right) = \frac{\ell n \left(\frac{I_g}{I_\ell}\right)}{t(\rho_\ell - \rho_g)} \qquad (24)$$

In single-phase flows it is clear that $t_\ell = t_g$, which appear as t in Equation 24. Implied in Equation 24 is the fact that for a given absorber the mass absorption coefficient $(\mu/\rho)$ is essentially constant at given gamma energies, regardless of physical state of the absorber. Thus, Equation 24 is valid for a single chemical species.

If a two-phase mixture occupies the channel, the emergent beam intensity can be written in the same form as Equations 22 and 23.

$$I = I_o \cdot \exp\left[ - \left(\frac{\mu}{\rho}\right) \bar{\rho} \, t - \left(\frac{\mu}{\rho}\right)_s \rho_s \, t_s \right] \qquad (25)$$

where $\bar{\rho}$ represents the mean mixture density.

In order to eliminate $I_o$ from Equation 25, Equation 22 or 23 may be used. Since in the potassium experimenta all-liquid flows are easier to achieve than all-vapor flows, Equation 22 is divided into Equation 25.

$$\ell n \frac{I}{I_\ell} = -\left(\frac{\mu}{\rho}\right) \bar{\rho}\, t + \left(\frac{\mu}{\rho}\right) \rho_\ell\, t$$

Inserting the value of $(\mu/\rho)$ from Equation 24,

$$\ell n \frac{I}{I_\ell} = \ell n \left(\frac{I_g}{I_\ell}\right) \left[\left(\rho_\ell t - \bar{\rho}\, t\right) \frac{1}{t(\rho_\ell - \rho_g)}\right]$$

Finally,

$$\frac{\ell n \left(\frac{I}{I_\ell}\right)}{\ell n \left(\frac{I_g}{I_\ell}\right)} = \frac{\rho_\ell - \bar{\rho}}{\rho_\ell - \rho_g} \qquad (26)$$

From Equation 26 the mean mixture density is obtained from the emergent beam intensity I. In addition, it is necessary to establish the single-phase intensities $I_g$ and $I_\ell$ from calibration runs.

It is easy to transform Equation 26 to make the void fraction $\alpha$ the dependent variable rather than the mean density $\bar{\rho}$. The void fraction by definition is the volume fraction occupied by vapor at a point (small region) in the two-phase flow. In measuring mean mixture densities by radiation attenuation, it is necessary to pass the rays through the entire channel or at least through some chord of the channel. Because of this technique, the void fractions obtained are not point values but are mean values occurring at the channel's axial location where the test equipment is placed. Hence, in this discussion the term "void fraction" will refer to the mean values so obtained. Let

$\alpha$ = void fraction

A = cross sectional flow area at a given channel position

For purposes of the following discussion, the void fraction may be thought of as the fraction of flow cross section occupied by vapor. Then

mass of liquid at a section per unit length = $\rho_\ell(1-\alpha)A$

mass of vapor at a section per unit length = $\rho_g\ \alpha\ A$

total mass at a section per unit length = $\bar{\rho}\ A$

By mass balance

$$\bar{\rho}\ A = \rho_\ell\ (1-\alpha)\ A + \rho_g\ \alpha\ A$$

so that

$$\bar{\rho} = \rho_g\ \alpha + \rho_\ell\ (1-\alpha) \tag{27}$$

which is the same as Equation 17 given in the Introduction. Insertion of Equation 27 into Equation 26 yields

$$\alpha = \frac{\ell n\left(I/I_\ell\right)}{\ell n\left(I_g/I_\ell\right)} \tag{28}$$

Equation 28 is valid for data reduction in obtaining void fractions as long as the two phases are sufficiently mixed to behave in pseudo-homogeneous fashion. This relationship is also valid for separated phase distributions, if the phases are distributed with respect to the gamma-ray beam as in Figure 65-a (54, 99, 106). Here the separated phases exist as lamina oriented perpendicular to the radiation beam.

The separated phase distribution of Figure 65-a represents one extreme case. Another extreme case is given in Figure 65-b where the phases exist as lamina oriented in the direction of the radiation beam. It can be readily shown (99, 106, 34) that the overall attenuation is expressed by

$$\alpha = \frac{I - I_\ell}{I_g - I_\ell} \tag{29}$$

Comparing the two extreme separated phase distributions given in Figure 65, with results expressed by Equations 28 and 29, it is apparent that the expression used for data reduction depends strongly on how the phases are oriented with respect to the radiation beam.

It was planned to run an air-water simulation study to try and determine the appropriate equation for use in data reduction. However, as reported in the Pressure Drop Study section, the two-phase flows obtained are almost certainly in the annular or dispersed regimes. Since a narrow gamma-ray beam was employed, the physical situation in annular flows corresponds to Figure 65-a, while the dispersed flows behave essentially homogeneously. Therefore, all data were reduced using Equation 28. Richardson (106) and

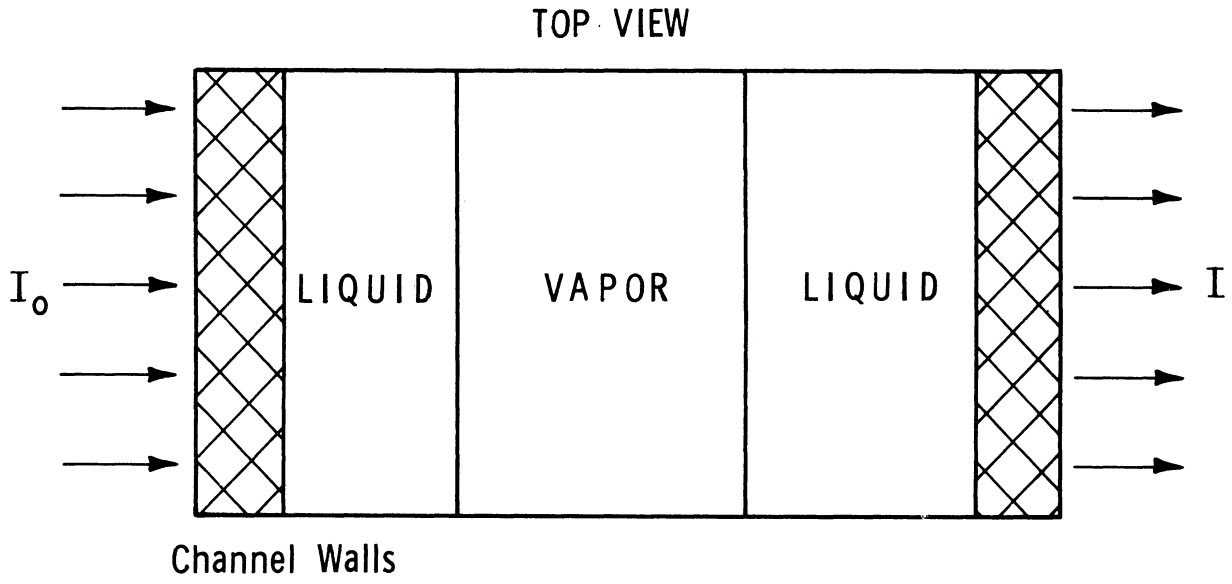


(a) Separated Phase Distribution Giving Overall Radiation Attenuation Same as for Homogeneous Mixture

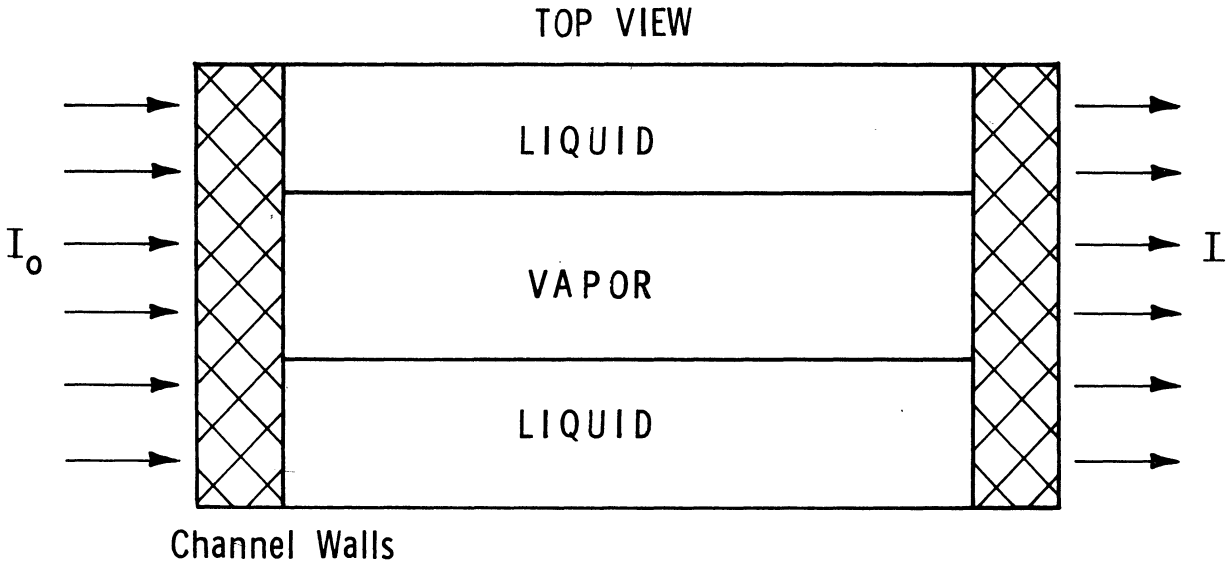


(b) Separated Phase Distribution Giving Overall Radiation Attenuation Completely Different from Homogeneous Mixture

Figure 65. Two Extreme Cases of Separated Phase Distribution.

Petrick (99) found their experimental air-water flows behaved essentially homogeneously and used Equation 28.

Detector count rates, N. rather than beam intensities can be used in Equations 28 and 29. Some investigators (54, 99, 106) have used a recorded voltage signal rather than count rates in their equations.

In utilizing Equation 28 or Equation 29 to calculate void fractions, care must be taken to account for temperature effects. Put more explicitly, if the single-phase emergent intensities are determined at flow temperatures different from the two-phase flow temperatures, the calculated void fractions will be in error. Experimental difficulties preclude making calibration measurements with each experimental measurement. Egen, Dingee, and Chastain (34) made a thorough analysis, showing clearly how to compensate for effects arising from different temperatures. The following discussion, based on their work, will show how appropriate temperature corrections can be made.

As an example, assume that a two-phase system is flowing essentially homogeneously so that the void fraction is given by

$$\alpha = \frac{\ell n\left(I/I_\ell\right)}{\ell n\left(I_g/I_\ell\right)} \tag{28}$$

To be strictly correct the I's in Equation 28 must all be measured at the same temperature. For an all-liquid flow at temperature $T_o$, the emergent beam intensity is obtained from Equation 22 as

$$\left(I_\ell\right)_{T_o} = I_o \exp\left\{ - \left[\left(\frac{\mu}{\rho}\right) \rho_\ell t_\ell\right]_{T_o} - \left[\left(\frac{\mu}{\rho}\right)_s \rho_s t_s\right]_{T_o}\right\} \tag{30}$$

where the subscript $T_o$ indicates the temperature dependence of the densities and mass absorption coefficients. Likewise for an all-vapor flow, Equation 23 gives

$$\left(I_g\right)_{T_o} = I_o \exp\left\{ - \left[\left(\frac{\mu}{\rho}\right) \rho_g t_g\right]_{T_o} - \left[\left(\frac{\mu}{\rho}\right)_s \rho_s t_s\right]_{T_o}\right\} \tag{31}$$

For single-phase flows $t_\ell = t_g = t$. Dividing Equations 30 and 31 and taking logarithms,

$$\ell n \left(\frac{I_g}{I_\ell}\right)_{T_o} = t \left(\frac{\mu}{\rho}\right)_{T_o} \cdot \left(\rho_\ell - \rho_g\right)_{T_o} \tag{32}$$

This equation may be extended immediately to any flow temperature T. Thus,

$$\ell n \left(\frac{I_g}{I_\ell}\right)_T = t \left(\frac{\mu}{\rho}\right)_T \cdot (\rho_\ell - \rho_g)_T \qquad (33)$$

Now, the mass absorption coefficient at a given gamma energy is essentially independent of temperature over appreciable temperature ranges (34). It is reasonable, then, to take $(\mu/\rho)$ as a constant. By dividing Equations 32 and 33 one obtains, upon rearrangement

$$\ell n \left(\frac{I_g}{I_\ell}\right)_T = \left[\ell n \left(\frac{I_g}{I_\ell}\right)_{T_o}\right] \left[\frac{(\rho_\ell - \rho_g)_T}{(\rho_\ell - \rho_g)_{T_o}}\right] \qquad (34)$$

It is convenient to let

$$C = \frac{\ell n \left(\frac{I_g}{I_\ell}\right)_{T_o}}{(\rho_\ell - \rho_g)_{T_o}} \qquad (35)$$

This constant C can be obtained from a single $I_g/I_\ell$ measurement at temperature $T_o$. Of course, it is assumed that fluid densities are known as functions of temperature. Using Equation 35, Equation 34 becomes

$$\ell n \left(\frac{I_g}{I_\ell}\right)_T = C (\rho_\ell - \rho_g)_T \qquad (36)$$

Equations 35 and 36 establish the denominator of Equation 28 as a function of temperature with only one measurement of $I_g/I_\ell$ necessary. Egen and coworkers (34) substantiated Equation 34 experimentally with water-steam data.

Consider next the numerator of Equation 28. Here also the $I_\ell$ value must be corrected to the same flow temperature as the I measurement. Recalling Equation 30 it readily follows that

$$\frac{(I_\ell)_{T_o}}{(I_\ell)_T} = \exp\left\{ -\left[\left(\frac{\mu}{\rho}\right) \rho_\ell t_\ell\right]_{T_o} - \left[\left(\frac{\mu}{\rho}\right)_s \rho_s t_s\right]_{T_o} + \left[\left(\frac{\mu}{\rho}\right) \rho_\ell t_\ell\right]_T + \left[\left(\frac{\mu}{\rho}\right)_s \rho_s T_s\right]_T \right\}$$

For the solid channel wall both the density and mass absorption coefficient may be taken as constant. Then

$$\ell n \frac{(I_\ell)_T}{(I_\ell)_{T_o}} = t \left(\frac{\mu}{\rho}\right) \left(\rho_{\ell_{T_o}} - \rho_{\ell_T}\right) \qquad (37)$$

It is valid to divide Equation 37 by Equation 32 which will eliminate the $(\mu/\rho)$ term assuming it is constant

$$\frac{\ell n \dfrac{(I_\ell)_T}{(I_\ell)_{T_o}}}{\ell n \left(\dfrac{I_g}{I_\ell}\right)_{T_o}} = \frac{\rho_{\ell_{T_o}} - \rho_{\ell_T}}{(\rho_\ell - \rho_g)_{T_o}}$$

By inserting Equation 35 and rearranging

$$(I_\ell)_T = (I_\ell)_{T_o} \cdot \exp\left[ C \left( \rho_{\ell_{T_o}} - \rho_{\ell_T} \right) \right] \tag{38}$$

Equation 38 is the desired result, as it corrects the all-liquid calibration value obtained at temperature $T_o$ to the temperature T of the two-phase flow. This, then, is the correction necessary in the numerator of Equation 28.

The two single-phase calibration values $I_g$ and $I_\ell$ in general are obtained at different temperatures, but to utilize Equation 35 both single-phase values are desired at the same calibration temperature $T_o$. The $I_\ell$ value can be adjusted quite easily to correspond to the temperature at which $I_g$ is obtained. Assume that $(I_g)T_o$ and $(I_\ell)_T$ are known and it is desired to adjust $(I_\ell)_T$ to $(I_\ell)_{T_o}$. From Equation 38, taking logarithms

$$\ell n\, (I_\ell)_{T_o} = \ell n\, (I_\ell)_T + C\, (\rho_{\ell_T} - \rho_{\ell_{T_o}})$$

Inserting the value of C from Equation 35 and rearranging,

$$\ell n\, (I_\ell)_{T_o} = \frac{\ell n\, (I_\ell)_T + \dfrac{\rho_{\ell_T} - \rho_{\ell_{T_o}}}{(\rho_\ell - \rho_g)_{T_o}}\, \ell n\, (I_g)_{T_o}}{1 + \dfrac{\rho_{\ell_T} - \rho_{\ell_{T_o}}}{(\rho_\ell - \rho_g)_{T_o}}} \tag{39}$$

Equation 39 provides the necessary adjustment in $I_\ell$ to allow evaluation of $(I_g/I_\ell)_{T_o}$ from calibration runs at two different temperatures. Equations 35 and 36 can then be easily applied.

In obtaining the temperature correction expressions, it should be noted that no assumptions were made as to phase distribution effects, except for the purpose of example. Thus, the corrective terms could be validly applied or adapted to any other valid data reduction equation.

DESCRIPTION OF EQUIPMENT

In determining void fractions by the radiation attenuation method, the most obvious necessities in addition to a flow test section are a suitable radiation source and detection system. Maurer (85) furnishes an extensive review of components used by various investigators. Shields for the source and detector must also be used, the designs of which vary widely, and many different types of electronic equipment have been used in detection systems.

Void fraction measurements were made at approximately the mid-point of the pressure drop section in the potassium test loop. Temperatures of the void fraction measurements were taken as the average between inlet and outlet thermocouples. This section will discuss specifications for the source, detection equipment, and shields.

A schematic diagram of the measuring system is given in Figure 66. Figure 67 provides a layout of the apparatus and indicates the types of shields specified for source and detector.

1. Source

The gamma-ray source used was Tm-170 (Thulium). The decay scheme for this nuclide is given in Figure 68 (32, 126). The relative occurrences of the two beta particles are 76 per cent and 24 per cent for the higher and lower energy betas, respectively.

A typical energy spectrum exhibited by Tm-170 is given in Figure 69 (85). The exact spectrum of gammas and X-rays will vary with sample size and cladding thickness. The peaks in the spectrum are due to an excited state of Yb-170. The most intense photon is a 0.053 Mev K X-ray which occurs from 5 per cent of the total Tm-170 disintegrations. The less intense peak is due to a 0.084 Mev unconverted gamma-ray, which occurs 5 per cent of the time. The excited Yb-170 also emits a 0.008 Mev L X-ray and a 0.002 Mev M X-ray. Although these two X-rays occur from 16 per cent of the total Tm-170 disintegrations, they are so weak that their transmission by the source capsule is negligible.

The equations developed in the previous section are based on a monoenergetic beam. Fortunately, the 0.053 Mev K X-ray is almost completely absorbed by the pipe wall, permitting the detector to see an essentially monoenergetic beam. The useful photon for these experiments is the 0.084 Mev gamma-ray. Figure 69 indicates the presence of Bremsstrahlung radiation caused by interactions of some of the Tm-170 beta particles with the encapsulation material.

Myers (94) discussed in detail the reasons for choosing Tm-170 as the gamma-ray source. It was necessary to obtain an isotope with a sufficiently long half-life to insure essentially constant source strength during any one experimental run. The 127-day half-life of Tm-170 meets this requirement, although it is short when considering experimental operations over several months. In long range use, however, corrections can be made for the decay.

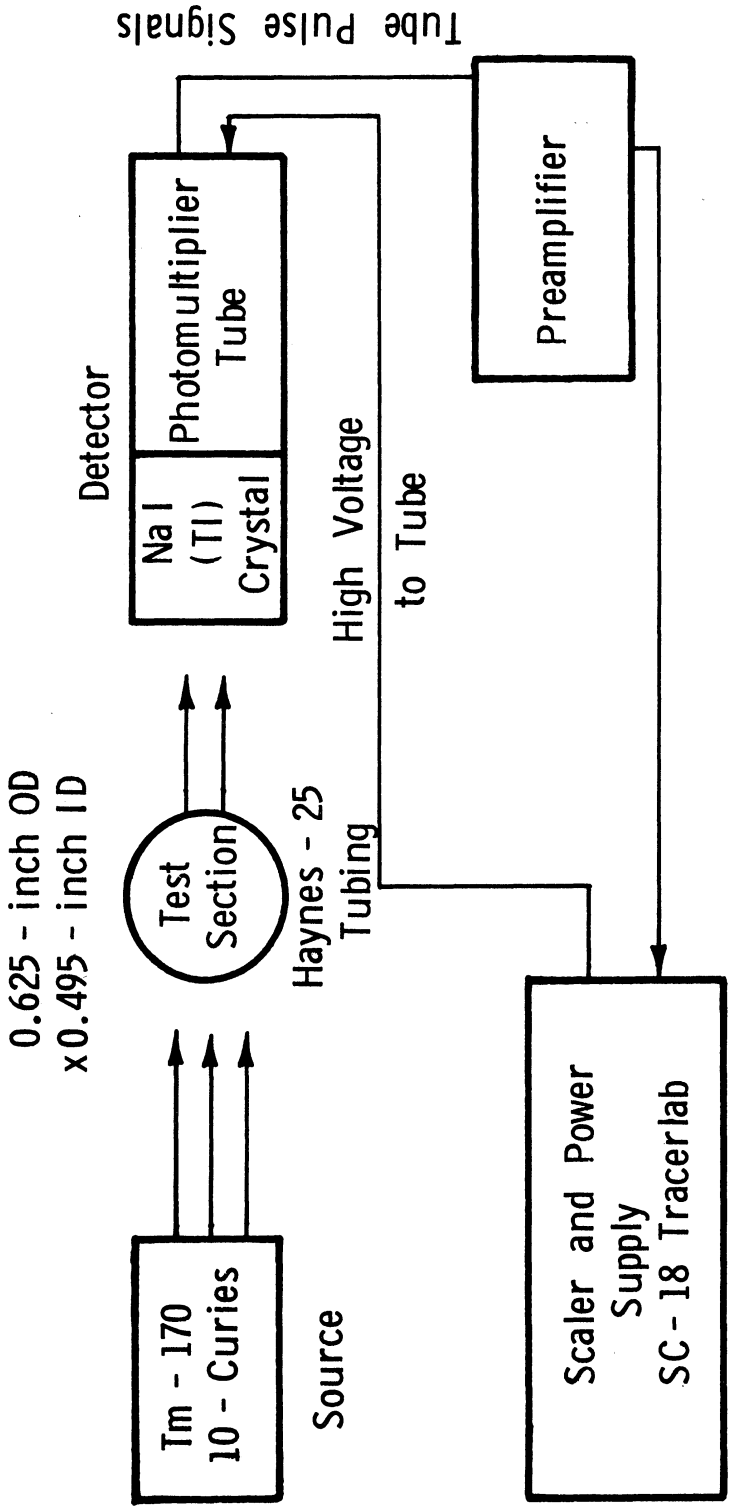


Figure 66. Schematic Diagram of Void Fraction Measuring System.

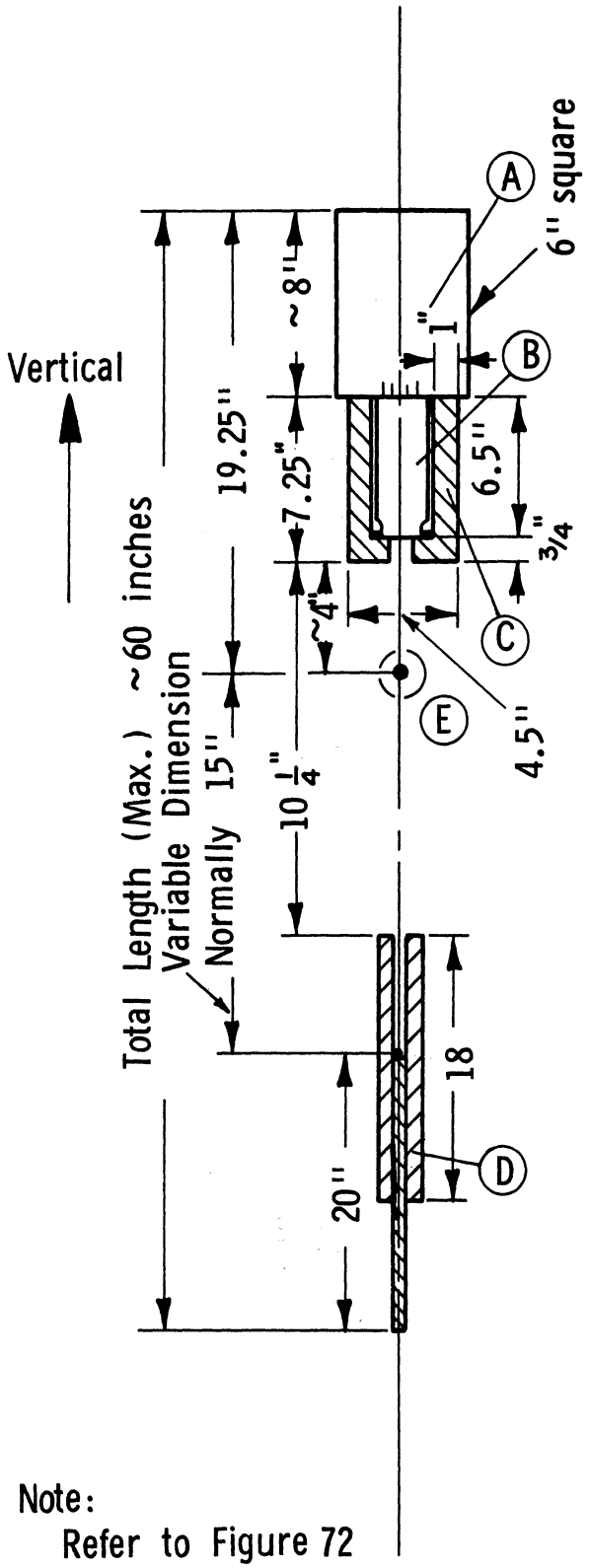


Key

A Preamplifier

B Harshaw Integral Line Scintillation Crystal & Photo-multiplier Tube, Type 6S4/E

C Steel Shield for Phototube, ~23 lbs.

D Source Shielding & Positioning Components ~21 lbs. Rod threaded to take source.

E Haynes 25 Tube 0.495-in. ID with 0.0625-in. wall

Note:
Refer to Figure 72 for details of both shields.

Figure 67. Layout of Void Fraction Measuring Apparatus.

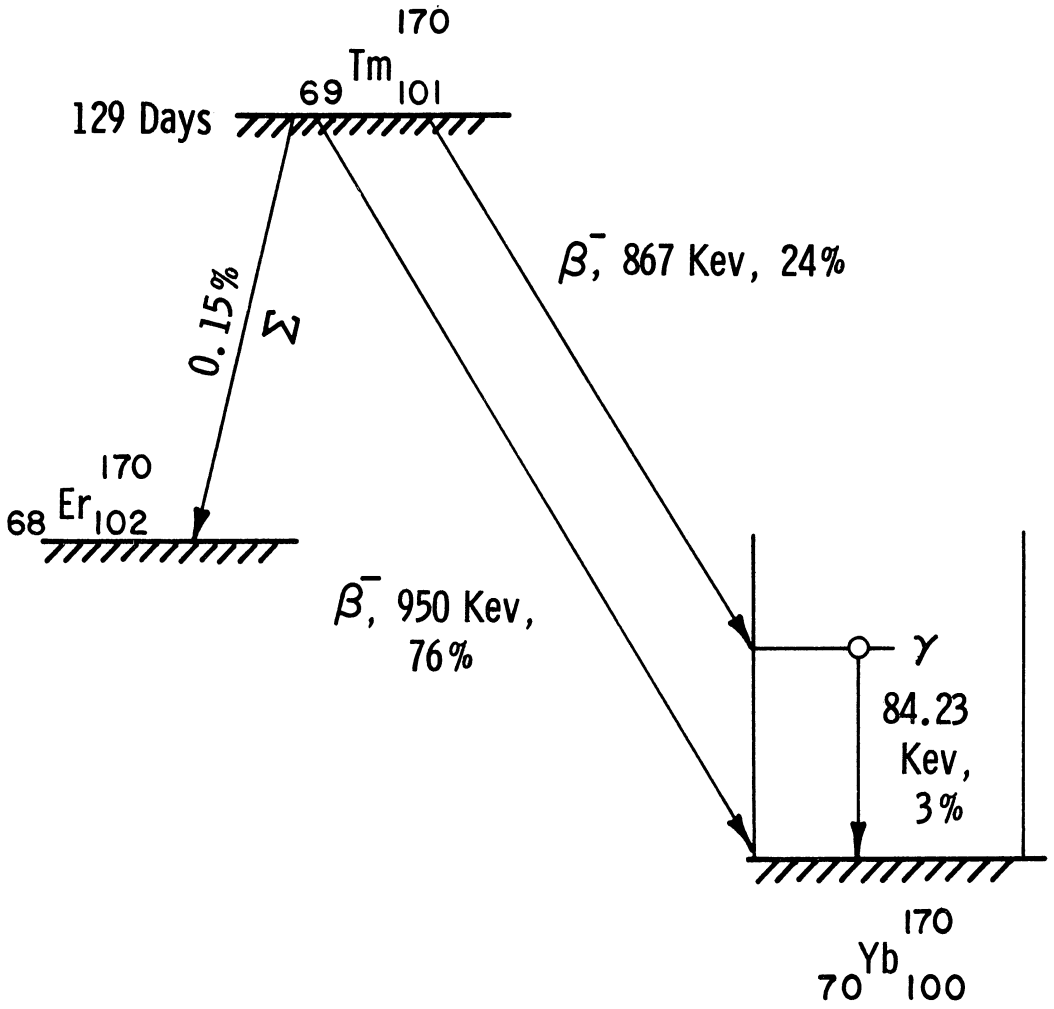


Legend:

Percent abundance is based on total Tm - 170 disintegrations.
Σ indicates orbital electron capture.
$\beta^-$ indicates beta particle emission.
γ indicates gamma ray emission.

Figure 68. Decay Scheme of Tm-170.

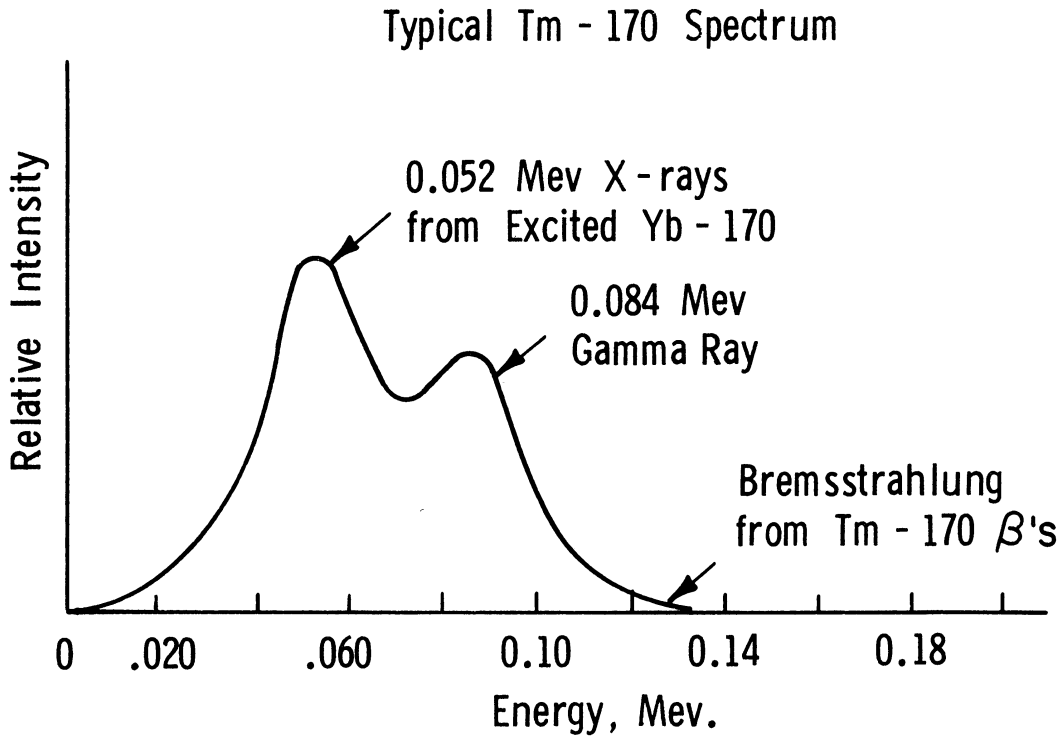


Figure 69. Typical Energy Spectrum of Tm-170.

In addition to half-life considerations, the photon energy and approximation to monoenergeticity were examined. The density ratio of the potassium vapor-liquid system is approximately the same as for the air-water system. This fact suggested choosing a low energy gamma emitter which would allow detection of small changes in mixture density. However, if a photon too low in energy were chosen, the constant attenuation due to the channel wall would lower the emergent intensity below detection level and also damp out sensitivity. Myers' predictions (94) showed that for photon energies lower than about 60 Kev the tube wall attenuation would require using an unreasonably large source. On the other hand, for energies greater than 100 Kev the sensitivity in the potassium experiments would suffer. These considerations, together with others discussed by Myers (94), led to the choice of Tm-170, which has a photon in the desirable energy range. For safety reasons, a beta decay source was preferred over an alpha decay type.

A nominal 10-curie Tm-170 source was purchased from Atomic Energy of Canada Limited (Ottawa). Preliminary calculations indicated that this strength is higher than necessary and could even lead to scaler overloading. However, the supplier offered Tm-170 radiography sources at 230 dollars for any strength up to 10 curies. Since experimental difficulties and delays were anticipated, it seemed wise to obtain the highest possible activity per unit cost. Excess strength was handled through collimation and shielding.

The source supplied by Atomic Energy of Canada had a strength of 9.8 curies on April 13, 1963. At the time of the potassium void fraction runs (August 22 through August 30, 1963) the source strength was about 4.7 curies.

The source is composed of metallic thulium and is encapsulated in stainless steel. Figure 70 provides an isometric view of the capsule and gives its main dimensions.

2. Detection Equipment

The schematic diagram of Figure 66 indicates the counting equipment which was employed. Scintillation detection was chosen over Geiger-Müller or proportional detection because of negligible dead time correction and high intrinsic counting efficiency.

The detector unit is an "Integral Line Assembly" produced by the Harshaw Chemical Company. It consists of a 1 1/2-in diameter by 1-in thick, thallium activated, sodium iodide crystal coupled optically to a 2-in photomultiplier tube. The assembly includes an external magnetic shield to minimize the effects of the various electric and magnetic fields present in the potassium test loop. The assembly obtained has a pulse height resolution* of 8.3 per cent at 661 Kev photon energy. The Harshaw literature (49) furnishes dimensions of these assemblies.

* Pulse height resolution is the width of the photopeak at half height divided by the mean pulse height of the photopeak.

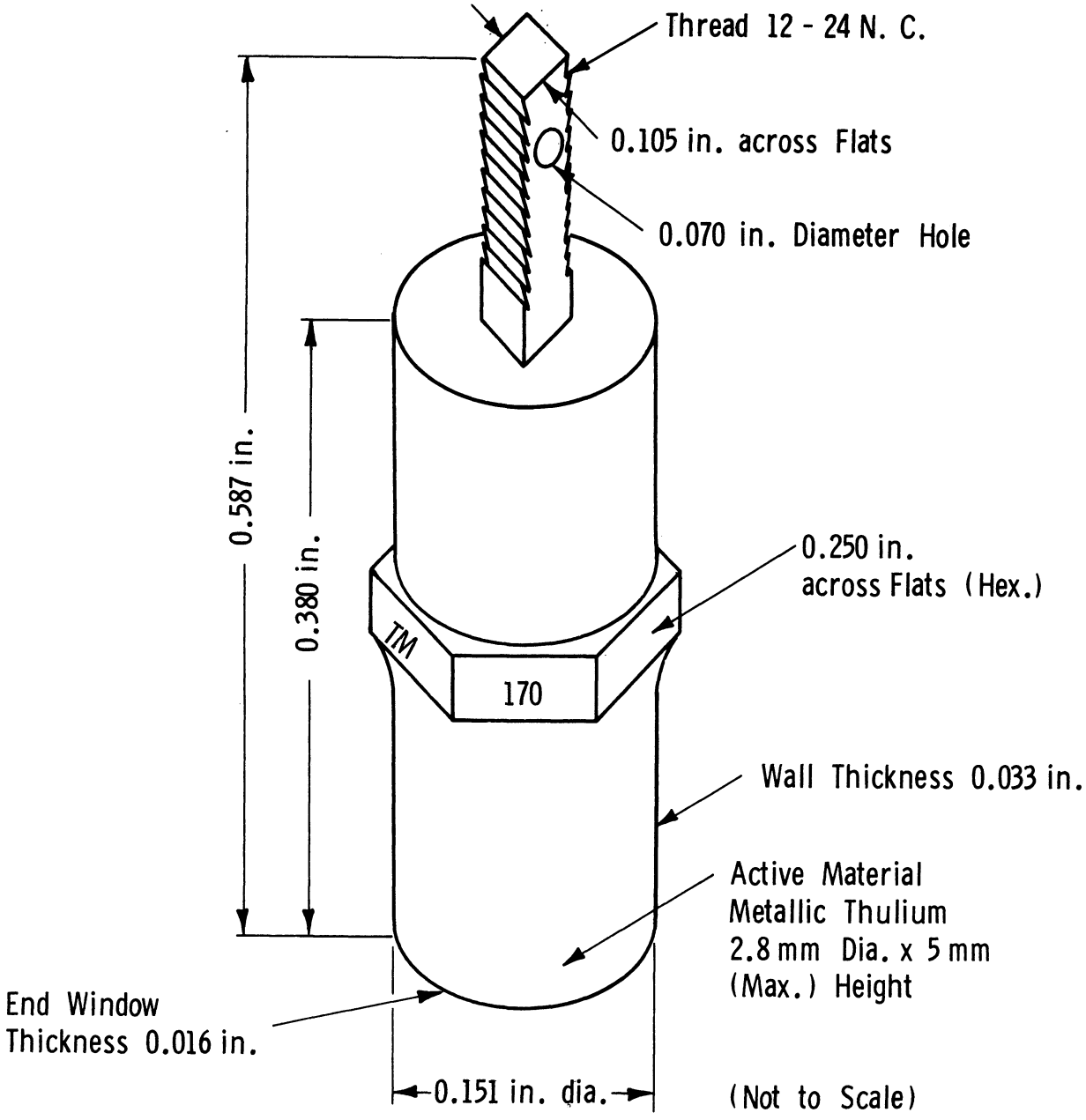


Figure 70. Tm-170 Gamma Ray Source.

Physically, the detection of gamma radiation by the scheme in Figure 66 is as follows. When a photon impinges on the NaI(Tl) crystal, the interaction in the crystal yields a flash of light. This light flash is picked up by the photomultiplier tube which converts it to a low level voltage pulse. This emf pulse must be amplified before it can drive a cable and furnish a signal to the scaler. The preamplifier provides the necessary amplification which has a high degree of linearity. The scaler has a discriminator which may be set to accept voltage pulses from the preamplifier only when the signal is above a certain level. The discrimination is necessary to eliminate effects due to amplifier and phototube noise. In the potassium experiments, the discriminator was set at 0.25 volt. For every emf pulse accepted by the discriminator, a count is registered by the scaler. Obviously, some photon interactions in the NaI(Tl) crystal are so weak that the amplified pulse is rejected by the discriminator. Thus, not every gamma photon striking the crystal produces a count.

The preamplifier was specially built to electronically match the scaler. The scaler is a Tracerlab SC-18 Superscaler. This scaler has a built-in high voltage power supply which is used to drive the phototube. The Tracerlab manual (112) gives complete instructions for operation and maintenance of this instrument. Table XVII summarizes the important features of this scaler.

Prior to flow experiments, the detection system was tested in background counting and also against a small Co-57 source. The main objective of the test was to locate the proper high voltage level to use in driving the photomultiplier tube. The results of this test are given in Figure 71, which shows the characteristic plateaus in the count rate versus tube voltage curves. It was desired to use a tube voltage such that the experimental counting would be on these plateaus. The count rate level at the plateau varies with the intensity of the detected radiation.

The results in Figure 71 indicate that a driving potential of 950 volts should allow operation on the count rate plateau, and this voltage was used in the potassium measurements.

Before concluding this discussion of the detection equipment, mention should be made of its efficiency. The resolving time of the photomultiplier tube is about 0.25 microsecond (49). Inorganic scintillation crystals such as NaI(Tl), due to their high density, have a high stopping power and consequently a greater counting efficiency for gamma rays than do gaseous detectors. The alkali halides--particularly NaI(Tl)--have the added advantage of high light output, transparency, and suitable refractive index. The high atomic number of inorganic scintillators aids in photon conversion.

The theoretical absorption coefficients of NaI(Tl) for gamma rays having energies ranging over three orders of magnitude are available (49). Using these coefficients, the theoretical efficiencies of crystals of various thicknesses can be obtained as a function of gamma energy. These theoretical or "intrinsic" efficiencies depend on source-to-crystal distance. They do not account for absorption by the crystal container or for the fact that only a fraction of the total interactions in the crystal are counted. (This latter factor depends on the scaler's discriminator setting). Price (102) presents

TABLE XVII

IMPORTANT FEATURES OF THE TRACERLAB

SC-18 SUPERSCALER

| | |
|---|---|
| (a) | A built-in mechanical register, preceded by an electronic scale of 1000 which provides for automatic "pre-set count" operation. |
| (b) | An odometer type timer which permits automatic "pre-set time" operation. |
| (c) | A high voltage power supply for driving the photomultiplier tube, continuously variable from 300 to 3000 v. Electronically regulated so that 1 per cent change in line voltage yields 0.2 v output change. Ripple and noise level limited to about 200 mv. |
| (d) | Resolving time of 5 microseconds. This implies count rates of up to 120,000 cpm with less than 1 per cent coincidence loss. |
| (e) | Input sensitivity (discrimination) adjustable from 0.20 to 0.35 v. |
| (f) | Electronic scaling system counts 1000 before pulsing the mechanical register. |
| (g) | Can totalize up to 9,999,999 counts. |

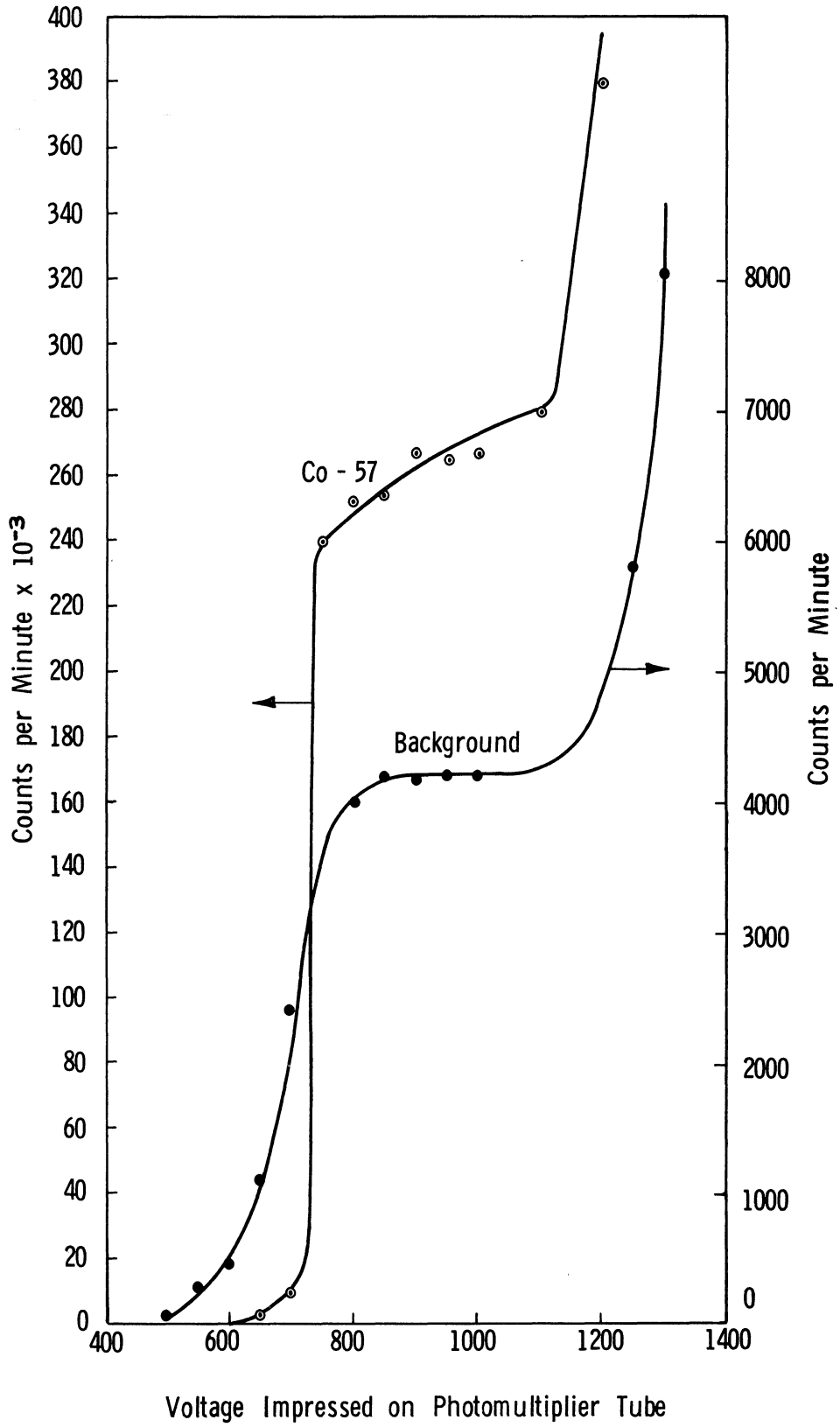


Figure 71. Count Rate as a Function of Voltage Impressed on Photomultiplier Tube.

intrinsic efficiencies for 1 1/2-in diameter by 1-in thick NaI(Tl) crystals. For the source-to-detector distances suggested in Figure 67 and for the low energy radiation employed, the theoretical detection efficiency approaches unity. Although actual detection efficiencies cannot be this high, one can confidently assume that they were greater than 0.50 and perhaps as high as 0.80.

3. Shields and Collimator

In the interest of personnel protection it was necessary to shield the Tm-170 source. The shielding employed was such that the narrow working beam impinged unhindered on the flow channel but radiation in all other directions was substantially reduced. The detector was also shielded in order to minimize the effect of background radiation on the count rate.

The source has an end output of 4.5 mr/hr at 1 meter per curie. This strength includes Bremsstrahlung radiation. Figure 67 shows the shields for both source and detector and indicates the method of varying the source-to-detector distance by adjusting the location of source inside the shield by means of the positioning rod. Figure 72 gives details of the shield designs. Both shields are made from seamless mechanical steel tubing.

The source shield was designed assuming that all the radiation is of 0.084 Mev energy, which was believed to allow considerable safety factor. Moreover, the design was based on a 10-curie strength. Even though these design precautions were taken, it was found that the steel tube did not stop the gamma rays as effectively as planned, and a 1/2-in thickness of lead sheet was fastened around the steel tube during the experiments. Even before the lead was added, however, the dose rate in the loop control room was well within the acceptable safe limit.

The output end of the source shield was tapped to accommodate a standard 3/4-in bolt from which the collimator was fabricated, as shown in Figure 73. The collimator was interchanged with a solid shut-off plug for background determinations. Unscattered background radiation--i.e., photons penetrating the 1 1/2-in long bolt piece--was negligible, according to the design calculations. The background radiation observed is attributed to scattering of beam photons. It is seen from Figure 73 that the collimated gamma beam was about 1/32-in in diameter.

The source and detector shields are accurately aligned on a common frame. The latter shield has 1-in thick walls for reduction of background effects. As shown in Figure 72, the face plate on the detector shield is removable to allow ease in changing the size of the window in front of the scintillation crystal.

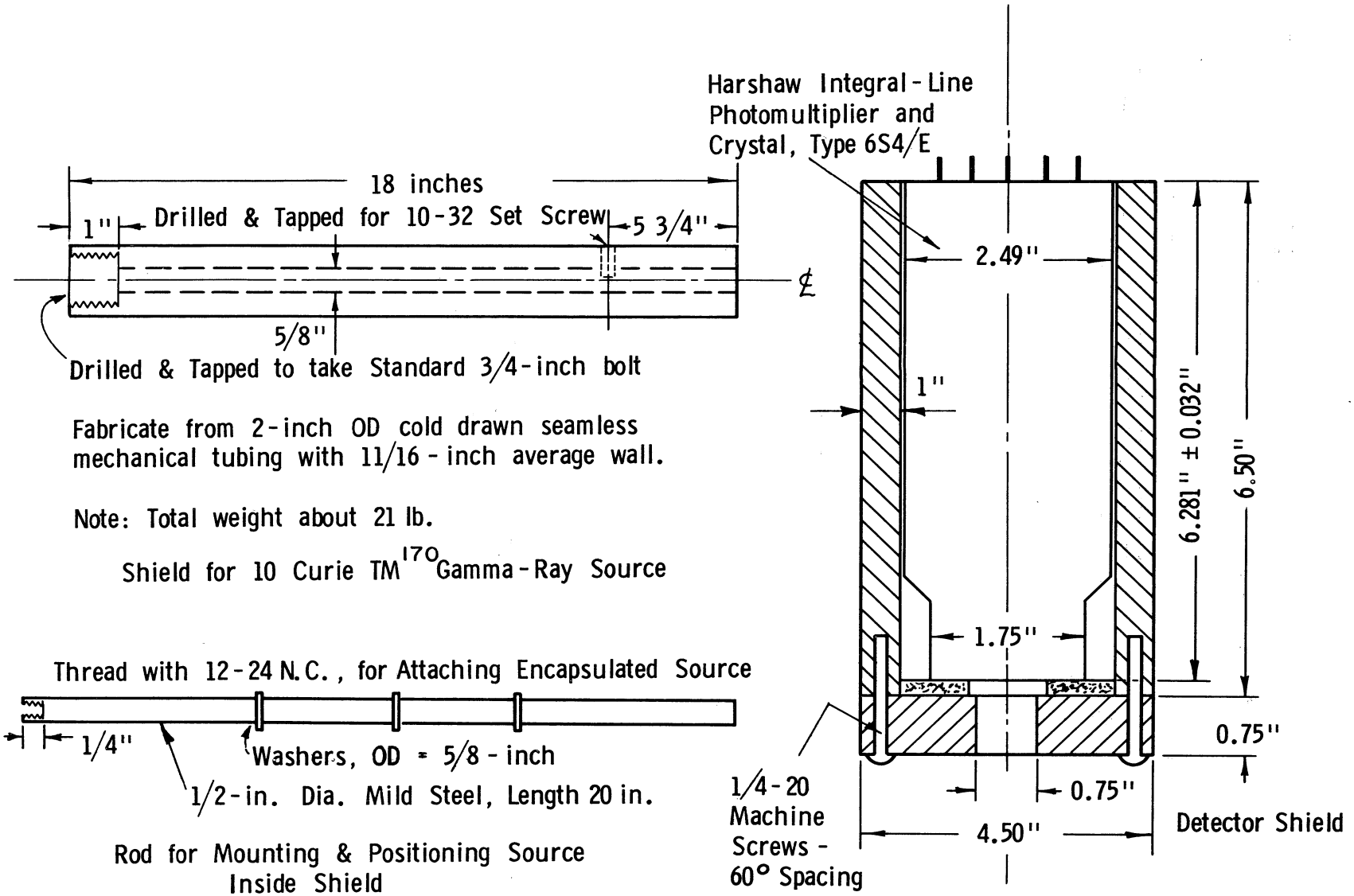


Figure 72. Source and Detector Shields.

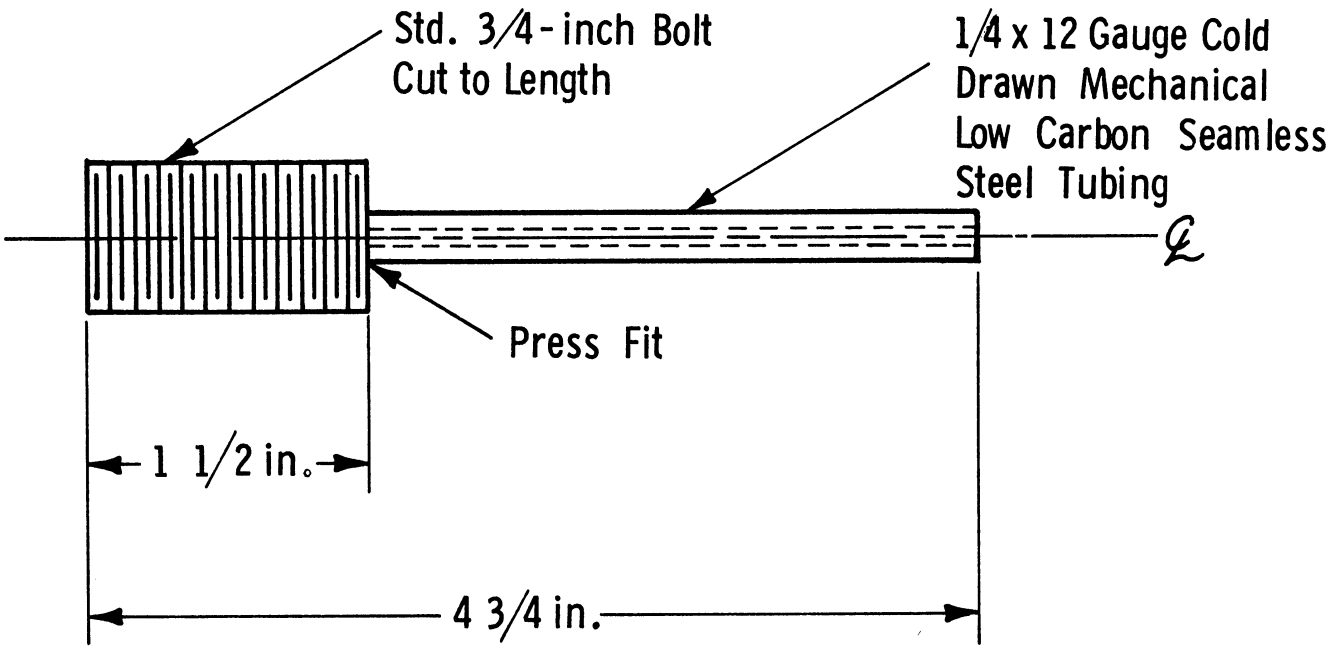


Notes:

1. 1/4 x 12 Gauge Tubing: 0.109 - inch Wall
   by 0.032 - inch ID

2. Cut second std. 3/4 - inch bolt to 1 1/2 - inch length. To be used as plug in background counting.

Figure 73. Gamma Ray Beam Collimator.

EXPERIMENTAL PROCEDURES

Whenever pressure drop data were recorded, gamma-ray attenuation readings were also taken. Therefore, the void fraction data were obtained over about the same flow rate and preheater power ranges as were the pressure drop data.

Detector counts were recorded for three-minute time intervals. Choice of a three-minute counting time was based on consideration of statistical error and coincidence loss. Statistical error arises from the random nature of the gamma emission process. It can be shown that the standard deviation in counting is usually equal to the square root of the number of counts recorded (102). It follows that the larger the number of counts read, the smaller the percentage the standard deviation is of the total. Hence, the probable error in counting is reduced as the number of counts is increased. Of course, an appreciable reduction in statistical error may result in prohibitively long counting times.

Although the statistical error is diminished by increasing the counting rate, some of the advantage is lost by inaccuracies introduced by coincidence loss in the counting system. Normally, the coincidence loss of a system is determined by that component which has the greatest dead time (i.e., the time interval immediately following a pulse during which no succeeding pulse will be counted). In this case, the scaler is the limiting component since it has a resolving time of 5 microseconds (112) as compared with about 0.25 microsecond for the scintillation detector (49). Although coincidence loss can be measured and subsequent data corrected for it, the following relation is valid for small corrections (112).

$$N = \frac{r}{1 - r\tau} \tag{40}$$

where $N$ = true count rate

$r$ = observed count rate

$\tau$ = dead time

The fraction of the true counting rate which is lost is equal to $r\tau$.

Preliminary experiments showed that three-minute counting periods would lead to counts in the neighborhood of $10^6$. For a million counts the standard deviation amounts to only 0.1 per cent, while the observed count rate produces a coincidence loss of 2.8 per cent. These same preliminary experiments established that an 18.25-in source-to-detector distance would be suitable (i.e., ten inches of positioning rod protruding from the source shield). This distance was maintained in all two-phase determinations. It was thus established that, for the source and geometry specified, a three-minute counting interval struck a good balance between statistical accuracy and coincidence loss.

The counts obtained in the two-phase experiments ranged from 600,000 to 1,500,000. The experimental procedure involved taking a series of three counts with the collimator in place. Then the collimator was replaced with the shut-off plug and another series of three counts taken. These latter counts measured background radiation striking the crystal. Deduction of the average corrected background count from the average corrected collimated count led to a count rate attributed primarily to the collimated beam (about 1/32-in in diameter). Usually six separate counts were recorded per data point, but occasionally seven or more counts were read if values seemed to drift. The approximately twenty minutes it took to make the gamma-ray attenuation readings usually fell within the time interval necessary for recording loop data.

A chromel-alumel thermocouple was attached to the outer surface of the detector shield. In the experiments so far, no attempt was made to control the detector temperature. The upper temperature limit for the photomultiplier tube is about 165°F. Sometimes the detector temperature approached this level, but it was always possible to cool the tube by use of the loop room exhaust fan. In fact, rough control of the detector temperature was possible with the fan. The photomultiplier tube temperature was recorded at each data run and ranged from 125 to 163°F.

The shield assembly was supported by and clamped to the framework of the loop housing. It was found that the pressure drop section moved only a negligible amount from thermal expansions. The source was aligned with the center of the flow tube by means of the collimator. Insulation was stripped off a segment of the test section and a 1/32-in welding rod inserted upward through the source shield and collimator, and pushed up to the channel. The shield assembly position was adjusted until the welding rod rested on the center of the tube. To allow for slight bend in the welding rod, it was rotated about its axis, letting the free end describe a circle. When this small circle centered on the pipe center, alignment was considered satisfactory. The alignment was checked several times during the course of the experiments, using this procedure.

Early measurements showed that too much background was scattering through the bolt portion of the collimator. To overcome this, a circular piece of lead was fitted over the end of the 1/4-in collimator tube. A steel cap 1/2-in thick was also placed over the collimator end to reduce the beam intensity somewhat.

The Theory section pointed out the necessity of obtaining single-phase calibration count rates. All-liquid values were obtained for an average flow temperature of 500°F. The all-vapor count was taken as an empty channel reading at 551°F. The temperature correcting equations were used in data reduction.

As mentioned previously, the detection system was operated with 950 volts impressed on the photomultiplier tube.

## RESULTS

The void fraction data are presented in Table XXII. Over half the results are at an average total mass flow of 256 lb/hr, although the entire range of flow rates is represented. The ratio of superficial vapor velocity to all-liquid velocity and the all-liquid Froude number are included in this tabulation, as suggested by the work of Kutateladze (69) and Smith, Tang, and Walker (115). Average temperature is the arithmetic average between readings of thermocouples TC-30 and TC-31. Average quality is the arithmetic average between inlet and outlet qualities in the pressure drop section.

The void fraction values were calculated from Equation 28, with proper temperature corrections being made in all cases. The slip velocity ratios were calculated from Equation 14.

Table XXII is arranged according to decreasing values of the Froude number, since Froude number is taken as a parameter. Figure 74 is a graphical presentation of the data, attempting to show void fraction as a function of the ratio of superficial vapor to total liquid velocities, taking Froude number as a parameter.

The overall ranges of pertinent variables may be summarized as follows:

| | | |
|---|---|---|
| a) | Void Fraction | 0.158 - 0.941 |
| b) | Slip Velocity Ratio | 5.7 - 3200 |
| c) | Froude Number | 0.29 - 9.05 |
| d) | Ratio of Superficial Vapor Velocity to Total Liquid Velocity | 66 - 1073 |
| e) | Total Mass Flow Rate | 129 - 736 |
| f) | Average Quality | 0.0200 - 0.1990 |
| g) | Average Temperature | 875 - 1312 |

## DISCUSSION OF RESULTS

Figure 74 shows the high degree of scatter in the void fraction data. Even for the comparatively narrow Froude number range 1.05-1.15 the data are too scattered to allow a curve to be drawn. Because of this large scatter, the data obtained to date must be considered preliminary.

It is believed that two experimental factors led to the failure in correlating the data. First, the photomultiplier tube temperature was not controlled, and it varied from 125 to 163°F. Since photomultiplier tubes are temperature sensitive, the detector temperature will have to be regulated in future experiments. Second, the placement of both the lead shield for background reduction and steel piece for reduction of beam intensity was a little sloppy. Slight changes in position could have contributed to the scatter. In future experiments these components should be more accurately machined.

One result can be stated from examination of Table XXII. Even though the slip ratios calculated from Equation 14 are scattered, the order of magnitude is indicated. It appears that potassium slip ratios, over the quality range observed are of the order of $10^2$.

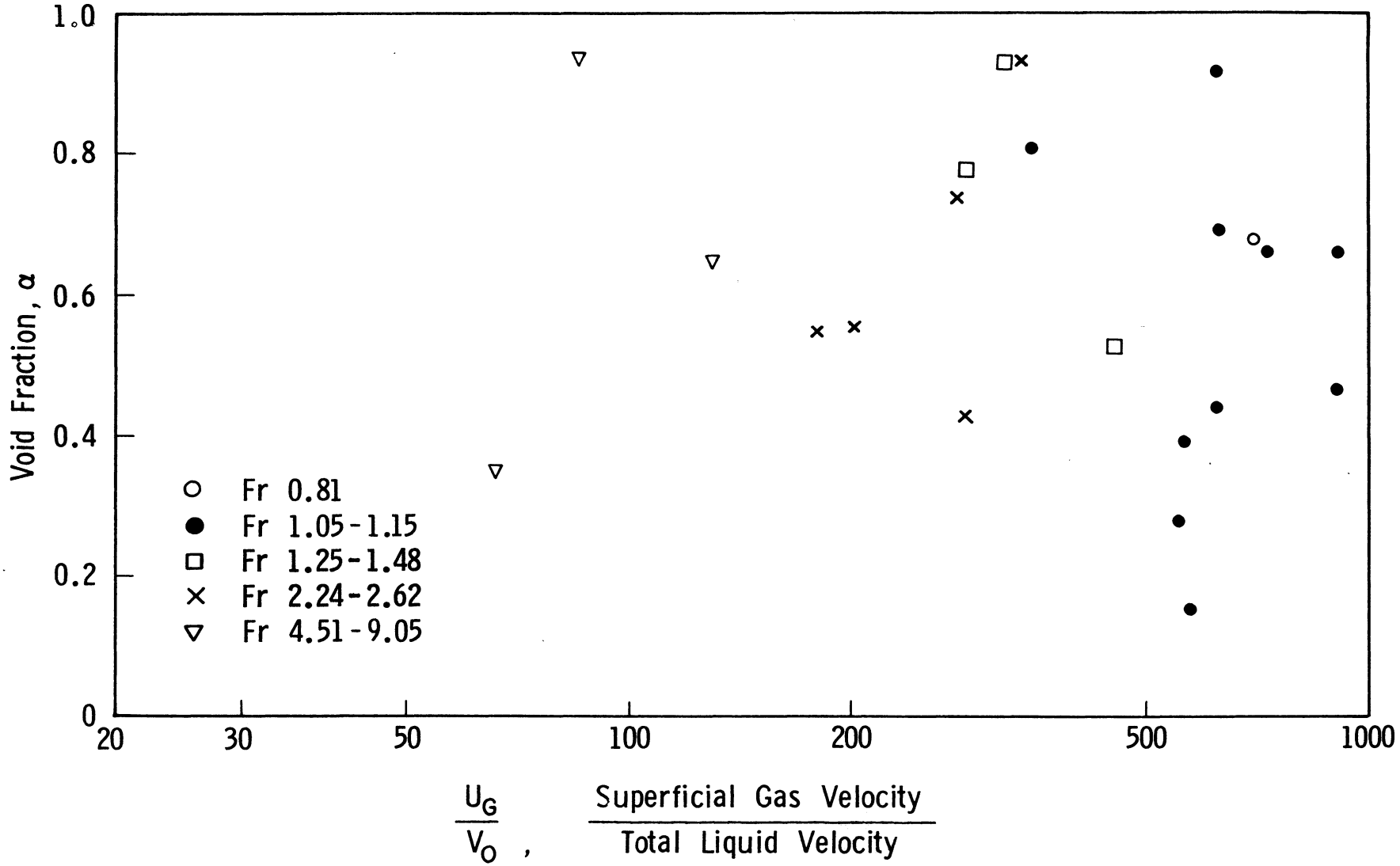


Figure 74. Void Fraction Results.

## CONCLUSIONS

Pressure drops occurring in nearly-adiabatic, evaporating two-phase flow of potassium have been determined as a function of average test section quality and total mass flow rate. For the low quality range 0.02 to 0.1, the pressure drop is established at 256 and 376 lb/hr flow rates. Over the somewhat more narrow quality range 0.03 to 0.06 the pressure drop is established as a function of total mass flow from 256 to 740 lb/hr. At the low flow rate 125 lb/hr, the pressure drop is established over the quality range 0.2 to 0.4.

Potassium two-phase pressure drops were found significantly higher than values for the steam-water system predicted by the Martinelli-Nelson method for the same flow parameters.

Void fraction values for two-phase potassium flows are reported. However, the scatter of the data is so severe that a correlation cannot be obtained. These void fraction data must, therefore, be regarded as preliminary.

# LIQUID METAL BOILING IN AGRAVIC FIELDS

Herman Merte, Jr.

## INTRODUCTION

As a consequence of the current interest in space flight and exploration with the attendant change in force fields, along with the fact that the devices involved will include heat transfer processes, a number of studies are being conducted to determine the significance of force fields on these processes.

Within certain limits force fields are of consequence with convective heat transfer processes only. For cases with no phase change, some success has been achieved in predicting the behavior of systems with variable body forces (87,113). For heat transfer with phase change, such as boiling, such success has been achieved only for specialized conditions.

A number of correlations for the maximum heat flux with pool boiling have been presented in the literature. A comprehensive discussion of the various correlations is given by Ivey (62). In most cases a dependence of the maximum heat flux on effective gravity is given as $(a/g)^{1/4}$. Experimental studies with variable effective gravity have tended to verify this dependency for water (30, 121) and for liquid nitrogen (88). In order to correlate the maximum heat flux for sodium with other fluids it was found necessary to include a Prandtl No. term (98). The experimental work was conducted at $a/g = 1$ only, and it might be injudicious to consider the $(a/g)^{1/4}$ dependency to hold, with no experimental verification, in light of other unusual heat transfer characteristics of liquid metals.

Film boiling in variable effective gravity fields with several geometries has been correlated well with Nusselt-Modified Rayliegh No. relations for liquid nitrogen (88) and Freon-113 (101). For the geometries used and a particular heater surface superheat, the film boiling heat flux exhibits a dependency of $(a/g)^{1/3}$, a characteristic of turbulent free convection. No experimental data is available for liquid metal film boiling in variable gravity fields.

With nucleate boiling at a heat flux well above the incipient boiling point it was observed for a given heat flux that a wide variation in effective gravity changed the heater surface superheat a relatively small amount. The measurements were made with the acceleration vector normal to a flat heating surface, and with a sphere, all at essentially atmospheric pressure. With liquid nitrogen these conclusions applied for the ranges $0 < a/g \leq 1$ (88) and $1 \leq a/g \leq 20$ (27), with liquid hydrogen with $a/g \simeq 0$ (114), with water over the range $1 \leq a/g \leq 20$ (87) and $20 \leq a/g \leq 40$ (31). With increasing effective gravity (27, 31, 87) the heater surface superheat increased somewhat for constant heat flux, resulting in a decrease in the "heat transfer coefficient," while with reduced gravities (88, 114) no changes could be detected.

A photographic study of pool boiling of water while under acceleration, along with heat transfer measurements, was made at low values of heat flux to avoid obscuring the field of view (47). The low heat flux, $q/A \cong 12{,}000$ Btu/hr-ft$^2$, coupled with the non-consistent subcoolings used render the heat transfer results inconclusive. It was observed that as acceleration increased, up to $a/g = 7$, the maximum bubble size and growth rate decreased. Again, no general conclusions can be drawn because of the variable subcoolings.

In spite of the relatively small effect of acceleration observed with nucleate boiling it should be recognized that due to the large slope of the $q/A - \Delta t_{sat}$ relation, were $\Delta t_{sat}$ the independent variable rather than the converse as in the experiments, changes of the body forces could change the heat flux by 50 - 100 per cent, a significant amount.

Potential space applications of small nuclear reactors cooled by boiling liquid metals have necessitated a better understanding of gravity effects with these media. For this reason the present research was initiated. Mercury was selected as the initial fluid to be used because the complexity of the experimental apparatus required is much less than would be required for other liquid metals. Again, in view of the gross differences in properties between liquid metals and other fluids, extensions of the behavior with boiling and variable gravity of non liquid metals to liquid metals would be tenuous with no experimental checks.

The direct effect of increasing the effective gravity field with nucleate boiling is to increase the buoyant forces acting on the vapor bubbles. The high rates of heat transfer possible with nucleate boiling have been ascribed in part to the intense agitation of the liquid at the heating surface by the bubbles. Insofar as this agitation is affected by varying the buoyant forces, variation of effective gravity will influence the gross heat transfer characteristics.

As a means for defining a criteria under which buoyant forces become significant a Froude number for the vapor bubbles is presented (26) as

$$F_R = \frac{3R^2\dot{R}^2 + R^3\ddot{R}}{R^3(a/g)g} \tag{41}$$

This represents an estimation of the ratio of the bubble dynamic (or inertia) force resulting from the momentum flow in the liquid surrounding a growing bubble, to the buoyant force. Substituting the expression for bubble growth in a superheated liquid derived by Forster and Zuber,

$$R\dot{R} = \left[\frac{\Delta T\, Cp_\ell \rho_\ell \sqrt{\pi\alpha}}{\lambda_{fg}\, \rho_v}\right]^2 \tag{42}$$

into Equation (41) results in:

$$F_R = \frac{2}{R^3\,(a/g)g} \left[ \frac{\Delta T\, Cp_\ell \rho_\ell \sqrt{\pi\alpha}}{\lambda_{fg}\, \rho_v} \right]^4 \qquad (43)$$

The magnitude of the Froude number in Equation (43) indicated the relative importance of inertia and buoyant forces in the growth of a bubble. When the Froude number is of the order of 1 these two forces have approximately equal value. Should this ratio be greater than unity then the inertia forces may be expected to predominate.

Calculations of the Froude number are given in the Table below for several saturated liquids, including mercury at two different pressures. For comparison purposes the values are presented for $\Delta T$ = 16°F, standard gravity and for a bubble radius of 0.05 inches. Experimental measurements of bubble sizes of boiling mercury are not available, but the number used appears to be of a reasonable magnitude.

TABLE XXIII

FROUDE NUMBERS FOR NUCLEATE BOILING OF SATURATED LIQUIDS

($a/g$ = 1, $\Delta T$ = 16°F, R = 0.05 inch)

| Liquid | Pressure-psi | Froude Number |
|---|---|---|
| $N_2$ | 15 | 0.452 |
| $O_2$ | 15 | 0.546 |
| $H_2$ | 15 | 0.352 |
| $H_2O$ | 15 | 13.1 |
| Hg | 16 | 681.0 |
| Hg | 300 | 0.0227 |

A number of interesting observations can be made concerning these values. From Equation (43) the Froude number is inversely proportional to $a/g$ and $R^3$. Research currently being independently conducted in the laboratory is concerned with a photographic study of nucleate boiling of water in the range $1 \leq a/g \leq 100$. Tentative results indicate that the maximum bubble diameter decreases by no more than 50 per cent over this range, or $R^3$ would decrease by no more than a factor of 8. With nucleate boiling of water and liquid nitrogen (27, 87) up to $a/g$ = 20, no dramatic changes in boiling characteristics were observed. The combination of $R^3$ and $a/g$ would result in a decrease in the Froude number by a factor of no more than 2.5. From Table XXIII the inertia forces for $N_2$ and $H_2O$ still retain relative significance.

With nucleate boiling of liquid nitrogen (88) and liquid hydrogen(114) under reduced gravity down to $a/g \approx 0$ no changes again could be detected in the boiling process. Reducing effective gravity increases the Froude number, assuming no significant changes in bubble growth characteristics, and hence inertia forces still dominate.

With mercury, it is noted that a large Froude number exists at low pressures, indicating that in this region increases in buoyant forces should have little effect. At high pressure, however, the Froude number decreases to 0.0227 in Table XXIII, and it is possible that rather significant changes will take place as a consequence of the system acceleration.

A number of assumptions are made in the computations of the Froude number, particularly as regards the significant bubble radii to be used. It thus becomes urgent that experimental measurements be made to determine the influence of increasing effective gravity fields on the boiling of mercury over a range of pressures.

EXPERIMENTAL PROGRAM

An experimental program was initiated to study the influence of increased effective gravity on nucleate pool boiling of saturated mercury. A centrifuge used in previous studies with other fluids (27, 87) is available in the laboratory and furnishes a means for attaining this increased effective gravity. The centrifuge is capable of accepting a test package of 10 inch maximum diameter, 12 inches maximum length, and having a maximum total mass of approximately 40 pounds to achieve an acceleration of $a/g = 20$. As will be seen, these conditions impose severe restrictions in the design of the experimental equipment necessary to study the boiling of mercury.

In order to identify the orientation between the heater surface and the body force vector and to minimize premature detachment of generated vapor bubbles by the gross liquid convection, a flat heat transfer surface was selected with an orientation such that the acceleration vector is perpendicular to it.

The range of experimental conditions are listed below:

1. Effective gravity - $1 \leq a/g \leq 20$. Imposed by the capacity of the centrifuge.

2. Pressure above liquid free surface - 15 to 300 $lb_f/in^2$. Limit imposed by compromise between acceleration desired and massiveness of pressure vessel required.

3. Heat flux - Non-boiling to approximately 500,000 $Btu/hr\text{-}ft^2$. The value of the maximum heat flux at atmospheric pressure is uncertain, but a review of the available data appears to indicate a probable value somewhat higher than this. Operation near the maximum heat flux is undesirable with this system because of the possibility of burnout and destruction of the heater.

4. Liquid depth - Approximately 1/2 inch to 4 inches above the heater surface.

This study is concerned with pool boiling of saturated mercury but it is necessary that the location of the desired saturated condition be defined. The high density of mercury results in a comparatively large hydrostatic pressure gradient with the attendant variation in saturation temperature with depth. With boiling of mercury at standard gravity (14) it was found that the bulk mercury temperature was essentially that of saturated mercury at the liquid-vapor interface, hence somewhat subcooled at the heating surface. With high force fields the subcooling effect may be expected to be intensified because of the increased hydrostatic pressure, for a given depth, and the more intense fluid motion between the heater surface and liquid-vapor interface. Similar effects were observed in high gravity work with water (87).

Since the boiling phenomenon is governed by conditions existing at the heating surface, it is necessary that the fluid be saturated at this location in order to specify that the results apply for saturated pool boiling. From the discussion above this will not be possible, and the next best condition will be to keep the subcooling at a minimum. To isolate the influence of system acceleration alone it will be necessary to maintain all other independent variables constant. These include heat flux, absolute pressure at the heater surface and hence saturation temperature there, and the degree of subcooling at the heater surface. If the bulk mercury temperature assumes the saturation temperature at the liquid-vapor interface, these conditions can be met by varying the depth of liquid with acceleration. This can be clarified by referring to Figure 75, a plot of hydrostatic pressure ( and thus local saturation temperature) as functions of fluid depth, distance from the heater surface and acceleration.

As an example, with liquid depth = 1 inch, at a/g - 20 the hydrostatic pressure at the heater surface will be approximately 24 psia and the saturation temperature approximately 728°F. With the bulk mercury at the saturation temperature of the liquid vapor interface the subcooling will be approximately 54°F. To maintain these same conditions at a/g = 10 will require a depth of 2 inches; at a/g = 5, 4 inches; at a/g = 1, 20 inches. It is thus obvious that conditions cannot be maintained constant over the entire range of accelerations, but will require division. Again, for example, the range $1 \leq a/g \leq 5$ can be covered for one set of conditions and $5 \leq a/g \leq 20$ for another set of conditions, with a check on the influence of changing these conditions at a/g = 5.

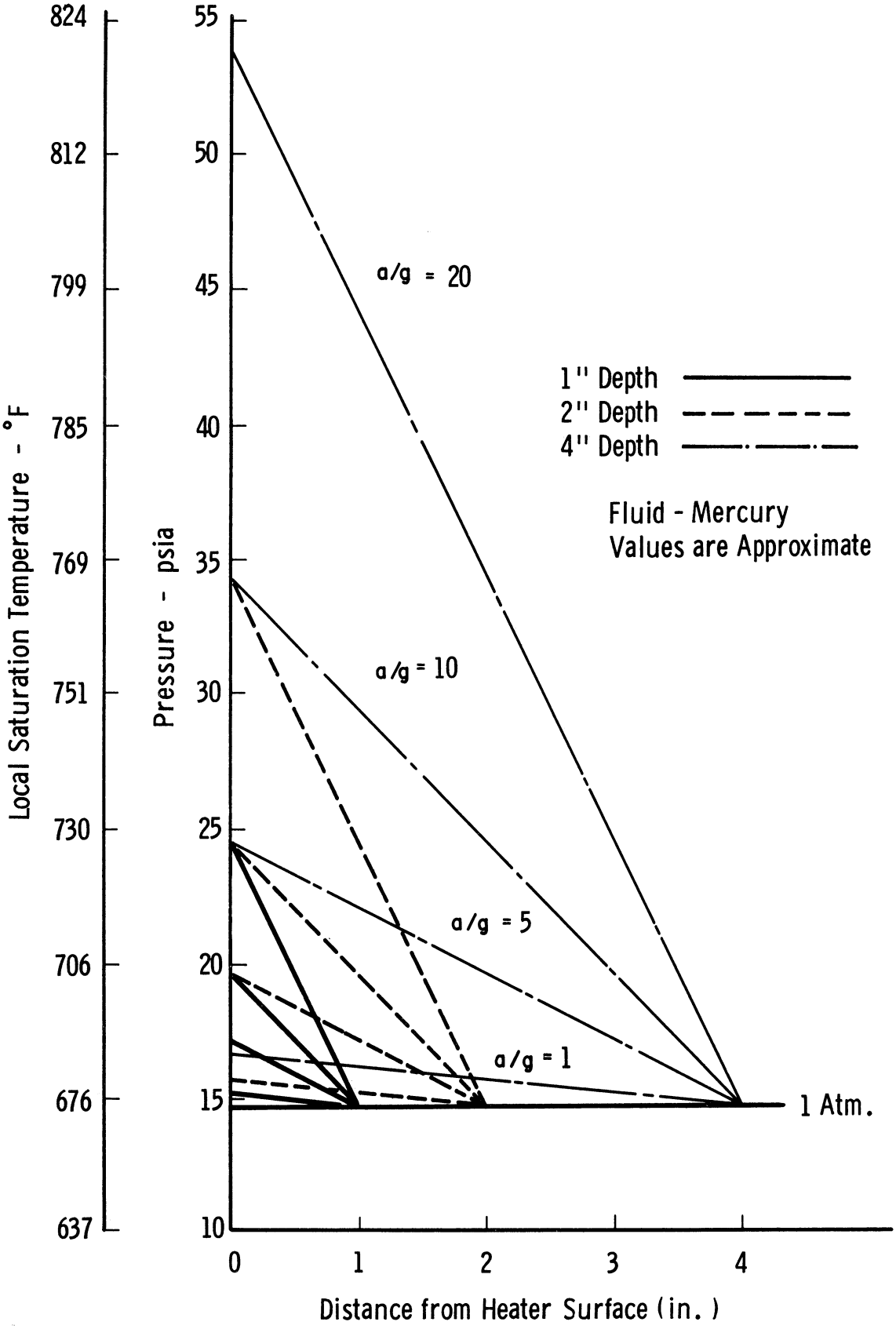


Figure 75. Variation of Hydrostatic Pressure with Acceleration.

EXPERIMENTAL APPARATUS

The final test vessel which was evolved and constructed for use with the centrifuge is shown in Figure 76. Various aspects of the design are discussed below.

Boiling Heat Transfer Surface: The maximum permissible overall size of the test vessel dictated a relatively small heat transfer surface area, since provision must be made within the vessel for instrumentation and insulation. It is desirable that the surface area be as large as practical in order that the disturbances introduced by provision for temperature measurements along with the heat losses be kept to a relatively small value. To a minor extent, the maximum heater surface area was also limited by the maximum power which could be transferred to the rotating assembly and taken within the pressure vessel. A heater surface diameter of 2 inches resulted, requiring approximately 3 KW to achieve a heat flux of $q/A = 500{,}000$ Btu/hr $ft^2$.

An electrical indirect method of heating was selected as being the most convenient, controllable and measureable. Seven commercial high-duty cartridge type heaters 3/8 inches in diameter by 2 1/2 inches long, centerless ground for close clearances, are inserted axially in one end of a 2-in diameter by 3 1/2-in long cylindrical piece of OFHC copper. The opposite end serves as the heat transfer surface. Copper was selected to minimize the temperature variations within the cylinder, and indeed was mandatory to achieve a temperature of 1100°F corresponding to 300 psia at the boiling surface without destruction of the cartridge heater elements.

To prevent attack of the copper by the mercury a 0.001-in thick foil of type 347 stainless steel is silver-brazed to the copper, resulting in intimate thermal contact between the foil and the copper. Extension of the foil from the heater surface furnishes a convenient seal between the heater and the inner-container side-wall. A thin foil is desirable for two reasons: the temperature drop across the foil is minimized, as is the heat loss from the edge of the heater due to the fin effect. A smaller temperature drop across the foil will permit a more accurate evaluation of the heating surface temperature, as the point nearest the boiling surface accessible to a thermocouple is the copper-stainless steel interface.

The surface temperature will be calculated by extrapolating temperatures measured with 2 thermocouples (encapsulated within 0.025-in OD stainless steel sheaths) located within 0.032 inches of the copper-stainless steel interface, and another located 1/2-in within the copper.

The copper cylinder is 1 inch longer than the inserted cartridge heaters in order that a uniform heat flux might exist at the boiling surface. It is estimated that the heat loss through the periphery of the foil amounts to less than 2 per cent of the total heat flux.

Figure 77 shown a view of the copper heater cylinder with the thin foil attached and with one of the cartridge heaters alongside.

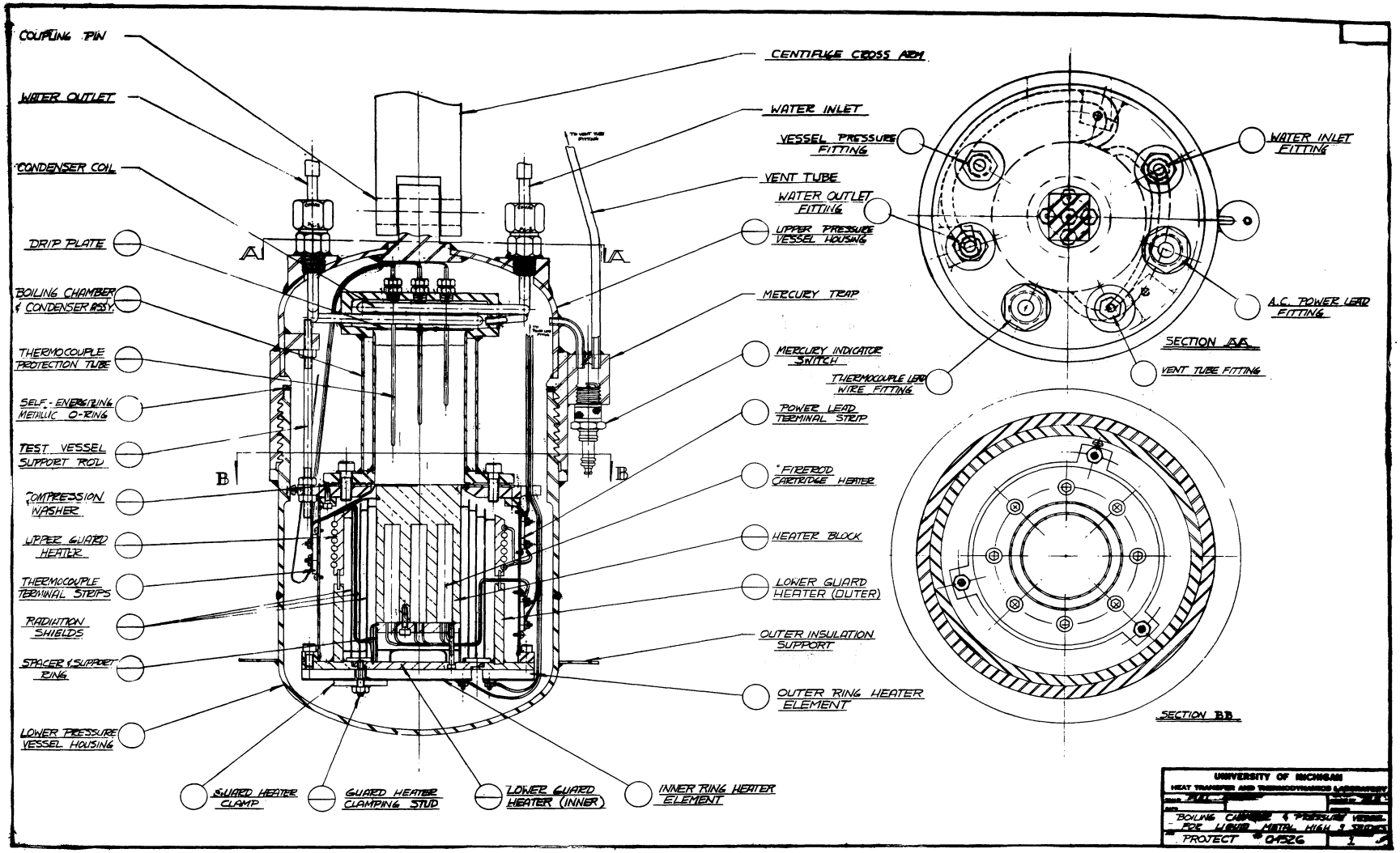


Figure 76. Test Vessel for Boiling Mercury Study Under High Gravity.

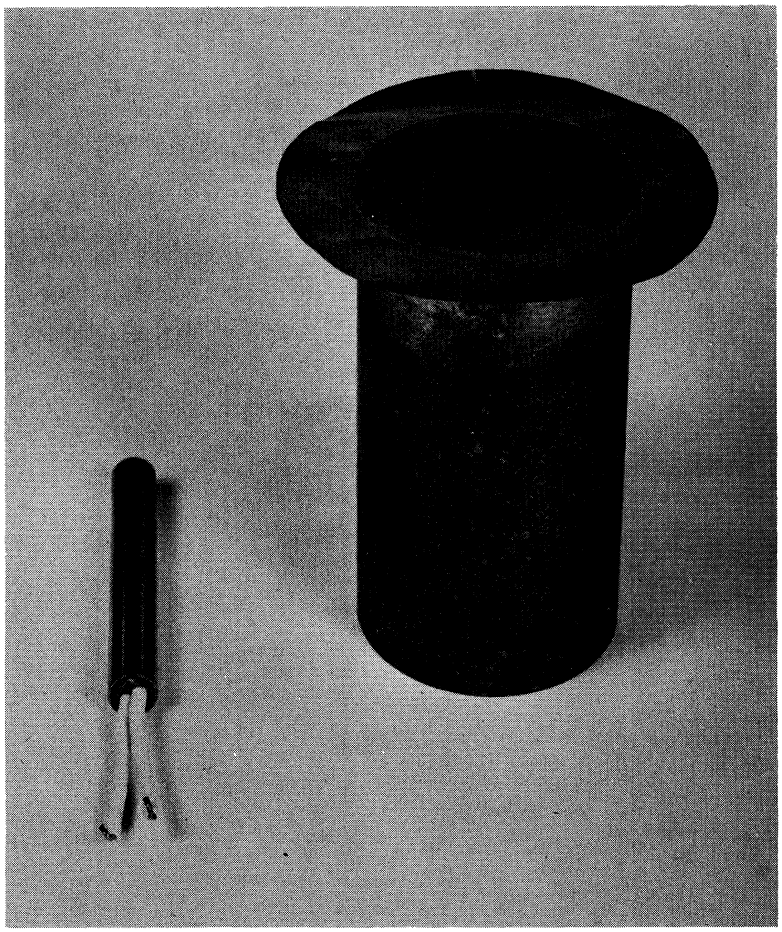

Figure 77. Copper Heater with Attached Stainless Steel Foil.

It was originally planned that the copper surfaces be chromium plated to prevent oxidation at the high temperature levels, but this has been eliminated since the operational procedure will entail initial evacuation and charging of the system with an inert gas such as helium or argon before heating begins.

A great deal of effort and time was necessary to develop the technique for achieving a good bond between the copper and stainless steel. An apparently successful bond was achieved by plating the stainless foil with .001-in thickness of silver, placing it in mechanical contact with the lapped copper surface, and heating the assembly to 1650°F in an argon atmosphere furnace, achieving what might be termed a silver-brazed joint by virtue of metallic diffusion. After a period of 6 months, while the apparatus was being prepared for assembly, a loose area was detected. It appeared that small gas pockets had been trapped between the two materials, resulting in an ineffective bond.

Prior to this, sample trials had been made by the same technique and the joint sectioned and observed under a metallurgical microscope, with no disparities in evidence.

The same technique has been repeated, but performing the heating within a high vacuum using the cartridge heaters as the heat source. This is also apparently successful, and an attempt will be made to verify the integrity with an ultrasonic transducer.

Guard Heater: The copper cylindrical heater is expected to operate at temperatures over the range 700°F - 1300°F. To insure that the measured power input is that passing through the boiling surface, heat losses are minimized by surrounding the cylinder with insulation, radiation shields and guard heaters as shown in Figure 76. A view of the disassembled components is given in Figure 78.

Since a temperature difference of as much as 200°F may exist in the axial direction within the copper cylinder at the higher heat flux, the guard heaters are divided into two independently measured and controlled zones: the upper periphery, and the lower periphery plus the underside. Differential thermocouples are to be installed in these zones between the cylinder and the guards for continuous monitoring.

Because of close clearances at the heater underside and insufficient flexibility of the wires to the cartridge heaters it was necessary to modify several elements in this region. To avoid severe assembly and disassembly problems it became necessary to rely on mechanical electrical connections to the cartridge heater lead wires. Pure nickel wires with ceramic fish-spine insulators are used as conductors within the pressure vessel.

Mercury Container and Condenser: The stainless steel foil skirt is clamped between two flanges as seen in Figure 76. The upper flange has two circular protuberances which crush into a copper washer on the underside of the foil to provide a high temperature seal. The entire heater assembly is supported by the lower flange, seen in the center of Figure 79.

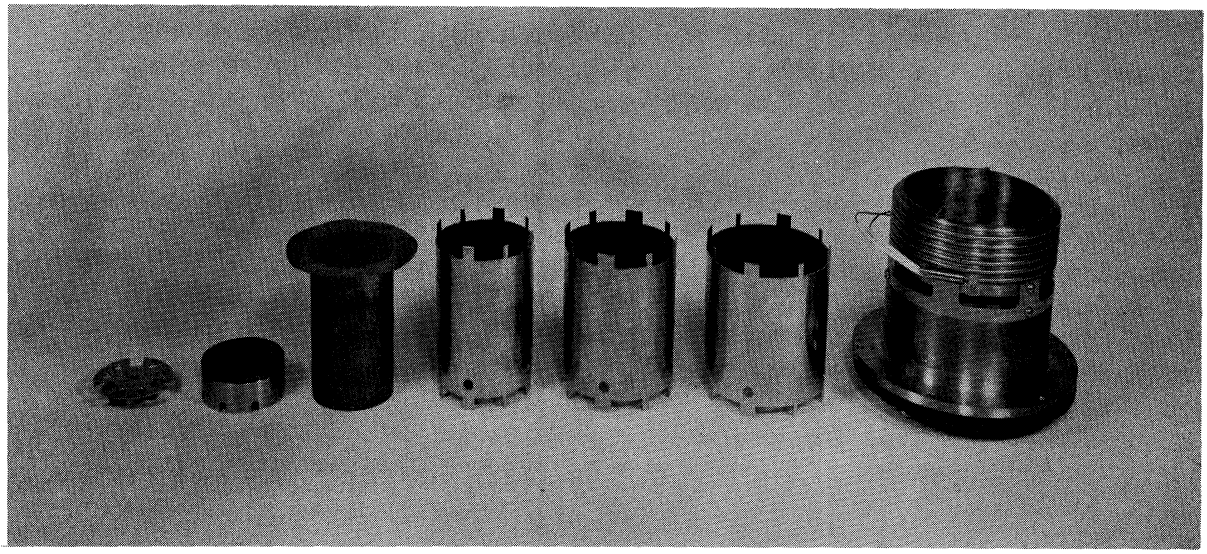

Figure 78. Copper Heater, Radiation Shields, and Guard Heaters.

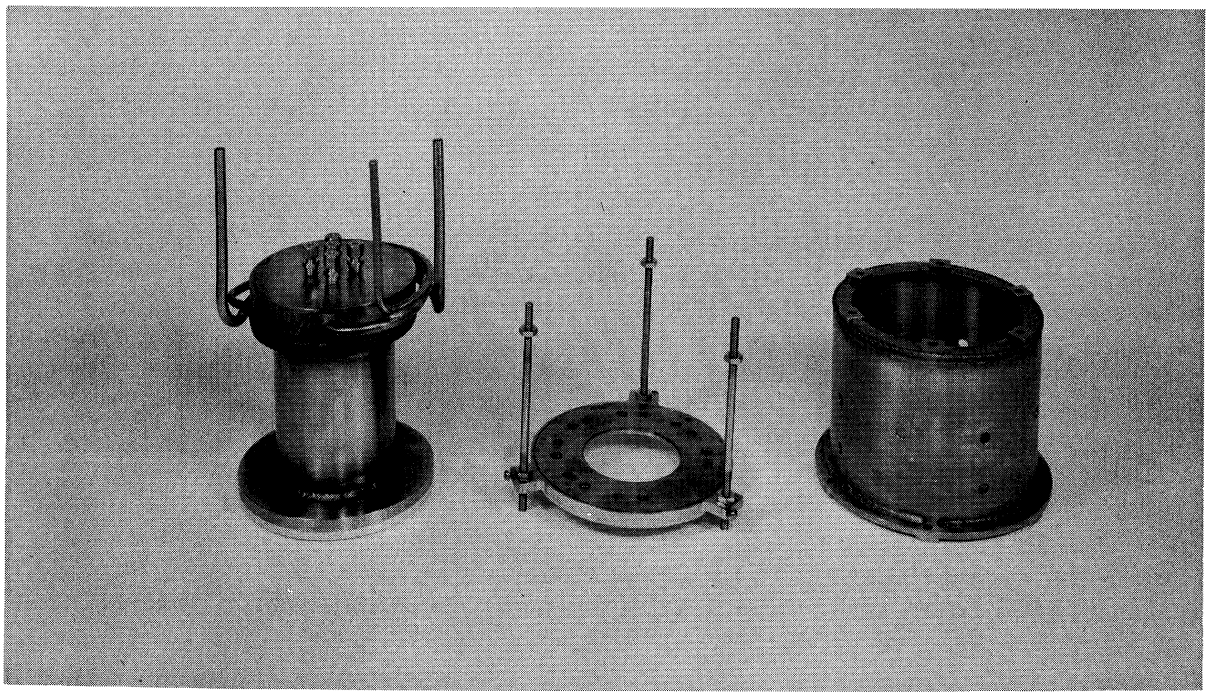

Figure 79. Mercury Container and Heater Support.

The upper flange also serves as the lower terminal of the double-walled mercury container. The upper end opens to a larger cavity in which a double row of coils is welded to serve as the mercury condenser. Beneath the coils is a so-called drip plate, a slightly dished disc of thin stainless steel with a number of small holes in it, acting as a countercurrent direct contact heat exchanger. If the condensed liquid mercury should become subcooled while in contact with the condenser coils, direct contact with the upflowing vapor through the holes is expected to reheat the liquid to near saturation temperature.

Thermocouples for measuring liquid temperatures are suspended from compression-type fittings threaded in the upper plate. Five tapped holes are in this plate and with the vent tube furnish the only access to the inner vessel once the unit is assembled.

Because of the complexity involved in assembling the test vessel, it is desirable that subsequent disassembly be kept at a minimum. To vary the liquid depth, mercury can be added and withdrawn from the inner vessel through the vent tube without disassembly. For data reduction purposes it is necessary that liquid depth be determined accurately. Careful metering of quantities added or withdrawn can accomplish this, but an independent direct method is incorporated by measuring the variation in resistance of a 30 gage pure iron wire with immersion depth in mercury. One electrical junction is made through the mercury and outer casing, and the other through a 20 gage tungsten wire insulated with quartz in passing through a compression fitting in the inner test chamber cover. The wire is held submerged in the liquid by means of a quartz extension rod as shown in Figure 80. No space exists in the outer pressure vessel cover to install the additional electrical connection required. Since liquid depth measurements under non-test conditions would suffice, access to the electrical lead is available by removing the test vessel pressurizing line.

Consideration was given to operating the test vessel as a closed vessel, regulating the system pressure by controlling the relation between heat input and output, but instabilities might be difficult to control because of the relatively low heat capacity of the system and the difficulty in regulating the condensation heat transfer rate.

External pressurization with an inert gas such as helium or argon will be used. This gas will have the effect of reducing the condensing heat transfer coefficient, requiring an increase in surface area of the condenser coils. The decreased condensing coefficient is beneficial, however, in that water under high velocity can be used as the coolant without achieving film boiling within the tubes.

Referring to Figures 76 and 79, operation under high pressure is attained by pressurizing the outer vessel. The inner vessel is vented to the pressure vessel via a tube which is welded to the inlet water line within the pressure vessel, and which then passes out of the pressure vessel through a suitable fitting, and then back to the pressure vessel through a mercury trap. Thus, any mercury vapor tending to pass through the vent line would be condensed in the water cooled part and reflux back to the inner vessel, or would

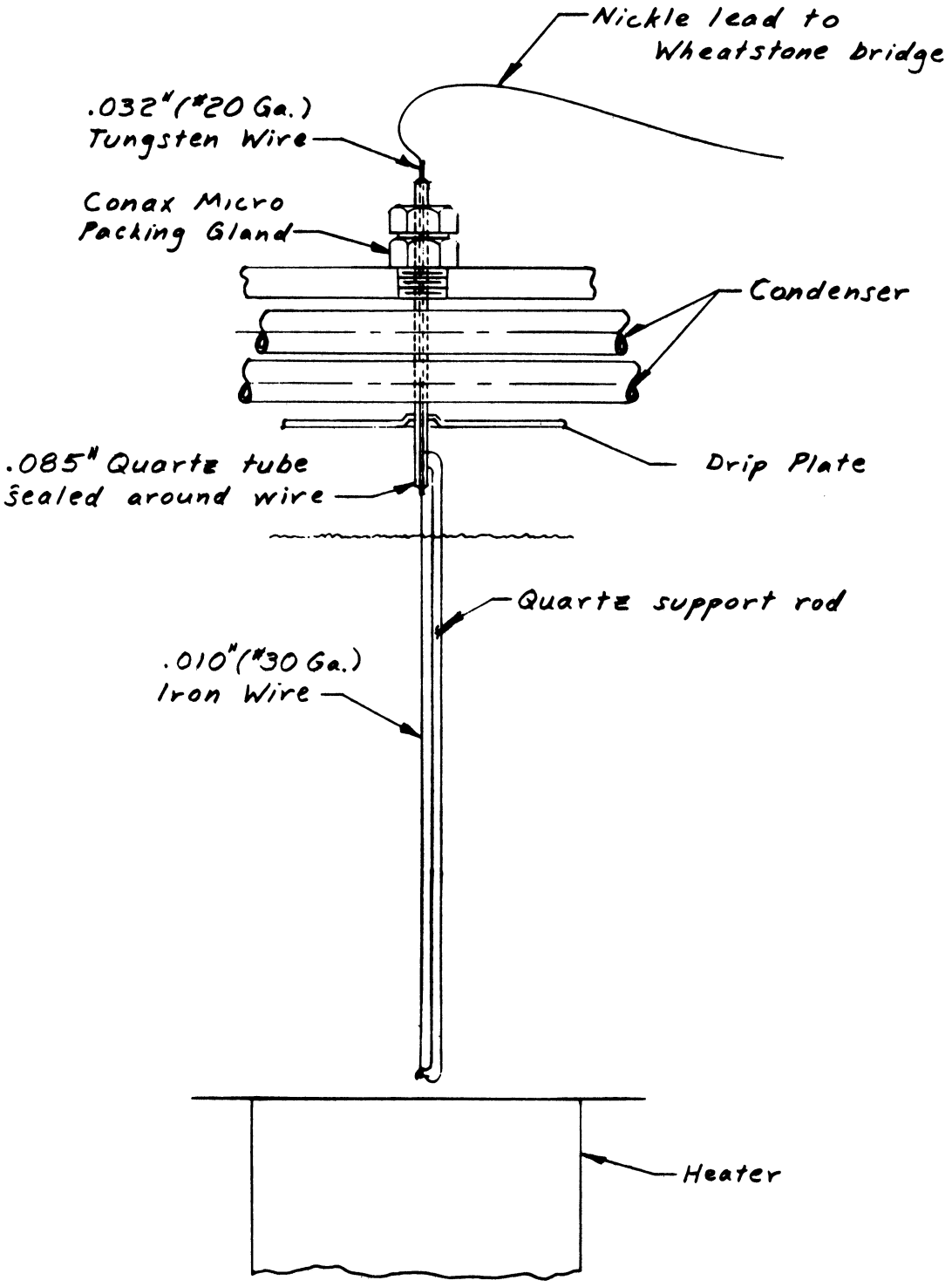


Figure 80. Liquid Level Indicator for Mercury.

be condensed in the air cooled external part and drop into the trap. An inverted spark plug in the trap will energize an electrical indicating circuit should any accumulation of mercury occur. These precautions are necessary to prevent the escape of mercury from the inner vessel.

Outer Pressure Vessel: The outer vessel consists of a welded construction of standard commercial stainless steel piping and elliptical caps. The two halves are shown in Figure 81, and are assembled with a buttress thread connection rather than the standard bolted flange technique for purposes of size and weight reduction. It was found necessary to chrome plate the threads to eliminate "galling" on assembly. The joint is sealed by a hollow self energizing stainless-steel O-ring, given a heavy plating of silver.

The vessel has been hydrostatically tested at 600 psi. As the maximum strength decreases at elevated temperatures, a conservative maximum operating pressure of 300 psi was selected.

The assembled outer pressure vessel and inner parts are shown in Figure 82. The inner vessel is supported from the upper half of the pressure vessel by way of stainless tension members threaded into welded pads. The use of these rods facilitates assembly of the entire vessel and also thermally isolates the pressure vessel from the lower part of the heater assembly, which has the highest temperature in the system. All pressure fittings are welded to bosses, which compensate for the decreased strength of the end cap.

Powdered high temperature insulation is to be used within the pressure vessel, and the ledge about the lower portion of the pressure vessel in Figure 82 is used to support magnesia-type insulation around the outside.

Temperature Measurement and Calibration: The temperature measurements within the pressure vessel are made with chromel-constantan thermocouples swaged in stainless steel tubing. The thermocouples within the copper heater are 0.025 inches in diameter while the remainder are 0.062 inches in diameter.

Figure 83 shows an equivalent thermocouple circuit required to achieve precision in the measurements. The thermocouples were calibrated from ambient to 900°F by comparison with a calibrated platinum resistance thermometer in a large constant temperature block. It is estimated that levels of temperature can be measured with $\pm$ 0.5°F accuracy while relative temperatures can be measured within $\pm$ 0.1°F. To achieve reproducibility it was found necessary to "age" the thermocouples at 1200°F for 24 hours, prior to calibration.

Centrifuge Assembly: Figure 84 schematically shows the test vessel, centrifuge and accessory equipment. The test vessel is pivoted on one end of the cross arm, thus maintaining the acceleration vector perpendicular to the heating surface at all g's. The mass and center of gravity of the counterweight are adjustable and will correspond to those values for the test vessel, in order that dynamic balance will exist at all rotational speeds.

A double fluid shaft seal is located at the upper end of the vertical shaft to furnish both the condenser coolant supply and the pressurizing gas supply.

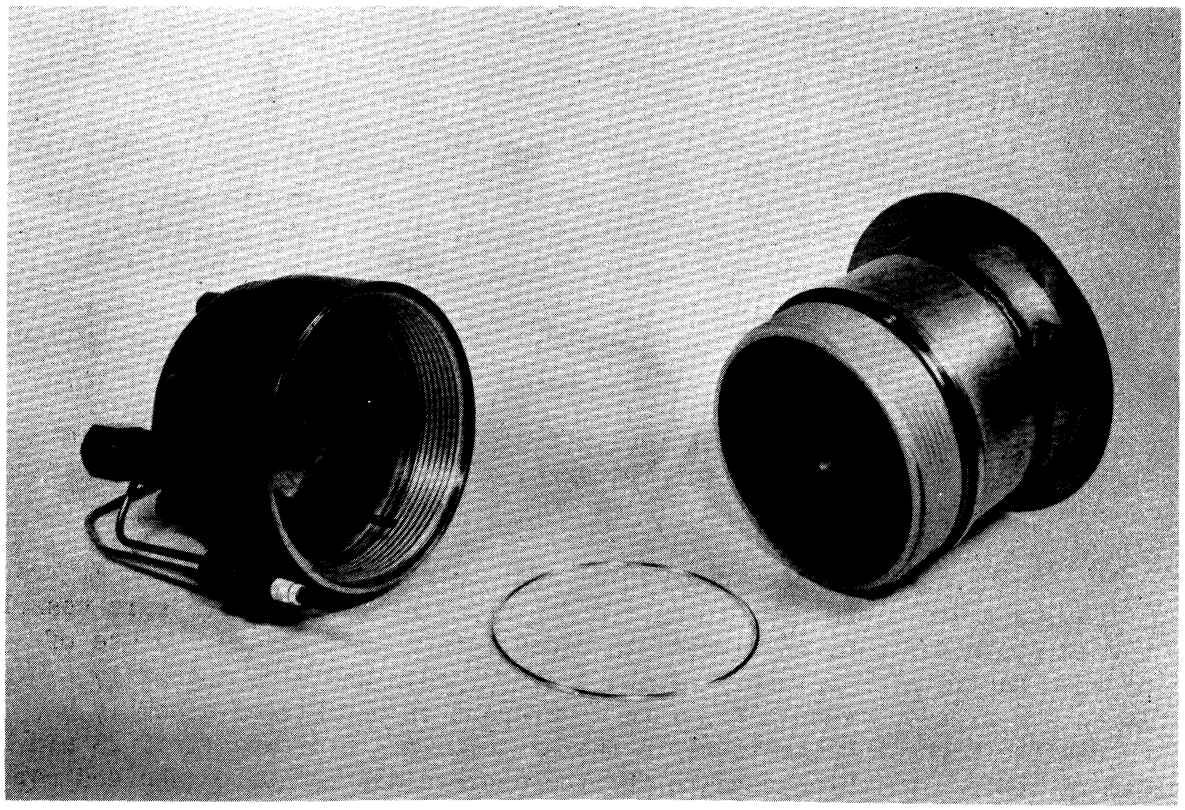

Figure 81. Pressure Vessel--Disassembled.

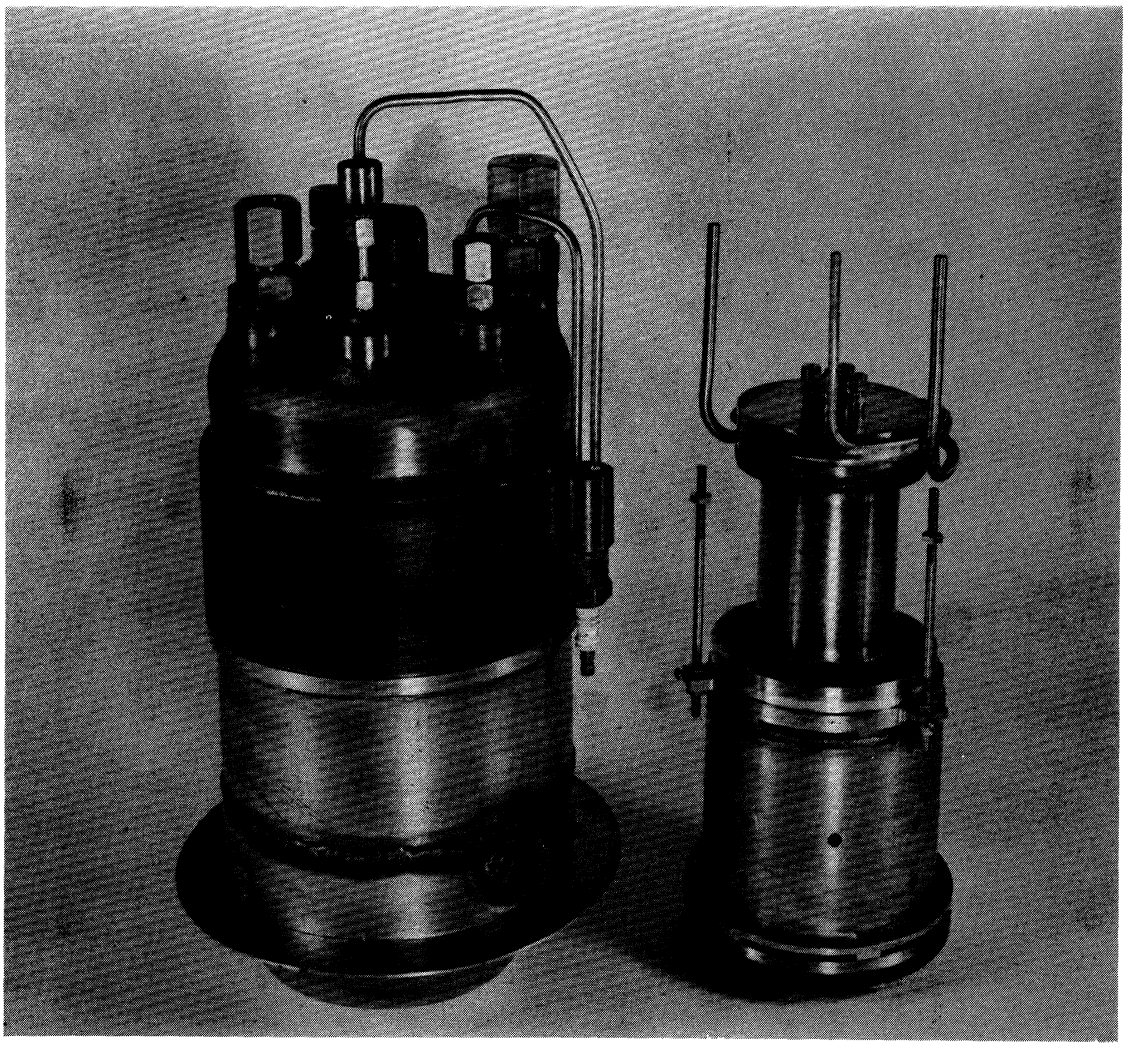

Figure 82. Assembled Pressure Vessel and Inner Test Vessel.

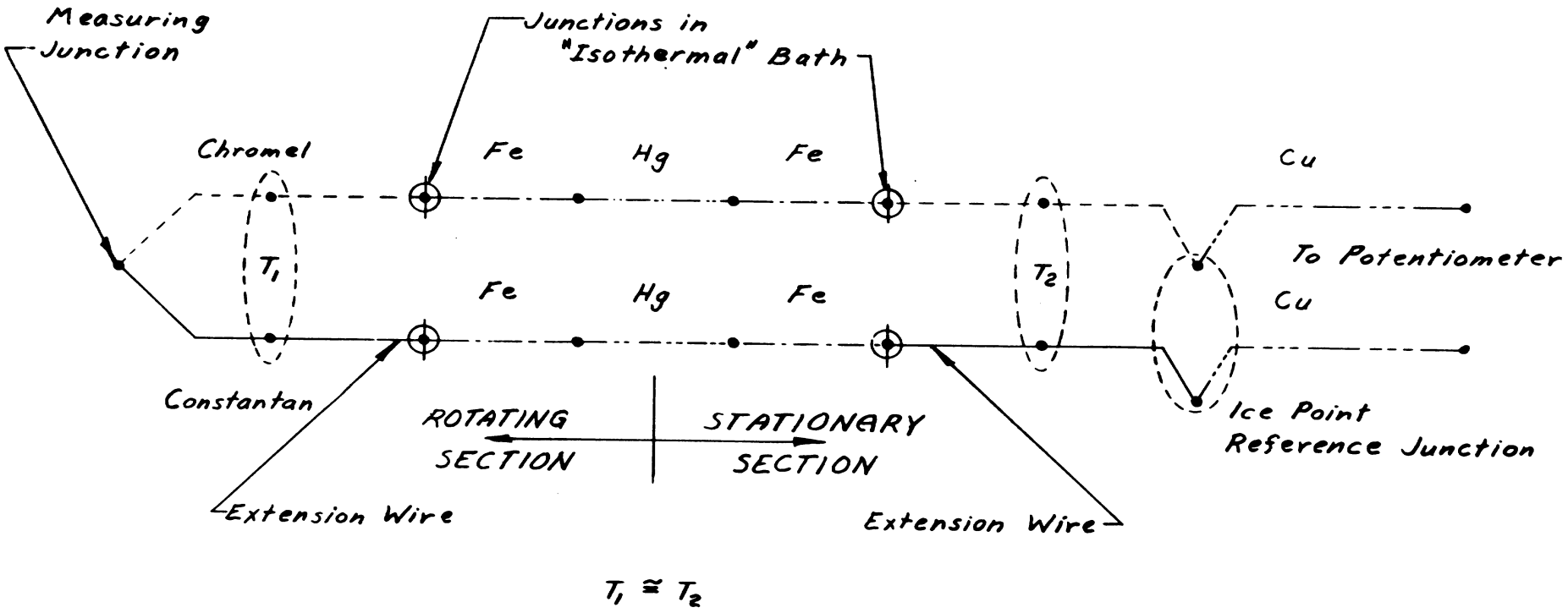


Figure 83. Equivalent Thermocouple Circuit for Temperature Measurement.

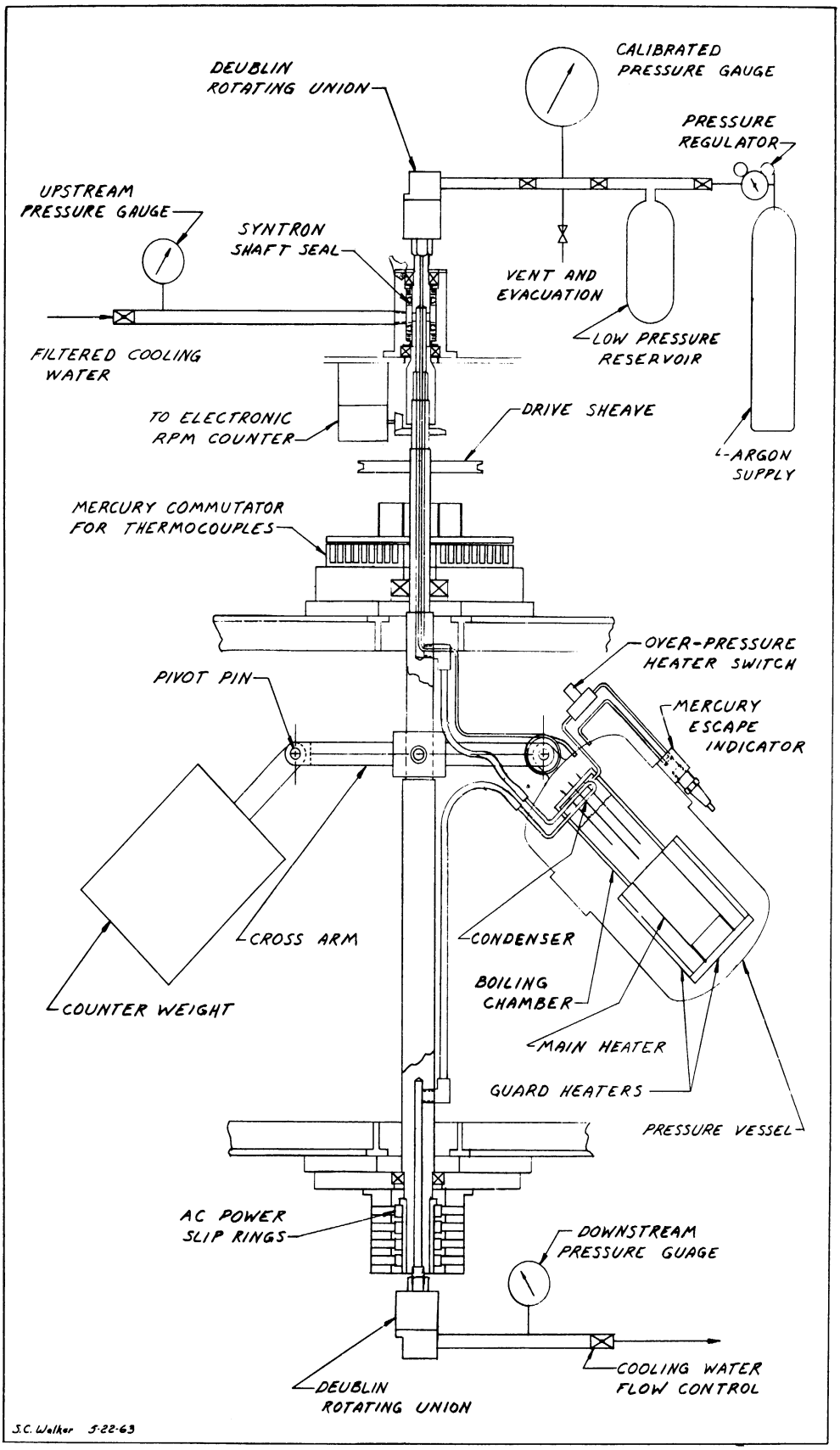


Figure 84. Mercury Boiling Test Vessel in Centrifuge.

An adjustable electrical pressure switch is shown mounted on the pressure vessel, in Figure 84 in the vent line, and is intended to cut off all power should the pressure exceed the operating pressure by a small amount.

In order to assure that the condenser coolant supply will completely fill the coils, a rotating seal and flow control valve are attached to the lower end of the vertical shaft.

An 8-ft high enclosure with 14-gage steel walls has been constructed about the centrifuge and terminates just below a building exhaust fan.

BIBLIOGRAPHY


1. Addoms, J. N. Sc.D. Thesis in Chemical Engineering, Massachusetts Institute of Technology. 1948.

2. Anderson, G. H. and Mantzouranis, B. G. "Two-Phase (Gas-Liquid) Flow Phenomena--I. Pressure Drop and Holdup for Two-Phase Flow in Vertical Tubes." Chemical Engineering Science. Vol. 12, 1960, p. 109.

3. Armand, A. A. et al. "Investigation of the Resistance During the Movement of Steam-Water Mixtures in a Heated Boiler Pipe at High Pressures." AERE-LIB/Trans-816, 1947.

4. Avery, G. W. "Effect of Surface Roughness on the Boiling of Mercury." M.S. Thesis in Chemical Engineering, Columbia University. 1960.

5. Baker, O. "Simultaneous Flow of Oil and Gas." Oil and Gas Journal. July 26, 1954. p. 185.

6. Balzhiser, R. E. et al. "Literature Survey on Liquid Metal Boiling." ASD-TR-61-594. The University of Michigan, Ann Arbor, Michigan. December, 1961.

7. Balzhiser, R. E. et al. Fourth Quarterly Report. The University of Michigan. Contract No. AF33(616)-8277. February, 1963.

8. Bankoff, S. G. et al. "On the Nature and Location of Bubble Nuclei in Boiling from Surfaces." Journal of Applied Physics. Vol. 29, No. 12, December, 1958, pp. 1739-1741.

9. Bankoff, S. G. "A Variable Density Single Fluid Model for Two-Phase Flow with Particular Reference to Steam-Water Flow." Journal of Heat Transfer. Vol. 82, November, 1960, p. 265.

10. Baroczy, C. J. "Correlation of Liquid Fraction in Two-Phase Flow with Application to Liquid Metals." NAA-SR-8171. Atomics International, Div. of North American Aviation, Inc., Canoga Park, California. April 15, 1963.

11. Bennett, J. A. R. "Two-Phase Flow in Gas-Liquid Systems: A Literature Survey." AERE CERI-2497. March, 1958.

12. Berensen, P. J. "Film-Boiling Heat Transfer from a Horizontal Surface." Journal of Heat Transfer. Vol. 83, August, 1961, p. 351.

13. Bertuzzi, A. F., Tek, M. R., and Poettmann, F. H. "Simultaneous Flow of Liquid and Gas Through Horizontal Pipe." Journal of Petroleum Technology. Vol. 8, January 17, 1956.

14. Bonilla, D. F. et al. "Pool Boiling Heat Transfer with Mercury." Reactor Heat Transfer Conference of 1956, TID-7529, Pt. 1, p. 324. (Also NYO-7638)

15. Bonilla, C. F. and Co-workers. "Alkali Metals Boiling and Condensing Investigations." General Electric Report No. ONE under NASA Contract NAS3-2528. September, 1962.

16. Braunlich, R. M. Thesis in Chemical Engineering, Massachusetts Institute of Technology. 1941.

17. Brown, R. A. S. and Govier, G. W. "High Speed Photography in the Study of Two-Phase Flow." Canadian Journal of Chemical Engineering. Vol. 39, 1961, p. 159.

18. Brown, R. A. S., Sullivan, G. A., and Govier, G. W. "The Upward Vertical Flow of Air-Water Mixtures--III. Effect of Gas Phase Density on Flow Pattern, Holdup and Pressure Drop." Canadian Journal of Chemical Engineering. Vol. 38, 1960, p. 62.

19. Calvert, S. and Williams, B. "Upward Cocurrent Annular Flow of Air and Water in Smooth Tubes." AIChE Journal. Vol. 1, 1955, p. 78.

20. Carslaw, H. S. and Jaeger, J. C. Conduction of Heat in Solids. Second Edition. Oxford Press, London. 1959.

21. Chang, Y. P. and Snyder, N. W. "Heat Transfer in Saturated Boiling." CEP Symposium Series. Vol. 56, No. 30, 1960, pp. 25-38.

22. Chang, Y. P. "Wave Theory of Heat Transfer in Film Boiling." Journal of Heat Transfer. Vol. 81, February, 1959, p. 1.

23. Chenoweth, J. M. and Martin, M. W. "Turbulent Two-Phase Flow." Petroleum Refiner. Vol. 34, No. 10, 1955, p. 151.

24. Chisolm, D. and Laird, A. D. K. "Two-Phase Flow in Rough Tubes." Transactions of ASME. Vol. 80, 1958, p. 276.

25. Cichelli, M. T. and Bonilla, C. F. "Heat Transfer to Liquids Boiling Under Pressure." Transactions of AIChE. Vol. 41, 1945, pp. 755-787.

26. Clark, J. A. and Merte, H. "Nucleate, Transition, and Film Boiling Heat Transfer at Zero Gravity," published in Advances in the Astronautical Sciences, Vol. 14, Physical and Biological Phenomena in a Weightless State, E. T. Benedict and R. W. Halliburton, Editors, Western Periodicals Co., North Hollywood, California. 1963. pp. 177.

27. Clark, J. A. and Merte, H. "Boiling Heat Transfer to a Cryogenic Fluid in Both Low and High Gravity Fields." Presented at the Eleventh International Congress of Refrigeration, Munich, Germany. August 27-September 4, 1963.

28. Colver, C. P. "Measurements of the Temperature Profiles Adjacent to the Surface During the Nucleate Boiling of Water and Methanol." M.S. Thesis in Chemical Engineering, University of Kansas. 1960.

29. Corty, C. and Foust, A. S. "Surface Variables in Nucleate Boiling." CEP Symposium Series. Vol. 51, 1955, p. 17.

30. Costello, C. P. and Adams, P. "Burnout Heat Fluxes in Pool Boiling at High Fluxes in Pool Boiling at High Acceleration." International Developments in Heat Transfer, Part II. ASME. 1961.

31. Costello, C. P. and Tuthill, W. "Effects of Accelerations on Nucleate Pool Boiling." CEP Symposium Series. Vol. 57, No. 32, 1961, p. 189.

32. Dzhelepov, B. S. and Peker, L. K. Decay Schemes of Radioactive Nuclei. Pergamon Press, New York, New York, 1961, pp. 497-499.

33. Dukler, A. E. "Fluid Mechanics and Heat Transfer in Vertical Falling Film Systems." ASME-AIChE Third National Heat Transfer Conference. August, 1959.

34. Egen, R. A., Dingee, D. A. and Chastain, J. W. "Vapor Formation and Behavior in Boiling Heat Transfer." BMI-1163. February 4, 1957.

35. Ellion, M. E. "A Study of the Mechanism of Boiling Heat Transfer." JPL-Memo No. 20-88. March 1, 1954.

36. Foerster, C. V. Private Communication. Coast Metals, Inc., Little Ferry, New Jersey.

37. Forster, H. K. and Greif, R. "Heat Transfer to a Boiling Liquid--Mechanism and Correlations." Journal of Heat Transfer. Transactions of ASME. Vol. 81, February, 1959, pp. 43-53.

38. Forster, H. K. and Zuber, N. "Dynamics of Vapor Bubbles and Boiling Heat Transfer." AIChE Journal. Vol. 1, No. 4, December, 1955, pp. 531-535.

39. Forster, H. K. and Zuber, N. "Growth of a Vapor Bubble in a Superheated Liquid." Journal of Applied Physics. Vol. 25, 1954, p. 474.

40. Gambill, W. R. "A Survey of Boiling Burnout." British Chemical Engineering. Vol. 8, No. 2, February, 1963, pp. 93-98.

41. Gambill, W. R. and Hoffman, H. W. "Boiling Liquid-Metal Heat Transfer." Space-Nuclear Conference, American Rocket Society, May 3-5, 1961.

42. Goldmann, K. "Selected Parameters for Two-Phase Flow of Sodium." Presented at Third Annual High Temperature Liquid Metal Heat Transfer Technology, Oak Ridge National Laboratory, Oak Ridge, Tennessee. September 4-6, 1963. To be published.

43. Goldsmith, A., Watermann, T. E., and Hirschorn, H. J. Handbook of Thermophysical Properties of Solid Materials. Macmillan Company, New York, New York, 1961, p. 963.

44. Govier, G. W. and Omer, M. M. "The Horizontal Pipeline Flow of Air-Water Mixtures." Canadian Journal of Chemical Engineering. Vol. 40, 1962, p. 93.

45. Govier, G. W., Radford, B. A. and Dunn, J. S. C. "The Upwards Vertical Flow of Air-Water Mixtures." Canadian Journal of Chemical Engineering. Vol. 35, 1957, p. 59.

46. Govier, G. W. and Short, W. L. "The Upward Vertical Flow of Air-Water Mixtures--III. Effect of Tubing Diameter on Flow Pattern, Holdup and Pressure Drop." Canadian Journal of Chemical Engineering. Vol. 36, 1958, p. 195.

47. Graham, R. W. and Hendricks, R. C. "A Study of the Effect of Multi-G Accelerations on Nucleate Boiling Ebullition." NASA-TN-D1196. May, 1963.

48. Gresham, W. A., Foster, P. A., and Kyle, R. J. "Review of the Literature on Two-Phase (Gas Liquid) Fluid Flow in Pipes." WADC-55-422. Part I. June, 1955.

49. "Harshaw Scintillation Phosphors." Harshaw Chemical Company, Cleveland, Ohio, 1962, p. 43.

50. "Haynes Alloy No. 25." Haynes Stellite Company, Kokomo, Indiana. 1960.

51. Heineman, J. B., Marchaterre, J. F., and Mehta, S. "Electromagnetic Flowmeters for Void Fraction Measurements in Two-Phase Metal Flow." Review of Scientific Instruments. Vol. 34, 1963, p. 399.

52. Hewitt, G. F. "Analysis of Annular Two Phase Flow: Application of the Dukler Analysis to Vertical Flow in a Tube." AERE-R-3680. January, 1961.

53. Hoogendoorn, C. J. "Gas-Liquid Flow in Horizontal Pipes." Chemical Engineering Science. Vol. 9, 1959, p. 205.

54. Hooker, H. H. and Popper, G. F. "A Gamma-Ray Attenuation Method for Void Fraction Determinations in Experimental Boiling Heat Transfer Test Facilities." ANL-5766. November, 1958.

55. Hosler, E. R. and Westwater, J. W. "Film Boiling on a Horizontal Plate." ARS Journal. Vol. 32, April, 1962, p. 553.

56. Houck, J. A. "Physical and Mechanical Properties of Commercial Molybdenum-Base Alloys." DMIC Report 140. November 30, 1960.

57. Hsu, S. T. and Schmidt, F. W. "Measured Variations in Local Surface Temperatures in Pool Boiling Water." ASME Paper No. 60-HT-32. 1960.

58. Hughmark, G. A. "Holdup in Gas-Liquid Flow." Chemical Engineering Progress. Vol. 58, April, 1962, p. 62.

59. Hughmark, G. A. and Pressburg, B. S. "Holdup and Pressure Drop with Gas-Liquid Flow in a Vertical Pipe." AIChE Journal. Vol. 7, 1961, p. 677.

60. Isbin, H. S., Moen, R. H., and Mosher, D. R. "Two-Phase Pressure Drops." AECU-2994. November, 1954.

61. Ishigai, S. et al. "Boiling Heat Transfer from a Flat Surface Facing Downward." Paper 26. International Heat Transfer Conference. 1961.

62. Ivey, H. J. "Acceleration and the Critical Heat Flux in Pool Boiling Heat Transfer." The Institution of Mechanical Engineers. Thermodynamics and Fluid Mechanics Group. 1962.

63. Ivey, H. J. and Morris, D. J. "On the Relevance of the Vapor-Liquid Exchange Mechanism for Subcooled Boiling Heat Transfer at High Pressure." AEEW-R-137. January, 1962.

64. Jackson, C. B. (Edit.) Liquid Metals Handbook: Na-NaK Supplement. Atomic Energy Commission and Bureau of Ships. Third Edition. 1955, pp. 32-45.

65. Jakob, M. Heat Transfer. Vol. 1, Chap. 29. John Wiley, New York, New York, 1949.

66. Korneev, M. I. "Investigation of Heat Transfer of Mercury and Magnesium Amalgams under Natural Circulation Conditions." Teploenergetika. Vol. 2, No. 7, July, 1955, pp. 25-29.

67. Korneev, M. I. Teploenergetika. Vol. 4, No. 44, 1955.

68. Kutateladze, S. S. "Heat Transfer in Condensation and Boiling." Second Edition. Moscow-Leningrad, 1952. AEC-tr-3770, August, 1959.

69. Kutateladze, S. S. et al. Liquid Metal Heat Transfer Media. Atomaya Energiia, Supplement No. 2. Translated by Consultants Bureau, Inc., New York, New York, 1959.

70. Kutateladze, S. S. and Schneiderman, L. L. "Experimental Study of the Influence of the Temperature of a Liquid on a Change in the Rate of Boiling." In Problems of Heat Transfer During a Change of State. A Collection of Articles. AEC-tr-3405. 1953.

71. Lady, E. D. "Low Flux Boiling." Ph.D. Thesis, The University of Michigan, Ann Arbor, Michigan. 1963.

72. Levy, S. "Generalized Correlation of Boiling Heat Transfer." Journal of Heat Transfer. ASME. Vol. 81, February, 1959, pp. 37-42.

73. Levy, S. "Theory of Pressure Drop and Heat Transfer for Annular Steady State Two-Phase Two-Component Flow." Second Midwestern Conference on Fluid Mechanics. Ohio State University Engineering Experiment Station. Bulletin 149, September, 1952, pp. 337-348.

74. Levy, S. "Steam Slip--Theoretical Prediction from Momentum Model." Journal of Heat Transfer. Vol. 82, May, 1960, p. 113.

75. Levy, S. "Prediction of Two-Phase Pressure Drop and Density Distribution From Mixing Length Theory." Journal of Heat Transfer. Vol. 85, May, 1963, p. 137.

76. Lin, C. et al. "Boiling Heat Transfer of Liquid Metals." JPRS-3512 (or 3531). Translated by Office of Technical Services. 1959.

77. Linning, D. L. "The Adiabatic Flow of Evaporating Fluids in Pipes of Uniform Bore." Institution of Mechanical Engineers. London. Proceedings (B). 1952, p. 64.

78. Lockhart, R. W. and Martinelli, R. C. "Proposed Correlation of Data for Isothermal Two-Phase, Two-Component Flow in Pipes." Chemical Engineering Progress. Vo. 45, 1949, p. 39.

79. Lyon, R. E., Foust, A. S., and Katz, D. L. "Boiling Heat Transfer with Liquid Metals." CEP Symposium Series No. 17. Vol. 51, 1955, pp. 41-47.

80. Madsen, N. and Bonilla, C. F. "Heat Transfer to Sodium Potassium Alloy in Pool Boiling." CEP Symposium Series. Vol. 56, 1960.

81. Martinelli, R. C. et al. "Isothermal Pressure Drop for Two-Phase Two-Component Flow in Horizontal Pipe." Transactions ASME. Vol. 66, 1944, p. 139.

82. Martinelli, R. C. and Nelson, D. B. "Prediction of Pressure Drop During Forced-Circulation Boiling of Water." Transactions ASME. Vol. 70, 1948, p. 695.

83. Martinelli, R. C., Putnam, J. A., and Lockhart, R. W. "Two-Phase Two-Component Flow in the Viscous Region." Transactions AIChE. Vol. 42, 1946, p. 681.

84. Masnovi, R. "Literature Survey of Two-Phase Fluid Flow." WAPD-TH-360, 1958.

85. Maurer, G. W. "The Measurement of the Densities of Flowing Fluids by Radioactivity Methods." M.S. Thesis, University of Pittsburgh, 1959.

86. McAdams, W. H. Heat Transmission. Chap. 10, 3rd Edition, McGraw-Hill Co., New York, New York, 1954.

87. Merte, H. and Clark, J. A. "Pool Boiling in an Accelerating System." Journal of Heat Transfer. Transactions ASME. Series C. Vol. 83, August, 1961, pp. 223-242.

88. Merte, H. and Clark, J. A. "Boiling Heat Transfer with Cryogenic Fluids at Standard, Fractional and Near-Zero Gravity." ASME Paper No. 63-HT-28. Presented at ASME-AIChE Heat Transfer Conference, Boston Massachusetts. August 11-14, 1963.

89. Mesler, R. B. and Banchero, J. T. "The Effect of Superatmospheric Pressures on Nucleate Boiling." AIChE Journal. Vol. 4, 1958, p. 102.

90. Misra, B. and Bonilla, C. F. Chemical Engineering Progress. Symposium Series. Vol. 52, 1956, p. 18.

91. Moore, F. D. and Mesler, R. B. "Micro-Layer Vaporization." AIChE Journal. Vol. 7, 1961, p. 62.

92. MSA Research Corporation. "Suggestions for Using MSAR NaK Shipping Containers." Callery, Pennsylvania. August 1, 1960.

93. Musinski, E. J. Private Communication. Ultra Carbon Corporation. December 20, 1962.

94. Myers, W. A. "A Method for Determining the Void Fraction of Two-Phase Potassium." Final Report for Course CME-690, University of Michigan, Ann Arbor, Michigan. May, 1963.

95. National Carbon Company, Engineering Handbook, 1957.

96. Neal, L. G. and Bankoff, S. G. "A High Resolution Resistivity Probe for Determination of Local Void Properties in Gas-Liquid Flow." Presented at 55th Annual Meeting of AIChE. Chicago. December 2-6, 1962.

97. Neal, L. G. "Local Parameters in Cocurrent Mercury-Nitrogen Flow." ANL-6625. January, 1963.

98. Noyes, R. C. "An Experimental Study of Sodium Pool Boiling Heat Transfer." Journal of Heat Transfer. Transactions ASME. Series C. Vol. 85, May, 1963, p. 125. (Also NAA-SR-6760.)

99. Petrick, M. "Two-Phase Air-Water Flow Phenomena." ANL-5787. March, 1958.

100. Pike, R. W. "The Adiabatic, Evaporating, Two-Phase Flow of Steam and Water in Horizontal Pipe." Ph.D. Thesis, Georgia Institute of Technology. 1962.

101. Pomerantz, M. L. "Film Boiling on a Horizontal Tube in Increased Gravity Fields." ASME Paper No. 63-HT-17. Presented at ASME-AIChE Heat Transfer Conference. Boston, Massachusetts. August 11-14, 1963.

102. Price, W. J. Nuclear Radiation Detection. McGraw-Hill Book Co., Inc. New York, New York. 1958, pp. 189-194.

103. "Proceedings of the Symposium on Two-Phase Fluid Flow." The Institution of Mechanical Engineering. London. 1962.

104. "Proceedings of the 1962 High-Temperature Liquid-Metal Heat Transfer Technology Meeting." Brookhaven National Laboratory, Upton, New York. Report BNL-756 (c-35). May 17-18, 1962.

105. "Proceedings of the 1963 High-Temperature Liquid-Metal Heat Transfer Technology Meeting." Oak Ridge National Laboratory, Oak Ridge, Tennessee. September 4-6, 1963. To be published.

106. Richardson, B. L. "Some Problems in Horizontal Two-Phase, Two-Component Flow." ANL-5949. December, 1958.

107. Rohsenow, W. M. "A Method of Correlating Heat-Transfer Data for Surface Boiling of Liquids." Transactions of ASME. Vol. 74, August, 1951, pp. 969-976.

108. Rohsenow, W. M. and Griffith, P. "Correlation of Maximum Heat Flux Data for Boiling of Saturated Liquids." Chap. 9 of Heat, Mass and Momentum Transfer. W. M. Rohsenow and H. Y. Choi. Prentice-Hall, New York, New York. 1961. (Also NP-5738.)

109. Rohsenow, W. M. Heat Transfer Symposium, 1952. Engineering Research Institute, University of Michigan. 1953, pp. 101-149.

110. Romie, F. E., Brorarney, S. W. and Giedt, W. H. "Heat Transfer to Boiling Mercury." Journal of Heat Transfer. Vol. 82, November, 1960. (Also ATL-A-102.)

111. Ros, N. C. J. "Simultaneous Flow of Gas and Liquid as Encountered in Oil Wells." Journal of Petroleum Technology. Vol. 13, October, 1961, p. 1037.

112. "SC-18 Superscaler: Operating and Maintenance Instructions." Tracerlab, Inc., Boston, Massachusetts. 1952.

113. Schmidt, E. H. W. "Heat Transmission by Natural Convection at High Centrifugal Acceleration in Water-Cooled Gas-Turbine Blades." The Institution of Mechanical Engineers-ASME. Proceedings of the General Discussion on Heat Transfer. September 11-13, 1951.

114. Sherley, Joan E. "Nucleate Boiling Heat Transfer Data for Liquid Hydrogen at Standard and Zero-Gravity." Published in Advances in Cryogenic Engineering. Volume 8. (K. D. Timmerhaus, Editor.) The Plenum Press. 1963.

115. Smith, C. R., Tang, Y. S. and Walker, C. L. "Slip Velocity in Two-Phase Metallic Fluids." Allison Division, General Motors Corporation. Indianapolis, Indiana. Engineering Department Report No. 2809. May 25, 1962.

116. Street, J. R. "A Study of Vertical Gas-Liquid Slug Flow." Ph.D. Thesis, The University of Michigan, Ann Arbor, Michigan. 1962.

117. Styrikovich, M. A. et al. "Some Relationships in Heat Transfer to Boiling Mercury in Forced Convection." Zhur. Tekh. Fiz. Vol. 10, 1940, pp. 1331-1339. (Also AEC-tr-3868.)

118. Taylor Volumetric Pressure Systems, Bulletin 98365. Taylor Instrument Company, Rochester, New York. February, 1961.

119. Taylor Transcope Recording Receiver 91J. Instructions for Taylor Instruments 3E211. Taylor Instrument Company, Rochester, New York. Issue 3.

120. Transaire Volumetric D-P Transmitter 205-T. Instructions for Taylor Instruments 2B204. Taylor Instrument Company, Rochester, New York. Preliminary Issue. March, 1959.

121. Usiskin, C. M. and Siegel, R. "An Experimental Study of Boiling in Reduced and Zero Gravity Fields." Journal of Heat Transfer, Transactions ASME. Series C. Vol. 83, August, 1961, pp. 243-251.

122. Van Camp, W. M. and St.Clair, C. R. ASME Paper No. 54-F-33. 1954.

123. Vohr, J. H. "Flow Patterns of Two-Phase Flow--A Survey of Literature." TID-11514. December 15, 1960.

124. Ward, H. C. et al. "Analytical Investigation of Two-Phase Vapor-Liquid Ratio Measuring Systems and Two-Phase Flow Literature Survey Supplement." WADC Report No. 59-230. August, 1959.

125. Weatherford, W. D. et al. "Properties of Inorganic Energy-Conversion and Heat Transfer Fluids for Space Applications." WADD Technical Report 61-96. November, 1961.

126. West, R. "Low-Energy Gamma-Ray Sources." Nucleonics. Volume 11, No. 2, pp. 20-23.

127. Westwater, J. W. American Scientist. Volume 47, 1959.

128. Westwater, J. W. and Santangelo, J. G. "Photograph Study of Boiling." Industrial Engineering Chemistry. August, 1955, p. 1605.

129. Wheeler, R. G. "Thermal Contact Conductance of Fuel Element Materials." General Electric Company, Hanford Atomic Products Operation, Richland, Washington.

130. Zuber, N. and Tribus, M. "Further Remarks on the Stability of Boiling Heat Transfer." AECU-3631. January, 1958.

131. Zuber, N. "Hydrodynamic Aspects of Boiling Heat Transfer." Ph.D. Thesis. Department of Engineering, U.C.L.A. June, 1959.

# APPENDIX A

## NUCLEATE BOILING AND BURNOUT DATA

TABLE I

NUCLEATE BOILING WATER DATA

| AMPS | VOLTS | HEAT FLUX $\frac{BTU}{(Hr)(Sq\ Ft)}$ | TEMPERATURES, °F | | |
|---|---|---|---|---|---|
| | | | Bulk | Tube | $\Delta T$ |
| Run: W-1 | | | | | |
| Pressure: | 1 Atmosphere | | | | |
| 19 | 0.3 | 1900 | 211 | 218 | 6.5 |
| 37 | 0.6 | 7200 | - | 228 | 15.1 |
| 50 | 0.8 | 13100 | - | 236 | 21.5 |
| 68 | 1.1 | 24200 | - | 241 | 23.5 |
| 88 | 1.5 | 40700 | - | 250 | 28.1 |
| 104 | 1.7 | 57000 | - | 257 | 30.7 |
| 124 | 2.1 | 80600 | - | 262 | 29.3 |
| 138 | 2.3 | 100000 | - | 270 | 32.1 |
| 150 | 2.5 | 118000 | - | 275 | 32.3 |
| Run: W-2 | | | | | |
| Pressure: | 1 Atmosphere | | | | |
| 20 | 0.3 | 2100 | 211 | 218 | 6.4 |
| 89 | 1.5 | 41600 | - | 256 | 33.8 |
| 121 | 2.0 | 76800 | - | 274 | 42.3 |
| 154 | 2.5 | 124000 | - | 291 | 46.6 |
| 183 | 3.1 | 176000 | - | 310 | 51.7 |
| Run: W-3 | | | | | |
| Pressure: | 1 Atmosphere | | | | |
| 25 | 0.4 | 3280 | 211 | 224 | 12.1 |
| 46 | 0.8 | 11100 | - | 232 | 18.0 |
| 69 | 1.2 | 25000 | 212 | 244 | 26.3 |
| 91 | 1.5 | 43500 | 212 | 254 | 31.3 |
| 126 | 2.1 | 83300 | 211 | 270 | 36.6 |
| 155 | 2.7 | 126000 | 211 | 286 | 41.1 |
| 188 | 3.1 | 186000 | 212 | 305 | 44.0 |
| Run: W-4 | | | | | |
| Pressure: | 1 Atmosphere | | | | |
| 23 | 0.5 | 3440 | 211 | 219 | 7.1 |
| 52 | 1.1 | 18700 | 212 | 238 | 22.0 |
| 72 | 1.5 | 34400 | 211 | 245 | 24.7 |
| 93 | 1.9 | 55700 | - | 253 | 27.0 |
| 123 | 2.4 | 92000 | - | 267 | 31.3 |
| 145 | 2.8 | 126000 | - | 279 | 34.1 |
| 166 | 2.9 | 154000 | - | 292 | 39.6 |
| 201 | 3.4 | 216000 | 212 | 313 | 43.9 |

TABLE I (continued)

NUCLEATE BOILING WATER DATA

| AMPS | VOLTS | HEAT FLUX $\frac{BTU}{(Hr)(Sq\ Ft)}$ | TEMPERATURES, °F | | |
|---|---|---|---|---|---|
| | | | Bulk | Tube | ΔT |
| Run: W-5 | | | | | |
| Pressure: | 169 psia | | | | |
| 31 | 0.4 | 4340 | 368 | 373 | 3.9 |
| 64 | 0.9 | 18500 | 368 | 384 | 11.4 |
| 103 | 1.5 | 48000 | 368 | 400 | 20.0 |
| 139 | 2.0 | 87400 | 370 | 424 | 34.2 |
| 176 | 2.5 | 140000 | 368 | 442 | 39.0 |
| 217 | 3.1 | 212000 | 369 | 469 | 48.0 |
| 237 | 3.4 | 253000 | 367 | 478 | 46.8 |
| 269 | 4.0 | 327000 | 367 | 497 | 47.3 |
| 288 | 4.1 | 374000 | 367 | 506 | 44.5 |
| 313 | 4.5 | 443000 | 368 | 528 | 49.3 |
| Run: W-6 | | | | | |
| Pressure: | 174 psia | | | | |
| 187 | 2.7 | 158000 | 369 | 440 | 30.6 |
| 308 | 4.4 | 429000 | 376 | 506 | 28.8 |
| 308 | 4.4 | 429000 | 372 | 509 | 31.8 |
| 62 | 0.9 | 17400 | 370 | 393 | 18.7 |

## TABLE II

## NUCLEATE BOILING POTASSIUM DATA

Run K-1
Tube 2 - Pool Depth $4\frac{1}{2}$ inches

April 2, 1963

| Pressure psia | Amps | Volts | Heat Flux Btu/(hr)(sq ft) | TEMPERATURES | | | | | | | | | | |
|---|---|---|---|---|---|---|---|---|---|---|---|---|---|---|
| | | | | Bulk | | Tube Top | | | Tube Side | | | Tube Bottom | | |
| | | | | EMF | °F | EMF | °F | ΔT, °F | EMF | °F | ΔT, °F | EMF | °F | ΔT, °F |
| 14.2 | 62 | 0.8 | 15 600 | 30.8 | 1364 | 31.1 | 1377 | 11.5 | 31.15 | 1379 | 14.0 | 31.15 | 1379 | 14.0 |
| | 87 | 1.2 | 32 900 | 30.8 | 1364 | 31.4 | 1389 | 21.8 | 31.35 | 1387 | 20.8 | 31.2 | 1381 | 15.0 |
| | 115 | 1.6 | 58 000 | 30.82 | 1365 | 31.55 | 1396 | 25.4 | 31.4 | 1389 | 20.1 | 31.3 | 1385 | 16.5 |
| | 150 | 2.0 | 94 500 | 30.9 | 1368 | 31.7 | 1402 | 24.8 | 31.55 | 1396 | 21.7 | 31.5 | 1394 | 20.3 |
| | 186 | 2.5 | 146 400 | 30.9 | 1368 | 31.98 | 1415 | 32.8 | 31.75 | 1405 | 27.3 | 31.7 | 1402 | 25.1 |
| | 219 | 2.9 | 200 000 | 30.85 | 1366 | 32.25 | 1426 | 40.6 | 31.9 | 1411 | 31.7 | 31.9 | 1411 | 32.9 |
| | 263 | 3.5 | 290 000 | 31.0 | 1372 | 32.5 | 1437 | 36.9 | 32.0 | 1415 | 23.7 | 31.95 | 1413 | 23.5 |
| | 303 | 4.0 | 382 000 | 31.05 | 1374 | 32.85 | 1453 | 41.0 | 32.2 | 1424 | 24.6 | 32.2 | 1424 | 26.9 |
| | 359 | 4.8 | 543 000 | 31.05 | 1374 | 33.3 | 1472 | 45.3 | 32.6 | 1442 | 31.9 | 32.4 | 1433 | 26.1 |
| | 0 | 0 | 0 | 31.0 | 1372 | 30.95 | 1370 | —— | 31.0 | 1372 | —— | 31.0 | 1372 | —— |

TABLE III

NUCLEATE BOILING POTASSIUM DATA

Run K-2
Tube 2 - Pool Depth $4\frac{1}{2}$ inches

April 2, 1963

| Pressure psia | Amps | Volts | Heat Flux Btu/(hr)(sq ft) | TEMPERATURES | | | | | | | | | | |
|---|---|---|---|---|---|---|---|---|---|---|---|---|---|---|
| | | | | Bulk | | Tube Top | | | Tube Side | | | Tube Bottom | | |
| | | | | EMF | °F | EMF | °F | ΔT,°F | EMF | °F | ΔT,°F | EMF | °F | ΔT,°F |
| 9.8 | 62 | 0.75 | 14 600 | 29.48 | 1307 | 29.50 | 1308 | — | 29.60 | 1312 | 4.0 | 29.4 | 1303 | — |
| | 113 | 1.4 | 49 800 | 29.48 | 1307 | 29.8 | 1321 | 9.2 | 29.80 | 1321 | 10.7 | 29.65 | 1314 | 4.0 |
| | 153 | 2.0 | 96 300 | 29.48 | 1307 | 30.07 | 1332 | 15.7 | 29.95 | 1327 | 13.6 | 29.8 | 1321 | 8.2 |
| | 197 | 2.6 | 162 000 | 29.48 | 1307 | 30.35 | 1344 | 21.3 | 30.15 | 1336 | 18.3 | 29.9 | 1325 | 8.2 |
| | 258 | 3.4 | 276 000 | 29.48 | 1307 | 30.75 | 1361 | 27.2 | 30.3 | 1342 | 16.6 | 30.1 | 1334 | 10.3 |
| | 288 | 3.8 | 345 000 | 29.48 | 1307 | 31.05 | 1374 | 33.6 | 30.4 | 1346 | 16.1 | 30.2 | 1338 | 10.1 |
| | 334 | 4.4 | 463 000 | 29.48 | 1307 | 31.45 | 1392 | 40.1 | 30.65 | 1357 | 19.2 | 30.35 | 1344 | 9.0 |

TABLE IV

NUCLEATE BOILING POTASSIUM DATA

Run K-3
Tube 2 - Pool Depth $4\frac{1}{2}$ inches

April 2, 1963

| Pressure psia | Amps | Volts | Heat Flux Btu/(hr)(sq ft) | TEMPERATURES | | | | | | | | | | |
|---|---|---|---|---|---|---|---|---|---|---|---|---|---|---|
| | | | | Bulk | | Tube Top | | | Tube Side | | | Tube Bottom | | |
| | | | | EMF | °F | EMF | °F | ΔT, °F | EMF | °F | ΔT, °F | EMF | °F | ΔT, °F |
| 0.7 | 0 | 0 | 0 | 20.85 | 941 | 20.85 | 941 | — | 20.85 | 941 | — | 20.90 | 943 | — |
| | 64 | 0.8 | 16 100 | 20.80 | 939 | 21.0 | 947 | 6.4 | 20.95 | 945 | 4.9 | 20.95 | 945 | 5.0 |
| | 96 | 1.2 | 36 200 | 20.80 | 939 | 21.2 | 955 | 12.5 | 21.1 | 951 | 9.6 | 21.05 | 949 | 7.8 |
| | 142 | 1.8 | 80 300 | 20.80 | 939 | 21.6 | 972 | 25.2 | 21.35 | 962 | 17.7 | 21.18 | 955 | 11.1 |
| | 174 | 2.2 | 121 000 | 20.85 | 941 | 21.87 | 984 | 31.3 | 21.45 | 966 | 17.0 | 21.25 | 958 | 9.7 |
| | 197 | 2.4 | 149 000 | 20.85 | 941 | 22.15 | 996 | 40.6 | 21.60 | 972 | 21.1 | 21.3 | 960 | 10.0 |
| 0.6 | 229 | 2.8 | 202 000 | 20.95 | 945 | 22.45 | 1008 | 43.4 | 21.8 | 981 | 22.6 | 21.5 | 970 | 12.8 |
| | 0 | 0 | 0 | 20.85 | 941 | 20.85 | 941 | — | 20.85 | 941 | — | 20.85 | 941 | — |

TABLE V

NUCLEATE BOILING POTASSIUM DATA

Run K-4
Tube 2 - Pool Depth $4\frac{1}{2}$ inches

April 7, 1963

| Pressure psia | Amps | Volts | Heat Flux Btu/(hr)(sq ft) | TEMPERATURES | | | | | | | | | | |
|---|---|---|---|---|---|---|---|---|---|---|---|---|---|---|
| | | | | Bulk | | Tube Top | | | Tube Side | | | Tube Bottom | | |
| | | | | EMF | °F | EMF | °F | ΔT, °F | EMF | °F | ΔT, °F | EMF | °F | ΔT, °F |
| 12.5 | 41 | 0.5 | 6 450 | 30.75 | 1361 | 30.9 | 1368 | 4.4 | 30.9 | 1368 | 4.6 | 30.95 | 1370 | 6.6 |
| | 72 | 1.0 | 22 700 | 30.75 | 1361 | 31.1 | 1377 | 11.8 | 31.1 | 1377 | 12.5 | 31.05 | 1374 | 9.6 |
| | 93 | 1.2 | 35 100 | 30.75 | 1361 | 31.2 | 1381 | 14.6 | 31.2 | 1381 | 15.7 | 31.1 | 1377 | 11.9 |
| | 113 | 1.5 | 53 500 | 30.83 | 1365 | 31.3 | 1385 | 14.8 | 31.3 | 1385 | 16.4 | 31.2 | 1381 | 12.8 |
| | 143 | 1.9 | 85 600 | 30.85 | 1366 | 31.5 | 1394 | 19.7 | 31.4 | 1389 | 17.3 | 31.35 | 1387 | 15.8 |
| | 165 | 2.2 | 114 000 | 30.85 | 1366 | 31.7 | 1402 | 24.9 | 31.5 | 1394 | 20.4 | 31.5 | 1394 | 21.1 |
| | 196 | 2.6 | 161 000 | 30.95 | 1370 | 31.9 | 1411 | 25.4 | 31.65 | 1400 | 19.3 | 31.6 | 1398 | 18.3 |
| | 217 | 2.9 | 198 000 | 31.05 | 1374 | 32.0 | 1415 | 21.8 | 31.75 | 1404 | 16.8 | 31.65 | 1400 | 14.0 |
| | 247 | 3.3 | 257 000 | 31.10 | 1377 | 32.3 | 1429 | 27.1 | 31.95 | 1413 | 18.9 | 31.8 | 1407 | 14.5 |
| | 260 | 3.6 | 294 000 | 31.19 | 1380 | 32.5 | 1437 | 28.4 | 32.1 | 1420 | 20.4 | 32.0 | 1415 | 17.2 |
| | 283 | 3.8 | 338 000 | 31.35 | 1387 | 32.65 | 1444 | 23.7 | 32.25 | 1426 | 16.5 | 32.1 | 1420 | 12.5 |
| | 307 | 4.05 | 391 000 | 31.45 | 1392 | 32.85 | 1452 | 23.1 | 32.45 | 1435 | 17.5 | 32.3 | 1429 | 13.8 |
| 14.0 | 339 | 4.5 | 482 000 | 31.55 | 1396 | 33.1 | 1464 | 21.3 | 32.65 | 1444 | 15.5 | 32.5 | 1437 | 11.9 |
| | 0 | 0 | 0 | 31.2 | 1381 | 31.2 | 1381 | —— | 31.2 | 1381 | —— | 31.2 | 1381 | —— |

TABLE VI

NUCLEATE BOILING POTASSIUM DATA

Run K-5
Tube 3 - Pool Depth 6 inches

April 20, 1963

| Pressure psia | Amps | Volts | Heat Flux Btu/(hr)(sq ft) | TEMPERATURES | | | | | | | | | | |
|---|---|---|---|---|---|---|---|---|---|---|---|---|---|---|
| | | | | Bulk | | Tube Top | | | Tube Side | | | Tube Bottom | | |
| | | | | EMF | °F | EMF | °F | ΔT,°F | EMF | °F | ΔT,°F | EMF | °F | ΔT,°F |
| 13.7 | 0 | 0 | 0 | 31.0 | 1372 | 31.0 | 1372 | | 31.0 | 1372 | | 31.0 | 1372 | |
| | 103 | 1.4 | 45 400 | 31.0 | 1372 | 31.2 | 1381 | 5.4 | 31.2 | 1381 | 6.3 | 31.4 | 1389 | 12.6 |
| | 145 | 2.0 | 91 300 | 31.05 | 1374 | 31.25 | 1383 | 1.8 | 31.25 | 1383 | 3.5 | 31.6 | 1398 | 15.1 |
| | 196 | 2.65 | 164 000 | 31.0 | 1372 | 31.45 | 1392 | 7.1 | 31.4 | 1389 | 7.1 | 31.9 | 1411 | 23.1 |
| | 227 | 3.01 | 215 000 | 31.0 | 1372 | 31.6 | 1398 | 9.0 | 31.5 | 1394 | 9.0 | 32.17 | 1423 | 30.1 |
| | 270 | 3.7 | 315 000 | 31.0 | 1372 | 31.7 | 1402 | 5.2 | 31.7 | 1403 | 12.0 | 32.55 | 1439 | 36.5 |
| | 309 | 4.2 | 409 000 | 31.02 | 1373 | 32.15 | 1422 | 16.7 | 31.85 | 1409 | 11.2 | 32.9 | 1455 | 42.3 |
| | 0 | 0 | 0 | 31.0 | 1372 | 31.0 | 1372 | — | 31.05 | 1374 | — | 31.0 | 1372 | — |

TABLE VII

NUCLEATE BOILING POTASSIUM DATA

Run K-6
Tube 3 - Pool Depth 6 inches

April 20, 1963

| Pressure psia | Amps | Volts | Heat Flux Btu/(hr)(sq ft) | TEMPERATURES | | | | | | | | | | |
|---|---|---|---|---|---|---|---|---|---|---|---|---|---|---|
| | | | | Bulk | | Tube Top | | | Tube Side | | | Tube Bottom | | |
| | | | | EMF | °F | EMF | °F | ΔT,°F | EMF | °F | ΔT,°F | EMF | °F | ΔT,°F |
| 6.06 | 0 | 0 | 0 | 27.65 | 1229 | 27.65 | 1229 | — | 27.65 | 1229 | — | 27.65 | 1229 | — |
| | 40 | 0.45 | 5 670 | 27.7 | 1231 | 27.70 | 1231 | — | 27.75 | 1233 | 1.7 | 27.75 | 1233 | 1.5 |
| | 103 | 1.40 | 45 400 | 27.75 | 1233 | 27.90 | 1239 | 2.4 | 27.90 | 1239 | 3.3 | 28.05 | 1246 | 8.6 |
| 6.05 | 156 | 2.05 | 101 000 | 27.6 | 1226 | 28.03 | 1245 | 11.1 | 27.85 | 1237 | 4.9 | 28.20 | 1252 | 16.2 |
| | 198 | 2.6 | 162 000 | 27.7 | 1231 | 28.15 | 1250 | 6.2 | 28.05 | 1246 | 5.2 | 28.55 | 1267 | 20.3 |
| | 248 | 3.3 | 258 000 | 27.7 | 1231 | 28.50 | 1265 | 13.7 | 28.25 | 1254 | 7.4 | 28.95 | 1284 | 28.0 |
| | 290 | 3.9 | 356 000 | 27.7 | 1231 | 28.75 | 1276 | 16.9 | 28.45 | 1263 | 10.5 | 29.45 | 1306 | 40.5 |
| | 0 | . 0 | 0 | 27.65 | 1229 | 27.80 | 1235 | — | 27.70 | 1231 | — | 27.70 | 1231 | — |

TABLE VIII

NUCLEATE BOILING POTASSIUM DATA

Run K-7
Tube 3 - Pool Depth 6 inches

April 20, 1963

| Pressure psia | Amps | Volts | Heat Flux Btu/(hr)(sq ft) | TEMPERATURES | | | | | | | | | | |
|---|---|---|---|---|---|---|---|---|---|---|---|---|---|---|
| | | | | Bulk | | Tube Top | | | Tube Side | | | Tube Bottom | | |
| | | | | EMF | °F | EMF | °F | ΔT, °F | EMF | °F | ΔT, °F | EMF | °F | ΔT, °F |
| 0.9 | 0 | 0 | 0 | 21.65 | 975 | 21.65 | 975 | — | 21.75 | 978 | — | 21.80 | 981 | — |
| | 36 | 0.4 | 4 530 | 21.6 | 972 | 21.65 | 975 | 2.6 | 21.75 | 978 | 5.7 | 21.80 | 981 | 8.6 |
| | 103 | 1.4 | 45 300 | 21.6 | 972 | 21.75 | 979 | 3.4 | 21.85 | 983 | 8.3 | 22.07 | 992 | 15.6 |
| | 147 | 1.9 | 87 800 | 21.55 | 970 | 21.90 | 985 | 8.1 | 21.95 | 987 | 11.7 | 22.35 | 1004 | 25.5 |
| | 169 | 2.2 | 117 000 | 21.4 | 964 | 21.90 | 985 | 11.8 | 21.90 | 985 | 13.9 | 22.45 | 1008 | 32.6 |
| | 198 | 2.6 | 162 000 | 21.4 | 964 | 21.95 | 987 | 10.2 | 21.92 | 986 | 12.2 | 22.6 | 1015 | 35.3 |
| | 232 | 3.0 | 219 000 | 21.4 | 964 | 22.05 | 991 | 9.7 | 22.0 | 989 | 11.7 | 22.85 | 1025 | 39.7 |
| | 0 | 0 | 0 | 21.35 | 962 | 21.35 | 962 | — | 21.35 | 962 | — | 21.40 | 964 | — |

TABLE IX

NUCLEATE BOILING POTASSIUM DATA

Run K-8
Tube 3 - Pool Depth 6 inches

April 20, 1963

| Pressure psia | Amps | Volts | Heat Flux Btu/(hr)(sq ft) | Depth In. | TEMPERATURES | | | | | | | | | | |
|---|---|---|---|---|---|---|---|---|---|---|---|---|---|---|---|
| | | | | | Bulk | | Tube Top | | | Tube Side | | | Tube Bottom | | |
| | | | | | EMF | °F | EMF | °F | ΔT, °F | EMF | °F | ΔT, °F | EMF | °F | ΔT, °F |
| 13 | 0 | 0 | 0 | 6 | 30.9 | 1368 | 30.85 | 1366 | | 30.8 | 1364 | | 30.7 | 1359 | |
| | | | | 5 | 30.9 | 1368 | 31.0 | 1372 | | 31.0 | 1372 | | 30.9 | 1368 | |
| | | | | 4 | 30.9 | 1368 | 31.0 | 1372 | | 31.0 | 1372 | | 30.9 | 1368 | |
| | | | | 3 | 30.9 | 1368 | 31.0 | 1372 | | 31.0 | 1372 | | 30.9 | 1368 | |
| | | | | 2 | 31.0 | 1372 | 31.0 | 1372 | | 31.0 | 1372 | | 30.9 | 1368 | |
| | | | | 1 | 30.9 | 1368 | 31.0 | 1372 | | 31.0 | 1372 | | 30.9 | 1368 | |
| | | | | 0 | 30.5 | 1351 | 31.0 | 1372 | | 31.0 | 1372 | | 30.9 | 1368 | |
| | 51 | 0.6 | 9 630 | 6 | 30.8 | 1364 | 30.95 | 1370 | 5.2 | 30.9 | 1368 | 3.4 | 30.9 | 1368 | 3.1 |
| | | | | 5 | 30.85 | 1366 | 30.85 | 1366 | | 30.9 | 1368 | | 30.9 | 1368 | |
| | | | | 4 | 30.95 | 1370 | 30.85 | 1366 | | 30.9 | 1368 | | 30.9 | 1368 | |
| | | | | 3 | 31.0 | 1372 | 30.85 | 1366 | | 30.8 | 1364 | | 30.8 | 1364 | |
| | | | | 2 | 31.05 | 1374 | 30.85 | 1366 | | 30.8 | 1364 | | 30.8 | 1364 | |
| | | | | 1 | 30.85 | 1366 | 30.85 | 1366 | | 30.9 | 1368 | | 30.9 | 1368 | |
| | | | | 0 | 30.5 | 1351 | 30.85 | 1366 | | 30.9 | 1368 | | 31.0 | 1372 | |

TABLE IX (continued)

NUCLEATE BOILING POTASSIUM DATA

Run K-8

April 20, 1963

| Pressure psia | Amps | Volts | Heat Flux Btu/(hr)(sq ft) | Depth In. | TEMPERATURES | | | | | | | | | | |
|---|---|---|---|---|---|---|---|---|---|---|---|---|---|---|---|
| | | | | | Bulk | | Tube Top | | | Tube Side | | | Tube Botton | | |
| | | | | | EMF | °F | EMF | °F | ΔT, °F | EMF | °F | ΔT, °F | EMF | °F | ΔT, °F |
| | 137 | 1.75 | 75 600 | 6 | 30.9 | 1368 | 31.35 | 1387 | 13.0 | 31.3 | 1385 | 12.4 | 31.6 | 1398 | 22.7 |
| | | | | 5 | 30.8 | 1364 | 31.35 | 1387 | | 31.3 | 1385 | | 31.6 | 1398 | |
| | | | | 4 | 31.0 | 1372 | 31.35 | 1387 | | 31.3 | 1385 | | 31.6 | 1398 | |
| | | | | 3 | 31.1 | 1377 | 31.30 | 1385 | | 31.2 | 1381 | | 31.6 | 1398 | |
| | | | | 2 | 31.2 | 1381 | 31.30 | 1385 | | 31.2 | 1381 | | 31.6 | 1398 | |
| | | | | 1 | 30.6 | 1355 | 31.30 | 1385 | | 31.2 | 1381 | | 31.6 | 1398 | |
| | | | | 0 | 30.8 | 1364 | 31.30 | 1385 | | 31.2 | 1381 | | 31.6 | 1398 | |
| | 237 | 3.05 | 228 000 | 6 | 30.9 | 1368 | 31.70 | 1402 | 16.0 | 31.5 | 1394 | 12.2 | 32.3 | 1428 | 37.9 |
| | | | | 5 | 31.0 | 1372 | 31.70 | 1402 | | 31.5 | 1394 | | 32.3 | 1428 | |
| | | | | 4 | 31.15 | 1379 | 31.70 | 1402 | | 31.5 | 1394 | | 32.3 | 1428 | |
| | | | | 3 | 31.25 | 1383 | 31.70 | 1402 | | 31.5 | 1394 | | 32.2 | 1424 | |
| | | | | 2 | 31.25 | 1383 | 31.70 | 1402 | | 31.5 | 1394 | | 32.2 | 1424 | |
| | | | | 1 | 31.0 | 1372 | 31.70 | 1402 | | 31.5 | 1394 | | 32.2 | 1424 | |
| | | | | 0 | 30.75 | 1362 | 31.70 | 1402 | | 31.5 | 1394 | | 32.2 | 1424 | |

TABLE IX (continued)

NUCLEATE BOILING POTASSIUM DATA

Run K-8

April 20, 1963

| Pressure psia | Amps | Volts | Heat Flux Btu/(hr)(sq ft) | Depth In. | TEMPERATURES | | | | | | | | | | | |
|---|---|---|---|---|---|---|---|---|---|---|---|---|---|---|---|---|
| | | | | | Bulk | | Tube Top | | | Tube Side | | | Tube Bottom | | | |
| | | | | | EMF | °F | EMF | °F | ΔT, °F | EMF | °F | ΔT, °F | EMF | °F | ΔT, °F |
| | 328 | 4.2 | 434 000 | 6 | 31.1 | 1377 | 32.3 | 1428 | 16.8 | 31.87 | 1410 | 6.8 | 33.2 | 1468 | 48.9 |
| | | | | 5 | 31.1 | 1377 | 32.3 | 1428 | | 31.87 | 1410 | | 33.2 | 1468 | |
| | | | | 4 | 31.25 | 1383 | 32.3 | 1428 | | 31.87 | 1410 | | 33.2 | 1468 | |
| | | | | 3 | 31.40 | 1389 | 32.3 | 1428 | | 31.87 | 1410 | | 33.2 | 1468 | |
| | | | | 2 | 31.35 | 1387 | 32.3 | 1428 | | 31.87 | 1410 | | 33.2 | 1468 | |
| | | | | 1 | 31.25 | 1383 | 32.3 | 1428 | | 31.87 | 1410 | | 33.2 | 1468 | |
| | | | | 0 | 31.05 | 1374 | 32.3 | 1428 | | 31.87 | 1410 | | 33.2 | 1468 | |

TABLE X

NUCLEATE BOILING POTASSIUM DATA

Run K-9
Tube 3 - Pool Depth 6 inches

April 20, 1963

| Pressure psia | Amps | Volts | Heat Flux Btu/(hr)(sq ft) | TEMPERATURES | | | | | | | | | | |
|---|---|---|---|---|---|---|---|---|---|---|---|---|---|---|
| | | | | Bulk | | Tube Top | | | Tube Side | | | Tube Bottom | | |
| | | | | EMF | °F | EMF | °F | ΔT, °F | EMF | °F | ΔT, °F | EMF | °F | ΔT, °F |
| 37 | 72 | 0.9 | 20 400 | 36.0 | 1592 | 36.0 | 1591 | — | 36.2 | 1601 | 7.8 | 36.25 | 1603 | 8.0 |
| | 113 | 1.4 | 49 800 | 36.53 | 1615 | 36.7 | 1623 | 4.1 | 36.95 | 1634 | 16.0 | 37.1 | 1641 | 21.2 |
| | 155 | 2.0 | 97 600 | 36.63 | 1619 | 36.95 | 1634 | 7.3 | 37.1 | 1641 | 16.1 | 37.4 | 1654 | 25.5 |
| | 207 | 2.6 | 169 000 | 36.78 | 1626 | 37.30 | 1650 | 10.7 | 37.3 | 1650 | 13.8 | 37.8 | 1672 | 29.6 |
| | 258 | 3.3 | 268 000 | 36.88 | 1631 | 37.60 | 1663 | 10.9 | 37.7 | 1667 | 19.8 | 38.5 | 1703 | 46.0 |
| 45 | 308 | 4.0 | 387 000 | 37.08 | 1639 | 37.85 | 1674 | 5.5 | 37.9 | 1676 | 13.6 | 38.9 | 1722 | 45.4 |

TABLE XI

NUCLEATE BOILING POTASSIUM DATA

Run K-10
Tube 4 - Pool Depth $6\frac{1}{2}$ inches

July 11, 1963

| Pressure psia | Amps | Volts | Heat Flux Btu/(hr)(sq ft) | TEMPERATURES | | | | | | | | | | |
|---|---|---|---|---|---|---|---|---|---|---|---|---|---|---|
| | | | | Bulk | | Tube Top | | | Tube Side | | | Tube Bottom | | |
| | | | | EMF | °F | EMF | °F | ΔT,°F | EMF | °F | ΔT,°F | EMF | °F | ΔT,°F |
| 3.8 | 0 | 0 | 0 | 26.1 | 1163 | 26.1 | 1163 | — | 26.1 | 1163 | — | 26.1 | 1163 | — |
| | 81 | 1.1 | 28 000 | 26.0 | 1158 | 26.45 | 1177 | 16.3 | 26.4 | 1175 | 14.6 | 26.35 | 1173 | 13.3 |
| | 160 | 2.2 | 111 000 | 26.3 | 1171 | 27.05 | 1203 | 21.3 | 26.9 | 1197 | 10.6 | 26.95 | 1199 | 15.3 |
| | 212 | 2.8 | 187 000 | 26.65 | 1186 | 27.7 | 1231 | 26.9 | 27.4 | 1218 | 16.1 | 27.4 | 1218 | 20.7 |
| | 247 | 3.3 | 257 000 | 26.9 | 1197 | 28.1 | 1248 | 26.1 | 27.75 | 1233 | 14.2 | 27.7 | 1231 | 18.5 |
| | 278 | 3.8 | 333 000 | 27.05 | 1203 | 28.5 | 1265 | 29.7 | 28.1 | 1248 | 16.7 | 27.95 | 1241 | 17.8 |
| | 202 | 2.7 | 172 000 | 27.15 | 1207 | 28.0 | 1244 | 20.4 | 27.7 | 1231 | 9.4 | 27.65 | 1229 | 11.6 |
| | 155 | 2.1 | 103 000 | 27.1 | 1205 | 27.95 | 1241 | 26.0 | 27.55 | 1224 | 10.3 | 27.6 | 1226 | 14.8 |
| 5.0 | 115 | 1.6 | 57 900 | 27.05 | 1203 | 27.75 | 1233 | 24.4 | 27.5 | 1222 | 14.1 | 27.55 | 1220 | 13.5 |
| | 72 | 1.0 | 22 700 | 26.95 | 1199 | 27.6 | 1226 | 24.8 | 27.35 | 1216 | 15.1 | 27.4 | 1218 | 17.6 |

TABLE XII

SUMMARY OF POTASSIUM BURNOUT MEASUREMENTS

| TUBE | METHOD OF DETER-MINATION[1] | PRESSURE PSIA | AMP | VOLTS | HEAT FLUX $\frac{BTU}{(Hr)(Sq\ Ft)}$ |
|---|---|---|---|---|---|
| 1 | DP | 0.164 | 258 | 3.5 | 285,000 |
| | DP | 0.152 | 258 | 3.5 | 285,000 |
| | CP | 15.0 | 395 | 5.3 | 660,000[2] |
| 2 | DP | 3.72 | 323 | 4.75 | 484,000 |
| | DP | 1.0 | 308 | 4.0 | 388,000 |
| | DP | 3.94 | 348 | 4.7 | 515,000 |
| | DP | 11.35 | 369 | 5.0 | 580,000 |
| 3 | DP | 14.6 | 359 | 4.85 | 550,000 |
| | DP | 0.715 | 307 | 4.2 | 407,000 |
| | DP | 1.42 | 330 | 4.5 | 468,000 |
| | CP | 22.2 | 400 | 5.3 | 669,000 |
| | CP | 13.9 | 379 | 5.0 | 598,000 |
| 4 | CP | 1.24 | 312 | 4.2 | 413,000 |
| | CP | 1.80 | 307 | 4.2 | 405,000 |
| | CP | 0.50 | 288 | 4.0 | 363,000 |
| | CP | 0.70 | 278 | 3.7 | 324,000 |
| | CP | 3.5 | 342 | 4.65 | 500,000 |
| | CP | 7.4 | 364 | 5.0 | 573,000[3] |

[1]DP = Decreasing pressure at constant heat flux
CP = Increasing heat flux at constant pressure

[2]Destructive burnout, tube shown in Figure 26

[3]Destructive burnout, tube shown in Figure 27

## APPENDIX B

## TREATMENT OF NUCLEATE BOILING DATA

In order to save a great deal of work in processing data, a computer program was written for the IBM 7090 digital computer at The University of Michigan Computing Center. For a particular boiling tube power setting, the program calculated the boiling tube heat flux, q/A, and temperature difference, $\Delta T$, between the boiling surface and liquid saturation (or free-surface) temperature. A separate curve was determined for each of the three boiling tube thermocouples. In addition, the data was correlated using a least-square subroutine to determine the best straight line log-log relationship for each run. However, curvature of the boiling curves at low fluxes (probably due to the influence of convection boiling) prevented a representative correlation. Thus, the least-square correlations were later discarded and are not present herein.

The boiling heat flux was determined by dividing the known tube surface area into the total power input to the tube, less any predetermined losses. The expression is:

$$q/A = \frac{cIV}{A}$$

where I and V are the DC current and DC voltage drop, respectively, across the graphite heating element, A the boiling tube OD area in sq. ft., and c the factor to convert watts to Btu/hr. The voltage drop across the heater element was determined from a measurement of the total voltage drop across the boiling tube assembly, less the lead losses. See Appendix E for a discussion of these losses.

Boiling surface temperatures were determined by averaging thermocouple readings in the tube wall and extrapolating to the surface. The boiling $\Delta T$ was calculated from the following:

$$\Delta T = \Delta Tc - q/A \left( \frac{\Delta x}{k} \right)$$

where $\Delta Tc$ represents the total temperature difference between the thermocouple and bulk temperatures, q/A the heat flux, $\Delta x$ the depth of the thermocouple junction in the tube surface, and k the effective thermal conductivity of the boiling tube material.

The value for $\Delta Tc$ was determined from thermocouple measurements while $\Delta x$ was determined by sectioning the boiling tube and visually measuring the depth to the center of the thermocouple junction. This was accomplished to an accuracy of $\pm$ 0.0005-in using a measuring microscope. The existence of a considerable mass of Nicrobraze surrounding each thermocouple and possessing a markedly different thermal conductivity than Haynes-25, made it very difficult to determine the effective value for the tube wall thermal conductivity in the vicinity of the thermocouple junctions. Reference (50) lists the thermal conductivity of Haynes-25 at a value of 120 Btu/(hr)(sq ft)(°F/in) at 800°F to 165 Btu/(hr)(sq ft)(°F/in) at 1400°F whereas the only available source (36) for Nicrobraze

AMS 4777 gives a value k = 377 Btu/(hr)(sq ft)(°F/in), assumed at ambient temperature.

For $\Delta x$ = 0.016-in, the numerical value of $\Delta x/k$ at 1400°F was bounded in the limits (0.0000428 using $k_{Nicrobraze}$) $< \Delta x/k <$ (0.000097 using $k_{Haynes-25}$), assuming $k_{Nicrobraze}$ was constant with temperature. This represents a $\Delta T$ variation at 500,000 Btu/(hr)(sq ft) of approximately 25°F.

In using k for Haynes-25 it was found in nearly all runs that at high fluxes the $\Delta T$ values decreased markedly with each incremental increase in flux. Since this was not believed to be possible, it indicated that the mass of the braze was indeed significant and served to distort the isotherms in the tube wall near each brazed thermocouple groove. The value for the effective k near a thermocouple groove should have been, as a minimum, that value in which $\Delta T$ remained constant with increasing flux. Calculations showed that this minimum k was between the Haynes-25 and the Nicrobraze values and gave on the average $\Delta T$ values about 15°F higher at a flux of 500,000 Btu/(hr)(sq ft) using the k for Haynes-25 alone.

Considering a boiling tube heat flux of 500,000 Btu/(hr)(sq ft), the two dimensional relaxation method for heat conduction was used to determine isotherms in the tube wall at the location of a braze filled thermocouple groove. From these calculations the temperature at the center of the brazed groove was about 10°F less than a similar wall location in the Haynes-25. Recall from above that this value was still 5°F less than required to yield non-decreasing $\Delta T$ values with increases in heat flux. The conclusion therefore was that the best value for the effective k should be that value (for a particular tube thermocouple) which gave a boiling curve with no reversal in slope.

# APPENDIX C

## ESTIMATION OF HEAT FLUX AND THE TEMPERATURE PROFILE IN THE BOILING TUBE

It might be expected that end effects in the boiling tube were significant inasmuch as the L/D ratio for the graphite heating element was only 5.45. Calculation of these effects was carried out by formulation of the differential equation for heat transfer from a cylinder with internal generation. Several simplifying assumptions were employed to permit an analytical solution. Also, adverse boundary conditions were specified in order to obtain an estimate of the maximum heat losses. The losses at the ends were considered to be approximately equal and therefore the longitudinal temperature profile was considered to be symmetrical about the midpoint of the tube. The analysis applied only to half of the tube, for which $x = 0$ to $x = \ell/2$, where $x = 0$ corresponds to the midpoint and $\ell$ the total length of the tube extending into the potassium pool.

The general one-dimensional problem is given in Carslaw and Jaeger (20). For specific boundary conditions, Lyon (79) solved the problem and determined errors in calculating the radial heat flux near the center of a Globar heating element. The present problem assumes no radial temperature gradients in the graphite (one-dimensional) and that all physical properties are constant with temperature.

The differential equation is:

$$\frac{d^2T}{dx^2} - \frac{4UT}{k_g D} = \frac{-cI^2R}{k_g V} \qquad \text{(C-1)}$$

where T = (temperature in the graphite) - (temperature of boiling potassium)

x = length dimension, $0 < x < \ell/2$

$k_g$ = thermal conductivity of graphite

U = overall heat transfer coefficient between graphite and boiling potassium

I = current

R = resistance of graphite

V = 1/2 volume of graphite

c = conversion factor from watts to Btu/hr

D = diameter of graphite heater

This equation includes a term for the radial surface heat transfer, and was formulated using an overall coefficient, U, which includes all interfacial and material resistances. The BN, Haynes-25, and interfacial resistances are contributors.

The boundary conditions for the graphite rod heater are:

$$\frac{dT}{dx} = 0 \qquad x = 0 \text{ (center of tube)} \qquad \text{C-2}$$

$$\frac{dT}{dx} = \frac{-k_{H-25}T}{k_g t} \qquad x = \ell/2 \text{ (free end of tube)} \qquad \text{C-3}$$

where $k_{H-25}$ = thermal conductivity of Haynes-25

$\ell$ = total length of graphite

t = thickness of Haynes-25 tube end.

The first boundary condition assumes equal heat transfer out each end of the graphite heater while the second condition is a heat balance at the interface between the graphite heater and the end of the Haynes-25 bayonet tube. This latter condition assumes infinite contact conductance between the graphite heater and Haynes-25 disk.

It should be pointed out that although symmetry was assumed in the rod, i.e., no heat transfer across the plane x = 0, the end of the rod which contacted molybdenum ($x = -\ell/2$) possessed a considerably different condition. However, since $I^2R$ dissipation in the molybdenum tended to reduce the magnitude of the graphite end losses, it was felt the largest loss occurred at the free end of the tube. Also, the $I^2R$ dissipation in the Haynes disk was neglected so that the actual loss would be somewhat less than that predicted here. Applying the two boundary conditions gives the following particular solution:

$$T = \frac{B/A^2}{\frac{k_g tA}{k_{H-25}} \sinh \frac{A\ell}{2} - \cosh \frac{A\ell}{2}} \cosh \frac{A\ell}{2} + \frac{B}{A^2} \qquad \text{C-4}$$

in the region $0 < x < \ell/2$ and where $A^2 = 4U/k_g D$ and $B = cI^2R/k_g V$.

This expression represents the temperature along the graphite heater and can be used to determine the heat loss out either end or the radial heat flux at any point along the boiling tube.

Using the following values: thermal conductivity of the graphite, $k_g$ = 20 Btu/(hr)(sq ft)(°F/ft), the thermal conductivity of Haynes-25, $k_{H-25}$ = 20 Btu/(hr)(sq ft)(°F/ft), the diameter of the graphite heater, D = 0.23-in, and the total length of the graphite heater, $\ell$ = 1.25-in, gives:

$$T = \frac{545 \frac{I^2R}{U} \cosh\left(\sqrt{10.4U}\, x\right)}{t\sqrt{10.4U} \sinh\left(\frac{\sqrt{10.4U}\ 1.25}{24}\right) - \cosh\left(\frac{\sqrt{10.4U}\ 1.25}{24}\right)} - \frac{545I^2R}{U} \qquad \text{C-5}$$

for $0 < x < 1.25/24$-ft.

To obtain the most adverse value for heat loss, the first term on the right hand side should be a maximum. This is accomplished by setting the thickness of the Haynes-25 end to zero or t = 0, then:

$$T = \frac{545I^2R}{U} - \frac{545\frac{I^2R}{U}\cosh(\sqrt{10.4U}\,x)}{\cosh\left(\frac{\sqrt{10.4U}\,1.25}{24}\right)} \qquad \text{C-6}$$

and

$$UT = 545I^2R - \frac{545I^2R}{\cosh\left(\frac{\sqrt{10.4U}\,1.25}{24}\right)}\cosh(\sqrt{10.4U}\,x) \qquad \text{C-7}$$

This expression is equivalent to:

$$\begin{pmatrix}\text{radial heat transfer}\\ \text{from boiling surface}\end{pmatrix} = \begin{pmatrix}\text{total heat}\\ \text{input}\end{pmatrix} - \text{(end loss)} \qquad \text{C-8}$$

The heat flux error at the center of the tube, where the thermocouples are embedded, is given by the following expression:

$$\text{Percent Error} = \left(\frac{\frac{545I^2R\cosh(\sqrt{10.4U}\,x)}{\cosh\left(\frac{\sqrt{10.4U}\,1.25}{24}\right)}100}{545I^2R}\right) \qquad \text{C-9}$$

Choosing the total heat transfer coefficients for the graphite-boron nitride contact and boron nitride-Haynes-25 contact (129), h(contacts) = 2000 Btu/(hr)(sq ft), the boiling heat transfer coefficient, h(boiling) = 10,000 Btu/(hr)(sq ft) and finally the thermal conductivity of the boron nitride sleeve (43), k(BN) = 15 Btu/(hr)(sq ft)(°F/ft), the overall heat transfer coefficient is calculated to be $U \cong 750$ Btu/(hr)(sq ft), and the heat flux error at the center of the tube is then:

$$\text{Percent Error} = \left(\frac{100}{\cosh\left(\frac{\sqrt{10.4(750)}\,1.25}{24}\right)}\right)_{x=0} = 2\% \qquad \text{C-10}$$

The average heat flux over the middle half of the boiling tube is determined from the following equation:

$$q/A)ave = \frac{\int_0^{\ell/4}(q/A)_x\,dx}{\ell/4 - 0} \qquad \text{C-11}$$

The value for the heat flux is given by Equation C-7, thus:

$$q/A)ave = \frac{\int_0^{\frac{1.25}{4(12)}} \left( 545I^2R - 545I^2R \frac{\cosh(\sqrt{10.4U}\, x)}{\cosh\left(\frac{\sqrt{10.4U}\ 1.25}{4}\right)} \right) dx}{1.25/4(12)} \qquad C\text{-}12$$

for U = 750

$$\begin{aligned} q/A)ave &= 545I^2R(1-0.0432) \\ &= 545I^2R(0.956) \end{aligned} \qquad C\text{-}13$$

Since the term $545I^2R$ represents the theoretical radial heat flux from the graphite rod, the average flux over the middle half of the tube is then 95.6% of this theoretical value.

In order to check these heat loss calculations against actual conditions, tube 4 was fabricated with the three thermocouples placed at different locations along the tube length. One thermocouple was located directly in the middle of the tube length while the other two were placed 1/4-in from each end. With this arrangement longitudinal temperature gradients were not detected up to fluxes over 300,000 Btu/(hr)(sq ft). This demonstrated that the heat flux was essentially uniform along the middle 60% of the tube and substantiated the calculations above.

In addition, the tube 4 assembly had a hole, 1/16-in diameter by approximately 1/4-in deep, drilled into the Swagelok fitting. The hole was fitted with a thermocouple such that the junction was approximately 1/2-in away from the end of the graphite heater contacting the molybdenum rod. The main guard heater surrounding the vessel shorted out during the heat-up cycle using this tube, so that the temperatures recorded by this thermocouple were actually much lower than would be normally expected and indicated heat losses from the tube, while operating without the use of the main guard heater. Even under this most adverse condition, the heat losses out the end of the tube contacting the molybdenum were as low as 0.13% at 333,000 Btu/(hr)(sq ft) to a high of 7.4% at 22,600 Btu/(hr)(sq ft). The lower value at the high flux was, at least in part, due to an increase in heat generation in the molybdenum.

The temperature profiles in the graphite were calculated using Equation C-6 at heat fluxes, based on the boiling tube OD, of $1x10^6$, $5x10^5$, and $1x10^5$ Btu/(hr)(sq ft). These are shown in Figure 35. The heat flux at any point along the graphite rod is determined by simply multiplying the temperature by 750.

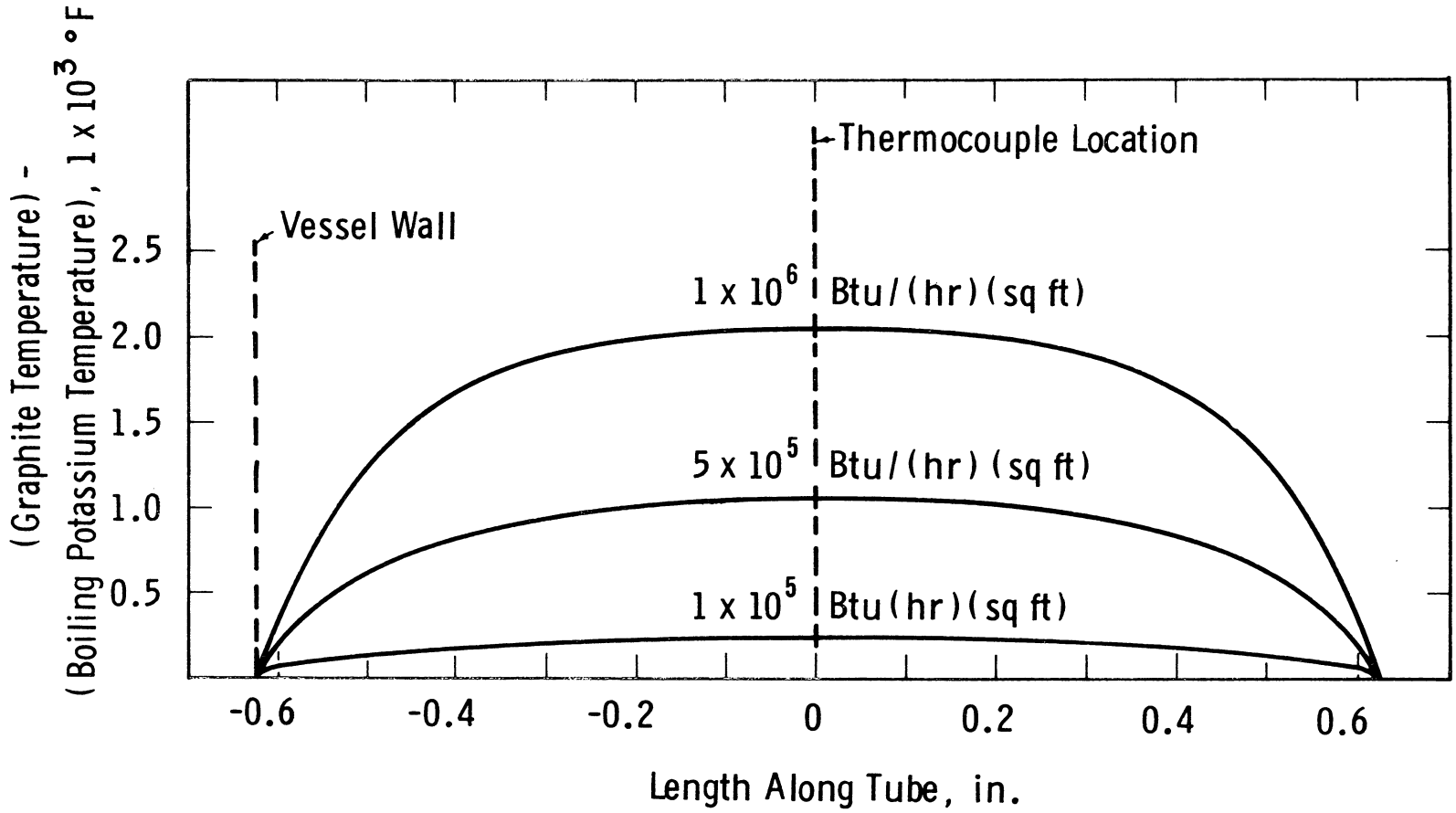


Figure 35. Temperature Profile of Graphite Heater in Boiling Tube.

## APPENDIX D

## DETERMINATION OF POWER LOSSES IN BOILING TUBE CIRCUITRY

Voltage measurements, made across the nickel bus bar and the boiling vessel wall, were used with the current to determine the total power to the boiling tube circuit. Included in the circuit were the nickel bus bar, the molybdenum rod, the graphite element, the end of the Haynes-25 boiling tube, the liquid metal bulk (which was in parallel with the Haynes-25 portion of the boiling tube), and finally the Haynes-25 boiling vessel.

One method used for obtaining lead losses involves experimentally measuring the resistance of the circuit with the graphite excluded. After tube 1 failed by melting in half, the liquid potassium was able to come in direct contact with the molybdenum rod. Thus, the power measurement included only lead losses in the circuit. The only losses not in this measurement were the contact losses between the graphite and molybdenum rod and the graphite and Haynes-25 tube end and the losses in the Haynes-25 tube end. The tube end loss was negligible. Contact losses were estimated from actual contact resistance data for graphite (95). Using a very conservative value for the contact pressure (400 psia--the calculated pressure was 1480 psia) the total loss for both contacts was 0.97 per cent of the total power input. From these findings the value determined by this method for the lead losses was considered quite reliable.

The actual power loss was measured for saturated potassium boiling at one atmosphere pressure and found to be 10.6 per cent of the total input. No measurements were made at other temperatures. However, since the total measured resistance of the boiling circuit remained very nearly constant over the operating temperature range, it was assumed that the lead resistances (thus power losses) and graphite heater resistance would maintain a constant value.

In order to obtain a definitive check of the above measurement, individual losses in the circuitry were computed from resistivity data. The total resistance of the tube circuit was represented as a series of resistences.

$$R_{total} = \frac{E}{I}\ \text{measured}$$

$$= R_{\text{nickel bus bar}} + R_{\text{moly rod}} + R_{\text{graphite}}$$

$$+ R_{\text{H-25 end}} + \frac{R_K R_{\text{H-25 tube}}}{R_K R_{\text{H-25 tube}}}$$

$$+ R_{\text{H-25 vessel}} + R_{\text{contacts}}$$

The fifth term on the right hand side of the equation represents the parallel circuit of the bulk potassium and Haynes-25 tube and the last term represents the sum of the electrical contact resistances at the various contact points.

Knowing the electrical resistivity, $\rho$, for each substance and using the relationship $R = \rho\ell/A$, where $\ell$ is the length and A the area, the individual resistences of the circuit were calculated. Resistances through the nickel bus bar, boiling tube end, and vessel wall were assumed negligible. Using values of electrical resistivities from references (50, 56, 93, 95, 125) the individual resistances were calculated to be: $R_{\text{moly rod}} = 0.0008$ ohms,

$R_{\text{contacts}} = 0.0004$ ohms, $R_{\text{graphite}} = 0.0122$ ohms, and

$$\frac{R_K R_{\text{H-25 tube}}}{R_K + R_{\text{H-25 tube}}} = 0.000046 \text{ ohms}.$$

The sum of these resistances is 0.0134 ohms with the lead losses accounting for 9 per cent of the total. This total calculated resistance compared to an average value of 0.0135 ohms for the total resistance measured experimentally. The lead losses calculated above gave a disagreement of only 1.6 per cent from the aforementioned experimentally measured value.

The percentage value ultimately used for lead losses in all data processing was 10 per cent. Comparison to the values above gave uncertainty limits of $\pm$ 1 per cent.

# APPENDIX E

## ESTIMATION OF ERRORS

### Heat Flux

The energy dissipated in the graphite heater was determined from a measurement of the total power to boiling tube circuit less power losses in electrical leads. The heat flux was then calculated by dividing the corrected power by the outside area of the boiling tube.

A calibrated ammeter and voltmeter were used to obtain total input power to the tube circuit. The uncertainty in reading the ammeter was about ± 0.5 amps whereas the voltmeter could be read to about ± 0.05 volt. The error in total input power could then be as much as ± 3.8 per cent at 50,000 Btu/(hr)(sq ft) and ± 1.3 per cent at 500,000 Btu/(hr)(sq ft).

Electrical lead losses are determined in Appendix D. The uncertainty in the value for these losses was thought to be ± 1 per cent of the total power input.

The effects of neglecting end losses in the graphite heater are analyzed in Appendix C. Neglecting longitudinal heat conduction in the tube wall or boron nitride sleeve, the total heat flux error at the center of the tube was calculated to be + 2 per cent. Over the middle half of the tube the calculated error was + 4.4 per cent.

The outside surface area was determined from the tube diameter and length. They were measured to a precision of 0.0005-in and 0.0156-in respectively. These variations correspond to a possible error in the tube area of ± 0.7 per cent. Overall errors at the center of the tube were therefore ± 7.5 per cent at a heat flux of 50,000 Btu(hr)(sq ft) and ± 5 per cent at 500,000 Btu/(hr)(sq ft).

### Temperatures

The three thermocouples used in tube 1 were calibrated against a Pt-Pt, 10% Rh thermocouple which was calibrated by the National Bureau of Standards. The average deviation from standard tables was + 0.32 per cent (+ 3.5°F) at 1100°F. All other thermocouples used in subsequent boiling tubes were made from the same lot of swaged assemblies. The liquid bulk thermocouple was calibrated against those of tube 1 at zero heat flux.

Principle errors in this study were caused from results involving temperature measurements. The temperature fluctuations in the tube wall were averaged and then extrapolated to the boiling tube surface. Since the temperature fluctuations were not always clearly defined with maximum and minimum deflections, some error in reading the mean value was inherent. This possible error was probably in the order of ± 3°F.

The best value for the calculated boiling tube wall temperature is discussed in Appendix B. Considering the results, the accuracy in the method is considered to be ± 5°F at 500,000 Btu/(hr)(sq ft).

Precision laboratory potentiometers (L and N No. 8662) and pen recorders were used to record emf for all thermocouples. Since the laboratory potentiometers and recorders could be read to within ± 0.005mv any error introduced by these instruments were completely overshadowed by errors above. The error in boiling $\Delta T$ values, therefore, would be ± 8°F at 500,000 Btu/(hr)(sq ft).

Pressure

The Bourdon pressure gauges were calibrated by a dead weight tester and could be accurately read to within ± 0.5 psia. The mercury manometer could be read to within 0.1 in Hg (0.049 psia).

# APPENDIX F

## PLOTS OF NUCLEATE BOILING

## POTASSIUM DATA

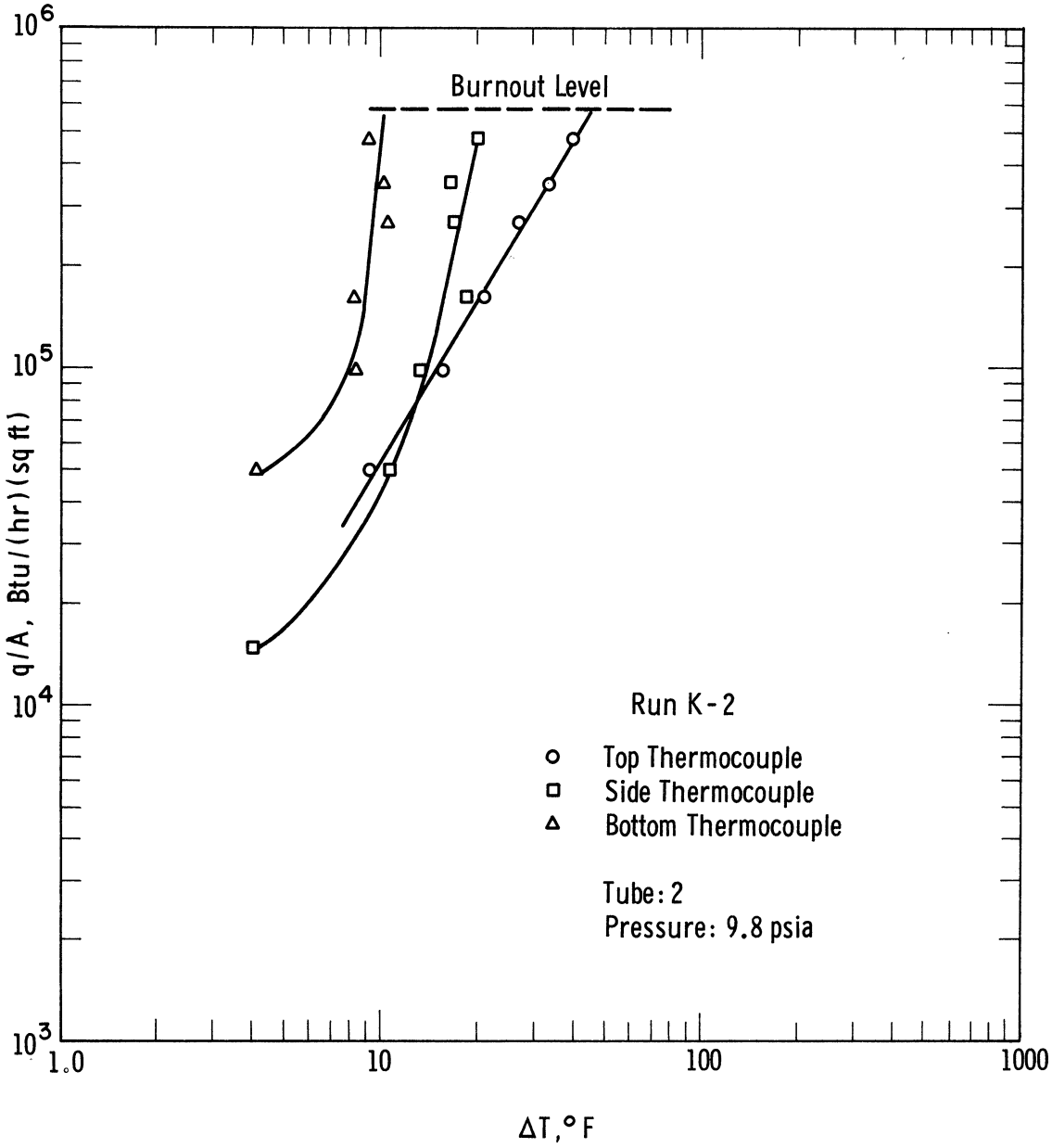


Figure 36. Boiling Data for Potassium Obtained at 9.8 psia using Tube 2 (Run K-2).

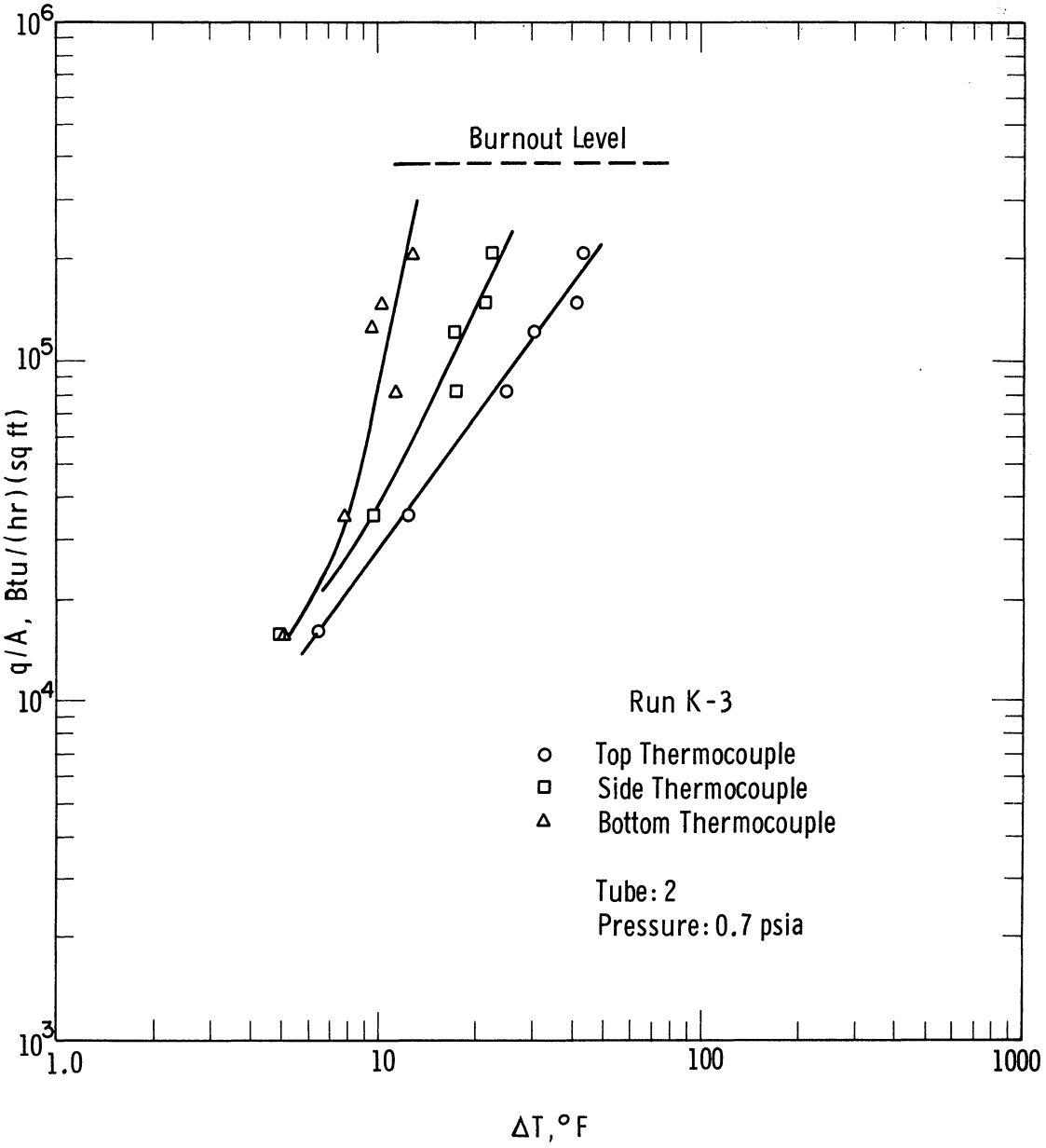


Figure 37. Boiling Data for Potassium Obtained at 0.7 psia using Tube 2 (Run K-3).

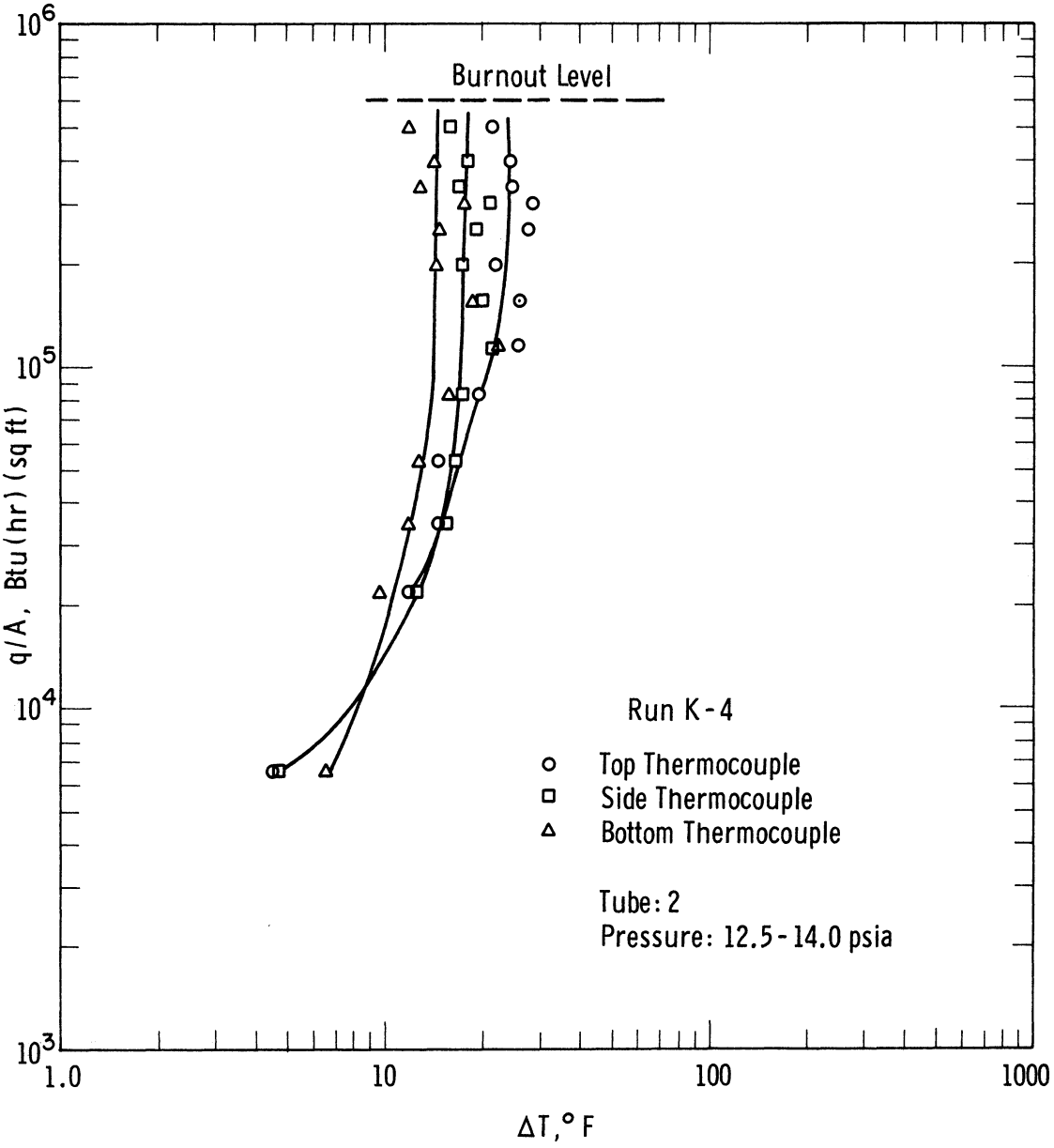


Figure 38. Boiling Data for Potassium Obtained in the Range 12.5 - 14.0 psia using Tube 2 (Run K-4).

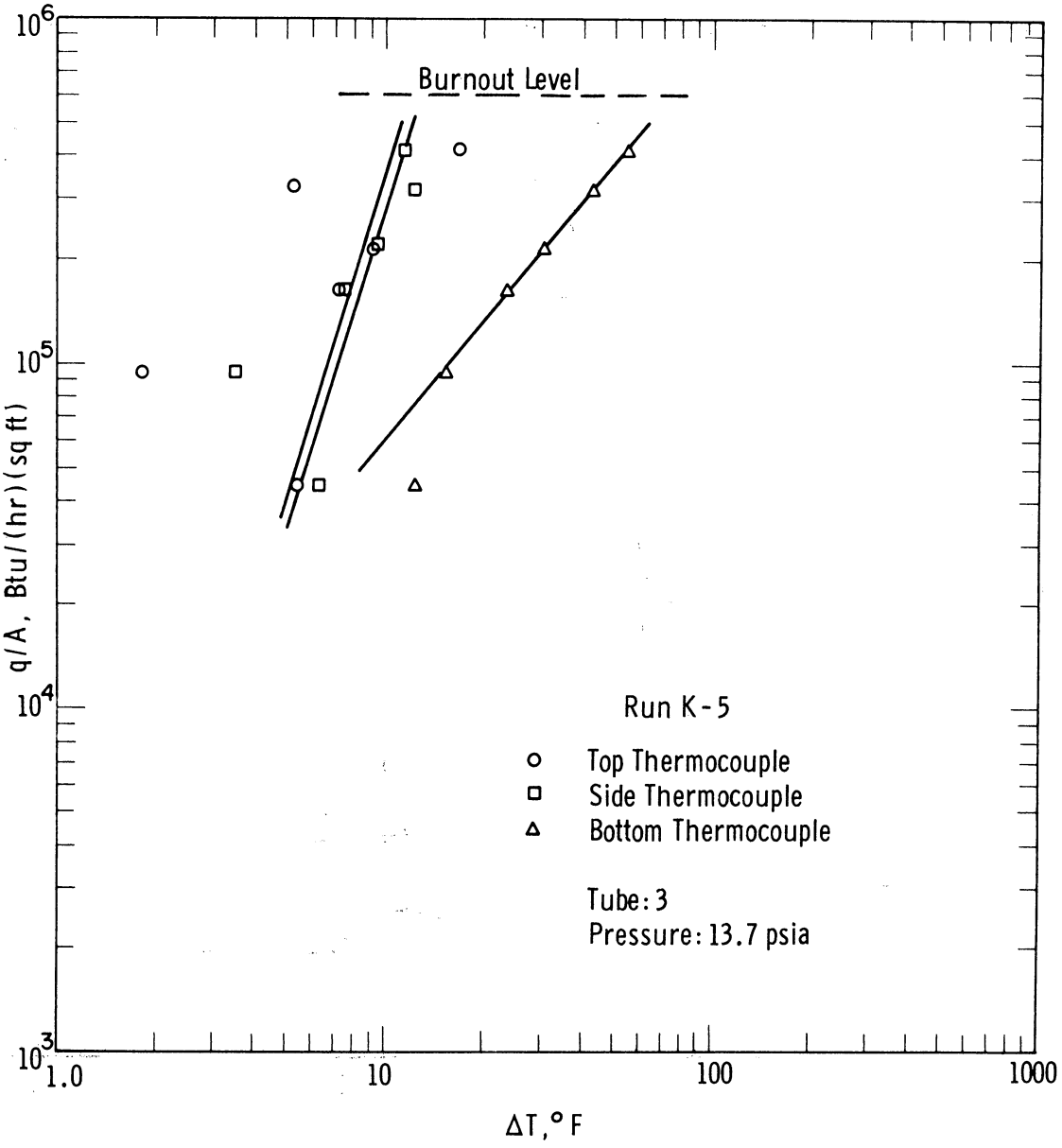


Figure 39. Boiling Data for Potassium Obtained at 13.7 psia using Tube 3 (Run K-5).

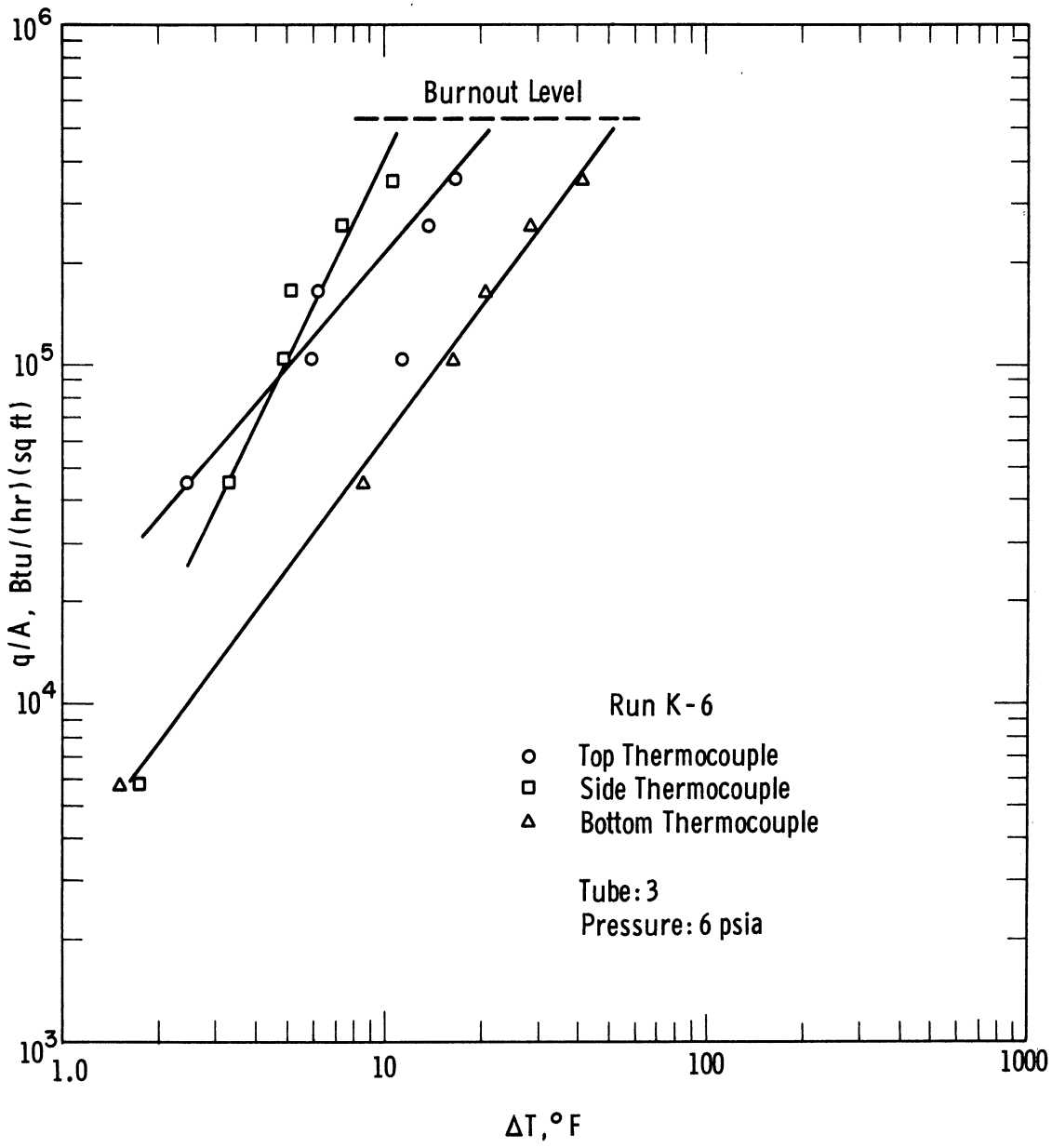


Figure 40. Boiling Data for Potassium Obtained at 6 psia using Tube 3 (Run K-6).

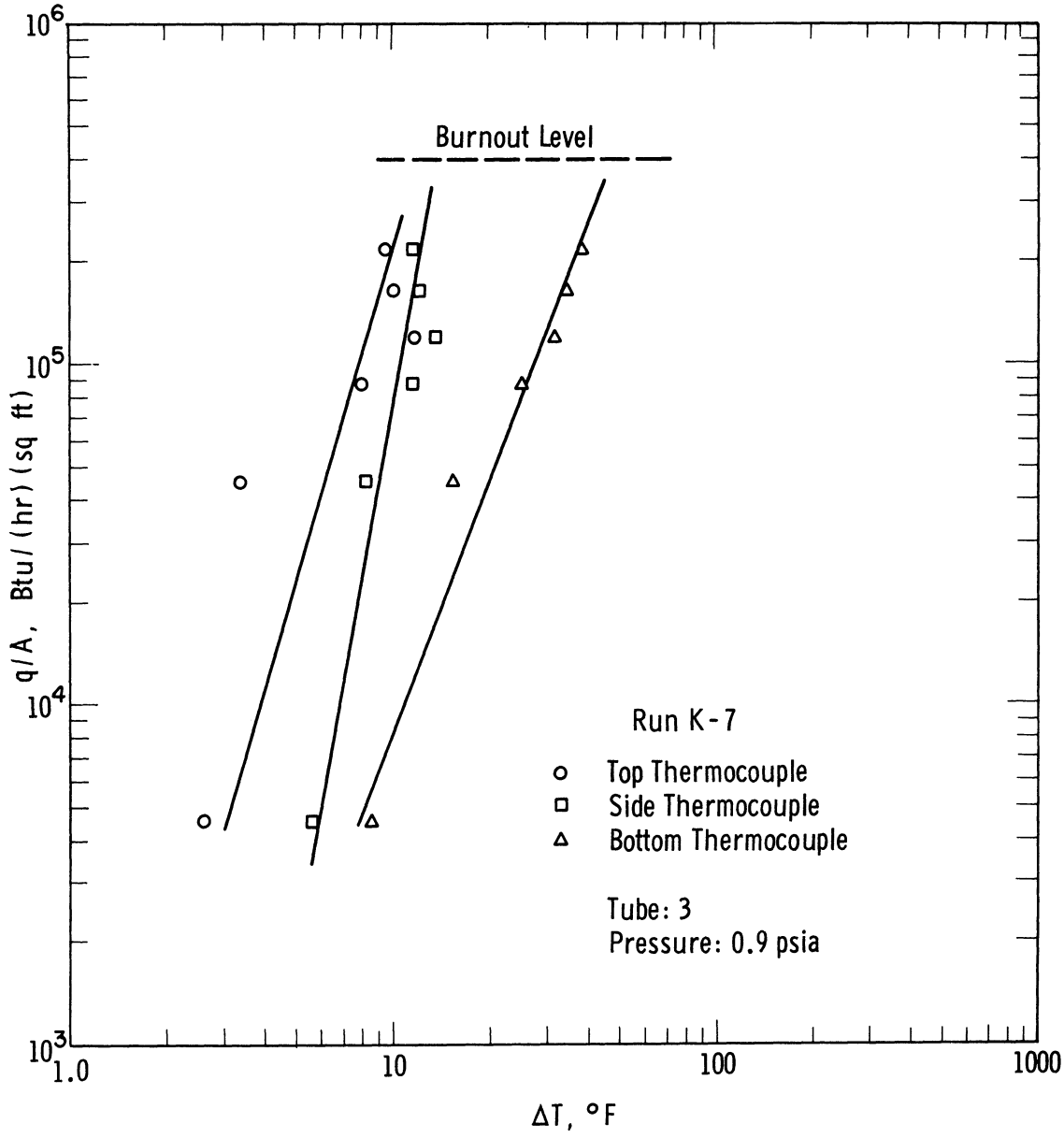


Figure 41. Boiling Data for Potassi ...u at 0.9 psia using Tube 3 (Run K-7).

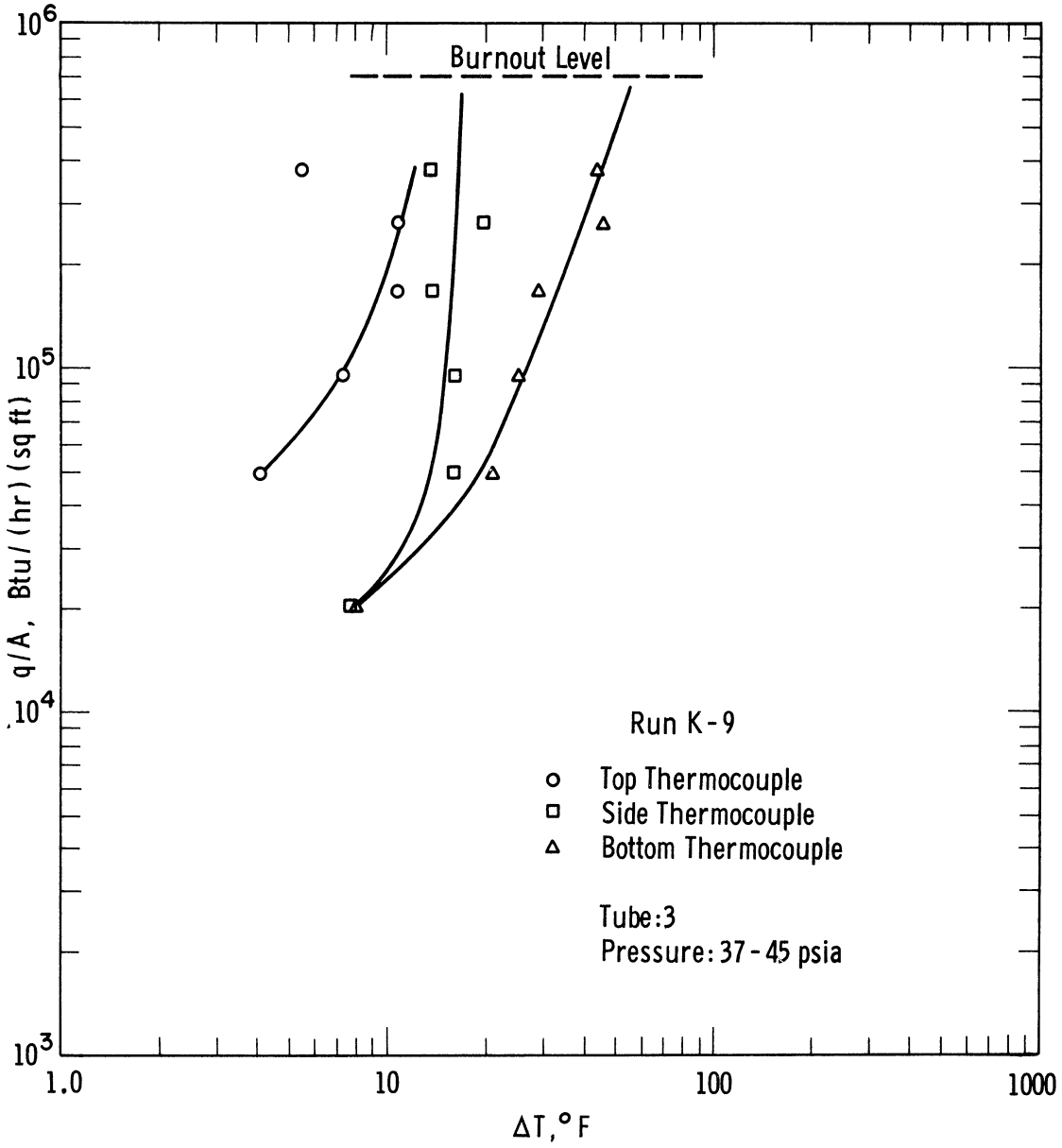


Figure 42. Boiling Data for Potassium Obtained in the Range 37 - 45 psia using Tube 3 (Run K-9).

## APPENDIX G

## PROCEDURE FOR FURNACE CALIBRATION OF MICRO-THERMOCOUPLES

The micro-thermocouples were calibrated using a Leeds and Northrup No. 9004 thermocouple checking furnace with a maximum temperature of 1800°F. Measurements were made on a Leeds and Northrup model 8662 laboratory potentiometer.

The micro-thermocouples are swaged assemblies with 0.020 ± 0.0005-in OD Inconel sheaths. The wires are 38-gauge Chromel-Alumel and are electrically insulated from each other and the sheath by magnesium oxide. The junctions are grounded to the sheath. The 10-in long Inconel sheath is connected to high-temperature Chromel-Alumel lead wire by means of a stainless steel transition fitting.

The micro-thermocouples along with a Pt/Pt-10% Rh thermocouple were inserted into a 1/2-in ID by 3/4-in OD by 9-in long stainless steel thermowell tied to a Haynes rod for support. A Pt/Pt-10% Rh thermocouple calibrated by the Bureau of Standards was tied to the outside of the thermowell with its junction flush with the bottom of the thermowell. All thermocouples were firmly pressed down to insure contact with the horizontal bottom of the thermowell.

The assembly was inserted into the furnace and the neck of the furnace packed with fiberfrax insulation to minimize heat losses. Approximately seven inches of the thermowell extended into the furnace with the remaining two inches located in the neck. The insulation completely covered the thermowell but the transition fittings of the micro-thermocouples extended just above the neck and were thus kept cool and could be checked for thermal contact with the bottom of the thermowell. The Pt/Pt-10% Rh and Chromel-Alumel thermocouples were hooked to separate switches which went through cold junctions immersed in an ice bath to the potentiometer.

The furnace was brought up to temperature with full power and then switched to manual control. Adjustment of a rheostat was then used to stabilize the temperature inside the furnace. A check on the transient response of the thermocouples inside the thermowell showed that approximately one-half hour was required for all temperatures to reach steady state. Careful adjustment of the rheostat could maintain the temperatures within two degrees F while the measurements were being taken.

Prior to taking a set of measurements, the potentiometer was checked against its internal standard cell. The secondary standard and then the Pt/Pt-10% Rh thermocouple in the thermowell were read. Then all Chromel-Alumel thermocouples were read followed by the two Pt/Pt-10% Rh thermocouples. The actual temperature, taken as that of the secondary standard, was linearly interpolated to give the true temperature for each micro-thermocouple. The Pt/Pt-10% Rh thermocouple in the thermowell may be sent to the Bureau of Standards at a later date as a further check on accuracy.

The recommended procedure for the furnace involved an immersion depth of 18 inches. This was not possible due to the short sheaths of the micro-thermocouples. Use of a copper equalizing block was not recommended for temperatures above 1000°F. The stainless steel thermowell which did not extend outside the furnace was used in place of a stainless steel equalizing block. Careful adjustment of the furnace rheostat after 30 minutes gave a furnace temperature drift of not more than 3°F per 5 minutes except at the highest temperatures, where a maximum of 8°F per 5 minutes was encountered.

APPENDIX H

TABLE XIV

FURNACE CALIBRATION OF MICRO-THERMOCOUPLES

| Standard | Inner Bottom | | Standard | Inner Top | |
|---|---|---|---|---|---|
| | Indicated | Calculated | | Indicated | Calculated |
| °F | °F | °F | °F | °F | °F |
| 608 | 618 | 607 | 605 | 567 | 598 |
| 797 | 807 | 797 | 798 | 762 | 798 |
| 993 | 1003 | 993 | 993 | 956 | 997 |
| 1186 | 1198 | 1189 | 1186 | 1148 | 1193 |
| 1379 | 1387 | 1379 | 1378 | 1334 | 1383 |
| 1588 | 1593 | 1586 | 1591 | 1526 | 1580 |

| Standard | Outer Bottom | | Standard | Outer Top | |
|---|---|---|---|---|---|
| | Indicated | Calculated | | Indicated | Calculated |
| °F | °F | °F | °F | °F | °F |
| 605 | 616 | 605 | 605 | 603 | 608 |
| 798 | 806 | 796 | 798 | 791 | 797 |
| 993 | 1003 | 994 | 993 | 984 | 991 |
| 1186 | 1197 | 1189 | 1186 | 1178 | 1185 |
| 1378 | 1386 | 1379 | 1378 | 1368 | 1376 |
| 1590 | 1594 | 1588 | 1590 | 1584 | 1593 |

Recheck on calibration data

| Standard | Inner Bottom | | Standard | Inner Top | |
|---|---|---|---|---|---|
| | Indicated | Calculated | | Indicated | Calculated |
| °F | °F | °F | °F | °F | °F |
| 624 | 635 | 624 | 625 | 582 | 614 |
| 1074 | 1083 | 1074 | 1074 | 1029 | 1071 |
| 1552 | 1554 | 1547 | 1550 | 1488 | 1541 |

| Standard | Outer Bottom | | Standard | Outer Top | |
|---|---|---|---|---|---|
| | Indicated | Calculated | | Indicated | Calculated |
| °F | °F | °F | °F | °F | °F |
| 625 | 637 | 626 | 625 | 621 | 626 |
| 1074 | 1084 | 1075 | 1074 | 1064 | 1071 |
| 1552 | 1554 | 1548 | 1552 | 1529 | 1539 |

TABLE XV

POTASSIUM BOILING DATA

| | Inner Radius Thermocouples | | Outer Radius Thermocouples | |
|---|---|---|---|---|
| Potassium | Bottom | Bottom-Top | Bottom | Bottom-Top |
| mv | mv | mv | mv | mv |
| VACUUM | | | | |
| 16.42 | 19.60 | 2.20 | 19.80 | 1.08 |
| 16.43 | 19.60 | 2.30 | 19.80 | 1.52 |
| 16.44 | 19.94 | 2.36 | 19.30 | 1.16 |
| 16.42 | 19.96 | 2.40 | 21.00 | 1.20 |
| 16.62 | 20.10 | 2.40 | 20.00 | 1.30 |
| 17.68 | 27.60 | 3.48 | 27.10 | 1.20 |
| 17.82 | 28.40 | 3.56 | 27.30 | 1.30 |
| 18.16 | 29.20 | 3.80 | 28.70 | 1.32 |
| 18.42 | 29.30 | 3.48 | 28.04 | 1.26 |
| 16.56 | 20.00 | 2.34 | 20.30 | 1.42 |
| 16.85 | 30.40 | 4.0 | 30.00 | 1.44 |
| 17.65 | 32.20 | 4.1 | 31.70 | 1.46 |
| 0.7 PSIA | | | | |
| 21.06 | 26.60 | 3.00 | 25.80 | 1.20 |
| 21.30 | 26.20 | 2.90 | 26.00 | 1.20 |
| 21.36 | 26.10 | 2.90 | 25.60 | 1.24 |
| 21.45 | 26.40 | 2.80 | 26.50 | 1.30 |
| 21.40 | 25.40 | 2.64 | 25.20 | 1.20 |
| 21.33 | 24.80 | 2.60 | 25.00 | 1.30 |
| 21.22 | 24.30 | 2.50 | 24.30 | 1.30 |
| 21.01 | 23.80 | 2.40 | 24.00 | 1.10 |
| 20.88 | 23.40 | 2.30 | 23.40 | 0.90 |
| 20.65 | 23.26 | 2.24 | 23.10 | 0.90 |
| 20.16 | 22.76 | 2.04 | 22.60 | 0.96 |
| 19.68 | 21.84 | 1.90 | 22.50 | 0.92 |
| 18.64 | 20.17 | 1.31 | 20.59 | 0.70 |

# APPENDIX I

## SAMPLE CALCULATION

Data

Pressure: 0.7 psia

Thermocouples in boiling plate:

| | | |
|---|---|---|
| Inner radius: | bottom | 26.60 mv |
| | bottom-top | 3.00 mv |
| Outer radius: | bottom | 25.80 mv |
| | bottom-top | 1.20 mv |
| Potassium: | | 21.06 mv |

Conversion to indicated temperatures:
(Leeds and Northrup Bulletin 077989, Issue 3)

| | | emf, mv | temp, °F |
|---|---|---|---|
| Inner radius: | bottom | 26.60 | 1184 |
| | top | 23.60 | 1057 |
| Outer radius: | bottom | 25.80 | 1150 |
| | top | 24.60 | 1099 |
| Potassium: | | 21.06 | 950* |

Conversion to actual temperatures:

| | | | | | | |
|---|---|---|---|---|---|---|
| Inner radius: | bottom | T | = | 1.0043 (1184) - 13.9 | = | 1175 |
| | top | T | = | 1.0238 (1057) + 18.0 | = | 1100 |
| Outer radius: | bottom | T | = | 1.0050 (1150) - 14.1 | = | 1142 |
| | top | T | = | 1.0040 (1099) + 2.7 | = | 1106 |

Calculation of inner flux and $\Delta T$:

Thermal conductivity of Cb-1 Zr

$$K = 25.88 + 0.0053 \left(\frac{1175 + 1100}{2}\right) = 31.91 \frac{\text{Btu}}{\text{hr-ft-°F}}$$

$$q/A = K \frac{\Delta T}{\Delta X} = \left(31.91 \frac{\text{Btu}}{\text{ft-hr-°F}}\right)\left(\frac{1175°\text{F} - 1100°\text{F}}{\frac{.1455}{12}\ \text{ft}}\right) = 197{,}000 \frac{\text{Btu}}{\text{hr-ft}^2}$$

---

* With the chart correction, the potassium temperature is 948°F. This correction has been omitted here because differences are involved.

$$T_{surface} = 1100 - \frac{25.5}{145.5}(1175-1100) = 1087$$

$$\Delta T = T_{surface} - T_{potassium} = 1087 - 950 = 137°F$$

Calculation of outer flux and $\Delta T$:

$$K = 25.88 + 0.0053\left(\frac{1142 + 1106}{2}\right) = 31.84 \frac{Btu}{hr\text{-}ft\text{-}°F}$$

$$q/A = K\frac{\Delta T}{\Delta X} = \left(31.84\frac{Btu}{ft\text{-}hr\text{-}°F}\right)\left(\frac{1142°F-1106°F}{.012125\ ft}\right) = 95,000 \frac{Btu}{hr\text{-}ft^2}$$

$$T_{surface} = 1106 - \frac{25.5}{145.5}(1142-1106) = 1100°F$$

$$\Delta T = 1100 - 950 = 150°F$$

# APPENDIX J

## SAFETY, SAMPLING AND CLEANING EQUIPMENT

Safety: Personnel entering the operations bay were required to wear long flame-resistant coats, leather gauntlets and a hard hat and a face shield. This equipment provided adequate protection although it was never put to a severe test. Several fires occurred during draining operations. Such fires were easily extinguished by applying Met-L-X powder with a scoop. The smoke was exhausted by a fan. Disposal of larger amounts ($\sim$1 gal) of alkalai metal was accomplished by dumping the metal outside in an isolated area and flushing it with large quantities of water. When large amounts of Met-L-X were interspersed with the metal, it would form a hard crusty mass in the bucket. In such cases, disposal required inverting the bucket on the ground, rapping it sharply to loosen the mass, then a breaking of the crust with a shovel before flushing it with water. In general, the disposal problem was much easier if Met-L-X was not present. Since potassium below 300°F could be drained from the system without a fire the use of Met-L-X was avoided by first cooling to below 300°F before draining.

Sampling: The easiest method of sampling a line was to cool the line to 280°F and let a fair amount of liquid metal run into a bucket. A drop of the discharge stream could be collected on the blade of a spatula. The spatula was allowed to cool for a moment and then placed in a beaker of methanol. The drop would rotate rapidly in the methanol until it was dissolved, but no fire occurred.

Cleaning Equipment: When small diameter equipment (which contained solid potassium or sodium) was to be salvaged, methanol was injected from a wash bottle followed by a rodding operation. If the reaction appeared to be going very slowly, the methanol was progressively diluted with water. Once the line was clear, it was flushed with water. For larger items, the methanol was added from a 10-ft piece of pipe with the operator behind a barricade. For expendable equipment (such as copper tubing) water would be played on the open end from a hose until the line was clear. This method usually resulted in small explosions, but was quick and effective. Heating a small line to drain it usually resulted in a fire.

## APPENDIX K

## UNCERTAINTY IN QUALITY DETERMINATION

An enthalpy balance is used to calculate inlet and outlet qualities for the pressure drop section. The inlet quality is given by

$$x_1 = \left[ \frac{Q_1 - Q_2 - Q_3}{\dot{m}} - (h_{\ell 3} - h_{\ell 1}) \right] \frac{1}{\lambda_3} \qquad \text{(K-1)}$$

where $x_1$ = quality at inlet of pressure drop section

$Q_1$ = heat supplied to preheaters (electrical), Btu/hr

$Q_2$ = heat loss from preheaters, Btu/hr

$Q_3$ = heat loss from heat transfer section, Btu/hr

$\dot{m}$ = total mass flow rate, lb/hr

$h_{\ell 1}$ = enthalpy of liquid entering preheaters, based on reading of TC-25, Btu/lb

$h_{\ell 3}$ = enthalpy of saturated liquid entering pressure drop section, based on reading of TC-30, Btu/lb

$\lambda_3$ = latent heat of vaporization, based on inlet temperature, TC-30, Btu/lb

The exit quality is given by

$$x_2 = \left[ \frac{Q_1 - Q_2 - Q_3 - Q_4}{\dot{m}} - (h_{\ell 4} - h_{\ell 1}) \right] \frac{1}{\lambda_4} \qquad \text{(K-2)}$$

where $x_2$ = quality at outlet of pressure drop section

$Q_4$ = heat loss from pressure drop section, Btu/hr

$h_{\ell 4}$ = enthalpy of saturated liquid leaving pressure drop section, based on reading of TC-31, Btu/lb

$\lambda_4$ = latent heat of vaporization, based on exit temperature, TC-31, Btu/lb

The average quality in the pressure drop section, which has been used in presenting results, is the arithmetic average of inlet and outlet qualities. From Equations (K-1) and (K-2), the average quality is

$$\bar{x} = \frac{Q_1 - Q_2 - Q_3 - Q_4/2}{\lambda\, \dot{m}} + \frac{2h_{\ell 1} - h_{\ell 3} - h_{\ell 4}}{2\lambda} \qquad \text{(K-3)}$$

where $\bar{x}$ = average quality in pressure drop section. In nearly every case $\lambda_3 \approx \lambda_4$, and this has been given in Equation (K-3) as $\lambda$.

For the purpose of assessing the uncertainty in average quality, all quantities on the right side of Equation (K-3) are taken as variables. The error or uncertainty in $\bar{x}$ may be written, using the notion of a differential of a function of several variables, as

$$\Delta\bar{x} = \frac{\partial\bar{x}}{\partial Q_1}\Delta Q_1 + \frac{\partial\bar{x}}{\partial Q_2}\Delta Q_2 + \frac{\partial\bar{x}}{\partial Q_3}\Delta Q_3 + \frac{\partial\bar{x}}{\partial Q_4}\Delta Q_4 + \frac{\partial\bar{x}}{\partial\dot{m}}\Delta\dot{m} \qquad \text{(K-4)}$$

$$+ \frac{\partial\bar{x}}{\partial\lambda}\Delta\lambda + \frac{\partial\bar{x}}{\partial h_{\ell 1}}\Delta h_{\ell 1} + \frac{\partial\bar{x}}{\partial h_{\ell 3}}\Delta h_{\ell 3} + \frac{\partial\bar{x}}{\partial h_{\ell 4}}\Delta h_{\ell 4}$$

where finite rather than infinitesimal differences are taken, as indicated by the $\Delta$'s.

The first five terms on the right side of Equation (K-4) contribute a component to $\Delta\bar{x}$ which may be considered the error due to uncertainties in measurements taken from the loop. The last four terms in Equation (K-4) contribute a component to $\Delta\bar{x}$ which is due to uncertainty in fluid properties. The temperatures in all cases were measured very accurately, and fluid properties such as density, enthalpy, and heat of vaporization are known as functions of temperature. Although there is some uncertainty in the values of fluid properties, particularly those of the vapor phase, it is assumed that these properties are known sufficiently accurately to allow one to consider the property component of $\Delta\bar{x}$ as negligible for the pure potassium. But these terms will be used here to determine the error arising from the use of pure-potassium properties for the 8 per cent sodium mixture.

It is convenient to break the $\Delta\bar{x}$ into its two components, as suggested above.

$$\Delta\bar{x}_{meas} = \frac{\partial x}{\partial Q_1}\Delta Q_1 + \frac{\partial\bar{x}}{\partial Q_2}\Delta Q_2 + \frac{\partial\bar{x}}{\partial Q_3}\Delta Q_3 + \frac{\partial\bar{x}}{\partial Q_4}\Delta Q_4 + \frac{\partial\bar{x}}{\partial\dot{m}}\Delta\dot{m} \qquad \text{(K-5)}$$

and

$$\Delta\bar{x}_{prop} = \frac{\partial\bar{x}}{\partial\lambda}\Delta\lambda + \frac{\partial\bar{x}}{\partial h_{\ell 1}}\Delta h_{\ell 1} + \frac{\partial\bar{x}}{\partial h_{\ell 3}}\Delta h_{\ell 3} + \frac{\partial\bar{x}}{\partial h_{\ell 4}}\Delta h_{\ell 4} \qquad \text{(K-6)}$$

where $\Delta\bar{x}_{meas}$ = component of $\Delta\bar{x}$ due to uncertainty in loop measurements

$\Delta\bar{x}_{prop}$ = component of $\Delta\bar{x}$ due to neglecting presence of 8 per cent sodium

From Equation (K-3), the following partial derivatives may be written

$$\frac{\partial \bar{x}}{\partial Q_1} = \frac{1}{\lambda \dot{m}}$$

$$\frac{\partial \bar{x}}{\partial Q_2} = \frac{\partial \bar{x}}{\partial Q_3} = -\frac{1}{\lambda \dot{m}}$$

$$\frac{\partial \bar{x}}{\partial Q_4} = -\frac{1}{2 \lambda \dot{m}}$$

$$\frac{\partial \bar{x}}{\partial \dot{m}} = -\frac{(Q_1 - Q_2 - Q_3 - Q_4/2)}{\lambda \dot{m}^2}$$

$$\frac{\partial \bar{x}}{\partial \lambda} = -\left[\frac{Q_1 - Q_2 - Q_3 - Q_4/2}{\dot{m} \lambda^2} + \frac{2h_{\ell 1} - h_{\ell 3} - h_{\ell 4}}{2 \lambda^2}\right] = -\frac{\bar{x}}{\lambda}$$

$$\frac{\partial \bar{x}}{\partial h_{\ell 1}} = \frac{1}{\lambda}$$

$$\frac{\partial \bar{x}}{\partial h_{\ell 3}} = \frac{\partial \bar{x}}{\partial h_{\ell 4}} = -\frac{1}{2 \lambda}$$

Inserting these derivatives in Equations (K-5) and (K-6),

$$\Delta \bar{x}_{meas} = \frac{1}{\lambda \dot{m}}\left[\Delta Q_1 - \Delta Q_2 - \Delta Q_3 - \frac{1}{2}\Delta Q_4 - \frac{(Q_1 - Q_2 - Q_3 - Q_4/2)\Delta \dot{m}}{\dot{m}}\right] \qquad \text{(K-7)}$$

$$\Delta \bar{x}_{prop} = \frac{1}{\lambda}\left[-\bar{x}\Delta\lambda + \Delta h_{\ell 1} - \frac{1}{2}\Delta h_{\ell 3} - \frac{1}{2}\Delta h_{\ell 4}\right] \qquad \text{(K-8)}$$

Equations (K-7) and (K-8) show that the error terms are worse when $\dot{m}$ is low, $\lambda$ is low (implying high temperature), and $Q_1$ is high.

The scatter in the heat loss correlation data shows the following uncertainties in heat losses.

| | |
|---|---|
| Preheaters | $\Delta Q_2 = \pm$ 1000 Btu/hr |
| Heat Transfer Section | $\Delta Q_3 = \pm$ 500 Btu/hr |
| Pressure Drop Section | $\Delta Q_4 = \pm$ 300 Btu/hr |

The power input to the preheaters is known to within 0.2 KW, so that

$$\Delta Q_1 = \pm 682 \text{ Btu/hr}$$

An error analysis, similar to this one, showed that the mass flow rate is known to within 7 lb/hr, that is

$$\Delta\dot{m} = \pm 7 \text{ lb/hr}$$

For pure potassium the $\Delta$'s in fluid properties are negligible, but the results of Table XVI may be used to evaluate the $\Delta$'s arising from neglect of sodium in the fluid.

A "worse case" chosen from the data will now be examined.

DATA POINT DESIGNATION 84-12(2)

$$\begin{aligned} Q_1 &= 64{,}500 \text{ Btu/hr} \\ Q_2 &= 9{,}800 \\ Q_3 &= 4{,}100 \\ Q_4 &= 1{,}500 \\ \dot{m} &= 122 \text{ lb/hr} \\ \bar{x} &= 0.380 \end{aligned}$$

with pure potassium properties

$$\begin{aligned} \lambda &= 850 \text{ Btu/lb} \\ h_{\ell 1} &= 261 \text{ Btu/lb} \\ h_{\ell 3} &= 349 \\ h_{\ell 4} &= 345 \end{aligned}$$

The data are at high temperature (1400°F), high preheat power and low flow rate. From Table XVI.

$$\begin{aligned} \Delta\lambda &= +(0.036)(850) = 30.6 \\ \Delta h_{\ell 1} &= +(0.051)(261) = 13.3 \\ \Delta h_{\ell 3} &= +(0.051)(349) = 17.8 \\ \Delta h_{\ell 4} &= +(0.051)(345) = 17.6 \end{aligned}$$

Using the average value between pure potassium and the mixture for $\lambda$, Equation (K-8) gives the property error.

$$\begin{aligned} \Delta\bar{x}_{prop} &= \frac{1}{865}\left[(-0.38)(30) + 13.3 - \frac{17.8}{2} - \frac{17.6}{2}\right] \\ &= \frac{-14.9}{865} = -0.0183 \end{aligned}$$

This error amounts to 4.8 per cent of the previously calculated $\bar{x} = 0.38$.

Again using an average value for $\lambda$, Equation (K-7) gives the error from measurement uncertainty. Here each $\Delta$ increment is given a sign which will make the error contribution in each case positive, yielding a worst value.

$$\Delta\bar{X}_{meas} = \frac{1}{(865)(122)}\left[682 + 1000 + 500 + \frac{300}{2} + \frac{(64{,}500-9800-4100-750)(7)}{122}\right]$$

$$= \frac{2332 + 2910}{(865)(122)} = \frac{5242}{(865)(122)} = 0.0495$$

This worst possible error amounts to 13 per cent of the calculated value $\bar{X} = 0.38$.

It must be remembered this is a "worst case." The $\Delta\bar{X}$ meas for other data points is not as severe, especially at higher flow rates. It should also be recalled that adjusting the physical properties will eliminate the $\Delta\bar{X}$ prop term.

# APPENDIX L

## TWO-PHASE FLOW INVESTIGATIONS
## EXPERIMENTAL DATA

TABLE XVIII

PRESSURE DROP DATA OBTAINED AT 2 MILLIVOLT AVERAGE FLOWMETER OUTPUT

MASS FLOW RATE: Average 256 lb/hr Range 210-289 lb/hr

| DATA POINT DESIG-NATION | MASS FLOW RATE lb/hr | PREHEATER POWER INPUT KW | INLET TEMPERATURE (TC 30) °F | OUTLET TEMPERATURE (TC 31) °F | INLET QUALITY $X_1$ | OUTLET QUALITY $X_2$ | AVERAGE QUALITY | PRESSURE DROP PSI |
|---|---|---|---|---|---|---|---|---|
| 56-7 | 271 | 19.2 | 1305 | 1237 | 0.1090 | 0.1200 | 0.1145 | 1.95 |
| 56-8 | 271 | 19.1 | 1322 | 1238 | 0.1070 | 0.1230 | 0.1150 | 1.95 |
| 56-9 | 246 | 19.1 | 1297 | 1225 | 0.1330 | 0.1420 | 0.1375 | 1.95 |
| 56-12 | 289 | 17.0 | 1244 | 1156 | 0.0870 | 0.1016 | 0.0943 | 1.73 |
| 56-121 | 289 | 16.8 | 1261 | 1159 | 0.0810 | 0.0995 | 0.0902 | 1.84 |
| 57-5 | 254 | 15.9 | 1221 | 1134 | 0.0827 | 0.1038 | 0.0932 | 2.44 |
| 57-6 | 232 | 15.9 | 1246 | 1127 | 0.1020 | 0.1220 | 0.1120 | 2.44 |
| 58-10 | 229 | 15.0 | 1238 | 1096 | 0.1015 | 0.1227 | 0.1121 | 2.13 |
| 58-11 | 278 | 14.9 | 1225 | 1102 | 0.0668 | 0.0856 | 0.0762 | 2.10 |
| 58-113 | 246 | 15.1 | 1205 | 1089 | 0.0931 | 0.1118 | 0.1025 | 2.16 |
| 58-115 | 266 | 15.1 | 1239 | 1094 | 0.0841 | 0.0968 | 0.0905 | 2.10 |
| 58-12 | 259 | 15.1 | 1184 | 1085 | 0.0839 | 0.1040 | 0.0939 | 2.02 |
| 58-122 | 250 | 15.0 | 1188 | 1099 | 0.0804 | 0.1057 | 0.0930 | 2.16 |
| 58-123 | 247 | 14.8 | 1208 | 1086 | 0.0863 | 0.1076 | 0.0969 | 2.06 |
| 59-4 | 285 | 13.7 | 1183 | 1058 | 0.0499 | 0.0715 | 0.0607 | 1.70 |
| 59-45 | 238 | 14.2 | 1160 | 1056 | 0.0765 | 0.0921 | 0.0843 | 1.70 |
| 59-5 | 210 | 14.1 | 1152 | 1038 | 0.1090 | 0.1230 | 0.1160 | 1.66 |
| 59-51 | 252 | 14.3 | 1171 | 1050 | 0.0698 | 0.0881 | 0.0789 | 1.95 |
| 59-53 | 286 | 14.2 | 1189 | 1063 | 0.0452 | 0.0645 | 0.0549 | 1.73 |
| 60-9 | 252 | 12.0 | 1121 | 994 | 0.0445 | 0.0676 | 0.0560 | 1.08 |
| 60-10 | 260 | 12.1 | 1088 | 1005 | 0.0500 | 0.0624 | 0.0562 | 1.12 |
| 60-102 | 256 | 12.0 | 1151 | 982 | 0.0411 | 0.0690 | 0.0550 | 1.15 |
| 60-104 | 256 | 12.0 | 1092 | 984 | 0.0511 | 0.0679 | 0.0595 | 1.12 |
| 60-11 | 254 | 12.0 | 1106 | 985 | 0.0479 | 0.0686 | 0.0582 | 1.08 |
| 61-1 | 256 | 11.3 | 1118 | 990 | 0.0420 | 0.0589 | 0.0505 | 0.975 |
| 61-2 | 256 | 11.3 | 1080 | 969 | 0.0398 | 0.0621 | 0.0510 | 0.975 |
| 61-3 | 251 | 11.2 | 1075 | 1036 | 0.0443 | 0.0488 | 0.0465 | 0.940 |
| 61-4 | 246 | 11.3 | 1037 | 974 | 0.0502 | 0.0675 | 0.0589 | 0.940 |
| 61-5 | 251 | 11.3 | 1080 | 979 | 0.0382 | 0.0639 | 0.0510 | 0.940 |
| 61-6 | 256 | 11.2 | 1175 | 983 | 0.0453 | 0.0594 | 0.0524 | 0.940 |
| 61-7 | 256 | 11.2 | 1091 | 991 | 0.0437 | 0.0584 | 0.0510 | 0.940 |
| 61-8 | 256 | 11.0 | 1075 | 971 | 0.0419 | 0.0582 | 0.0500 | 0.795 |
| 62-84 | 256 | 11.0 | 1081 | 966 | 0.0397 | 0.0570 | 0.0483 | 0.940 |
| 62-9 | 247 | 11.0 | 1070 | 990 | 0.0453 | 0.0576 | 0.0515 | 0.865 |
| 62-10 | 256 | 11.3 | 1109 | 992 | 0.0488 | 0.0590 | 0.0539 | 0.865 |
| 63-2 | 264 | 7.4 | 926 | 855 | 0.0143 | 0.0257 | 0.0200 | 0.0545 |
| 64-10 | 258 | 9.0 | 971 | 887 | 0.0187 | 0.0333 | 0.0260 | 0.271 |
| 64-103 | 251 | 9.0 | 974 | 889 | 0.0252 | 0.0394 | 0.0323 | 0.289 |
| 64-11 | 251 | 9.1 | 981 | 896 | 0.0258 | 0.0414 | 0.0336 | 0.307 |
| 64-12 | 255 | 9.0 | 983 | 896 | 0.0222 | 0.0378 | 0.0300 | 0.307 |
| 64-2 | 255 | 9.0 | 984 | 898 | 0.0222 | 0.0378 | 0.0300 | 0.324 |

TABLE XVIII (Continued)

PRESSURE DROP DATA OBTAINED AT 2 MILLIVOLT AVERAGE FLOWMETER OUTPUT

MASS FLOW RATE: Average 256 lb/hr Range 210-289 lb/hr

| DATA POINT DESIG-NATION | MASS FLOW RATE lb/hr | PREHEATER POWER INPUT KW | INLET TEMPERATURE (TC 30) °F | OUTLET TEMPERATURE (TC 31) °F | INLET QUALITY $X_1$ | OUTLET QUALITY $X_2$ | AVERAGE QUALITY | PRESSURE DROP PSI |
|---|---|---|---|---|---|---|---|---|
| 65-7 | 257 | 10.0 | 1046 | 940 | 0.0227 | 0.0463 | 0.0345 | 0.595 |
| 65-8 | 257 | 10.0 | 1042 | 940 | 0.0227 | 0.0463 | 0.0345 | 0.612 |
| 65-9 | 253 | 9.8 | 1040 | 939 | 0.0216 | 0.0446 | 0.0331 | 0.595 |
| 65-10 | 257 | 10.0 | 1046 | 940 | 0.0227 | 0.0463 | 0.0345 | 0.612 |
| 66-4 | 256 | 11.0 | 1095 | 986 | 0.0403 | 0.0580 | 0.0492 | 1.01 |
| 66-5 | 260 | 11.1 | 1096 | 988 | 0.0397 | 0.0576 | 0.0487 | 1.05 |
| 66-6 | 259 | 11.0 | 1090 | 984 | 0.0409 | 0.0576 | 0.0493 | 1.08 |
| 66-62 | 260 | 11.1 | 1102 | 983 | 0.0386 | 0.0589 | 0.0487 | 1.08 |
| 66-7 | 256 | 11.1 | 1100 | 997 | 0.0398 | 0.0600 | 0.0499 | 1.08 |
| 82-12(1) | 250 | 11.1 | 1106 | 985 | 0.0404 | 0.0617 | 0.0510 | 1.01 |
| 82-1 | 264 | 7.3 | 949 | 872 | 0.0091 | 0.0228 | 0.0159 | 0.091 |
| 82-3 | 254 | 10.0 | 1023 | 925 | 0.0249 | 0.0458 | 0.0353 | 0.47 |
| 82-4 | 254 | 10.0 | 1030 | 930 | 0.0249 | 0.0458 | 0.0353 | 0.54 |
| 82-12(2) | 228 | 11.0 | 1081 | 974 | 0.0454 | 0.0628 | 0.0541 | 0.95 |

NOTE: The number preceding the dash in DATA POINT DESIGNATION refers to the page number in University of Michigan Research Institute Data Book No.3496 on which the raw data are recorded. The number following the dash refers to the time readings were taken.

TABLE XIX

PRESSURE DROP DATA OBTAINED AT 3 MILLIVOLT AVERAGE FLOWMETER OUTPUT

MASS FLOW RATE: Average 376 lb/hr Range 352-400 lb/hr

| DATA POINT DESIG-NATION | MASS FLOW RATE lb/hr | PREHEATER POWER INPUT KW | INLET TEMPERATURE (TC 30) °F | OUTLET TEMPERATURE (TC 31) °F | INLET QUALITY $X_1$ | OUTLET QUALITY $X_2$ | AVERAGE QUALITY | PRESSURE DROP PSI |
|---|---|---|---|---|---|---|---|---|
| 50-2 | 382 | 12.0 | 1091 | 982 | 0.0097 | 0.0300 | 0.0199 | 0.74 |
| 50-3 | 356 | 12.0 | 1103 | 994 | 0.0157 | 0.0370 | 0.0264 | 0.58 |
| 50-4 | 363 | 13.0 | 1137 | 1016 | 0.0158 | 0.0371 | 0.0265 | 0.82 |
| 50-5 | 383 | 12.9 | 1150 | 1029 | 0.0110 | 0.0350 | 0.0230 | 0.96 |
| 50-6 | 387 | 13.1 | 1127 | 1014 | 0.0163 | 0.0390 | 0.0277 | 0.80 |
| 51-10 | 354 | 13.8 | 1170 | 1056 | 0.0354 | 0.0500 | 0.0427 | 1.63 |
| 51-11 | 390 | 14.0 | 1174 | 1047 | 0.0458 | 0.0466 | 0.0462 | 1.63 |
| 51-12 | 382 | 13.8 | 1152 | 1056 | 0.0300 | 0.0466 | 0.0383 | 1.70 |
| 52-4 | 376 | 15.0 | 1203 | 1000 | 0.0405 | 0.0544 | 0.0475 | 2.24 |
| 52-5 | 366 | 15.0 | 1213 | 1090 | 0.0390 | 0.0624 | 0.0507 | 2.24 |
| 52-6 | 365 | 15.0 | 1214 | 1089 | 0.0413 | 0.0545 | 0.0484 | 2.24 |
| 52-9 | 377 | 16.2 | 1244 | 1127 | 0.0501 | 0.0646 | 0.0574 | 2.60 |
| 52-10 | 400 | 16.0 | 1213 | 1109 | 0.0355 | 0.0585 | 0.0470 | 2.56 |
| 53-102 | 400 | 16.0 | 1227 | 1118 | 0.0380 | 0.0575 | 0.0478 | 2.55 |
| 53-2 | 395 | 16.9 | 1263 | 1148 | 0.0405 | 0.0625 | 0.0515 | 3.00 |
| 53-3 | 385 | 16.8 | 1264 | 1149 | 0.0434 | 0.0640 | 0.0537 | 3.00 |
| 54-85 | 370 | 18.0 | 1277 | 1171 | 0.0580 | 0.0765 | 0.0672 | 2.37 |
| 54-10 | 400 | 18.0 | 1292 | 1178 | 0.0475 | 0.0665 | 0.0570 | 2.37 |
| 55-3 | 374 | 19.0 | 1314 | 1205 | 0.0651 | 0.0793 | 0.0722 | 2.44 |
| 55-34 | 380 | 18.8 | 1311 | 1207 | 0.0582 | 0.0758 | 0.0670 | 2.38 |
| 55-4 | 386 | 19.2 | 1304 | 1208 | 0.0623 | 0.0794 | 0.0709 | 2.44 |
| 67-12 | 372 | 11.0 | 1070 | 972 | 0.0138 | 0.0308 | 0.0223 | 0.65 |
| 67-123 | 365 | 11.0 | 1070 | 971 | 0.0134 | 0.0302 | 0.0218 | 0.65 |
| 67-1 | 374 | 11.0 | 1065 | 966 | 0.0134 | 0.0314 | 0.0224 | 0.65 |
| 67-2 | 365 | 11.0 | 1057 | 960 | 0.0190 | 0.0358 | 0.0274 | 0.65 |
| 68-7 | 378 | 16.5 | 1333 | 1258 | 0.0769 | 0.0925 | 0.0847 | 2.75 |
| 68-8 | 378 | 16.3 | 1307 | 1264 | 0.0885 | 0.0940 | 0.0913 | 2.78 |
| 68-9 | 352 | 16.3 | 1341 | 1282 | 0.0955 | 0.1060 | 0.1007 | 2.82 |
| 75-7 | 366 | 19.0 | 1344 | 1293 | 0.0934 | 0.0985 | 0.0959 | 2.16 |
| 75-8 | 376 | 19.3 | 1335 | 1290 | 0.0908 | 0.0988 | 0.0948 | 2.06 |
| 75-9 | 360 | 18.9 | 1361 | 1295 | 0.0915 | 0.1018 | 0.0967 | 2.06 |
| 81-3 | 351 | 15.0 | 1187 | 1092 | 0.0507 | 0.0635 | 0.0571 | 2.24 |
| 81-7 | 358 | 16.1 | 1226 | 1100 | 0.0515 | 0.0692 | 0.0603 | 2.46 |
| 83-3 | 356 | 10.0 | 1044 | 953 | 0.0123 | 0.0284 | 0.0203 | 0.58 |

NOTE: DATA POINT DESIGNATION has the same significance as in Table XVIII.

TABLE XX

PRESSURE DROP DATA OBTAINED AT 4, 5, 6, AND 1 MILLIVOLT AVERAGE FLOWMETER OUTPUTS

| AVERAGE FLOWMETER OUTPUT Millivolts | DATA POINT DESIG-NATION | MASS FLOW RATE lb/hr | PREHEATER POWER INPUT KW | INLET TEM-PERATURE (TC 30) °F | OUTLET TEM-PERATURE (TC 31) °F | INLET QUALITY $X_1$ | OUTLET QUALITY $X_2$ | AVERAGE QUALITY | PRESSURE DROP PSI | MASS FLOW RATE (lb/hr) Average Range |
|---|---|---|---|---|---|---|---|---|---|---|
| | 69-11 | 486 | 16.1 | 1350 | 1258 | 0.0562 | 0.0659 | 0.0610 | 2.96 | |
| | 69-12 | 484 | 16.1 | 1321 | 1256 | 0.0555 | 0.0653 | 0.0604 | 3.03 | |
| | 69-1 | 498 | 16.2 | 1338 | 1270 | 0.0530 | 0.0594 | 0.0562 | 3.06 | |
| | 69-14 | 498 | 16.2 | 1320 | 1252 | 0.0484 | 0.0615 | 0.0549 | 3.10 | |
| | 69-2 | 498 | 16.2 | 1310 | 1242 | 0.0484 | 0.0626 | 0.0555 | 3.06 | |
| | 74-3 | 481 | 18.7 | 1350 | 1271 | 0.0573 | 0.0712 | 0.0642 | 2.38 | |
| 4 | 74-4 | 500 | 18.7 | 1340 | 1256 | 0.0525 | 0.0645 | 0.0585 | 2.38 | 479 |
| | 74-5 | 485 | 18.6 | 1341 | 1257 | 0.0568 | 0.0698 | 0.0633 | 2.38 | 440-500 |
| | 83-9(1) | 461 | 15.8 | 1328 | 1238 | 0.0507 | 0.0671 | 0.0589 | 2.92 | |
| | 83-10(1) | 459 | 16.6 | 1310 | 1242 | 0.0553 | 0.0680 | 0.0616 | 3.07 | |
| | 83-8(2) | 485 | 16.9 | 1323 | 1236 | 0.0458 | 0.0634 | 0.0546 | 2.06 | |
| | 83-9(2) | 440 | 16.9 | 1327 | 1242 | 0.0560 | 0.0720 | 0.0640 | 2.06 | |
| | 84-12(1) | 450 | 18.5 | 1339 | 1266 | 0.0681 | 0.0830 | 0.0755 | 2.38 | |
| | 70-12 | 613 | 16.7 | 1312 | 1236 | 0.0384 | 0.0507 | 0.0445 | 3.07 | |
| | 70-1 | 590 | 16.5 | 1308 | 1234 | 0.0356 | 0.0512 | 0.0434 | 3.03 | |
| | 73-8 | 615 | 18.3 | 1345 | 1274 | 0.0349 | 0.0485 | 0.0417 | 2.44 | |
| | 73-9 | 590 | 18.4 | 1349 | 1265 | 0.0425 | 0.0536 | 0.0480 | 2.44 | |
| 5 | 73-10 | 611 | 18.0 | 1348 | 1259 | 0.0356 | 0.0482 | 0.0419 | 2.44 | 607 |
| | 73-11 | 613 | 18.0 | 1344 | 1261 | 0.0335 | 0.0458 | 0.0397 | 2.44 | 590-637 |
| | 83-10 | 637 | 16.7 | 1327 | 1242 | 0.0167 | 0.0341 | 0.0254 | 2.06 | |
| | 84-6 | 597 | 19.0 | 1356 | 1253 | 0.0340 | 0.0578 | 0.0454 | 2.44 | |
| | 84-7 | 597 | 19.0 | 1349 | 1277 | 0.0375 | 0.0533 | 0.0474 | 2.49 | |
| | 71-11 | 730 | 17.0 | 1317 | 1250 | 0.0213 | 0.0330 | 0.0271 | 1.95 | |
| | 72-2 | 701 | 18.5 | 1353 | 1264 | 0.0280 | 0.0440 | 0.0360 | 2.58 | |
| | 72-3 | 727 | 18.2 | 1357 | 1257 | 0.0248 | 0.0444 | 0.0346 | 2.58 | |
| 6 | 72-4 | 740 | 18.5 | 1353 | 1268 | 0.0260 | 0.0411 | 0.0335 | 2.33 | 725 |
| | 72-5 | 732 | 18.5 | 1358 | 1272 | 0.0243 | 0.0409 | 0.0326 | 2.58 | 701-740 |
| | 84-1 | 710 | 18.8 | 1350 | 1262 | 0.0419 | 0.0607 | 0.0513 | 2.38 | |
| | 83-4 | 732 | 16.5 | 1307 | 1230 | 0.0224 | 0.0366 | 0.0295 | 2.86 | |
| | 76-1 | 115 | 18.8 | 1395 | 1375 | 0.402 | 0.399 | 0.400 | 1.08 | |
| | 76-2 | 125 | 18.9 | 1385 | 1388 | 0.374 | 0.363 | 0.368 | 1.08 | |
| | 76-3 | 124 | 19.0 | 1432 | 1399 | 0.378 | 0.368 | 0.373 | 1.08 | |
| | 77-7 | 128 | 15.0 | 1290 | 1265 | 0.286 | 0.280 | 0.283 | 1.08 | |
| | 77-8 | 125 | 15.0 | 1285 | 1254 | 0.294 | 0.291 | 0.292 | 1.08 | |
| | 77-9 | 110 | 14.9 | 1267 | 1252 | 0.342 | 0.335 | 0.338 | 1.08 | |
| 1 | 78-12 | 125 | 11.2 | 1184 | 1143 | 0.211 | 0.210 | 0.210 | 0.76 | 125 |
| | 78-1 | 129 | 11.1 | 1183 | 1128 | 0.197 | 0.201 | 0.199 | 0.86 | 110-134 |
| | 84-11 | 126 | 18.8 | 1364 | 1337 | 0.360 | 0.356 | 0.358 | 1.18 | |
| | 84-12(2) | 122 | 18.9 | 1388 | 1378 | 0.379 | 0.383 | 0.381 | 1.18 | |
| | 85-4 | 125 | 15.0 | 1331 | 1314 | 0.294 | 0.290 | 0.292 | 1.08 | |
| | 85-5 | 134 | 15.0 | 1318 | 1296 | 0.267 | 0.264 | 0.265 | 1.08 | |
| | 85-6 | 131 | 15.0 | 1320 | 1281 | 0.271 | 0.271 | 0.271 | 1.18 | |
| | 85-11 | 125 | 11.1 | 1202 | 1164 | 0.210 | 0.204 | 0.207 | 0.76 | |

NOTE: DATA POINT DESIGNATION has the same significance as in Table XVIII.

TABLE XXI

SELECTED DATA USED IN PREPARING FIGURE 62

| DATA POINT DESIGNATION | MASS FLOW RATE lb/hr | AVERAGE QUALITY | PRESSURE DROP PSI | RANGE OF AVERAGE QUALITY |
|---|---|---|---|---|
| 69-11 | 486 | 0.0610 | 2.96 | |
| 69-12 | 484 | 0.0604 | 3.03 | |
| 69-1 | 498 | 0.0562 | 3.06 | 0.055 |
| 69-2 | 498 | 0.0555 | 3.06 | to |
| 74-3 | 481 | 0.0642 | 2.38 | 0.0642 |
| 74-4 | 500 | 0.0585 | 2.38 | |
| 74-5 | 485 | 0.0633 | 2.38 | |
| 83-9(1) | 461 | 0.0589 | 2.92 | |
| 83-10(1) | 459 | 0.0616 | 3.07 | |
| 83-9(2) | 440 | 0.0640 | 2.06 | Parametric |
| 52-9 | 377 | 0.0574 | 2.60 | Value |
| 54-10 | 400 | 0.0570 | 2.37 | 0.06 |
| 81-3 | 351 | 0.0571 | 2.24 | |
| 81-7 | 358 | 0.0603 | 2.46 | |
| 59-4 | 285 | 0.0607 | 1.70 | |
| 60-9 | 252 | 0.0560 | 1.08 | |
| 60-10 | 260 | 0.0562 | 1.12 | |
| 60-102 | 256 | 0.0550 | 1.15 | |
| 60-104 | 256 | 0.0595 | 1.12 | |
| 60-11 | 254 | 0.0582 | 1.08 | |
| 61-4 | 246 | 0.0589 | 0.94 | |
| 70-12 | 613 | 0.0445 | 3.07 | |
| 70-1 | 590 | 0.0434 | 3.03 | |
| 73-8 | 615 | 0.0417 | 2.44 | 0.0353 to 0.0445 |
| 73-10 | 611 | 0.0419 | 2.44 | Parametric |
| 73-11 | 613 | 0.0397 | 2.44 | Value |
| 72-2 | 701 | 0.0360 | 2.58 | 0.04 |
| 51-10 | 354 | 0.0427 | 1.63 | |
| 51-12 | 382 | 0.0383 | 1.70 | |
| 82-3 | 254 | 0.0353 | 0.47 | |
| 82-4 | 254 | 0.0353 | 0.54 | |

TABLE XXI (Continued)

SELECTED DATA USED IN PREPARING FIGURE 62

| DATA POINT DESIGNATION | MASS FLOW RATE lb/hr | AVERAGE QUALITY | PRESSURE DROP PSI | RANGE OF AVERAGE QUALITY |
|---|---|---|---|---|
| 83-10 | 637 | 0.0254 | 2.06 | |
| 71-11 | 730 | 0.0271 | 1.95 | |
| 72-3 | 727 | 0.0346 | 2.58 | 0.0254 |
| 72-4 | 740 | 0.0335 | 2.33 | to |
| 72-5 | 732 | 0.0326 | 2.58 | 0.0346 |
| 83-4 | 732 | 0.0295 | 2.86 | |
| 50-2 | 382 | 0.0264 | 0.58 | Parametric |
| 50-4 | 363 | 0.0265 | 0.82 | Value |
| 50-6 | 387 | 0.0277 | 0.80 | 0.03 |
| 64-10 | 258 | 0.0260 | 0.271 | |
| 64-103 | 251 | 0.0323 | 0.289 | |
| 64-11 | 251 | 0.0336 | 0.307 | |
| 64-12 | 255 | 0.0300 | 0.307 | |
| 64-2 | 255 | 0.0300 | 0.324 | |
| 65-7 | 257 | 0.0345 | 0.595 | |
| 65-8 | 257 | 0.0345 | 0.612 | |
| 65-9 | 253 | 0.0331 | 0.595 | |
| 65-10 | 257 | 0.0345 | 0.612 | |

NOTE: DATA POINT DESIGNATION has the same significance as in Table XVIII.

TABLE XXII

VOID FRACTION DATA

| Average Temperature °F | Average Quality | Total Mass Flow Rate lb/hr | Ratio of Superficial Vapor Velocity to Total Liquid Velocity, $U_g/V_o$ | All-Liquid Froude Number $V_o^2/gD$ | Void Fraction $\alpha$ | Slip Velocity Ratio $V_g/V_\ell$ |
|---|---|---|---|---|---|---|
| 1156 | 0.1990 | 129 | 1073 | 0.29 | 0.811 | 311 |
| 933 | 0.0265 | 253 | 700 | 0.81 | 0.682 | 335 |
| 933 | 0.0278 | 255 | 732 | 1.05 | 0.636 | 432 |
| 1034 | 0.0527 | 252 | 629 | 1.06 | 0.445 | 830 |
| 993 | 0.0345 | 257 | 567 | 1.09 | 0.394 | 904 |
| 1271 | 0.1375 | 246 | 352 | 1.10 | 0.810 | 47 |
| 1145 | 0.0957 | 252 | 551 | 1.10 | 0.283 | 1555 |
| 1047 | 0.0572 | 256 | 630 | 1.10 | 0.698 | 288 |
| 1047 | 0.0569 | 257 | 625 | 1.10 | 0.924 | 55 |
| 1037 | 0.0493 | 258 | 573 | 1.10 | 0.158 | 3200 |
| 875 | 0.0200 | 270 | 908 | 1.15 | 0.468 | 1052 |
| 875 | 0.0200 | 270 | 908 | 1.15 | 0.664 | 470 |
| 1118 | 0.0669 | 269 | 453 | 1.25 | 0.529 | 433 |
| 1277 | 0.1150 | 271 | 286 | 1.33 | 0.781 | 91 |
| 1214 | 0.0902 | 289 | 326 | 1.48 | 0.935 | 25 |
| 1021 | 0.0220 | 368 | 286 | 2.24 | 0.427 | 393 |
| 1312 | 0.1007 | 352 | 201 | 2.28 | 0.558 | 178 |
| 1105 | 0.0383 | 382 | 278 | 2.49 | 0.745 | 99 |
| 1260 | 0.0670 | 380 | 183 | 2.60 | 0.550 | 161 |
| 1110 | 0.0462 | 390 | 335 | 2.62 | 0.938 | 23 |
| 1286 | 0.0556 | 498 | 131 | 4.51 | 0.647 | 75 |
| 1302 | 0.0408 | 612 | 86 | 6.81 | 0.941 | 5.7 |
| 1310 | 0.0330 | 736 | 66 | 9.05 | 0.347 | 129 |

NOTES:

1. Densities used in data reduction are from Weatherford, et al (125).

2. Total liquid velocity $V_o$ is based on total mass flow rate at average temperature.

3. $V_g$ and $V_\ell$ are mean phase velocities based on cross sectional area occupied by each phase.

4. Superficial vapor velocity $U_g$ is based on tube cross section.

INDEX INFORMATION SHEET

RTD-TDR-63-4130. INVESTIGATION OF LIQUID METAL BOILING HEAT TRANSFER.

(Unclassified) Univ. of Michigan, Balzhiser, Richard E. et al. C: AF 33(616)-8277. P: 3145. T: 314507. In DDC. In OTS. Personnel in the College of Engineering at The University of Michigan have been conducting both analytical and experimental investigations involving liquid metal boiling heat transfer under contract with the Research and Technology Division, Wright-Patterson Air Force Base, Ohio. A study of saturated pool boiling of potassium in the nucleate regime has supported the nucleate boiling data of Bonilla and Coworkers at Columbis University. Values for the critical heat flux were determined experimentally over a pressure range of 0.1 psia to 22 psia. The data fall substantially above the theoretical predictions of Zuber and Tribus, Rohsenow and Kutateladze. The results are of the same magnitude as predicted by Noyes of Atomics International based on his experimental work with sodium at the lower end of this pressure range. The slope of the burnout flux versus pressure curve is much flatter than was predicted by Noyes on the basis of his data and a modified version of the hydrodynamic "correlations." At atmospheric pressure the burnout flux was found to be approximately 600,000 Btu/(hr)(sq ft). Significant temperature fluctuations were observed in the potassion pool during the course of these investigations. Superheating was attributed to the difficulty in establishing nucleating sites at the heat transfer surface in view of the strong wetting tendencies of the potassium and its high thermal diffusivity. The latter served to dissipate rapidly the energy required for nucleation in the boundary layer. Preliminary data in the stable film boiling regime have not yielded conclusive results. The studies to date have confirmed the superheating tendencies of alkali metal systems. Operation which was believed to have been in a stable film boiling regime produced fluxes much larger than predicted by analytical studies. Further data should be forthcoming for this apparatus shortly. The forced circulation studies have been plagued by a number of difficulties which have required substantial effort and time to resolve. Loop operation commenced in the spring of 1963, but was terminated shortly thereafter when persistent plugging difficulties in the primary potassium circuit prevented further operation. These difficulties were finally overcome during the summer months following the installation of a zirconium chip hot trap and potassium circulation has proceeded without difficulty since that time. An apparent break in the test section region has prevented the attainment of heat transfer results and has resulted in the contamination of the potassium circuit with sodium. The contamination was slight and it was possible to obtain two-phase pressure drop data and void fraction measurements with this apparatus. These results suggest that the Martinelli-Nelson correlation predicts pressure drops substantially lower than those observed experimentally at qualities up to 40 per cent. Agravic studies with mercury have not produced data. The fabrication of the apparatus is nearing completion and initial check out procedures should begin shortly. The program calls for the pool boiling of mercury at pressures up to 300 psia and accelerations up to 20 times that of normal gravity. The apparatus is capable of producing fluxes up to 500,000 Btu/(hr)(sq ft).